

Investigations of Open-Framework Metal Sulfite, Sulfite-Oxalate and related Materials

By

TIWARI RANJAY KUMAR

CHEM11201204008

**National Institute of Science Education and
Research, Bhubaneswar**

*A thesis submitted to the
Board of Studies in Chemical Sciences
In partial fulfillment of requirements
for the Degree of*

DOCTOR OF PHILOSOPHY

of

HOMI BHABHA NATIONAL INSTITUTE



January, 2019

Homi Bhabha National Institute¹

Recommendations of the Viva Voce Committee

2. As members of the Viva Voce Committee, we certify that we have read the dissertation prepared by Tiwari Ranjay Kumar entitled "Investigations of Open-Framework Metal Sulfite, Sulfite-Oxalate and related Materials" and recommend that it may be accepted as fulfilling the thesis requirement for the award of Degree of Doctor of Philosophy.

Chairman - Prof. A. Srinivasan



Date:

25.1.19

Guide / Convener - Dr. J. N. Behera



Date:

25/1/2019

Examiner - Prof. Tapas K. Maji



Date:

25/1/2019

Member 1- Dr. C. S. Purohit



Date:

25/01/19

Member 2- Dr. Nagendra K. Sharma



Date:

25.01.19

Member 3- Dr. Joydeep Bhattacharjee



Date:

25/01/19

Final approval and acceptance of this thesis is contingent upon the candidate's submission of the final copies of the thesis to HBNI.

I/We hereby certify that I/we have read this thesis prepared under my/our direction and recommend that it may be accepted as fulfilling the thesis requirement.

Date: 25/01/2019



(Dr. J. N. Behera)

Place: NISER, Bhubaneswar

Guide

¹ This page is to be included only for final submission after successful completion of viva voce.

STATEMENT BY AUTHOR

This dissertation has been submitted in partial fulfillment of requirements for an advanced degree at Homi Bhabha National Institute (HBNI) and is deposited in the Library to be made available to borrowers under rules of the HBNI.

Brief quotations from this dissertation are allowable without special permission, provided that accurate acknowledgement of source is made. Requests for permission for extended quotation from or reproduction of this manuscript in whole or in part may be granted by the Competent Authority of HBNI when in his or her judgment the proposed use of the material is in the interests of scholarship. In all other instances, however, permission must be obtained from the author.


Tiwari Ranjay Kumar

DECLARATION

I, hereby declare that the investigation presented in the thesis has been carried out by me. The work is original and has not been submitted earlier as a whole or in part for a degree / diploma at this or any other Institution / University.


Tiwari Ranjay Kumar

List of Publications arising from the thesis

Journal

1. “H–bond Supported Coordination Polymers of Transition Metal Sulfites with Different Dimensionalities”, Ranjay K. Tiwari, Jitendra Kumar and J. N. Behera, *RSC Adv.* **2015**, *5*, 78389-78395.
2. “Organically Templated Linear Metal Sulfites”, Ranjay K. Tiwari, Jitendra Kumar and J. N. Behera, *RSC Adv.* **2015**, *5*, 96034-96041.
3. “The First Organically Templated Open-Framework Metal-Sulfites with Layered and Three-Dimensional Diamondoid Structures”, Ranjay K. Tiwari, Jitendra Kumar and J. N. Behera, *Chem. Commun.* **2016**, *52*, 1282- 1285.
4. “Organic–Inorganic Hybrid Three-Dimensional Metal Sulfite- Oxalate with Honeycomb-like Structures”, Ranjay K. Tiwari, and J. N. Behera, *Dalton Trans.* **2017**, *46*, 5911- 5917.
5. “Organically-Templated Inorganic–Organic Hybrid Metal (Zn and Cd) Sulphite- Oxalate with Layered and Three-Dimensional Structures”, Ranjay K. Tiwari, Jitendra Kumar, and J. N. Behera, *Dalton Trans.* **2017**, *46*, 15939-15946.
6. “Hybrid Materials Based on Transition Metal–BTC–Benzimidazole: Solvent Assisted Crystallographic and Structural Switching”, Ranjay K. Tiwari and J. N. Behera, *CrystEngComm*, **2018**, *20*, 6602-6612.

Others

1. “Structural Tuning of Anion-Templated Motifs with External Stimuli through Crystal-to-Crystal Transformation”, A. S. Singh, R. K. Tiwari, M. M. Lee, J. N. Behera, S.-S. Sun and V. Chandrashekhar, *Chem. Eur. J.* **2017**, *23*, 762- 766.
2. “Two Novel 3D-MOFs (Ca-TATB and Co-HKUST): Synthesis, Structure and Characterization”, Subba Reddy Mari, Neha Chauhan, Ranjay K. Tiwari, Jitendra Kumar, J. N. Behera, *Inorganica Chim. Acta*, **2018**, *478*, 8-14.
3. “Thermal Induced 1D to 2D Polymer Conversion Accompanied by Major Packing Changes in a Single-Crystal-to-Single-Crystal Transformation”, Ashutosh S. Singh, Amjad Ali, Ranjay K. Tiwari, J. N. Behera, Shih -S. Sun, Vadapalli Chandrasekhar, *CrystEngComm*, **2018**, *20*, 2346-2350.
4. “Hexanuclear Zn(II) and Mononuclear Cu(II) Complexes: Synthesis, Structural Characterization and Evaluation of their Biological Prospects”, Shyam Mondal, Manosree Chatterjee, Ranjay K. Tiwari, J. N. Behera, Nripen Chanda, Sourav Biswas, Tanmoy Saha, *Appl. Organomet. Chem.*, **2019** (Revised Manuscript submitted for publication).
5. “Chiral Lanthanide Sulfite-Acetate Open-Framework Layered Materials: Synthesis, Structure and Characterization”, Ranjay K. Tiwari, Ipsha Shruti, J. N. Behera, *Inorg. Chem.*, **2019** (Manuscript submitted for publication).
6. “Synthesis and Characterization of Metal Tri-Hydroxy-benzene-Tri-Sulfonate Based Framework Materials”, Ranjay K. Tiwari, and J. N. Behera, *Daton Trans.*, **2019** (Manuscript submitted for publication).

Conferences

1. Oral talk on “Open-framework Metal Sulfites and Sulfite-Oxalate Based on Honeycomb-like Structures” at IINCM-2017, organized by NISER Bhubaneswar (22nd Dec, 2017)
2. Poster presentation on “Open-Framework Metal Sulfites and Sulfite-Oxalate Based on Honeycomb-like Structures” in 24th Congress & General Assembly of the International Union of Crystallography 2017 held at Hyderabad, 21-28 August 2017.
3. Attended a workshop in "Rigaku Oxford Diffraction: CrysAlisPro and Olex2 Workshop" in 24th Congress & General Assembly of the International Union of Crystallography 2017 held at Hyderabad, 21-28 August 2017.
4. Attended a workshop in "X-ray Structure Determination" under Global Initiative of Academic Networks (GIAN) scheme of the Ministry of Human Resource & Development (MHRD), held at Jiwaji University, Gwalior, 13-26 June 2016.
5. Poster Presentation on “Controlled Synthesis of Heterometallic Oxide from Single-Source Precursors” in Indo-French Symposium on Functional Metal-Organics held at NISER, Bhubaneswar, 24-26 February 2014.

Ranjay
Tiwari Ranjay Kumar

Dedicated to

My beloved family

ACKNOWLEDGEMENTS

I would like to express my gratitude to *Dr. J. N. Behera*, my guide, for continuous support, encouragement and patience exhibited, inspiring me with his knowledge, to pursue and find answers to existing problems.

I am very thankful to Prof. Sudhakar Panda, Director-NISER for the Laboratory facilities and infrastructure, DAE for financial support. I thank my doctoral committee members Dr. C. S. Purohit, Dr. Nagendra K. Sharma, Prof. A Srinivasan and Dr. Joydeep Bhattacharjee. Besides this I am grateful to Dr. K. Senapati (SPS) for magnetic measurement and Dr. R. Vaidhyanathan for gas adsorption study. I thank all others faculties in SCS and scientific officer Dr. Arun Kumar for their support. Also, I thank to Mr. Deepak Behera, Mr. Sanjay, Mr. Amit, Mr. Raj Kumar for help provide to learn and analyses of the X-ray, NMR and Mass analyses.

I would like to thank my senior Dr. Pratap Deheri, Dr. Jitendra Kumar and Dr. Subba Reddy Marri. I would also like to thank my lab mates Ipsha, Rambabu, Neha, Vineet, Himansu, and Niharika who have worked with us in different time their help, support and cooperation during these years.

I specially thank to Villa no. 224 members Om, Dr. Abhash, Dr. Ashim, Dr. Prabhat, Dinesh and all my friends in NISER with great gratitude, especially, Dr. Giri, Amarnath, Manas, Tanmay, Ajesh, Adi, Tapas, Santosh, Amrish, and Rahul.

Finally, above all I thank my teachers, father (Dashrath J. Tiwari), mother (Malti Tiwari) and family members (Dhananjay, Manjay, Shweta, Renu, Tara) for their unconditional love, care, affection and support.


Tiwari Ranjay Kumar

CONTENTS

Thesis title	i
Recommendations of Viva Voce Board	ii
Statement by the Author	iii
Declaration	iv
Publication List	v
Dedications	viii
Acknowledgements	ix
Contents	x
Synopsis	xi
List of Schemes	xxxii
List of Figures	xxxii
List of Tables	xlvi
List of Abbreviations	xlix
Chapter 1	1
Chapter 2	53
Chapter 3	119
Chapter 4	163
Chapter 5	195

Synopsis

The thesis consists of five chapters. Chapter-1 describes the open-framework materials and difficulties involved in the synthesis of sulfite-based framework materials. Chapter-2 describes the syntheses and applications of the metal sulfites framework. Metal sulfite-oxalate based framework materials syntheses and applications are described in Chapter-3 followed by a discussion on the structural changes of THBTS³⁻ ligand in the presence of the metal cation and organic cation in Chapter-4. The last chapter (Chapter-5) covers syntheses and applications of inorganic and organic hybrid materials based on the BTC benzimidazole and imidazole framework materials.

Chapter 1: Open-Framework Materials

Open-framework materials having are in the interesting due to their novel structural diversity with their various application and properties such as sorption, catalysis and electrical conductivity etc^{1,2}. The open-framework materials studies started with the aluminium silicate and then spread to the large subjective area using different primary building units of the structure such as phosphate, sulfate, selenate with interesting structure and properties which are well characterized by the single crystal X-Ray diffraction and other techniques³⁻⁶. Moving to another direction with one less oxygen atom in the oxyanions like phosphite, selenite, tellurite etc. provide the structural diversity and the different binding modes to the fewer availability of oxygen atom⁷⁻⁸. The sulfite anion which possesses a lone pair of electrons on sulfur atom may have significant influence in directing the structural topology by providing crystal in non-centrosymmetric space group to the resultant open-framework materials akin to selenite

and tellurite anions which show SHG^{9,10}. Open-framework materials using pyramidal SO_3^{2-} ion as the building unit are very few, as it gets oxidized to SO_4^{2-} during the synthetic condition¹¹.

Chapter 2: Metal Sulfite Open-Framework Materials

This chapter contains synthesis, crystal structure, thermal study and application of a varying structural diversity of organically templated and coordination polymers based on a transition metal sulfite a 1D chain, 2D, and 3D open-framework materials.

Organically-templated One-Dimensional Metal Sulfites¹²

The reaction of zinc(II) acetate or manganese(II) acetate with sodium disulfite in presence of varying organic amines afford six novel 1D-coordination polymers namely $[(\text{C}_3\text{H}_{10}\text{N})_2] [\text{Zn}(\text{SO}_3)_2]$, **1**, $[(\text{C}_3\text{H}_{12}\text{N}_2)] [\text{Zn}(\text{SO}_3)_2]$, **2**, $[(\text{C}_4\text{H}_{14}\text{N}_2)] [\text{Zn}(\text{SO}_3)_2]$, **3**, $[(\text{C}_6\text{H}_{18}\text{N}_2)] [\text{Zn}(\text{SO}_3)_2]$, **4**, $[(\text{C}_4\text{H}_{12}\text{N}_2)] [\text{Zn}(\text{SO}_3)_2] \cdot (\text{H}_2\text{O})$, **5** and $[(\text{C}_4\text{H}_{12}\text{N}_2)] [\text{Mn}(\text{SO}_3)_2(\text{H}_2\text{O})_2] \cdot 2\text{H}_2\text{O}$, **6** based on metal-sulfites coordination. **1-5** differs with one another only in terms of organic amine which acts as a template in all zinc-based compounds, but the basic unit for the formation of 1D polymer based on ZnO_4 tetrahedron remains same (Fig.1). In all the cases, Zn(II) ion is tetrahedrally coordinated with four sulfite anions and the ZnO_4 tetrahedra are joined together by their vertices to give 1D-polymer. In the case of **6**, Mn(II) ion adopts octahedral geometry and these octahedrons are joined with sulfite anions another to give 1D-polymer.

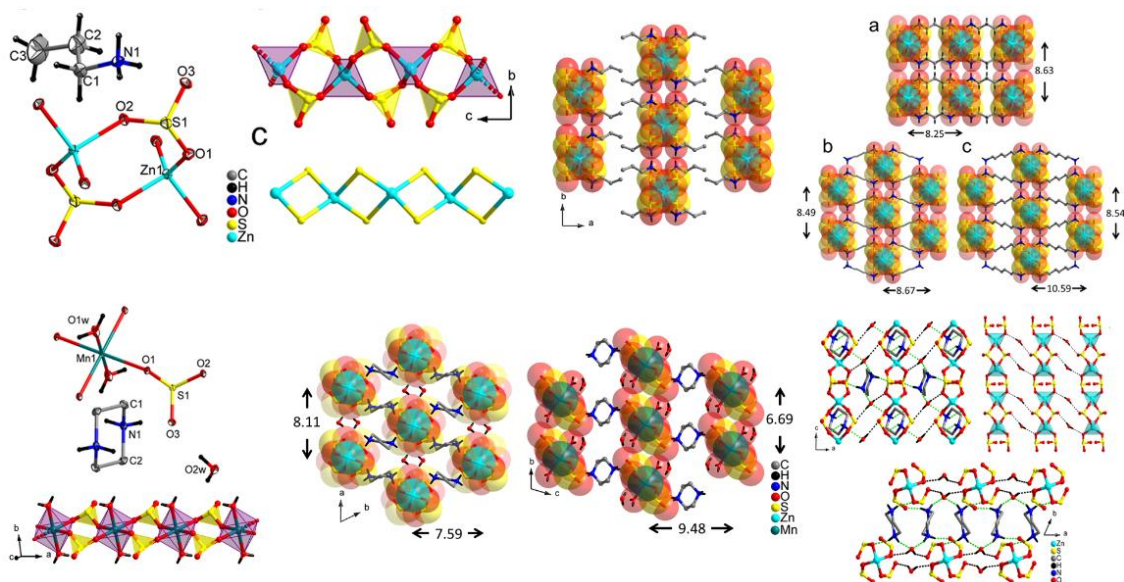


Fig.1. The asymmetric unit of amine templated one-dimensional ZnSO₃ and MnSO₃ chain with their molecular and H-bonding pattern.



The **7** featured a two-dimensional structure and it was synthesized by the hydrothermal method in the mild condition in which organic amine coordinated to metal and balanced the charge neutrality. **7** crystallizes in the monoclinic crystal system having a $P2_1/c$ space group. In this case the *in-situ* auto-oxidation of Co(II) precursor to Co(III) species is observed. Both the Co(III) ions have octahedral geometries. The coordination sphere of each Co(III) ion consists of four amino nitrogen atoms from the organic base and two sulfur atoms from two identical SO₃²⁻ occupying the axial sites. In the crystal lattice of **7**, the Co(III) ions and Na(I) ions are coordinated to SO₃²⁻ anion and forms an infinite 2D layer in the *bc*-plane where each SO₃²⁻ anion is coordinated with two Na(I) ions and one Co(III) anion (Fig. 2a).

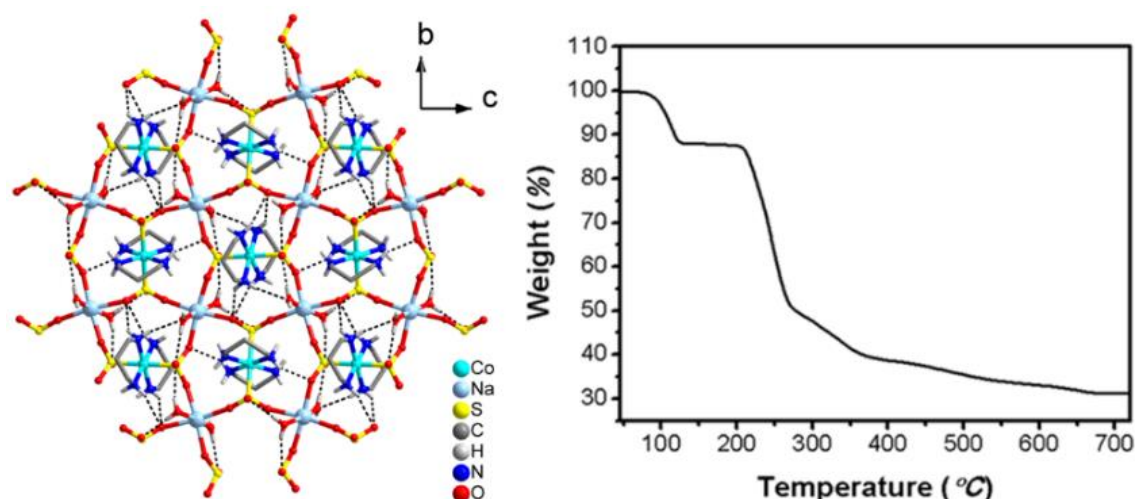


Fig. 2. (a) Part of 2D-crystal lattice of $[(C_3N_2H_{10})_2NaCo(SO_3)_2(H_2O)_2].H_2O$, **7** and (b) TGA of $[(C_3N_2H_{10})_2NaCo(SO_3)_2(H_2O)_2].H_2O$, **7**.

$[C_2H_{10}N_2][Zn_3(SO_3)_4]$, **9.**¹⁴

9 as block shape single crystals have a monoclinic system with a $C2/c$ space group. Two crystallographically independent Zn(II) ions are encountered in the asymmetric unit with one atom having half occupancy. Both the unique sulfite anions offer all three oxygen atoms towards Zn(II) coordination in $\eta^1\mu^3$ -manner however with significant differences. Two $S(2)O_3^{2-}$ anions coordinates three zinc ions in a way to form a sulfite capped triangular node $[Zn_3(SO_3)_2]$ where three adjacent ZnO_4 tetrahedra are interconnected. These nodes are further interconnected by $S(1)O_3^{2-}$ anion to generate a layer in bc -plane with embedded 4, 6 and 8-membered rings (Fig. 3).

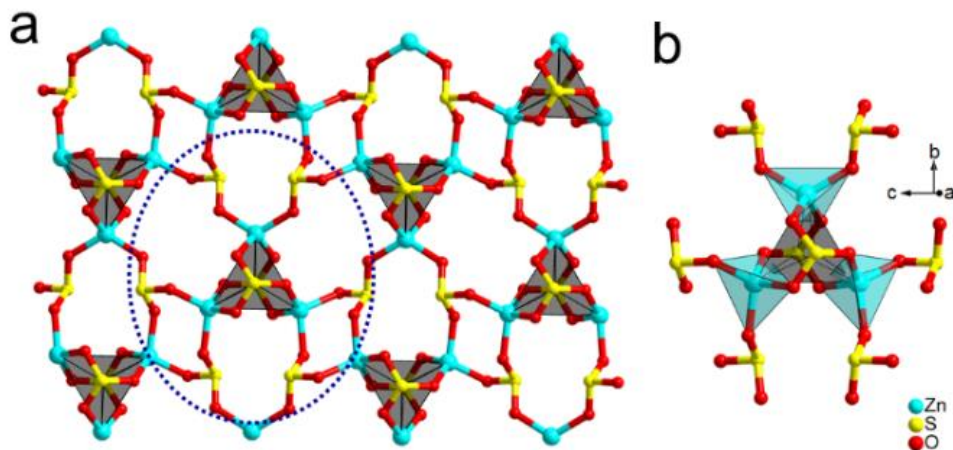


Fig. 3. (a) Part of the 2D-crystal lattice of $[\text{C}_2\text{H}_{10}\text{N}_2][\text{Zn}_3(\text{SO}_3)_4]$, **9** (b) connectivity of Zn and sulfite ion.

$[\text{CN}_3\text{H}_6]_2[\text{Zn}(\text{SO}_3)_2]$, **10**¹⁴

The colorless Plate-like crystals of **10** were adopted an orthorhombic crystal system with a non-centrosymmetric space group $Fdd2$. The crystal lattice is composed of ZnO_4 tetrahedra connecting four SO_3^{2-} pyramidal units through Zn-O-S links. The SO_3^{2-} with two oxygens and Zn(II) ions coordinated in a bidentate fashion giving rise to a 3D network.

The 3D network is composed of a 12-membered ring system having six ZnO_4 and six SO_3 units arranged alternately. Each ring is occupied by the guanidinium cations which held *via* strong N-H \cdots O hydrogen bonding interactions (Fig. 4). The crystal lattice of **10** is composed of strictly alternating ZnO_4 tetrahedra SO_3 pyramids *via* vertex sharing forms distorted adamantane-like topology to give rise to an infinite, anionic 3D-diamondoid network. Interestingly, part of the crystal lattice can also be visualized as a helix running along b -axis with a pitch length of 12.12 Å where the grooves are occupied by the guanidinium cation and the plane is pointing toward the helical axis.

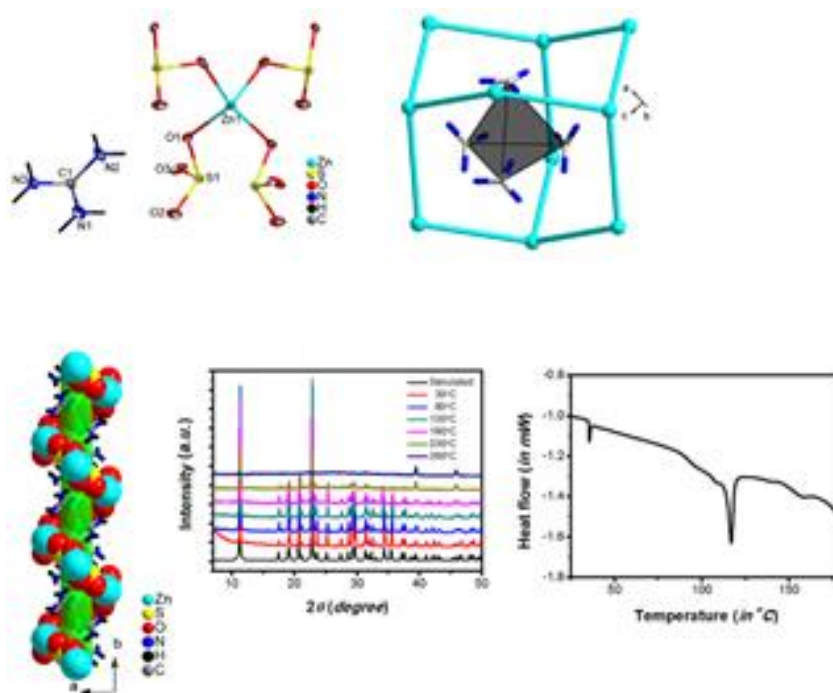


Fig. 4. (a) Asymmetric unit of $[\text{CN}_3\text{H}_6]_2[\text{Zn}(\text{SO}_3)_2]$, **10** where unique atoms are labelled, (b) adamantane type topology, (c) Helical structure in **10**, (d) temperature dependent PXRD and (e) DSC spectrum of **10**.

Chapter 3: Metal Sulfite-Oxalate Open-Framework Materials

This chapter enclosed synthesis, magnetic and photoluminescence studies of metal sulfite-oxalate open-framework materials. All the compounds are synthesized under hydrothermal conditions. These compounds are well characterized with single crystal X-ray diffractometer, PXRD, TGA, and DSC.

$[\text{Zn}_2(\text{SO}_3)_2(\text{C}_2\text{O}_4)_{0.5}(\text{C}_6\text{N}_2\text{H}_{13})] \cdot (\text{H}_2\text{O})_2$, **11**¹⁷. Compound **11** was synthesized hydrothermally and show a layered structure, it crystallizes in the monoclinic crystal system with a $P21/c$ space group. The asymmetric unit contains zinc, sulfite, DABCO, oxalate and a water molecule. The penta coordinated Zn and tetrahedral Zn is connected

through sulfite anions and form a one-dimensional chain, the oxalate anion acts as a bridge and it connects two chains and forms layered structure (Fig. 5). The complex start decomposing from room temperatures and result in ZnO after reaching 700 °C.

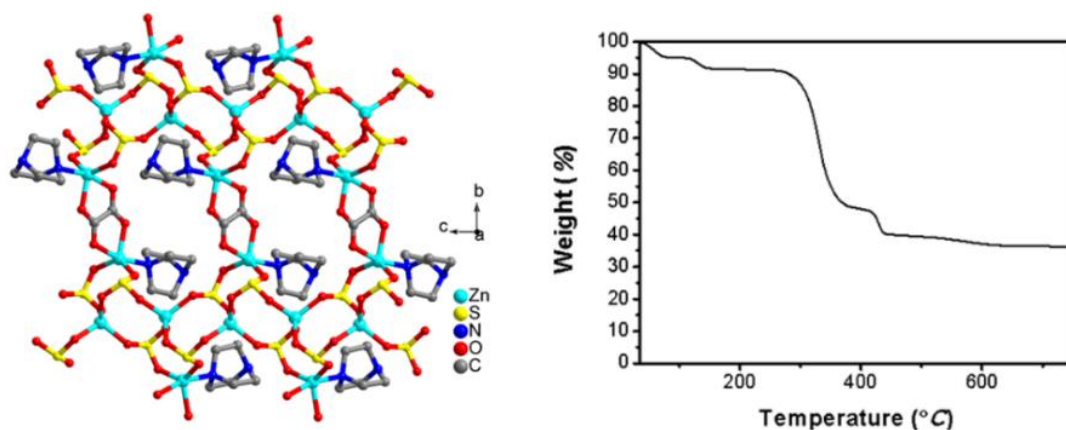


Fig. 5. Part of the 2D-crystal lattice of $[\text{Zn}_2(\text{SO}_3)_2(\text{C}_2\text{O}_4)_{0.5}(\text{C}_6\text{N}_2\text{H}_{13})] \cdot (\text{H}_2\text{O})_2$, **11** and TGA Profile diagram

$[\text{C}_4\text{N}_2\text{H}_{12}]_{0.5}[\text{Zn}_2(\text{SO}_3)_2(\text{C}_2\text{O}_4)_{0.5}(\text{H}_2\text{O})_2]$, **12**¹⁷.

12 was obtained by the hydrothermal method by keeping similar reaction condition for **11** and introducing piperazine, **12** crystallize in tetragonal crystal system with $P4_2/mnm$ space group having an infinite three-dimensional network with Zn(II) as central atom and sulfite and oxalate as counter anions, Zn has two different environments, one has tetrahedral and other show octahedral geometry (Fig. 6). The piperazine was situated in the cavity. The TGA curve shows that it stables up to 110 °C and start decomposing which results in ZnO as a calcined product.

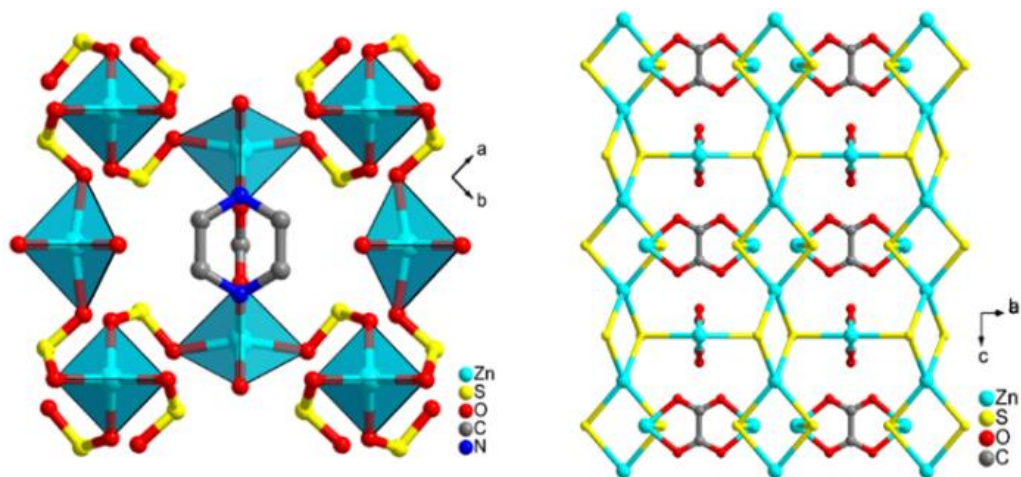


Fig. 6. (a) Part of the 3D-crystal lattice of $[\text{C}_4\text{N}_2\text{H}_{12}]_{0.5}[\text{Zn}_2(\text{SO}_3)_2(\text{C}_2\text{O}_4)_{0.5}(\text{H}_2\text{O})_2]$, **12** along *c*-axis and (b) 3D-Crystal lattice of **12**, showing the interconnection of Zn_2S_2 chains.



The zinc ions were replaced with cadmium ions and we got **13** which crystallizes in a triclinic crystal system having *P*-1 space group and showed a two-dimensional structure with embedded a one-dimensional channel. The inorganic framework was composed of hepta coordinated Cd1 and octahedra Cd2 connected to oxalate and sulfite *via* edge sharing with S2 and corner-sharing S1 of sulfite and *vice-versa*, and form a one-dimensional channel. The charge of Inorganic framework was balanced by the presence of half molecules of two unique protonated piperazine cations which are situated in the interlayer as well as in the cavity of the one-dimensional channel (Fig. 7).

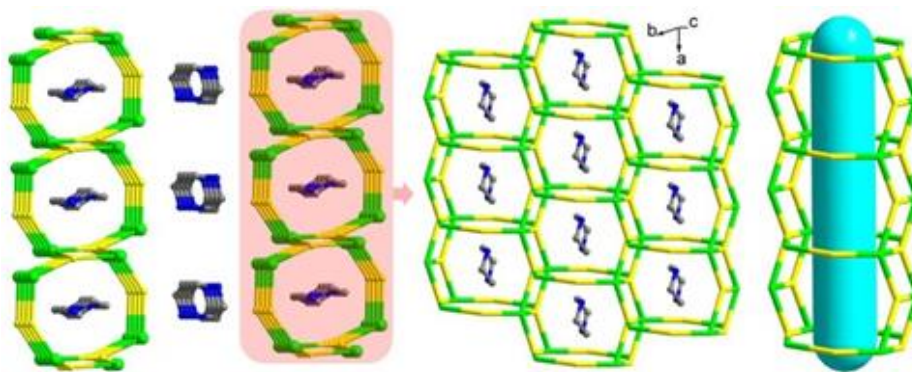


Fig. 7. (a) Part of crystal lattice of the $[\text{C}_4\text{N}_2\text{H}_{12}][\text{Cd}_2(\text{SO}_3)_2(\text{C}_2\text{O}_4)(\text{H}_2\text{O})]\cdot\text{H}_2\text{O}$, **13** as viewed close to a -axis; (b) A layer structure in case of **13** in ab -plane; (c) embedded 1D channel along a -axis having 8 and 4-member rings within the layers.

$[\text{Na}_2\text{Mn}_2(\text{C}_2\text{O}_4)(\text{SO}_3)_2(\text{H}_2\text{O})_2]$, **14¹⁸.**

The crystal lattice of **14**, which consists of the alternating MnO_4 tetrahedron and SO_3 trigonal pyramids linked through their corner to form the layer structure in the bc -plane with 4-member rings. The organic anions oxalate moiety connects the two-manganese ion to form a chain along a -axis. Further oxalate ion is acting as a bridge and connects the two manganese sulfite layers in the a -axis, forming honeycomb-like structure and results in the infinite 3D network (Fig 8). The magnetic study of **14** suggests that the material is essentially paramagnetic with antiferromagnetic interactions exhibiting only short-range order (Fig. 8).

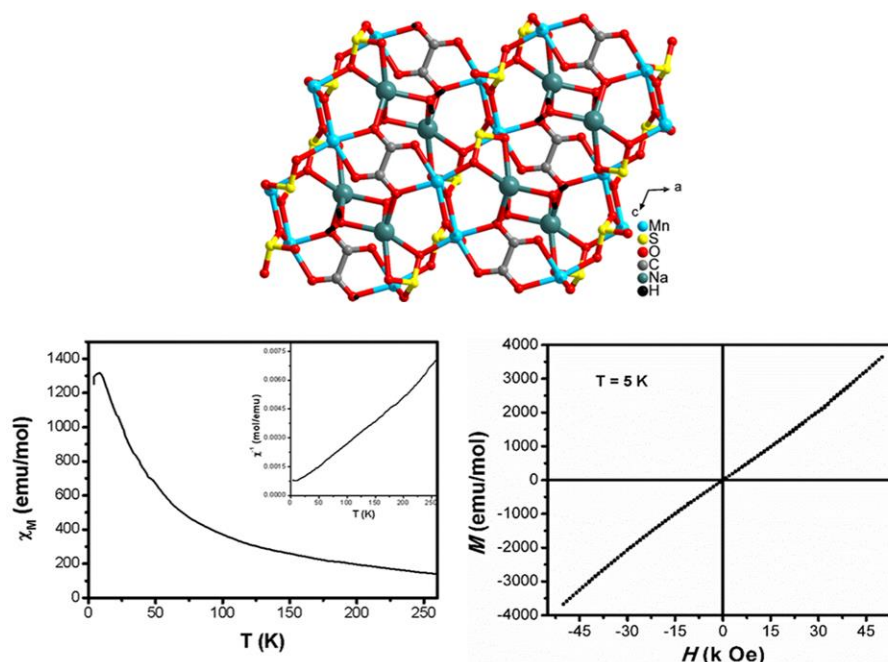


Fig. 8. (a) 3D packing of **14**, (b) MT and MH cycle of $[\text{Na}_2\text{Mn}_2(\text{C}_2\text{O}_4)(\text{SO}_3)_2(\text{H}_2\text{O})_2]$, **14**.

$[\text{NaEu}(\text{C}_2\text{O}_4)(\text{SO}_3)(\text{H}_2\text{O})_3]$, **15**¹⁸.

The crystal lattice of **15** is packed in such a way that alternate arrangement of EuO_9 and SO_3^{2-} polyhedra forms an infinite one-dimensional ladder-like chain along a -axis, containing 4-membered rings formed by the two Eu and two sulfite moiety. EuO_9 and oxalate anion forms the honeycomb-like layered structure in bc -plane (Fig. 9). The photoluminescence emission spectra (PL) of compound **15** upon excitation at 395 nm shows four expected peaks for the $^5\text{D}_0 \rightarrow ^7\text{F}_j$ transitions, it emits sharp intense red emission band at 616 nm, which is its characteristic emission due to the electric dipole transition ($^5\text{D}_0 \rightarrow ^7\text{F}_2$) of central Eu (III) metal ion (Fig. 9).

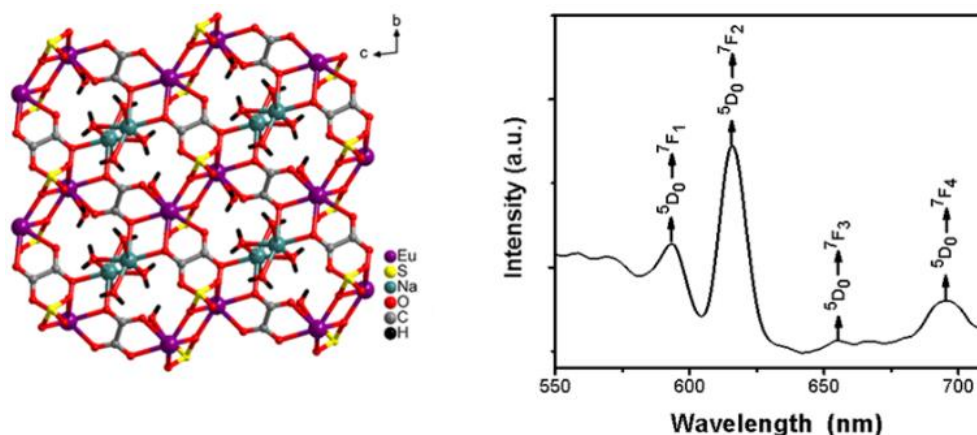


Fig. 9. (a) 3D packing and (b) Photoluminescence spectrum of **15**.

Chapter 4: Metal Benzene tri-hydroxy, tri-sulfonate Framework Materials

This chapter contains the synthesis and the structural change observed when changing the metal cations and organic bases. The trihydroxy-benzene-trisulfonate ligand was synthesized by the reported procedure¹⁹.



16 was synthesized by the slow evaporation method, **16** crystallizes in the monoclinic crystal system with a $P2_1/n$ space group. The asymmetric unit contains one ligand surrounded by the four melamine and four water molecules. The melamine and ligand form an H-bonded three-dimensional framework. The ligand itself forms a helical structure with a water molecule. The Melamine, ligand and water molecule are strongly bonded *via* H-bonding (Fig 10.).

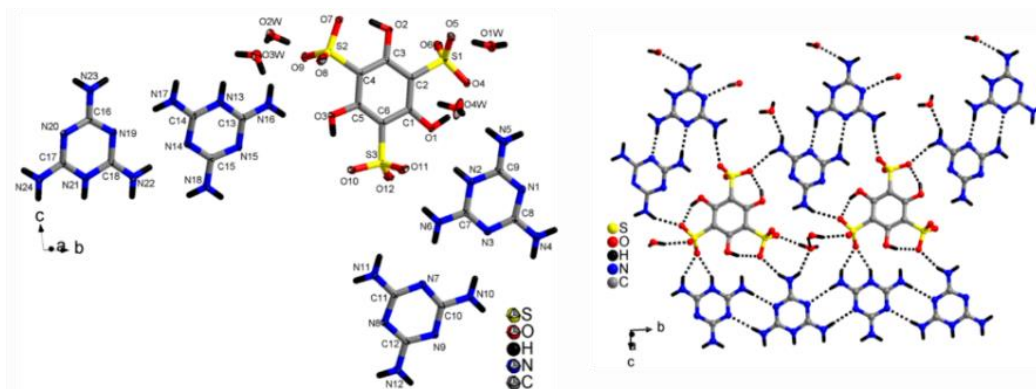


Fig. 10. (a) Asymmetric unit of $(C_3N_6H_7)_4(C_6H_3O_9S_3)(H_2O)_4$, **16** and (b) Lattice diagram and H-bonding in $(C_3N_6H_7)_4(C_6H_3O_9S_3)(H_2O)_4$, **16**

$[Na_2(C_6H_3O_3S_3)(CN_3H_6)(H_2O)](H_2O)$, **17.**

We replaced the melamine with guanidine we got a two-dimensional framework with ordered structure and the interesting part is that in presence of guanidine H atom is moving and forming tetrahedral geometry at the para position with losing the aromaticity and sulfonate ligand came outside the plane. It crystallizes in the orthorhombic crystal system with a $Cmca$ space group.

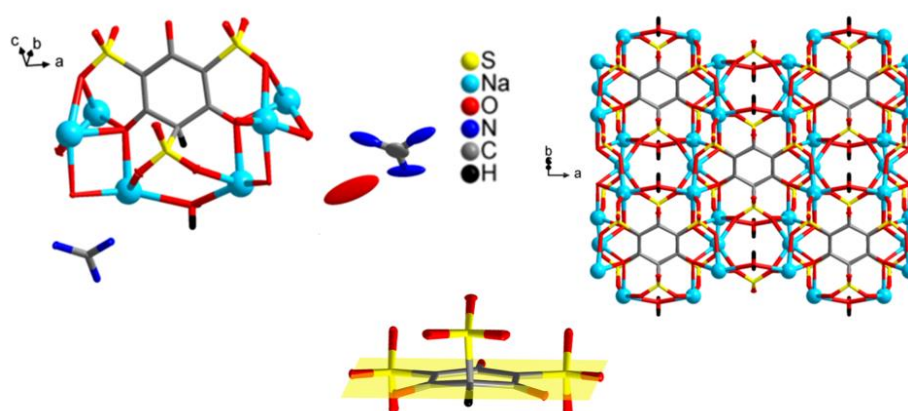


Fig. 11. (a) The asymmetric unit of $[Na_2(C_6H_3O_3S_3)(CN_3H_6)(H_2O)](H_2O)$, **17**, (b) Lattice diagram of **17** and (c) A non-planar tetrahedral arrangement of ligand.

The asymmetric unit contains one benzene tri-hydroxy tri-sulfonate ligand, two half moieties of guanidine, two sodium and one water molecule. The bond angle between distorted sulfonate and H atom is 104.23° (Fig 11).

[K₃(C₆H₃O₉S₃)(H₂O)₃], 18.

We replaced the guanidine carbonate with K₂CO₃ we got chiral three-dimensional framework with ordered structure. The crystal has an orthorhombic crystal system with a *Cmca* space group. The asymmetric unit contains two potassium and one ligand molecule two water molecule. The K-O bond distance ranges from 2.95 to 3.15 Å. The Potassium ions have loosely bonded and coordinated to 8 neighbor oxygen atoms. In the complex the water molecule itself forming a water channel. The distance between two water molecules is 2.85 and 3.18 Å (Fig. 12).

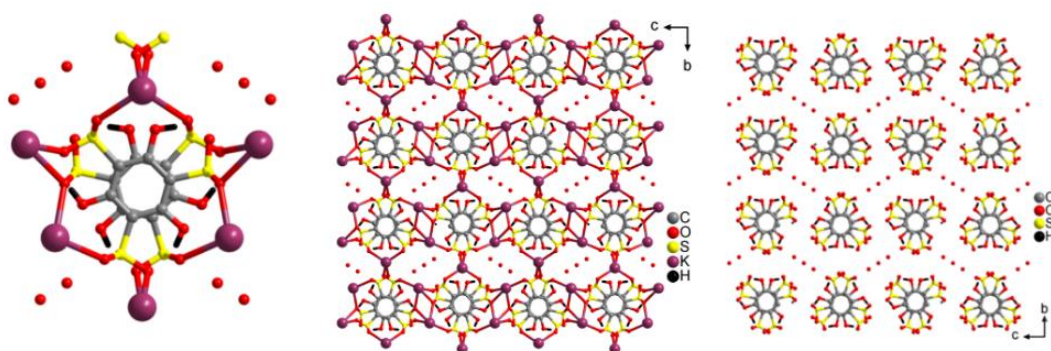


Fig. 12. (a) The asymmetric unit of **18**, (b) Lattice diagram of **18** and (c) H-bonding between the ligand and water channel where K is omitted for clarity.

[C₄N₂H₁₃]₂[Cd₂(C₆H₃O₃S₃)(H₂O)₂].(H₂O), 19.

Here we introducing d¹⁰ Cd metal ions and got a one-dimensional chain. The colorless crystals of **19** crystallize in the monoclinic crystal system with the *P2₁/c* space group.

The asymmetric unit contains two cadmium, one DABCO and one sulfonate ligand. The central atom Cadmium ion has octahedral geometry and connected with surrounding two aqua ligand, two sulfonate oxygen and two hydroxy oxygen. The central metal cadmium surrounded by two ligands, the bond length of Cd-O is 2.5 Å. The two-cadmium linked together *via* edge sharing and forming a linear one-dimensional chain along *c*-axis (Fig 13.). The partially protonated DABCO lying the space between two chains.

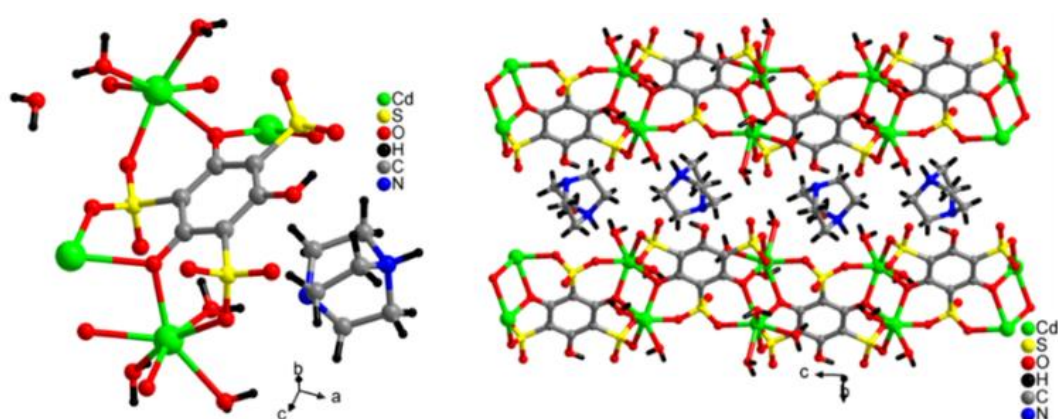


Fig. 13. (a) Asymmetric unit of $[\text{C}_4\text{N}_2\text{H}_{13}]_2[\text{Cd}_2(\text{C}_6\text{H}_3\text{O}_3\text{S}_3)(\text{H}_2\text{O})_2] \cdot (\text{H}_2\text{O})$, **19** and (b) Lattice diagram of $[\text{C}_4\text{N}_2\text{H}_{13}]_2[\text{Cd}_2(\text{C}_6\text{H}_3\text{O}_3\text{S}_3)(\text{H}_2\text{O})_2] \cdot (\text{H}_2\text{O})$, **19**.

Chapter 5: Inorganic-Organic Hybrid Materials

This chapter describes the synthesis, magnetic property and dielectric constant of compounds. **20-25** was synthesized by the solvothermal method, Metal acetate hydrate, 1,3,5-benzene tricarboxylic acid (BTC), and Imidazole (Im)/ Benzimidazole (BIm), in (1:1:1) were mixed in DMF and sealed in 7 mL autoclave and heated at 120 ° C.

[Co₆(formate)₆(BTC)₆(Im)₆], 20.

The Pink color crystals of **20** crystallize in trigonal *R*-3 spacegroup shows a layered structure. The metal centre Co ions have octahedral geometry and connected with the oxygen of three formates, two carboxylates (BTC) and one nitrogen of the Im group. The bond valence sum calculations show +2 oxidation state of Co ions. The hexagonal cluster of Co ions displays a layered structure of **20**. The six Co ions, six formates, six BTC and six IM moiety forming a hexagonal cluster and this cluster are extended through BTC and forms a layered structure. It shows antiferromagnetic behavior.

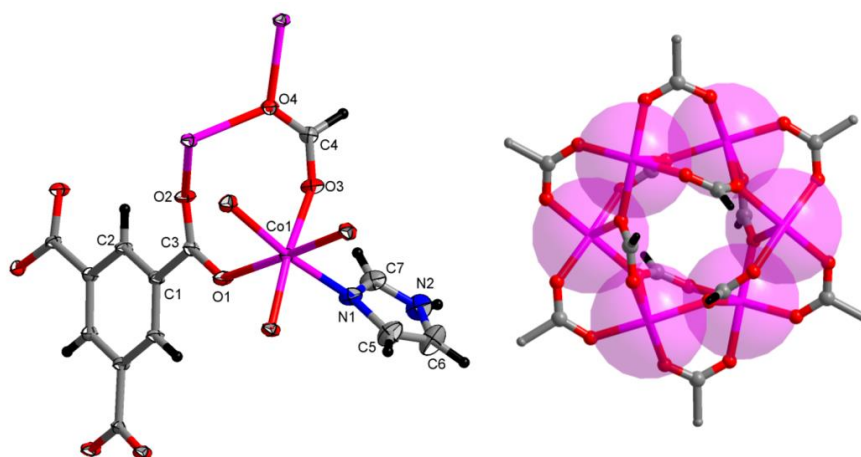


Fig. 14. (a) Asymmetric unit of [Co₆(formate)₆(BTC)₆(Im)₆], **20** where unique atoms are labelled and (b) A hexanuclear Co cluster.

[(CH₃)₂NH₂][Cu(BTC)₃(Im)], 21.

21 was synthesized under solvothermal condition. The blue color crystal was crystallized in the monoclinic crystal system having a *P*2₁/*n* space group. The central Cu metal surrounded by the three carboxylates of BTC and one Imidazole. The Cu atoms present in a distorted square-planar geometry with oxygen and nitrogen atoms.

The 2 Copper and 2 BTC unit together form 4-membered rings, 4 copper and 4 BTC unit form 8-membered rings. The 4-membered ring and 8-membered rings together extend and forms wave-like layered structure running in *bc*-plane. The anionic framework was balanced by the dimethylamine.

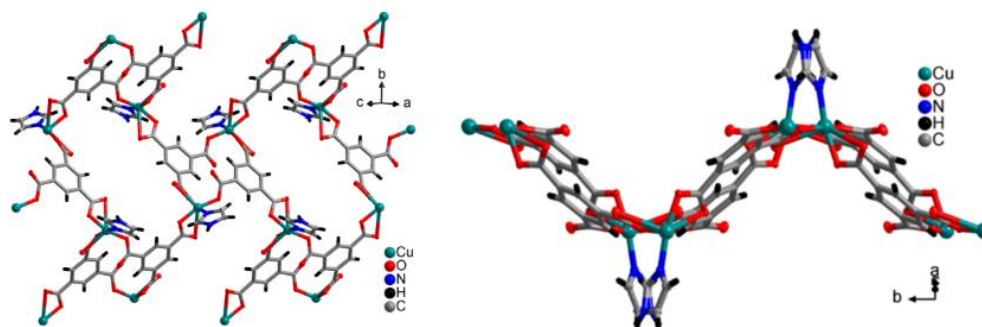


Fig. 15. (a and b) layered structure of $[(\text{CH}_3)_2\text{NH}_2][\text{Cu}(\text{BTC})_3(\text{Im})]$, **21**.

$[\text{Co}_4(\text{BTC})_3(\text{BIm})_6][\text{solvent}]$, **23.**

The paddlewheel type three-dimensional of compound **23** was synthesized by the solvothermal method, which crystallizes in a monoclinic crystal system with a $C2/c$ space group. The Co ions show a 3D framework constructed from paddlewheel Co_2 tetracarboxylic and triangular BTC linkers. The two crystallographically equivalent Co ions have a square pyramidal geometry where the four equatorial positions are occupied by carboxylate oxygen atoms, $\text{Co}-\text{O}_{\text{carboxylate}}$ bond lengths are 2.010(3) Å. Each paddlewheel unit in **23** is locked by four carboxylate groups from four equivalent BTC linkers, and each BTC linker connects three paddlewheel units, resulting in the 3D (3,4)-connected network.

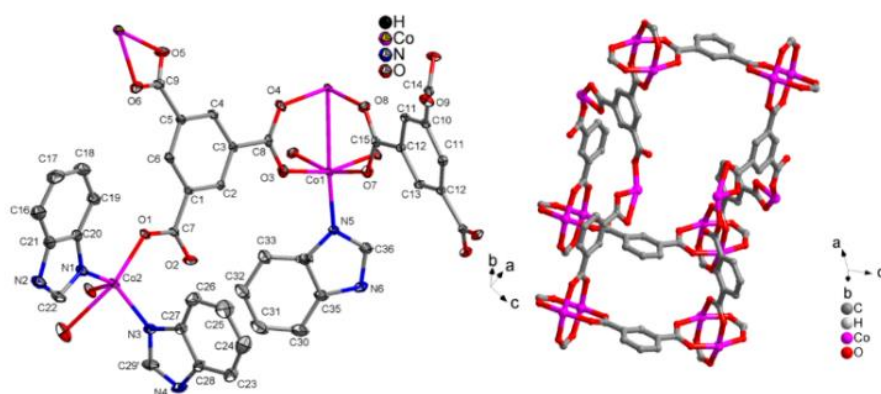


Fig. 16. (a) Asymmetric unit of $[\text{Co}_4(\text{BTC})_3(\text{BIm})_6][\text{solvent}]$, **23**; where unique atoms are labeled (b) Paddlewheel type of structure of $[\text{Co}_4(\text{BTC})_3(\text{BIm})_6][\text{solvent}]$, **23**.

$[\text{Cu}_3(\text{BTC})_2(\text{BIm})_6][\text{solvent}]$, **24.**

24 show a layered structure, the plate shape blue crystals crystalizes in the rhombohedral crystal system with an $R\bar{3}$ space group. The asymmetric unit of **24** contains one copper, two BTC and six BIm unit. The central metal Cu, coordinated by the two BTC group and two BIm moiety. The six copper and six BTC units are alternatively formed hexagonal sheet, the BIm is out of the plane of CuBTC plane and the angle between the planes is 83.29° .

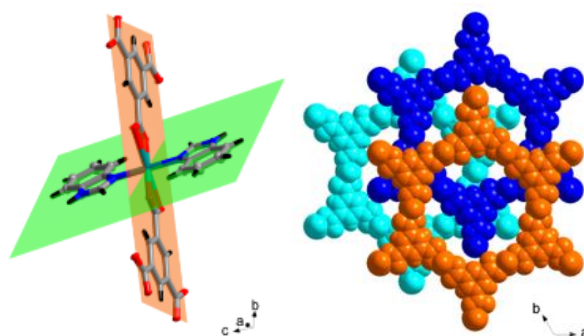


Fig. 17. (a) Intersection plane in $[\text{Cu}_3(\text{BTC})_2(\text{BIm})_6]$, **24** and (b) ABC-stacking of a hexagonal sheet of **24**.

$[(\text{CH}_3\text{CH}_2)_2\text{NH}_2][\text{Zn}(\text{BTC})_3(\text{BIm})].(\text{H}_2\text{O})$ **25**.

Compound **25** was synthesized similar to compound **24** by changing Zn ions and results in a three-dimensional network. The SCXRD analysis of **25** shows plate shape colorless crystal and crystallizes in the orthorhombic crystal system with a $P2_1/n$ space group. The asymmetric unit of **25** contains one zinc ion, one BTC, one BIm, one diethylamine and one lattice water molecule. The central metal Zn ions are coordinated by the three oxygen of the three BTC group and one with the nitrogen of BIm moiety. **25** shows the dielectric property.

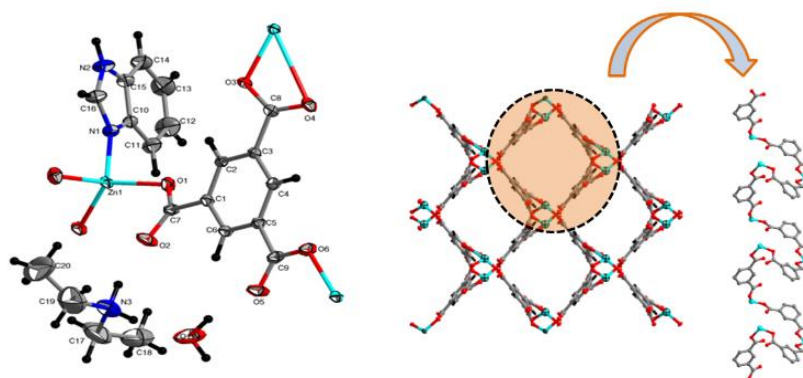


Fig. 18. (a) Asymmetric unit of $[(\text{CH}_3\text{CH}_2)_2\text{NH}_2][\text{Zn}(\text{BTC})_3(\text{BIm})].(\text{H}_2\text{O})$, **25**, where unique atoms are labeled (b) 3D packing of **25**.

References:

- (1) Natarajan, S.; Mandal, S. *Angew. Chem. Int. Ed.* **2008**, *47*, 4798.
- (2) Talin, A. A.; Centrone, A.; Ford, A. C.; Foster, M. E.; Stavila, V.; Haney, P.; Kinney, R. A.; Szalai, V.; El Gabaly, F.; Yoon, H. P.; Léonard, F.; Allendorf, M. D. *Science* **2014**, *343*, 66.
- (3) Francis, R. J.; Jacobson, A. J. *Angew. Chem. Int. Ed.* **2001**, *40*, 2879.

- (4) Murugavel, R.; Choudhury, A.; Walawalkar, M. G.; Pothiraja, R.; Rao, C. N. R. *Chem. Rev.* **2008**, *108*, 3549.
- (5) Choudhury, A.; Krishnamoorthy, J.; Rao, C. N. R. *Chem. Commun.* **2001**, 2610.
- (6) Pasha, I.; Choudhury, A.; Rao, C. N. R. *J. Solid State Chem.* **2003**, *174*, 386.
- (7) Jing, X.-M.; Tan, Y.-B.; Xiao, L.-W.; Liu, Y.-L. *Inorg. Chem. Commun.* **2015**, *57*, 75.
- (8) Papaefstathiou, G. S.; Subrahmanyam, K. S.; Armatas, G. S.; Malliakas, C. D.; Kanatzidis, M. G.; Manos, M. J. *CrystEngComm* **2014**, *16*, 3483.
- (9) Kong, F.; Sun, C.-F.; Yang, B.-P.; Mao, J.-G. *Second-order nonlinear optical materials based on metal iodates, selenites, and tellurites*; Springer GmbH: Berlin, Germany, 2012; Vol. 144.
- (10) Miras, H. N.; Woollins, J. D.; Slawin, A. M.; Raptis, R.; Baran, P.; Kabanos, T. *A. Dalton Trans.* **2003**, 3668.
- (11) Meyer, B. *Sulfur, energy, and environment*; Elsevier, 2013.
- (12) Tiwari, R. K.; Kumar, J.; Behera, J. N. *RSC Adv.* **2015**, *5*, 96034.
- (13) Tiwari, R. K.; Kumar, J.; Behera, J. N. *RSC Adv.* **2015**, *5*, 78389.
- (14) Tiwari, R. K.; Kumar, J.; Behera, J. N. *Chem. Commun.* **2016**, *52*, 1282.
- (15) Harrison, W. T. A.; Phillips, M. L. F.; Stanchfield, J.; Nenoff, T. M. *Angew. Chem., Int. Ed.* **2000**, *39*, 3808.
- (16) Harrison, W. T. A.; Phillips, M. L. F.; Nenoff, T. M. *J. Chem. Soc., Dalton Trans.* **2001**, 2459.
- (17) Tiwari, R. K.; Kumar, J.; Behera, J. N. *Dalton Trans.* **2017**, *46*, 15939.
- (18) Tiwari, R. K.; Behera, J. N. *Dalton Trans.* **2017**, *46*, 5911.

- (19) Hurd, J. A.; Vaidhyanathan, R.; Thangadurai, V.; Ratcliffe, C. I.; Moudrakovski, I. L.; Shimizu, G. K. H. *Nat. Chem.* **2009**, *1*, 705.

List of Schemes

1. Scheme Shape-selective catalysis diagram describing the three types of selectivity: reactant, product and transition state selectivity in the zeolite. 8
- 1.1

List of Figures

1. Figure An idealized framework structure of the cloverite mineral, with extra-large pore openings comprising of 20 [(Si/Al)O₄] units. 7
- 1.1
2. Figure Calculated lattice energies with density of silica structures. 9
- 1.2
3. Figure A perspective view of pentasils ZSM-5 structure with extra-large pore. 11
- 1.3
4. Figure The secondary building units (SBUs) found in the zeolitic framework of aluminosilicates framework family with the legend indicating the type of ring present in the unit. 12
- 1.4
5. Figure Perspective view of the AlPO₄ framework structure, VPI-5 (VFI) type zeolite with 18-membered ring. 16
- 1.5
6. Figure Polyhedral representation of the three-dimensional cobalt phosphate [C₂N₂H₁₀][Co₄(PO₄)₄].H₂O⁶⁵, showing the 8-membered channel along the *b*-axis. (Amine molecules are omitted for clarity). 18
- 1.6
7. Figure (a) A viewing direction of JU-98 along the *y*-axis, with 12-membered ring channels and occupies methyl-viologen, (b) UV/Vis spectrum of JU-98 with photochromic effect on a single 19
- 1.7

crystal of JU-98 and (c) Field-induced surface photovoltage spectra of JU98.

8. Figure 1.8 (a) 1D zinc sulfate chain along the *c*-axis and (b) Lattice diagram of (EMIm)₂[Zn(SO₄)₂]. 22
9. Figure 1.9 Polyhedral view of three-dimensional zinc sulfate comprising of ZnO₄ and SO₄ tetrahedra in [(CN₃H₆)₂][Zn(SO₄)₂], and the presence of 12-membered channels. 23
- 10 Figure 1.10 (a) The 3D structure of [Na(NpO₂)(SeO₄)(H₂O)] constructed by neptunyl (V) selenate ribbons with open channels along the *b*-axis direction filled by Na⁺ cations (blue balls) and H₂O molecules and (b) The depiction of an individual ribbon of corner-sharing green NpO₇ pentagonal bipyramids decorated by orange SeO₄ tetrahedra. 24
11. Figure 1.11 The inorganic layer of [La₂(SeO₄)₄]²⁻ in [La₂(SeO₄)₄(H₂O)₃][C₂N₂H₁₀]·H₂O, with the capping and bridging of the LaO₉ dimers by two selenate units, resulting in corner-shares 4-membered rings along the *a*-axis. 25
12. Figure 1.12 The layered structure of [C₂N₂H₁₀][CdCl₂(HSeO₃)₂], with 8-membered ring aperture. 27
13. Figure 1.13 Crystal lattice of 3D structure of [NaY(SeO₃)₂], where blue color indicate Y; green color show Se; yellow color indicate Na and red color for O. 28
14. Figure 1.14 Type 1 phase matching curve for NCS [NaY(SeO₃)₂]. 28

15. Figure Polyhedral view of sheets in the *ab*-plane of 30
 1.15 $(\text{C}_4\text{NH}_{12})_2[\text{Zn}_3(\text{HPO}_3)_4]$ showing the 24-membered ring
 channels present in this material.
16. Figure Polyhedral view of the three-dimensional 31
 1.16 $[\text{H}_6\text{PEHA}][(\text{GaOH})_9(\text{HPO}_3)_{12}](\text{NTHU-15})$ showing the 18-
 membered ring channels present in this material and (b) Gas
 sorption isotherms of NTHU-15 of H_2 , CO_2 (triangles), CH_4
 (squares), and N_2 (circles) for 15-PEHA, adsorption curves
 measured at 77 K.
17. Figure Structures of hypophosphite and formate ligands. 32
 1.17
18. Figure Polyhedral view of the three-dimensional of 32
 1.18 $[\text{Mn}(\text{H}_2\text{PO}_2)_2]_n \cdot (\text{DMF})_{0.11}$, and temperature dependent
 magnetic susceptibility.
19. Figure The coordination modes of carboxylate, when the linking units 33
 1.19 are changed from dicarboxylates to tricarboxylates, the
 topology of the ligand is also changed from a two-point-linker
 to a three-point-linker, hence, the different networks will be
 resulted.
20. Figure Crystal structure of 437-MOF, (a) Ball and stick model of 35
 1.20 BTTB ligands and (b) Viewing direction of the 3-D framework
 and the space-filling model showing regular 1D hexagonal
 channels.
21. Figure Transformation of a zinc oxalate dimer (a), to a linear chain 36
 1.21 (1D) structure (b), a pseudo two-dimensional structure with

	honeycomb apertures (c) and a 3-dimensional framework structure (d).	
22.	Figure 1.22 Pressure as a function of temperature and percentage fill of water in a sealed vessel.	38
23.	Figure 1.23 (a) A schematic of Teflon TM -lined, stainless autoclave typically used in the laboratory and (b) The external view of the autoclave used for the synthesis described in this thesis with Teflon inserts.	40
24.	Figure 1.24 Diffraction of X-Ray by crystals.	41
25.	Figure 1.25 TGA profile diagram.	43
26.	Figure 1.26 DSC Profile diagram.	43
27.	Figure 1.27 Schematic diagram of VSM.	45
28.	Figure 2.1 The schematic representation of the observed coordination modes for the sulfite anion, where X is the transition metal and/or alkali metal.	58
29.	Figure 2.2 (a) ORTEP diagram of compound 1 at 25% probability level where asymmetric unit atoms were labeled, (b) Formation of the 1D chain due to zinc sulfite coordination (part of the lattice is omitted for clarity) and (c) Interconnected Zn ₂ S ₂ dimeric units to generate 1D chain (the oxygen atom were ignored).	65

30. Figure (a) Crystal lattice of compound **1** as observed along the *c*-axis 66
 2.3 showing the interchain space where the $[\text{Zn}(\text{SO}_3)]_\infty$ chain in the space-filling model and (b) A layered structure as a result of H-bonding interaction (shown with fragmented bonds and hydrogen on carbon are omitted).
31. Figure (a) The molecular structure of compound **2** with unique atoms 68
 2.4 are labeled (ellipsoid probability is 25%), (b) Part of the crystal lattice of compound **2** viewed along *b*-axis (space fill model) compound **2** and (c) H-bonding pattern in compound **2**.
32. Figure (a) The molecular structure of compound **3** with unique atoms 70
 2.5 are labeled (ellipsoid probability is 25 %), (b) Part of the crystal lattice of compound **3** viewed along the *c*-axis (space fill model) compound **3** and (c) H-bonding pattern in compound **3**.
33. Figure (a) The molecular structure of compound **4** with unique atoms 72
 2.6 are labeled (ellipsoid probability is 25%), (b) Part of the crystal lattice of compound **4** viewed along the *c*-axis (space fill model) and (c) H-bonding pattern in compound **4**.
34. Figure Part of the crystal lattice of (a) compound **2** as viewed along the 74
 2.7 *b*-axis, (b) compound **3** as viewed along the *c*-axis and (c) compound **4** as viewed along the *c*-axis.
35. Figure An H-bonded 3D lattice of compounds (a) **2**, (b) **3** and (c) **4** 74
 2.8 (part of the lattice is omitted for clarity).
36. Figure The molecular structure of (a) compound **5** and (b) compound 77
 2.9 **6** at 25 % ellipsoid probability level (unique atoms are labeled);

View of 1D structure with interconnected ZnO_4 tetrahedron for compound **5** (c) and MnO_6 octahedron for compound **6** (d).

37. Figure 2.10 Part of the crystal lattice of (a) compound **5** and (b) compound **6** showing the positions and orientations of water and protonated piperazine molecules. 77
38. Figure 2.11 (a) H-bonded lattice of compound **5**, (b) water molecule-mediated H-bonding in the lattice as viewed close to the *b*-axis and (c) involvement of piperazine molecules in the lattice as shown with green color fragmented bonds (H-bonds are represented with fragmented bonds). 78
39. Figure 2.12 (a) H-bonding in compound **6** through piperazine molecules giving an H-bonded 2D structure in the *ac*-plane; (b) A water molecule-mediated H-bonding in the lattice and (c) H-bonded lattice highlighting the extension through water and piperazine H-bonding as represented with a different color rectangle. 79
40. Figure 2.13 The molecular unit of $[(\text{C}_3\text{N}_2\text{H}_{10})_2\text{NaCo}(\text{SO}_3)_2(\text{H}_2\text{O})_2]\cdot\text{H}_2\text{O}$, **7** where unique atoms are labeled. 81
41. Figure 2.14 (a) View of the two-dimensional layer of $[(\text{C}_3\text{N}_2\text{H}_{10})_2\text{NaCo}(\text{SO}_3)_2(\text{H}_2\text{O})_2]\cdot\text{H}_2\text{O}$, **7**, with H-bonding scheme (fragmented bonds) and (b) Interconnection of different layers *via* H-bonding as viewed along *c*-axis. Part of the crystal lattice has been omitted for clarity. 83
42. Figure 2.15 Interconnection of different layers *via* H-bonding through water molecules in the $[(\text{C}_3\text{N}_2\text{H}_{10})_2\text{NaCo}(\text{SO}_3)_2(\text{H}_2\text{O})_2]\cdot\text{H}_2\text{O}$, **7**. 84

43. Figure 2.16 Asymmetric unit of compound **8** where unique atoms are labeled. 86
44. Figure 2.17 (a) View of the layer in $[(C_6N_4H_{18})Zn_3(SO_3)_3]$, **8**, as viewed close to *b*-axis (green polyhedra represent the Zn3 ions and blue polyhedra represent Zn1 or Zn2 ions, respectively), (b) View of the crystal lattice along the *a*-axis showing the position of coordinated organic amines and (c) Coordination of sulfite anions in the crystal lattice of compound **8**. 87
45. Figure 2.18 (a) Interconnected sheets of honeycomb structure within a layer of $[(C_6N_4H_{18})Zn_3(SO_3)_3]$, **8**, composed of alternate Zn1 and Zn2 ions (b) Arrangement of two hexagonal sheet in the lattice and (c) Position of amine coordinated Zn3 ion in hexagonal space. 88
46. Figure 2.19 Molecular structure of $[C_2H_{10}N_2][Zn_3(SO_3)_4]$, **9** where unique atoms are labeled. 89
47. Figure 2.20 (a) Crystal lattice of $[C_2H_{10}N_2][Zn_3(SO_3)_4]$, **9** showing an infinite anionic layer as viewed close to *a*-axis and (b) The arrangement of Zn(II) ions in a triangular node having $[Zn_3S_2O_{12}]^{10-}$ fragment capped by two sulfite groups as highlighted in (a). 90
48. Figure 2.21 (a) A layer structure of $[C_2H_{10}N_2][Zn_3(SO_3)_4]$, **9** with embedded 4, 6 and 8-membered rings (MR); excluding the oxygen atoms (ignoring the intervening sulfite oxygen atoms). 91
49. Figure 2.22 Interconnection of a triangular node in compound **9** via H-bonding interaction shown with fragmented bonds (part of the 92

lattice is omitted and protonated ethylenediamine is shown with a different color for clarity).

50. Figure 2.23 Molecular unit of $[\text{CN}_3\text{H}_6]_2[\text{Zn}(\text{SO}_3)_2]$ **10**, where unique atoms are labeled. 93
51. Figure 2.24 (a) 12-membered ring with alternating ZnO_4 tetrahedra and SO_3 pyramids templated by guanidinium cation in $[\text{CN}_3\text{H}_6]_2[\text{Zn}(\text{SO}_3)_2]$, **10**, H-bonding are shown with fragmented bonds and (b) Adamantane topology adopted by four 12-membered rings in the lattice of compound **10**, the position of guanidinium cation in a tetrahedral arrangement is also highlighted with grey color; Part of the lattice has been omitted for clarity). 94
52. Figure 2.25 12-membered ring with Zn-S atoms in an adamantane topology in the compound **10**. 95
53. Figure 2.26 (a) A 3D-Crystal lattice of compound **10** with guanidinium cations at the center of 12-MR window and (b) helical assembly observed in compound **10** (guanidinium cations in (a) are represented with different color for better visualization). 96
54. Figure 2.27 Adsorption isotherms for N_2 on $[\text{CN}_3\text{H}_6]_2[\text{Zn}(\text{SO}_3)_2]$, **10**. 97
55. Figure 2.28 (a) DSC profile diagram of compound **10**. 97
56. Figure 2.29 (a) Dielectric constant profile of $[\text{CN}_3\text{H}_6]_2[\text{Zn}(\text{SO}_3)_2]$, **10** and (b) Dielectric constant (real part) vs. frequency profile of compound **10** at different temperatures. 98

57. Figure Thermogravimetric analysis for compounds **2-10**. 99
2.30
58. Figure Temperature-dependent PXRD pattern of $[\text{CN}_3\text{H}_6]_2[\text{Zn}(\text{SO}_3)_2]$, **10**. 102
2.31
59. Figure The PXRD pattern of the complex $[\text{C}_3\text{H}_{12}\text{N}_2][\text{Zn}(\text{SO}_3)_2]$, **2** 115
2.32 showing the phase purity of as-synthesized material.
60. Figure PXRD pattern for (a) $[\text{C}_4\text{H}_{14}\text{N}_2][\text{Zn}(\text{SO}_3)_2]$, **3**; (b) 115
2.33 $[\text{C}_6\text{H}_{18}\text{N}_2][\text{Zn}(\text{SO}_3)_2]$, **4**; (c) $[\text{C}_4\text{H}_{12}\text{N}_2][\text{Zn}(\text{SO}_3)_2]\cdot\text{H}_2\text{O}$, **5** and
(d) $[\text{C}_4\text{H}_{12}\text{N}_2][\text{Mn}(\text{SO}_3)_2(\text{H}_2\text{O})_2]\cdot 2\text{H}_2\text{O}$, **6**.
61. Figure PXRD pattern for (a) $[(\text{C}_3\text{N}_2\text{H}_{10})_2\text{NaCo}(\text{SO}_3)_2(\text{H}_2\text{O})_2]\cdot\text{H}_2\text{O}$, **7** 116
2.34 and (b) $[(\text{C}_6\text{N}_4\text{H}_{18})\text{Zn}_3(\text{SO}_3)_3]$, **8**.
62. Figure PXRD pattern for (a) $[\text{C}_2\text{H}_{10}\text{N}_2][\text{Zn}_3(\text{SO}_3)_4]$, **9** and (b) 116
2.35 $[\text{CN}_3\text{H}_6]_2[\text{Zn}(\text{SO}_3)_2]$, **10**.
63. Figure (a) Asymmetric unit of $[\text{Zn}_2(\text{SO}_3)_2(\text{C}_2\text{O}_4)_{0.5}(\text{C}_6\text{N}_2\text{H}_{13})]\cdot(\text{H}_2\text{O})_2$, **11** 128
3.1 **11** at 20% ellipsoidal probability where unique atoms were
labelled and (b) Part of 2D-crystal lattice of
 $[\text{Zn}_2(\text{SO}_3)_2(\text{C}_2\text{O}_4)_{0.5}(\text{C}_6\text{N}_2\text{H}_{13})]\cdot(\text{H}_2\text{O})_2$, **11** highlighting
 $[\text{Zn}(\text{SO}_3)]_\infty$ 1D chains (N atom is coming from mono
protonated DABCO cation has been partly removed for clarity).
64. Figure Bifurcated H-bonding interaction in 130
3.2 $[\text{Zn}_2(\text{SO}_3)_2(\text{C}_2\text{O}_4)_{0.5}(\text{C}_6\text{N}_2\text{H}_{13})]\cdot(\text{H}_2\text{O})_2$, **11**, through partially
protonated DABCO cations.
65. Figure (a) Asymmetric unit of 131
3.3 $[\text{C}_4\text{N}_2\text{H}_{12}]_{0.5}[\text{Zn}_2(\text{SO}_3)_2(\text{C}_2\text{O}_4)_{0.5}(\text{H}_2\text{O})_2]$, **12** at 25% ellipsoidal
probability (unique atoms were labelled; disordered piperazine

- is also shown), (b) Part of the 3D-crystal lattice of $[\text{C}_4\text{N}_2\text{H}_{12}]_{0.5}[\text{Zn}_2(\text{SO}_3)_2(\text{C}_2\text{O}_4)_{0.5}(\text{H}_2\text{O})_2]$, **12** as viewed along the *c*-axis and (c) Formation of $[\text{Zn}(\text{SO}_3)]_\infty$ chain along the *c*-axis which is highlighted in 'b' (as viewed close to the *b*-axis).
66. Figure 3D-Crystal lattice of $[\text{C}_4\text{N}_2\text{H}_{12}]_{0.5}[\text{Zn}_2(\text{SO}_3)_2(\text{C}_2\text{O}_4)_{0.5}(\text{H}_2\text{O})_2]$, **12**, showing interconnection of Zn_2S_2 chains (excluding the intervening O atoms) running along *c*-axis (a) *via* Zn-sulfite coordination and (b) *via* Zn-oxalate coordination (H-bonding through aqua ligand is also shown with fragmented bonds along crystallographic position of disordered protonated piperazine cation). 133
67. Figure H-bonding interaction in case of $[\text{C}_4\text{N}_2\text{H}_{12}]_{0.5}[\text{Zn}_2(\text{SO}_3)_2(\text{C}_2\text{O}_4)_{0.5}(\text{H}_2\text{O})_2]$, **12** between protonated piperazine and oxalate oxygen atoms (black fragmented bonds), 12-membered rings are also visible. 134
68. Figure The asymmetric unit of $[\text{C}_4\text{N}_2\text{H}_{12}][\text{Cd}_2(\text{SO}_3)_2(\text{C}_2\text{O}_4)(\text{H}_2\text{O})].(\text{H}_2\text{O})]$, **13** with 15% ellipsoidal probability. 135
69. Figure (a) Part of crystal lattice of the $[\text{C}_4\text{N}_2\text{H}_{12}][\text{Cd}_2(\text{SO}_3)_2(\text{C}_2\text{O}_4)(\text{H}_2\text{O})].\text{H}_2\text{O}$, **13** as viewed close to *a*-axis, (b) The layered structure in case of compound **13** in the *ab*-plane and (c) Embedded 1D channel along the *a*-axis having 8 and 4-membered rings within the layers (The oxygen atoms have been omitted for clarity, S = yellow, Cd = green, N = blue and C = grey). 136

70. Figure (a) Four sets of $\text{CdO}_{6/7}$ polyhedrons for the construction of 1D channel as a result of sulfite and oxalate coordination in compound **13** and (b) Part of the 1D channel highlighted in ‘a’ shows formation of ribbon structure in compound **13**. 137
3.8
71. Figure H-bonding pattern in $[\text{C}_4\text{N}_2\text{H}_{12}][\text{Cd}_2(\text{SO}_3)_2(\text{C}_2\text{O}_4)(\text{H}_2\text{O})]\cdot\text{H}_2\text{O}$, **13**. 138
3.9
72. Figure The Molecular unit of $[\text{Na}_2\text{Mn}_2(\text{C}_2\text{O}_4)(\text{SO}_3)_2(\text{H}_2\text{O})_2]$, **14** with 25% ellipsoidal probability (unique atoms were labeled). 140
3.10
73. Figure (a) MnSO_3 layer of $[\text{Na}_2\text{Mn}_2(\text{C}_2\text{O}_4)(\text{SO}_3)_2(\text{H}_2\text{O})_2]$, **14**, in the bc -plane, (b) the arrangement of Mn-oxalate chain along a -axis (c) 3D honeycomb structure of compound **14** and (d) Na-oxalate chain along c -axis $[\text{Na}_2\text{Mn}_2(\text{C}_2\text{O}_4)(\text{SO}_3)_2(\text{H}_2\text{O})_2]$, **14**. 141
3.11
74. Figure Na oxalate chain along the c -axis in $[\text{Na}_2\text{Mn}_2(\text{C}_2\text{O}_4)(\text{SO}_3)_2(\text{H}_2\text{O})_2]$, **14**. 142
3.12
75. Figure (a) The crystal lattice of $[\text{Na}_2\text{Mn}_2(\text{C}_2\text{O}_4)(\text{SO}_3)_2(\text{H}_2\text{O})_2]$, **14** showing an infinite anionic 3D network and (b) H-bonding pattern in compound **14** (Na is omitted for the clarity). 142
3.13
76. Figure (a) Temperature dependence graph of magnetic susceptibility and inverse susceptibility of compound **14** at 1000 Oe, (b) Temperature dependent $\chi_m T$ plot of compound **14** and (c) M-H cycle of compound **14** at 5 K. 143
3.14
77. Figure The asymmetric unit of $[\text{NaEu}(\text{C}_2\text{O}_4)(\text{SO}_3)(\text{H}_2\text{O})_3]$, **15** with 45% ellipsoidal probability (the unique atoms are labeled). 144
3.15

78. Figure 3.16 Distorted octahedral geometry of Na ion in $[\text{NaEu}(\text{C}_2\text{O}_4)(\text{SO}_3)(\text{H}_2\text{O})_3]$, **15**. 145
79. Figure 3.17 (a) 1D Europium-sulfite chain in $[\text{NaEu}(\text{C}_2\text{O}_4)(\text{SO}_3)(\text{H}_2\text{O})_3]$, **15** with 4-membered rings window, (b) Eu-oxalate honeycomb structure in compound **15**, (c and d) Aqua bridge Na-oxalate 3D network, (e) The 3D crystal lattice of compound **15**, and (f) The honeycomb structure of compound **15** where the aqua bridge Na ions are omitted. 146
80. Figure 3.18 (a) H-bonding pattern of $[\text{NaEu}(\text{C}_2\text{O}_4)(\text{SO}_3)(\text{H}_2\text{O})_3]$, **15** and (b) H-bonding pattern of $[\text{NaEu}(\text{C}_2\text{O}_4)(\text{SO}_3)(\text{H}_2\text{O})_3]$, **15** where Na ions are deleted for clarity. 147
81. Figure 3.19 Photoluminescence emission spectrum of $[\text{NaEu}(\text{C}_2\text{O}_4)(\text{SO}_3)(\text{H}_2\text{O})_3]$, **15** at room temperature. 148
82. Figure 3.20 TGA profile diagram for compounds **11-15**. 149
83. Figure 3.21 DSC spectra of compounds **11-15**. 151
84. Figure 3.22 PXRD pattern for (a) $[\text{Zn}_2(\text{SO}_3)_2(\text{C}_2\text{O}_4)_{0.5}(\text{C}_6\text{N}_2\text{H}_{13})] \cdot (\text{H}_2\text{O})_2$, **11**, (b) $[\text{C}_4\text{N}_2\text{H}_{12}]_{0.5}[\text{Zn}_2(\text{SO}_3)_2(\text{C}_2\text{O}_4)_{0.5}(\text{H}_2\text{O})_2]$, **12** and (c) $[\text{C}_4\text{N}_2\text{H}_{12}][\text{Cd}_2(\text{SO}_3)_2(\text{C}_2\text{O}_4)(\text{H}_2\text{O})] \cdot (\text{H}_2\text{O})$ **13**. 160
85. Figure 3.23 PXRD pattern for (a) $[\text{Na}_2\text{Mn}_2(\text{C}_2\text{O}_4)(\text{SO}_3)_2(\text{H}_2\text{O})_2]$, **14** and (b) $[\text{NaEu}(\text{C}_2\text{O}_4)(\text{SO}_3)(\text{H}_2\text{O})_3]$, **15**. 160
86. Figure 4.1 Coordination mode of THBTS^{3-} ligand with metals. 167

87. Figure (a) Asymmetric unit of compound **16** with ellipsoidal probability 15% and unique atoms are labelled and (b) H-Bonded helix structure of ligands and water molecules. 172
- 4.2
88. Figure (a and b) H-bonding pattern between (THBTS)³⁻ ligand water and melamine units. 174
- 4.3
89. Figure (a) Molecular Structure of [Na₂(C₆H₃O₃S₃)(CN₃H₆)(H₂O)].(H₂O), **17**, (b) Coordination mode of (THBTS)³⁻ ligand with surrounding Na ions and (c) A non-planar tetrahedral arrangement of (THBTS)³⁻ ligand in compound **17**. 175
- 4.4
90. Figure (a) A single layer of [Na₂(C₆H₃O₃S₃)(CN₃H₆)(H₂O)].(H₂O), **17**, (b) Infinite Na- sulfonate chain running along the *b*-axis, (c) H-bonding pattern in [Na₂(C₆H₃O₃S₃)(CN₃H₆)(H₂O)].(H₂O), **17**, (d) H-bonding between (THBTS)³⁻ ligand, water and guanidinium and (e) Arrangement of guanidinium and water molecule. 176
- 4.5
91. Figure (a) Asymmetric unit of [K₃(C₆H₃O₉S₃)(H₂O)₃], **18**, (b) Lattice diagram of [K₃(C₆H₃O₉S₃)(H₂O)₃], **18**, (c) A water channel in [K₃(C₆H₃O₉S₃)(H₂O)₃], **18** where potassium ions are omitted and (d) Coordination mode of potassium and (THBTS)³⁻ ligands along *a*-axis where K1 ions are blue and K2 ions in turquoise color. 178
- 4.6
92. Figure (a) K2 chain in compound **18** running parallel to K1 chain, (b) K1 chain in compound **18** and (c) Potassium ions at equilateral triangle position in the compound **18**. 180
- 4.7

93. Figure 4.8 H-bonding pattern in $[\text{K}_3(\text{C}_6\text{H}_3\text{O}_9\text{S}_3)(\text{H}_2\text{O})_3]$, **18**. 181
94. Figure 4.9 (a) Asymmetric unit of $[\text{C}_4\text{N}_2\text{H}_{13}]_2[\text{Cd}_2(\text{C}_6\text{H}_3\text{O}_3\text{S}_3)(\text{H}_2\text{O})_2].(\text{H}_2\text{O})$, **19**, where unique atoms are labeled, (b) Lattice diagram of $[\text{C}_4\text{N}_2\text{H}_{13}]_2[\text{Cd}_2(\text{C}_6\text{H}_3\text{O}_3\text{S}_3)(\text{H}_2\text{O})_2].(\text{H}_2\text{O})$, **19** and (c) Cd chain running along *c*-axis in $[\text{C}_4\text{N}_2\text{H}_{13}]_2[\text{Cd}_2(\text{C}_6\text{H}_3\text{O}_3\text{S}_3)(\text{H}_2\text{O})_2].(\text{H}_2\text{O})$, **19**. 182
95. Figure 4.10 (a and b) H-bonding pattern in $[\text{C}_4\text{N}_2\text{H}_{13}]_2[\text{Cd}_2(\text{C}_6\text{H}_3\text{O}_3\text{S}_3)(\text{H}_2\text{O})_2].(\text{H}_2\text{O})$, **19** from different viewing direction(in case of (a) DABCO units are omitted). 184
96. Figure 4.11 TGA Profile diagram for compounds **16-19**. 185
97. Figure 4.12 PXRD pattern of the compounds (a) $[(\text{C}_3\text{N}_6\text{H}_6)(\text{C}_3\text{N}_6\text{H}_7)_3(\text{C}_6\text{H}_3\text{O}_9\text{S}_3).(\text{H}_2\text{O})_4]$, **16**, (b) $[\text{Na}_2(\text{C}_6\text{H}_3\text{O}_3\text{S}_3)(\text{CN}_3\text{H}_6)(\text{H}_2\text{O})](\text{H}_2\text{O})$, **17**, (c) $[\text{K}_3(\text{C}_6\text{H}_3\text{O}_9\text{S}_3)(\text{H}_2\text{O})_3]$, **18** and (d) $[\text{C}_4\text{N}_2\text{H}_{13}]_2[\text{Cd}_2(\text{C}_6\text{H}_3\text{O}_3\text{S}_3)(\text{H}_2\text{O})_2].(\text{H}_2\text{O})$, **19** showing the phase purity of as-synthesized material. 191
98. Figure 5.1 (a) Asymmetric unit of $[\text{Co}_6(\text{formate})_6(\text{BTC})_6(\text{Im})_6]$, **20** with 35% ellipsoidal probability where unique atoms are labeled, (b) A hexagonal cluster of Co(II) ions, (c) A layer structure of compound **20** viewing along the *c*-axis and Co(II) ions were shown by space filling and (d) Lattice packing diagram of compound **20**. 203

99. Figure (a) Crystal lattice of $[\text{Co}_6(\text{formate})_6(\text{BTC})_6(\text{Im})_6]$, **20**, with 204
 5.2 Co(II) ions are in hexagonal arrangement and (b) ABC-stacking
 of layers in $[\text{Co}_6(\text{formate})_6(\text{BTC})_6(\text{Im})_6]$, **20**, in the *ab*-plane.
100. Figure (a) Temperature dependence graph of the magnetic 205
 5.3 susceptibility and χ^{-1} of compound **20** at external magnetic field
 100 Oe, (b) Temperature dependent $\chi_M T$ curve of compound **20**
 and (c) field dependent magnetization of compound **20** at 2, 5,
 10, 20, 40, 80 and 300 K.
101. Figure (a) Asymmetric unit of $[(\text{CH}_3)_2\text{NH}_2][\text{Cu}(\text{BTC})(\text{Im})]$, **21**, where 207
 5.4 unique atoms are labeled, (b) crystal lattice view of a layered
 structure of $[(\text{CH}_3)_2\text{NH}_2][\text{Cu}(\text{BTC})(\text{Im})]$ with 8 and 4-
 membered rings and (c) A wave-like arrangement of
 $[(\text{CH}_3)_2\text{NH}_2][\text{Cu}(\text{BTC})(\text{Im})]$ layer in the *bc*- plane.
102. Figure (a) Lattice packing of two layers $[(\text{CH}_3)_2\text{NH}_2][\text{Cu}(\text{BTC})(\text{Im})]$, 208
 5.5 **21** and (b) The Cu-BTC layer in $[(\text{CH}_3)_2\text{NH}_2][\text{Cu}(\text{BTC})(\text{Im})]$,
21, where Im unit omitted.
103. Figure The asymmetric unit of $[\text{Zn}_2(\text{HBTC})_2((\text{Im})(\text{H}_2\text{O}))]$, **22**, with 209
 5.6 20% ellipsoidal probability, where unique atoms are labeled.
104. Figure (a) One dimensional ribbon running along *a*-axis in 210
 5.7 $[\text{Zn}_2(\text{HBTC})_2((\text{Im})(\text{H}_2\text{O}))]$, **22**, (b) Crystal lattice of compound
22 viewing along *a*-axis, (c) Coordination mode of Zn(II) ions
 in compound **22**, and (d) A pi-pi interactions between two BTC
 units to provide extra stability.
105. Figure H-bonding pattern in compound **22** along *a*-axis between the 212
 5.8 imine NH, carboxylate oxygen and aqua ligands.

106. Figure (a) The asymmetric unit of $[\text{Co}_4(\text{BTC})_3(\text{BIm})_6][\text{solvent}]$, **23**, as 214
5.9 ORTEP diagram with 15% probability level where unique atoms are labeled, (b) Part of the 3D-crystal lattice of compound **23**, (c) Interconnection of paddlewheel units along the *c*-axis and (d) Embedded helical assemblies running along the *b*-axis as a result of tetrahedrally coordinated Co^{+2} ions, interconnection of such assemblies through paddlewheel type of structure along the *a*-axis.
107. Figure (a and b) H bonding interaction between BIm NH group and 215
5.10 carboxylate oxygen atoms.
108. Figure (a) Asymmetric unit of $[\text{Cu}_3(\text{BTC})_2(\text{BIm})_6][\text{solvent}]$, **24** at 15% 217
5.11 probability level where unique atoms are labelled, (b) A hexagonal 12-membered rings in compound **24**, (c) A bronze hexagonal sheet like structure in the lattice of compound **24**, (d) Intersection of BTC and BIm plane in compound **24**, (e) ABC-type stacking of layers in the crystal lattice and (f) H-bonding between -NH of BIm and carboxylate of BTC unit.
109. Figure (a) Asymmetric unit of 219
5.12 $[(\text{CH}_3\text{CH}_2)_2\text{NH}_2][\text{Zn}(\text{BTC})(\text{BIm})].(\text{H}_2\text{O})$, **25**, as ORTEP diagram at 25% probability level, (b) Part of the crystal lattice of compound **25** (as viewed along the *b*-axis) where diethyl ammonium cations are shown in green color and (c) Embedded helical assembly in compound **25** as highlighted in 'b'.
110. Figure A six-membered ring of Zn(II) ions and BTC unit in the 3D 220
5.13 packing of $[(\text{CH}_3\text{CH}_2)_2\text{NH}_2][\text{Zn}(\text{BTC})(\text{BIm})].(\text{H}_2\text{O})$, **25**.

111.	Figure	Dielectric profile diagrams of compound 25 (a) Temperature dependent dielectric constant at various frequency, (b) Dielectric constant vs frequency at different temperature and (c) Frequency dependent real part of impedance graph.	221
	5.14		
112.	Figure	TGA profile diagram of compounds 20-25 .	222
	5.15		
113.	Figure	PXRD pattern for (a) $[\text{Co}_6(\text{formate})_6(\text{BTC})_6(\text{Im})_6]$, 20 , (b) $[(\text{CH}_3)_2\text{NH}_2][\text{Cu}(\text{BTC})(\text{Im})]$, 21 , (c) $[\text{Zn}_2(\text{HBTC})_2((\text{Im})(\text{H}_2\text{O}))]$, 22 , (d) $[\text{Co}_4(\text{BTC})_3(\text{BIm})_6][\text{solvent}]$, 23 , (e) $[\text{Cu}_3(\text{BTC})_2(\text{BIm})_6][\text{solvent}]$, 24 and (f) $[(\text{CH}_3\text{CH}_2)_2\text{NH}_2][\text{Zn}(\text{BTC})(\text{BIm})].(\text{H}_2\text{O})$, 25 .	232
	5.16		

List of Tables

1.	Table	Milestone in zeolite preparation and application	5
	1.1		
2.	Table	Information obtained from powder X-ray diffraction	41
	1.2		
3.	Table	Synthetic conditions and molar ratios for the preparation of compounds 1-10	61
	2.1		
4.	Table	Crystal structure refinement parameters for compounds 1-10	107
	2.2		
5.	Table	Complete list of bond lengths [\AA] and bond angles [$^\circ$] for compounds 1-10	110
	2.3		
6.	Table	Hydrogen bonding table for compounds 1-10	113
	2.4		

7.	Table	Synthetic conditions and molar ratios for the preparation of 11-15	125
	3.1		
8.	Table	Crystal structure refinement parameters for compounds 11-15	155
	3.2		
9.	Table	Selected bond lengths for compounds 11-15	157
	3.3		
10.	Table	Hydrogen bonding table for compounds 11-15	158
	3.4		
11.	Table	Crystallographic table of compounds 16-19	189
	4.1		
12.	Table	Selected bond length tables for compounds 16-19	190
	4.2		
13.	Table	Synthetic conditions and molar ratios for the preparation of compounds 20-25	201
	5.1		
14.	Table	Crystallographic structure refinement parameter tables for compounds 20-25	228
	5.2		
15.	Table	Selected bond length tables of compounds 20-25	229
	5.3		
16.	Table	Hydrogen bonding table for compounds 20-25	231
	5.4		

List of Abbreviations

PBUs	Primary building units
SBU _s	Secondary building units
AlPO ₄ _s	Aluminophosphates
AlSiO ₄ _s	Aluminosilicates
DACH	Diamino cyclohexane
SDA	Structure directing agent
SHG	Second harmonic generation
PIP	piperzine
EN	ethylenediamine
DABCO	1, 4-diaza bicycle [2, 2, 2] octane
DMF	dimethylformamide
DEF	diethylformamide
TGA	Thermogravmetric analysis
PXRD	Powder X-ray diffraction
SCXRD	Single crystal X-ray diffraction
FTIR	Fourier transform infrared
HCO ₂ ⁻	formate
CCD	Cambridge crystallographic data
DAP	1, 3-Diaminopropane
GC	Guanidine carbonate
Gu	Guanidinium
TAEA	<i>tris</i> -(2-aminoethyl) amine

HMDA	hexamethylenediamine
DAB	1, 4-Diaminobutane
BVS	Bond valance sum
RH	Relative humidity
AC	Alternating Current
3D	Three-dimensional
2D	Two-dimensional
1D	One-dimensional
ZFC	Zero field-cooled
FC	Field-cooled
ILs	Ionic liquids
TMOs	Transition metal oxides
CPs	Conducting polymers
PA	<i>n</i> -propylamine
THBTS	Trihydroxy-benzene-trisulfonate
BTC	1, 3, 5-Benzenetricarboxylic acid
BDC	1, 4-Benzenedicarboxylic acid
Im	Imidazole
BIm	Benzimidazole
COF	Covalent Organic Framework
MOF	Metal Organic Framework
OAc	acetate
equiv.	Equivalents
h	hours

min

minutes

UV

Ultraviolet

Chapter 1

OPEN-FRAMEWORK AND HYBRID MATERIALS - A BRIEF OVERVIEW

1.1. Introduction	3
1.2. Development of molecular sieves	3
1.2.1. Framework density	6
1.2.2. Applications of Zeolites	7
1.2.3. Solvothermal synthesis of zeolite	9
1.2.4. Open-framework/zeolite building blocks	11
1.2.5. Metal organic frameworks/ zeolite secondary building units (SBU's)	12
1.3. Templating in the construction of microporous materials	13
1.3.1. Types of templates	13
1.3.2. Role of templating	14
1.4. Open-framework metal phosphates	15
1.4.1. Aluminophosphates	15
1.4.2. Other metal phosphates	17
1.4.2.1. Cobalt phosphate open-framework	17
1.4.2.2. Zinc phosphate open-framework	18
1.5. Metal sulfates, selenates, selenites, phosphite, hypophosphite open-framework	20
1.5.1. Metal sulfates open-framework	20
1.5.1.1. 1D Zinc sulfate open-framework (EMIm) ₂ [Zn(SO ₄) ₂]	21
1.5.1.2. 3D Zinc sulfate network [(CN ₃ H ₆) ₂][Zn(SO ₄) ₂]	22
1.5.2. Metal selenates open-framework	23
1.5.2.1. Neptunium selenate open-framework [Na(NpO ₂)(SeO ₄)(H ₂ O)]	24

1.5.2.2. Lanthanum based selenate framework [La ₂ (SeO ₄) ₄ (H ₂ O) ₃] [C ₂ N ₂ H ₁₀]·H ₂ O	25
1.5.3. Metal selenite open-framework	26
1.5.3.1. 2D cadmium selenite open-framework [C ₂ N ₂ H ₁₀][CdCl ₂ (HSeO ₃) ₂]	26
1.5.3.2. 3D mixed metal selenite open-framework [NaY(SeO ₃) ₂]	27
1.5.4. Metal phosphites open-framework	29
1.5.4.1. Zinc phosphite open-framework (C ₄ NH ₁₂) ₂ [Zn ₃ (HPO ₃) ₄]	29
1.5.4.2. Gallium phosphite open-framework (NTHU-15)	30
1.5.5 Metal hypophosphite open-framework	31
1.5.5.1. Manganese hypophosphite open-framework	32
1.6. Metal carboxylates Frameworks	33
1.6.1. Carboxylate Ligands	33
1.6.2. Metal carboxylates frameworks	34
1.6.3. Hierarchy of structures in open-framework metal carboxylates	35
1.7. Synthesis and characterization techniques of open-framework inorganic structures	37
1.7.1 Materials characterizations	40
1.7.1.1 X-Ray diffraction	40
1.7.1.2. Thermal analysis	42
1.7.1.3. Gas adsorption study	44
1.7.1.4. Vibrating sample magnetometry (VSM)	44
1.7.1.5. Fourier transfer infra-red spectroscopy	45
1.8. References	46

1.1. Introduction:

Solid state chemistry is interesting in the field of science, engineering, and applications. It includes the synthesis of inorganic, organic, and organometallic solid materials with open architecture with novel structures, physical/ chemical properties. Their application is well studied in the field of drug delivery^{1,2}, gas sorption³⁻⁵ and separation⁶⁻⁸, catalysis⁹⁻¹¹, magnetism¹²⁻¹⁵, proton conduction^{16,17} and electrical conductors¹⁸⁻²⁰. Today's, researcher main effort is in designing or fabrication of an organic, inorganic and/or organometallic small molecule. These smaller units can be self-assembled to a larger framework to function as a single entity to achieve predefined properties that can be explored for defined applications.

The self-assembled large framework materials are interesting to both researcher and engineers for a large number of voids/ pores with a rigid framework. These porous materials are classified based on the pore size; microporous (2 nm), mesoporous (2-50 nm) and macroporous (larger than 50 nm). Inorganic open-frameworks with micropores (pore size ranging from 0.5 nm to 2 nm) are termed as molecular sieves. Molecular sieves, in the field of gas absorption, catalysis, magnetic and electrical applications have attracted immense research interest.

In this chapter; a brief history of molecular sieves developments, their classifications, synthesis, and applications are discussed.

1.2. Development of molecular sieves:

Zeolites are the first known molecular sieves and are discovered by the Swedish mineralogist Axel F. Cronstedt in 1756^{21,22}. Zeolite also is known as hydrated

aluminosilicates with an ordered framework. The ordered structure possesses a large number of micro-pores where water molecule is trapped. Heating the zeolite at high temperature liberates the water vapors and hence termed as 'zeolite' that is derived from the Greek words "zeo" and "lithos" means "to boil" and "stone" respectively. Zeolites have the ability to absorb reversibly both liquids as well as gas without losing the framework structures²³⁻²⁶.

The further development of this porous solid concept is carried forward by the J. W. Mc Bain²⁷. He has reported the molecular absorption and desorption by chabazite a natural mineral with a pore size of 0.5 nm²⁸. Till date, around 40 naturally occurring zeolite has been discovered. Synthetic Zeolites were introduced in the early 1940s, by Barrer and Milton^{29,30}. The field of synthetic zeolites and their applications is expanding rapidly and approximately 133 zeolites have been synthesized in the laboratory.

Zeolite structures are described with a 3-capital letter code (International Zeolite Association (IZA)). For example; Zeolite faujasite is described by FAU-x, FAU stands for faujasite and x is a number of rings. The 5th edition of the *Atlas of Zeolite Framework Types* published by IZA describes 133 zeolites structures³¹. The theoretical calculations predicted the thermodynamic stability of others zeolites is possible³². These mathematical modelling works have motivated other researchers in this field for research and development of another zeolite system that can be targeted for specific applications³³. The progress in the field of zeolite research, developments and their applications are recorded in Table 1.1.

Table 1.1 Milestone in zeolite preparation and application

Mid 1930s-1940s	Pioneering work of Barrer in adsorption and synthesis
1949-1954:	Discovery and synthesis of zeolites A, X, Y (Milton-Breck)
1954:	Commercialization of zeolites A, X, Y (Union Carbide). Applications in <ul style="list-style-type: none"> ● drying, n-iso/-alkane separation (Union Carbide, 1959) ● catalysis: isomerization on Y (Union Carbide, 1959), cracking on X and Y (Mobil, 1962) ● ion exchange: detergents, A zeolites instead of phosphates (Hankel, 1974)
1967-1969:	Synthesis of high silica zeolites MFI and BEA (mobil) Applications of MFI in shape selective process Xylene isomerization and production (1974)
1980s:	Secondary synthesis (dealumination, isomorphous substitution)
1982-1986:	Synthesis of aluminophosphates, SAPO, MeAPO, (Union Carbide) Application in Isodewaxing (SAPO 11, Chevron, 1997) Methanol to olefins (SAPO 34, UOP-Norsk Hydro)
1983:	Synthesis of titanium silicates TSI (Enichem) Application in phenol hydroxylation (1986)
1992:	MCM 41 mesoporous molecular sieves (Mobil)
1994, 1998:	Nanocrystalline zeolites, delamination (Corma)

Zeolites are aluminosilicates and consisted of $[\text{SiO}_4]^{4-}$ and $[\text{AlO}_4]^{5-}$ tetrahedra framework interconnected through corner sharing O atoms. The O-(Si/Al)-O angle is nearly 109° i.e. tetrahedral. But Si-O-(Si/Al) bond angles can vary over wide range $\sim 125^\circ$ to $\sim 180^\circ$ between two connecting tetrahedral. If the centre of all tetrahedron is only Si^{4+} , the overall structure is electronically neutral. However, in aluminosilicates; Al^{3+} substitute some of the Si^{4+} , resulting in the negatively charged framework. This developed negative charge is balanced by other metal ions (Na^+ , Mg^{2+} , Ca^{2+} , K^+) or organic cations at the interstitials

sites forming an extra-framework featuring pores. Empirically, zeolites are represented by $M_{y/n}[(1-y)SiO_2 \cdot yAlO_2] \cdot xH_2O$.

The novel microstructure of zeolites is due to the micro-porosity resulted from the rigid corner sharing SiO_2/AlO_2 -tetrahedra. In the framework, the amount of Al ions can be varied. The absent of aluminium in the framework results in completely silicious polymorphs of silica. However, the limit of $Si/Al = 1$ in the framework is not possible. The electrostatic repulsion between negative charges arises from adjacent AlO_4^- leads to the collapse of the structural framework³⁴.

1.2.1. Framework density:

The zeolites and zeolite-derivative materials are differentiated on the basis of framework density. Framework density is the number of tetrahedra per 1000 \AA^3 . For the ideal porous aluminosilicates, the number of the tetrahedral unit is ~ 21 . Lower framework density than 21 have a higher open structure and vice-versa. For example, the condensed silicate structures like. α -quartz, cristobalite, and tridymite have framework density of ~ 20 . Generally, in zeolites, the framework density value ranges from 12-19. However, in certain zeolite such as Cloverite, a gallophosphate, have a 20-membered ring system, that has a density value of 11.1 (Fig. 1.1)³⁵.

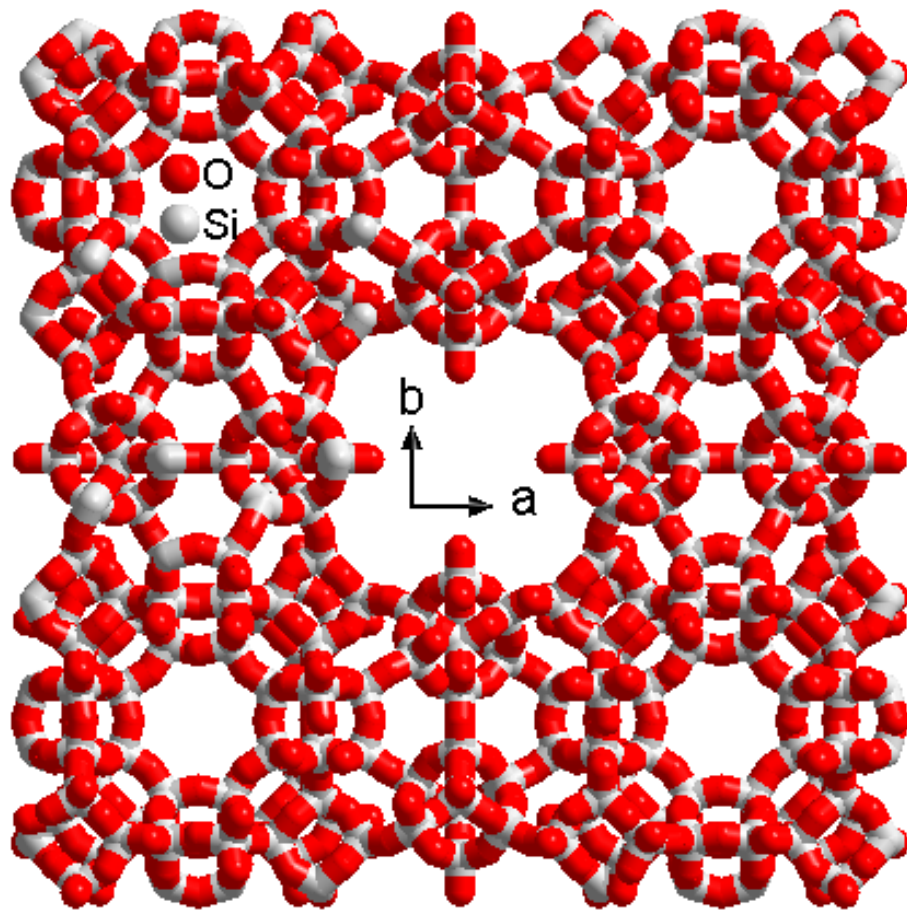


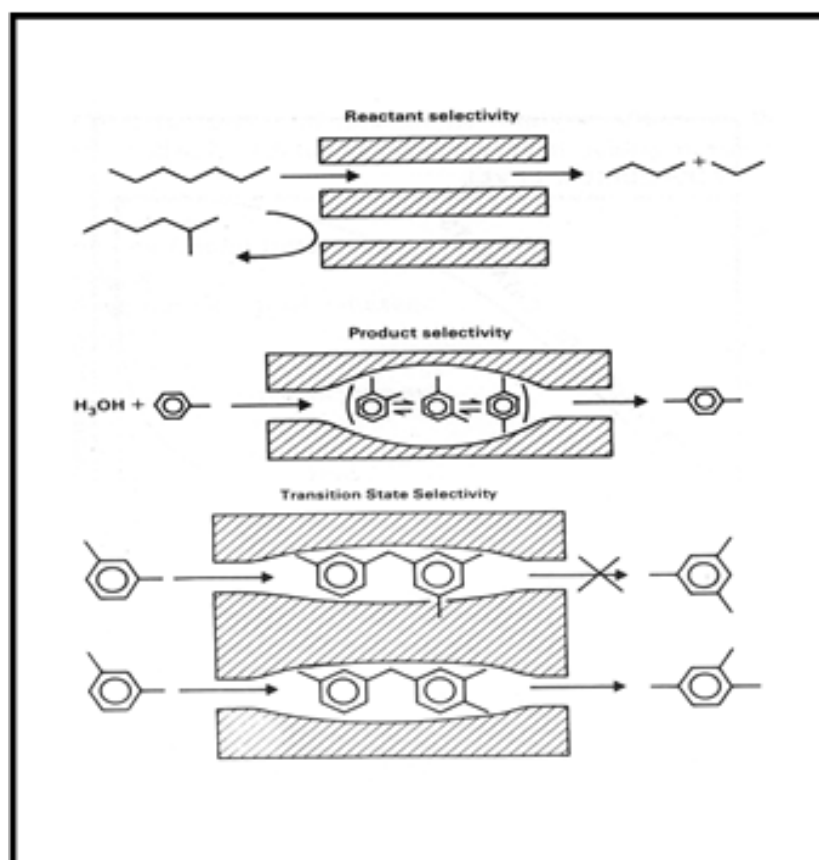
Fig. 1.1. An idealized framework structure of the cloverite mineral, with extra-large pore openings comprising of 20 [(Si/Al)O₄] units.

1.2.2. Applications of Zeolites:

One of the major application of zeolite is in the field of ion exchange. The interstitial inorganic or organic cations are loosely connected with oxygen atoms and are easily exchangeable. This easily exchangeable ion makes it a strong candidate in the applications of water purifications, gas purifications, gas sensing etc. The other major application includes catalysis in industrial chemical synthesis. The catalyst depends upon two factors; (a) accessibility of catalytically active centers to reactants, and (b) the shape and size of the penetrant molecules. The catalytic active centers can be manipulated by altering the framework electric charge by manipulating tetrahedral Si⁴⁺ ions and Al³⁺ ions ratio.

In the zeolite framework; when Si^{4+} is substituted by an Al^{3+} , resulted in a negative charge at the center promoting a weak Lewis acid^{36,37} or the charge imbalance is compensated by an OH^- ions instead of oxygen at the corner. This OH^- acts as a strong Brønsted acid. The zeolites are also utilized as a shape-selective catalyst which depends upon the zeolites shape and cavity size and provides the direction to the selective type of reaction³⁸.

Shape selectivity works by the selectivity of reactant, product and also transition-state shape selectivity. This selectivity in chemical reactions is outlined below (scheme 1.1)³⁸. The shape selective catalysis has been used in the case of hydrocarbon cracking as a catalyst for gasoline synthesis. The shape selectivity of zeolites has also been used in the isomerization-polymerization of p-xylene for mass-production of polyester³⁹.



Scheme 1.1. Shape-selective catalysis diagram describing the three types of selectivity: reactant, product and transition state selectivity in the zeolite.

1.2.3. Solvothermal synthesis of zeolite:

The molecular sieves are thermodynamically metastable phase owing to highly dense negatively charged oxygen atom. The calculated lattice energies of the framework structures decrease with the framework density (Fig. 1.2). The hypothetical and experimental calorimetric information supports that zeolites are 8-20 kJmol⁻¹ less stable than quartz⁴⁰⁻⁴³.

Hence, in the development of zeolite kinetics played an extensive role in determining the phase formation. The arrangement of framework relies upon Si/Al stoichiometric, nature of solvents and synthetic conditions. The preparation of zeolitic materials complies Ostwald's law of progressive reactions. This law states that an underlying metastable phase is progressively transformed into a thermodynamically more stable phase until the most stable phase is obtained.

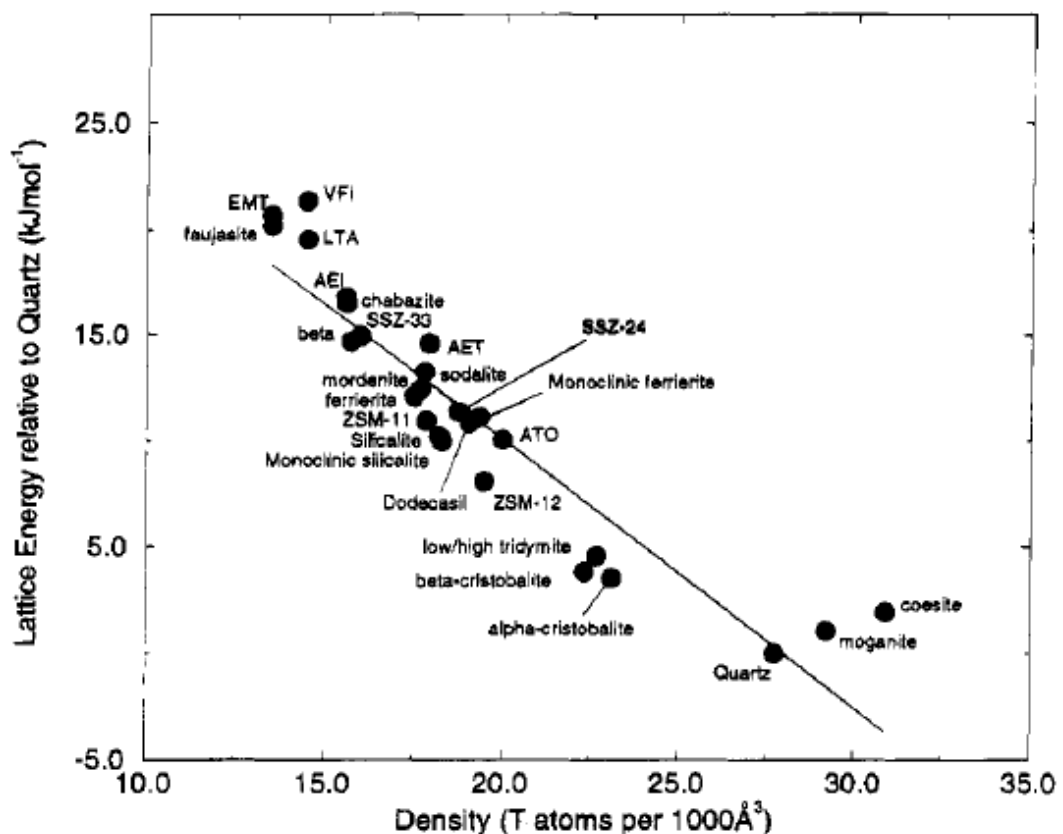


Fig. 1.2 Calculated lattice energies with density of silica structures.

Typically, zeolites materials have been prepared by hydrothermally in presence of reactive alkali metal aluminosilicate gels at low temperatures (60–180 °C) and pressure (autogenous pressure of 30-910 bar range). The hydrated alkali metal acts as the template for the growth of zeolites. This leads to solution mediated crystallization of aluminosilicate amorphous gel and development of templated zeolite subunit. Variation in the gel composition, temperature, charge compensating cation, time of reaction and the pH value (generally greater than 12) yield a range of low-silica zeolites⁴⁴.

In hydrothermal synthesis, water molecule occupies the internal voids of the zeolite. The liberation of the water is possible by heating. Zeolites hold their basic structural integrity upon removal of water molecules makes them distinct from other porous hydrates such as CaSO₄. The crystallinity in the zeolite framework makes sure that the pore gaps are homogeneous and can promptly segregate across the molecules with dimensional contrast under 1 Å, hence they are named molecular sieves.

In zeolite synthesis; organic bases can be used as a substitution for inorganic bases^{45,46}. The utilization of hydroxides of quaternary ammonium ions or organic amines empowered the direct synthesis of high silica content zeolites. These organic nitrogen compounds aggregates act as a template molecule and joined into the final product where they replace the usual charge adjusting cation. The quaternary amines have two important roles; i) templating of new cage structures which is occasional in the aqueous method and ii) the expansive size of these cations, a contrast to the conventional metal cation. Also, the organic cation can be expelled ordinarily from the zeolite by leaching, ion exchange and calcination leaving behind the acid form of the zeolite.

Barrer and Denny and Kerr and Kokotailo ideas in the utilization of organic bases in zeolite preparations leads to many fascinating outcomes⁴⁵. The organic compounds have been effective especially in delivering to extremely silica-rich zeolites e.g. pentasils ZSM-5 (Fig. 1.3) and ZSM-11. The preparation of Al-free ends individually form of ZSM-5 and ZSM-11, named as silicalite I and silicalite II⁴⁷ respectively has been possible.

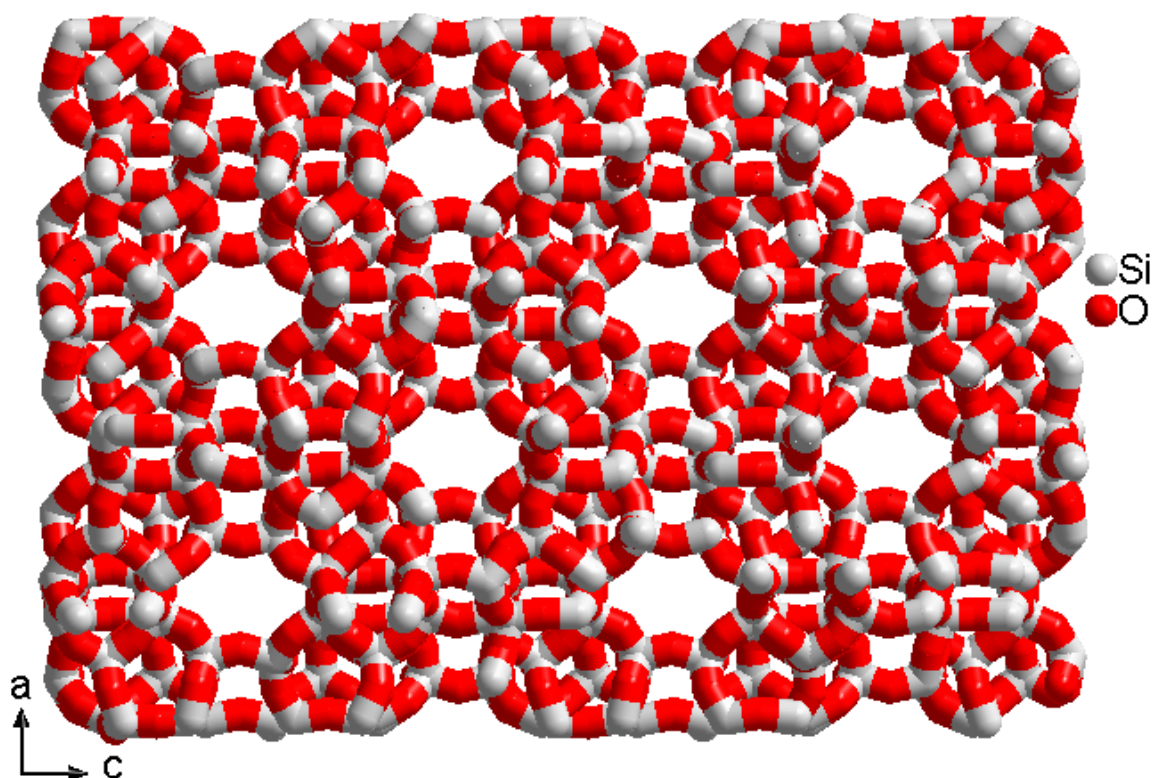


Fig. 1.3 A perspective view of pentasils ZSM-5 structure with extra-large pore.

1.2.4. Open-framework/ zeolite building blocks:

The open-frameworks can be divided into three different categories depending on the building units: 1) Zeolites consisting of $\text{SiO}_4/\text{AlO}_4$ tetrahedra, 2) Zeo-types consisting of phosphate, sulfate, selenate and tellurate tetrahedra and 3) Oxyanions like phosphite, selenite, and tellurites. The complicated structures of the open-framework can be implicated from basic building units used in the synthesis. The neutral framework of zeolite molecular sieves can be depicted as four-corner oxygen connected 3D frameworks.

1.2.5. Metal-Organic Frameworks/ zeolite Secondary building units (SBU's):

In the open-framework; $\text{SiO}_4/\text{AlO}_4$, phosphate, selenate, tellurate-tetrahedra, and Selenite, phosphites-pyramidal forms the primary building units. The interlinking of these primary building block is determined by the secondary building unit⁴⁸. The SBU is represented as $-\text{[Si-O-Si]}-$, $-\text{[Si-O-Al]}-$, $-\text{[Al-O-P]}-$; the central atoms bridging through oxygen atom. The number of primary building block interconnected controlled the geometry of the SBUs (Fig 1.4). For example; four primary units can be interconnected through a rectangle, the six-member unit can be connected through hexagon. A twelve-member unit can be connected through three rectangles or a double hexagonal geometry. However, the interconnection can be through a mixture of geometry too.

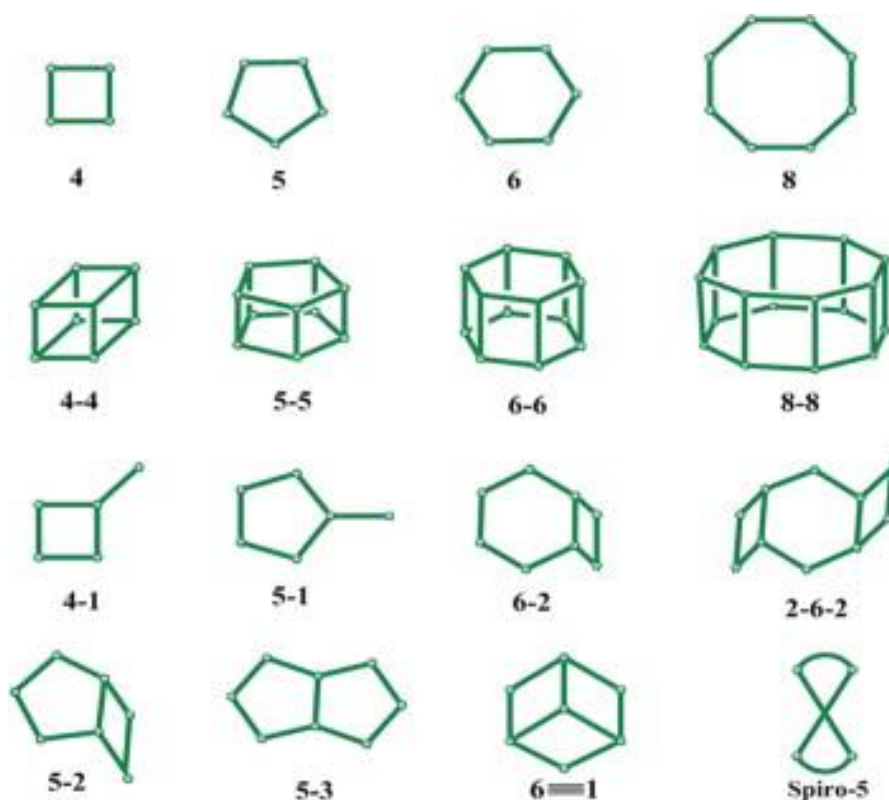


Fig. 1.4. The secondary building units (SBUs) found in the zeolitic framework of aluminosilicates framework family with the legend indicating the type of ring present in the unit.

In zeolite, the rigid primary unit is interconnected directly through the oxygen atom. But in Metal-Organic Frameworks (MOFs), both oxygen atom and organic ligand play as bridging groups. Appropriate synthesis conditions make it possible to obtain desired inorganic SBUs and retain the structural integrity of the organic linkers. This SBU approach leads the final structure of the MOF crystal toward a small number of preferred topologies. The stability of these frameworks can be mathematically modelled and a specific MOFs can be synthesized⁴⁹.

1.3. Templating in the Construction of Microporous Materials:

Templating in open-framework materials synthesis is described as; “the phenomenon occurring during either the gelation or the nucleation process whereby the organic species organizes oxide tetrahedra into a particular geometric topology around itself and thus provides the initial building block for a particular structure type.”⁵⁰ The synthesis of open-framework materials in presence of an organic base which acts as a structure directing agents (templating agents), are carried out under hydrothermal or solvothermal and results in crystallization of reactive aluminophosphate gels similar to the synthesis of high-silica zeolites materials. The structure directing agent (templating species) plays an important role in the framework which can control and dictate the formation of categorical structures by occupying the pore and voids of the structure.

1.3.1. Types of templates:

A large number of organic templates can be aided in the synthesis of open-framework materials. Earlier, more than 100 template species such as quaternary ammonium cations and various organic amines including primary, secondary, tertiary, cyclic amines and alkanolamines have been used in open-framework synthesis (MOFs). The selection of a templating agents' dependent on the ligand which is going to be used. For large ligands,

the size of the template should be large such that it can make significant interaction with the moieties of the cavity. The smaller ligand in such case may stick to side way of the cavity.

Stable metal-ligand building units such as $\text{Cp}_2\text{Co}^{2+}$ and $\text{Co}(\text{en})_3^{3+}$, have also been utilized as a part of the synthesis of Aluminum phosphate frameworks (AIPO). Morris and coworker have used the ionic liquids for the synthesis of SIZ-n-type AIPO materials^{51,52}. The ionic liquid acts both as a solvent and organic template.

There are possibilities for one-template giving multiple-structure and multiple-template provide one-structure, this phenomenon is amazing in open-framework AIPOs. For instance, di-n-propylamine (Pr_2NH) has been utilized in the preparation of at least ten different AIPO framework structure types, for example AIPO₄-11, -31, -39, -41, -43, -46, -47, -50, H3/MCM-1, and H1/VPI-5/MCM-9, displaying low structure specificity. However, few structures promptly frame from a wide range of templates. For example, AIPO₄-5 is significantly templated and can be synthesized with > 25 distinct templates.

1.3.2. Role of templating:

Templating agent goes inside the cavity and is bonded through ionic, H-bonding or van der Waals interaction. This stabilizes the pore within the frameworks and determines the shape and size of the pores. After the formation of the framework templating agents can be removed by thermal treatment. Templating has been discussed quite frequently in the synthesis of zeolite and the related effect on the open-framework materials^{53,54}. However, the interactions between the templating agents and the structures are known as templating effect, is not completely understood.

To understand the templating phenomena, we need to study the gelation mechanism of the aluminium-silicates, alumina-phosphate/phosphite, nucleation, and growth mechanism of MOFs. The gel chemistry plays a vital role in MOFs developments as it has a structure-directing effect. With the change in the organic bases (organic template), the gel chemistry of aluminophosphate is modified. The templating agents crystallize with the frameworks and stabilize voids and also balance the framework charge. For example, in AlPO_4 -12 and -21, ethylenediamine stabilizes and balances the negative charge of the AlPO_4 anionic framework.²⁹

The protonated template cations, not only balance the charge and neutralize of macroanionic layers but also stabilizes the structure. This H-bonding stabilizes the layered structures and also determine the stacking factor of the layers⁵⁵. However, the templating effect is less coherent in the preparation of open-framework of AlPOs.

1.4. Open-framework metal phosphates

1.4.1. Aluminophosphates:

In 1982 Flanigen and co-workers built up the new generation of microporous materials aluminophosphates, AlPO_n (n refers to structural type)^{56,57}. The structure of AlPO_4 (AlPO) is an iso-electronic structure with SiO_2 unit where both the Al and P endorse tetrahedral coordination environment as Si in SiO_2 . The synthetic methodology of aluminophosphate is similar to that of zeolite.

The basic structural chemistry of open-framework AlPOs is way different from that of aluminosilicate zeolites. The Al ions have four, five and/or six coordination with surrounding oxygen atoms in AlPOs materials⁵⁸, in contrast to tetrahedral coordination in aluminosilicate zeolites. The P atom can bind with neighboring Al through variable $-\text{[P-O-}$

Al]- covalent bond. Moreover, the strict repeated rotation of Al and P tetrahedral in AlPOs allows forming 8, 12, 14, 18 and 20-membered rings arrangement (Fig 1.5). However, in aluminosilicate, it is restricted to five/ seven members ring.

For example, aluminophosphates, VPI-5 (Fig. 1.5), $[\text{Al}_3\text{P}_3\text{O}_{12}]\cdot(\text{H}_2\text{O})_7$, contains three-dimensional channels with an 18-membered ring aperture and have a free diameter of 12-13 Å⁵⁹. The structure is composed of AlO_4 , $\text{AlO}_4(\text{H}_2\text{O})_2$ and PO_4 units. The AlPO structures are acquired by using organic amine templates that interact with the frameworks through the H-bonding. The frameworks of AlPOs family are thermally unstable as compared to the aluminosilicate zeolites where the structures are stabilized by some inorganic cations or quaternary ammonium cations.

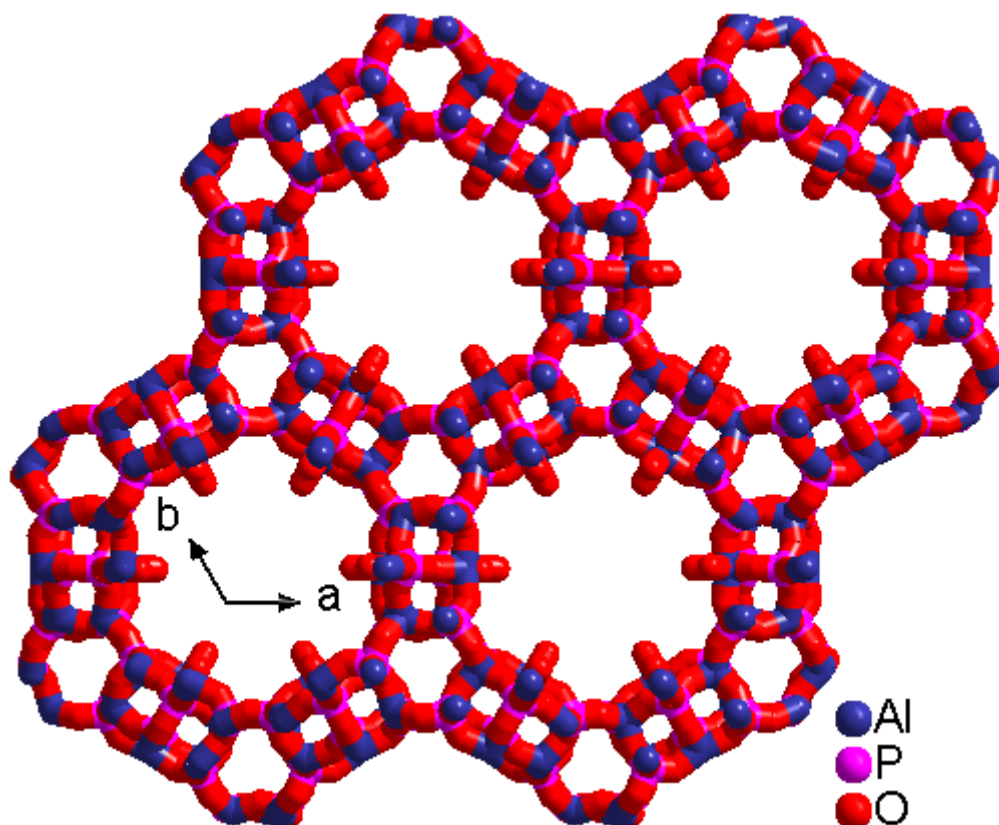


Fig. 1.5. Perspective view of the AlPO_4 framework structure, VPI-5 (VFI) type zeolite with 18-membered ring.

1.4.2. Other metal phosphates:

Empowered by the achievement of doping transition metal ions into the AlPO_4 frameworks, researchers have developed a wide range of AlPO_4 based frameworks that fully/ partially replaces Al by Ga, In, Be, Mg, Zn, Sn, and Sb, as well as transition metals e.g. Mo, V, Fe, Co, Ti, Zr, Mn, Ni, and Sc^{60-63,64}. Since transition metals can be in variable valence states; it can possess a diverse coordination number. Such materials containing oxide-fluoride and phosphate offer an incredible arrangement of frameworks extension.

1.4.2.1. Cobalt phosphate open-framework:

Cobalt metal is among the few known other metals like zinc, manganese and vanadium promptly display variable coordination of 4, 5 or 6. The first known open-framework of cobalt phosphate family is $[\text{C}_2\text{N}_2\text{H}_{10}][\text{Co}_4(\text{PO}_4)_4]\cdot\text{H}_2\text{O}$. It shows a pseudo-tetragonal three-dimensional framework structure.⁶⁵ Followed by a numerous cobalt phosphates framework have been made^{63,66}.

The ethylenediamine templated cobalt phosphate shows a three-dimensional structure with a channel structure. Both structural and magnetic transitions at low temperatures have been reported for this Co-phosphate framework⁶⁷. A three-dimensional cobalt phosphate constructed by the vertex sharing linkage of the CoO_4 and PO_4 tetrahedra is shown in Fig. 1.6.

This Co-phosphate framework has two-fold four-membered rings (D4R) connected to each other by means of oxygen to eight other D4R units through Co-O-P linkages producing an eight-membered channel through the *b*-axis⁶⁷. It shows paramagnetic behavior with antiferromagnetic interaction. It is proton non-conductive in anhydrous

conditions. But the proton conductivity increases to $2.05 \times 10^{-3} \text{ S cm}^{-1}$ at 329 K with the assistance of 98% humidity conditions ⁶⁸.

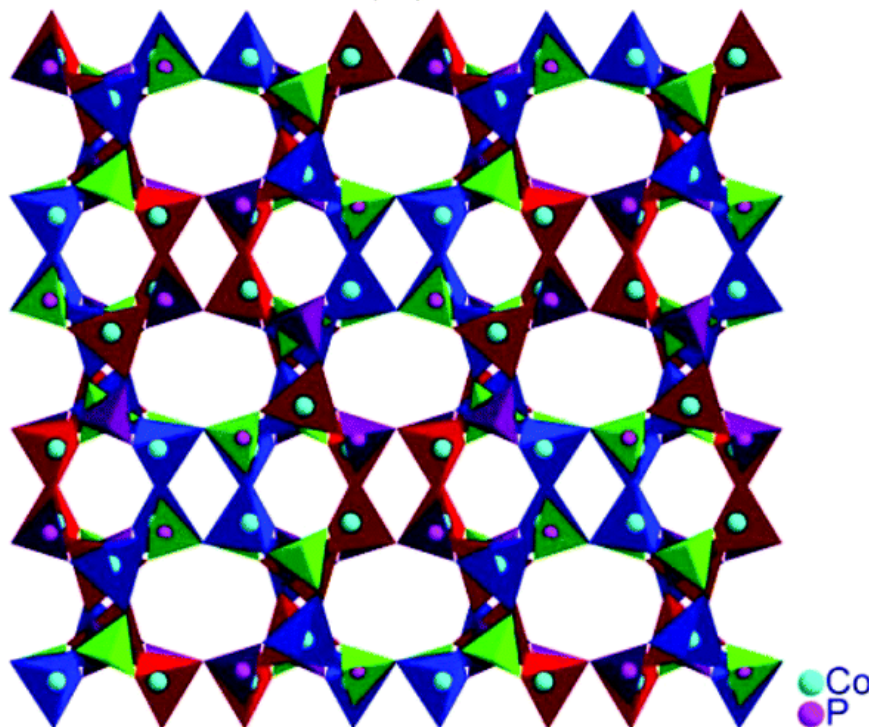


Fig. 1.6. Polyhedral representation of the three-dimensional cobalt phosphate $[\text{C}_2\text{N}_2\text{H}_{10}][\text{Co}_4(\text{PO}_4)_4]\cdot\text{H}_2\text{O}$ ⁶⁵, showing the 8-membered channel along the *b*-axis. (Amine molecules are omitted for clarity).

1.4.2.2. Zinc phosphate open-framework:

The Zinc phosphates are well studied as compared to others metal ions. Zinc atoms also have variable coordination mode similar to Co atoms in a phosphate framework⁶⁴. In general, the Zn atoms prefer tetrahedral than the penta-coordination or octahedra. In $[\text{C}_{12}\text{H}_{14}\text{N}_2][\text{Zn}_6(\text{PO}_4)_4(\text{HPO}_4)(\text{H}_2\text{O})_2]$ (JU98), the zinc phosphate anionic framework are formed by edge sharing of ZnO_4 tetrahedra with PO_4 tetrahedra⁶⁹.

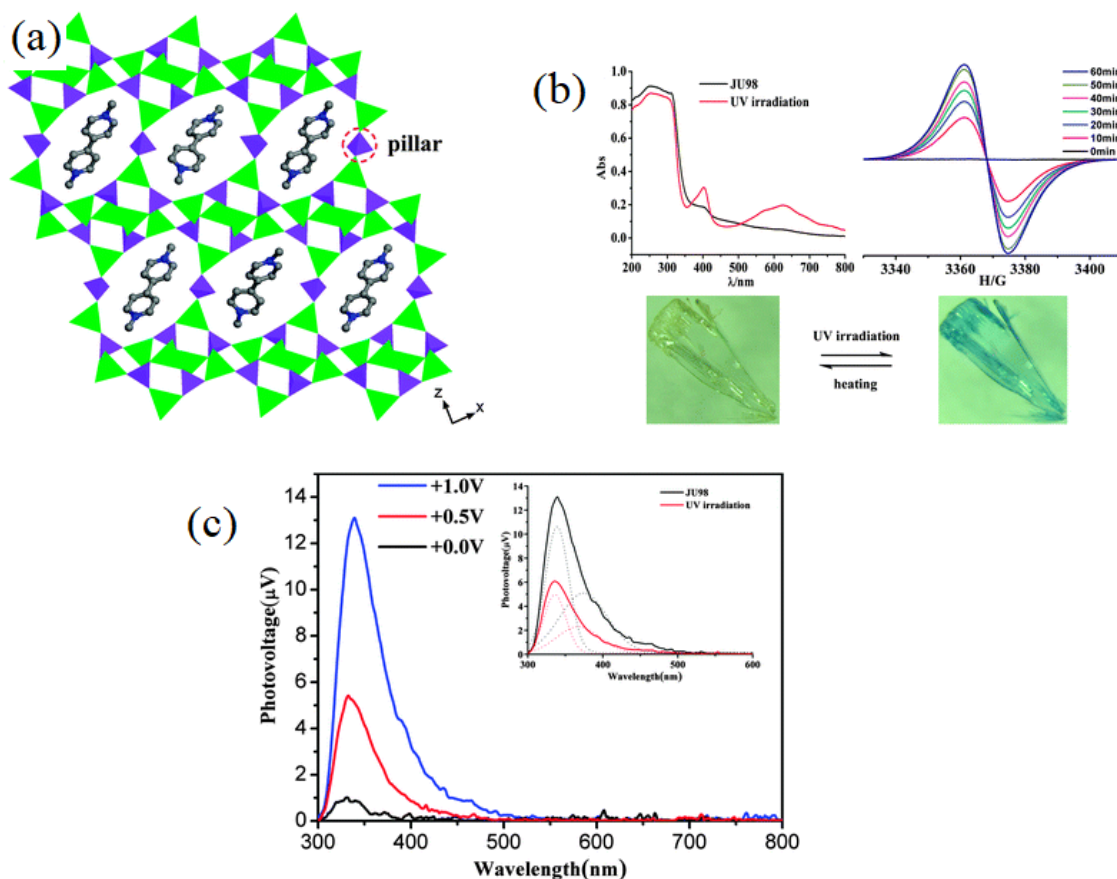


Fig. 1.7. (a) A viewing direction of JU-98 along the y -axis, with 12-membered ring channels and occupies methyl-viologen, (b) UV/Vis spectrum of JU-98 with photochromic effect on a single crystal of JU-98 and (c) Field-induced surface photovoltage spectra of JU98.

The framework of zinc phosphates contains a 3D pillared-layered structure with the 1D, 12-membered channel ($9.0 \times 5.6 \text{ \AA}$) which extends in the crystallographic b -axis. The structure is isostructural with NTHU-9 with an edge-sharing 3-ring chain and ladder like 4-membered ring chain. The organic template methyl-viologen are located in the 12-membered ring channel Fig. 1.7b. It shows reversible photochromic properties from colorless to blue in UV irradiation^{69,53}. It also possesses reversible photovoltaic activity, photoluminescence properties, and n -type semiconductor properties (Fig. 1.7c)⁶⁹

1.5. Metal sulfates, selenates, selenites, phosphite, and hypophosphite open-framework:

The substitution of phosphate by other oxyanions like sulfates, selenites, selenates and so on can offer a large number of variations in inorganic open-framework materials. The differences arise due to the difference in formal charge and oxidation state of the central atom like P, S, Se, and Si. This affects the degree of covalency and the strength of the bonds constructed by these oxyanions with the metal centers. In $-\text{[S-O-M]}-$, sulfur has a higher negative charge compared to Si/P in $-\text{[Si-O-M]}-$ or $-\text{[P-O-M]}-$ bonds. The sulfate bonds are more ionic in nature and form a stable structure with comparatively low valent metal ions. However, it is not clear why the sulfate ion constructs a less number of open-framework structures with metal ions. Currently, a few organically templated open-framework metal sulfates have been reported.^{70,71}

Amine-templated metal selenites and selenates have also been reported recently with open-framework structures⁷². These materials are also prepared by techniques used for metal phosphates synthesis. The salts of the oxyanions with the organic amines have been utilized as precursors for the development of these inorganic open-framework materials.

1.5.1. Metal sulfates open-framework:

The sulfate anion has stable perfect tetrahedron geometry and able to construct expanded infinite novel network structures with similar topology to metal silicates, metal phosphates etc. In 1970, a three-dimensional organically templated zinc sulfate was reported by Morimoto and Lingafelter⁷³. However, the sulfate based open-frameworks following the work of Rao's and co-workers on the synthesis of cadmium sulfates in the year 2001⁷⁴.

It is quite challenging to construct the sulfate-based open-frameworks. Though a sulfur atom is just next to the phosphorous group, the S-O bond order is 0.5 Å which is less than the 0.75 Å of phosphate (P-O) tetrahedral unit. The S-O bond length is less covalent than the P-O and Si-O bond and resulted in less framework networking. The structure of sulfate anions is close to oxalate anions and have comparatively high reactivity.

The metal sulfate open-framework having chain, sheet, and 3D network structures are synthesized. The sulfate polyhedra are connected to metal polyhedra through a common oxygen atom through corner sharing. The metals are interconnected with fluoride and oxygen *via* -M-O-M- and -M-F-M- connection within the polyhedra and constructing a magnetic chain or magnetic layers termed as Kagome layers⁷⁵⁻⁷⁷. Within the Kagome layers, due to the electron sharing inequality between O and F atoms the system shows magnetic frustrations.

1.5.1.1. One-dimensional metal sulfate (EMIm)₂[Zn(SO₄)₂]:

Zinc sulfate open-framework based on (EMIm)₂[Zn(SO₄)₂], enclosing an organic amine has been synthesized by the Kitagawa utilizing the ionic liquid⁷⁸. The amines lie in the inter-chain space and stabilized a one-dimensional chain. In this zinc sulfate chain, [Zn(SO₄)₂]²⁻, the alternate Zn tetrahedra share the corner with four sulfate tetrahedra in a trans-fashion (Fig 1.8). The (EMIm)₂[Zn(SO₄)₂], chain produce EMIm⁺ cation at 240 °C and the ionic conductivity increases nearly to 1.1 × 10⁻⁴ S cm⁻¹.

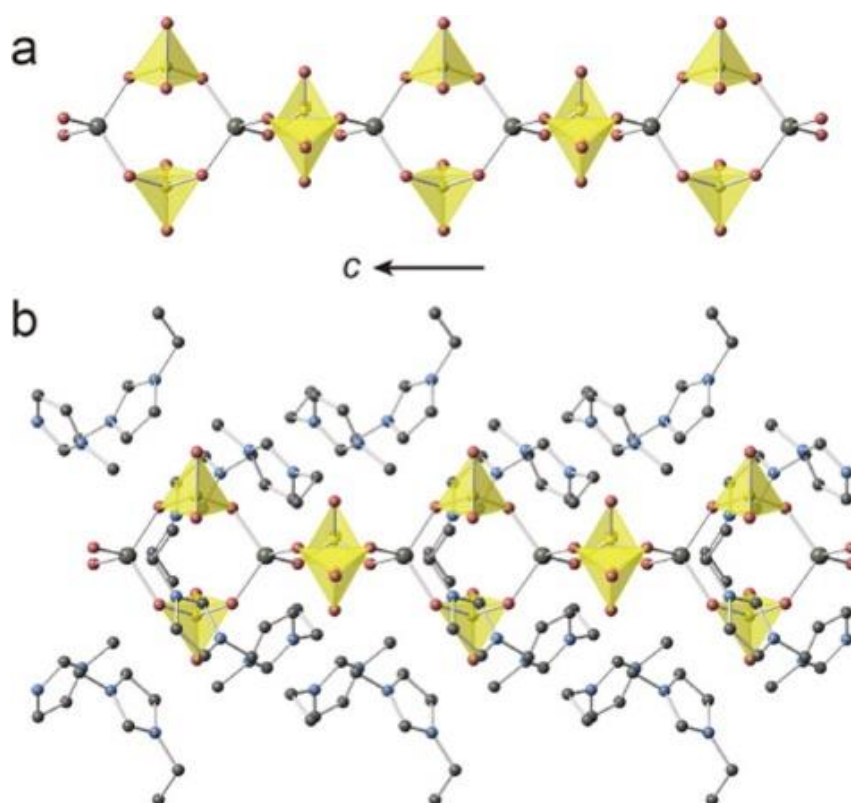


Fig. 1.8. (a) 1D zinc sulfate chain along the c -axis and (b) Lattice diagram of $(\text{EMIm})_2[\text{Zn}(\text{SO}_4)_2]$ ⁷⁸.

1.5.1.2. 3D Zinc sulfate network $[(\text{CN}_3\text{H}_6)_2][\text{Zn}(\text{SO}_4)_2]$:

The $[(\text{CN}_3\text{H}_6)_2][\text{Zn}(\text{SO}_4)_2]$, 3D network is made up of the alternating arrangement of ZnO_4 and SO_4 tetrahedra with vertex sharing⁷⁶. The polyhedral bonding of the ZnO_4 and SO_4 results in an infinite three-dimensional network. This forms a 12-membered ring system, made up of six ZnO_4 and six SO_4 units. The network has a two-dimensional intersecting channels running along a and b - axes, with no channels apparent in the c -axis. Well-ordered guanidinium cations are located in all the 12-membered ring windows (Fig. 1.9) and interact with the zinc sulfate framework through N-H...O H-bonding. The structure resembles that of diamond and is similar to that of a three-dimensional zinc phosphite⁹² and of a guanidinium-templated zinc phosphate.⁹³

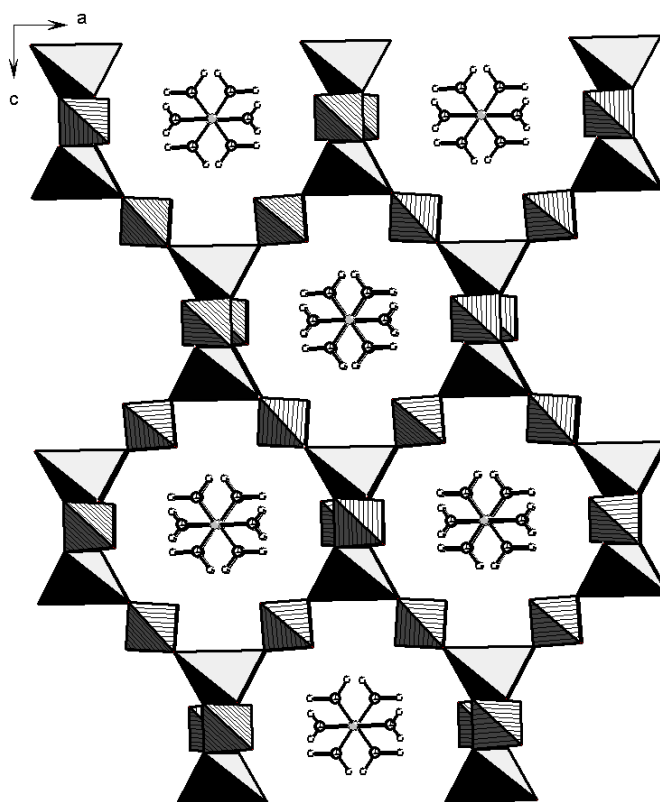


Fig. 1.9. Polyhedral view of three-dimensional zinc sulfate comprising of ZnO_4 and SO_4 tetrahedra in $[(CN_3H_6)_2][Zn(SO_4)_2]$, and the presence of 12-membered channels.

1.5.2. Metal selenates open-framework:

The next oxyanion of chalcogenide group is selenate. It has a similar structure to phosphate and sulfate and has tetrahedral geometry. The selenate anion is less stable in the hydrothermal condition. As the Se has stable oxidation state is +4 so it has the tendency to reduce the selenate (Se^{+6}) anion to form selenite (Se^{+4}) it is reverse from the sulfate case⁷⁹, here the S in sulfite has +4 oxidation state and it oxidized to the most stable oxidation state in sulfate i.e. +6. The reduction potential of selenate (Se^{+6})/selenite (Se^{+4}) couple is 0.03 V where sulfite (S^{+4})/ sulfate (S^{+6}) couple has 0.119 V in alkaline medium. Therefore, it becomes necessary to prepare them in an acidic medium. Hence the organically templated metal selenate less explored.

1.5.2.1. Neptunium based Selenate framework $[\text{Na}(\text{NpO}_2)(\text{SeO}_4)(\text{H}_2\text{O})]^{80}$:

In 2012, Solhohm and his lab member work on Np based selenate framework⁸⁰. They synthesized the 3D framework of $[\text{Na}(\text{NpO}_2)(\text{SeO}_4)(\text{H}_2\text{O})]$ (Fig. 1.10). In the polyhedron, Np ions share their corner and forms ribbon. These ribbons share its oxygen atoms with tetrahedra of selenate through vertices sharing and form a three-dimensional open-framework with three different channels along the *b*-axis. The free spaces or channels are filled with the Na ions and water molecules.

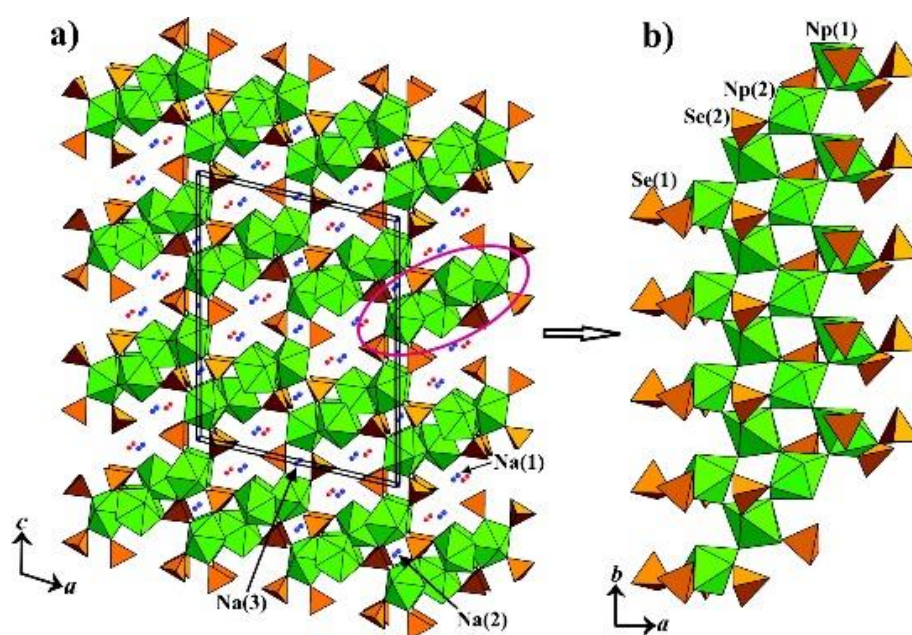


Fig. 1.10 (a) The 3D structure of $[\text{Na}(\text{NpO}_2)(\text{SeO}_4)(\text{H}_2\text{O})]$ constructed by neptunyl (V) selenate ribbons with open channels along the *b*-axis direction filled by Na^+ cations (blue balls) and H_2O molecules and (b) The depiction of an individual ribbon of corner-sharing green NpO_7 pentagonal bipyramids decorated by orange SeO_4 tetrahedra.

All the Np ions are bonded to two oxygen atoms linear way and form NpO^{2+} ions which further connected with five selenates in the equatorial plane and form bipyramidal geometry. The Np ions in the ribbon are connected to each other through

Cation-Cation Interactions. The complex shows ferromagnetic behavior, the average N_p effective moment of $\mu_{\text{eff}} = 3.65(10) \mu_B$ and Weiss constant of $\theta = 14(1)$ K. with ferromagnetic spin ordering at $6.5(2)$ K.

1.5.2.2. Lanthanum based selenate framework $[\text{La}_2(\text{SeO}_4)_4(\text{H}_2\text{O})_3]$ $[\text{C}_2\text{N}_2\text{H}_{10}]\cdot\text{H}_2\text{O}$ ⁸¹:

Organically template three-dimensional lanthanide selenate open-framework was developed using the hydrothermal method by Rao *et al*⁸¹. The three-dimensional anionic $[\text{La}_2(\text{SeO}_4)_4(\text{H}_2\text{O})_3]^{2-}$ framework form from the $\text{LaO}_{8/9}$ polyhedra, SeO_4 tetrahedra, and a water molecule (Fig.1.11). The negative charge is balanced with protonated ethylenediamine which occupies the cavity space.

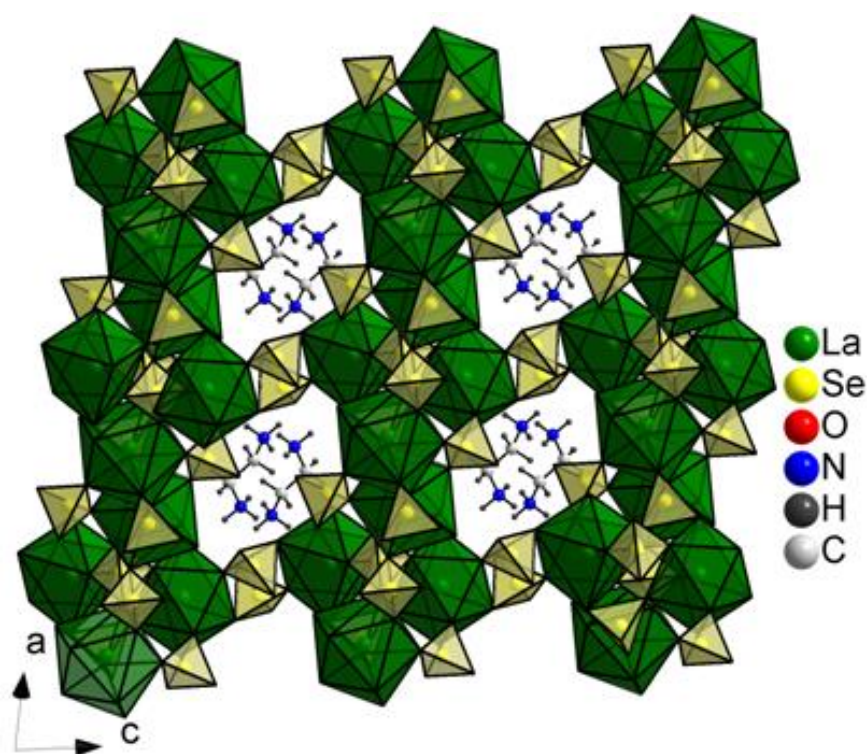


Fig. 1.11. The inorganic layer of $[\text{La}_2(\text{SeO}_4)_4]^{2-}$ in $[\text{La}_2(\text{SeO}_4)_4(\text{H}_2\text{O})_3]$ $[\text{C}_2\text{N}_2\text{H}_{10}]\cdot\text{H}_2\text{O}$, with the capping and bridging of the LaO_9 dimers by two selenate units, resulting in corner-shares 4-membered rings along the a -axis.

LaO₈ are capped with four selenates through corner sharing and LaO₉ are edge sharing with selenate polyhedral. The alternate La polyhedral and selenate tetrahedral forms chain along the *c*-axis. The chains are interconnected by Se(2) selenate ions and forming a layered structure in the *ab*-plane with 4 and 8-membered rings. Further, the layers connected by the Se(4)O₄ in the *c*-axis and forming a 3D framework with 12-membered rings along *a* and *b*-axes.

1.5.3. Metal selenites open-framework:

The framework based on selenite attracted immense research interest because of the desirable role of the lone pair of electrons as an invisible structure-dictating agent. The presence of a stereochemically active lone pair of electrons on Se(IV) prompt pyramidal coordination for the selenite species. Because of the presence of a lone pair of electrons, metal selenites have a tendency to crystallize in non-centrosymmetric structures leading to fascinating physical properties (due to the acentric lone pair of electron present after metal selenite complex formation); for example, non-linear optical second harmonic generation (SHG)^{79,82}.

The Se^{IV}/Se⁰ ions pair has a low reduction potential under hydrothermal conditions. This will lead to a reduction of Se^{IV} to metallic Se formation during hydrothermal synthesis. And hence, the preparation of amine-templated open-framework metal selenites is challenging. The organically templated iron (III) and zinc (II) selenite with 3D structure are reported by Harrison *et al.*⁸³ Rao *et al.*^{84,85}.

1.5.3.1. 2D cadmium selenites open-framework [C₂N₂H₁₀][CdCl₂(HSeO₃)₂]:

Depending upon the connectivity mode between the various metal atoms and selenite units provides a range of the two-dimensional metal selenites design. In

[C₂N₂H₁₀][CdCl₂(HSeO₃)₂], the Cd polyhedra connected to four groups of selenites through vertex sharing and two Cl atoms at axial position⁸⁶. The 4 Cd polyhedral and 4 selenite anions are alternatively arranged and forming 8-membered rings (Fig. 1.12)⁸⁶.

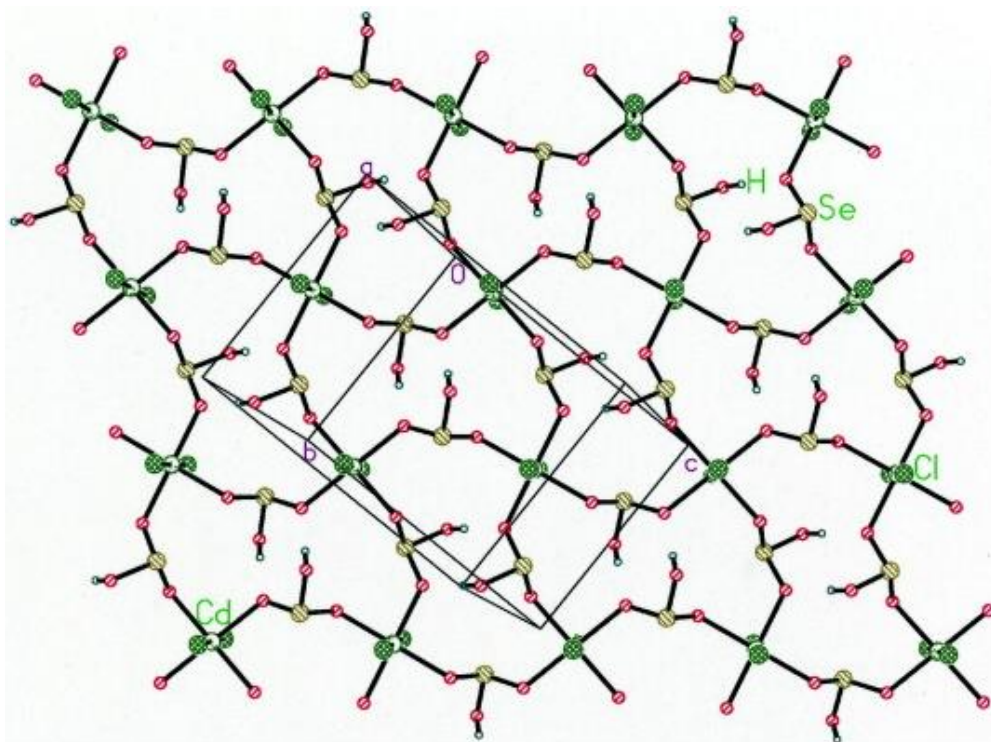


Fig. 1.12. The layered structure of [C₂N₂H₁₀][CdCl₂(HSeO₃)₂], with 8-membered ring aperture.

1.5.3.2. 3D Mixed metal selenite open-framework [NaY(SeO₃)₂]:

In 2014 Ok and *et al.* synthesized the three-dimensional network of [NaY(SeO₃)₂] hydrothermally⁸⁷. The selenite shares three oxygen atoms *via* corner sharing to three Y(III) ions and two oxygen atoms with two sodium ions. The other selenite shares their oxygen atoms to two Y(III) ions through corner and edge-sharing and two oxygen atoms of selenite connected to two sodium with Se-O-Na linkage. The polyhedra YO₇ mono-capped trigonal prism and trigonal pyramidal SeO₃ together forming a three-dimensional structure. The YO₇ polyhedra are forming zigzag chains through vertex-sharing polyhedra and further trigonal pyramidal SeO₃ interconnect the chain resulting 3D backbone (Fig. 1.13).

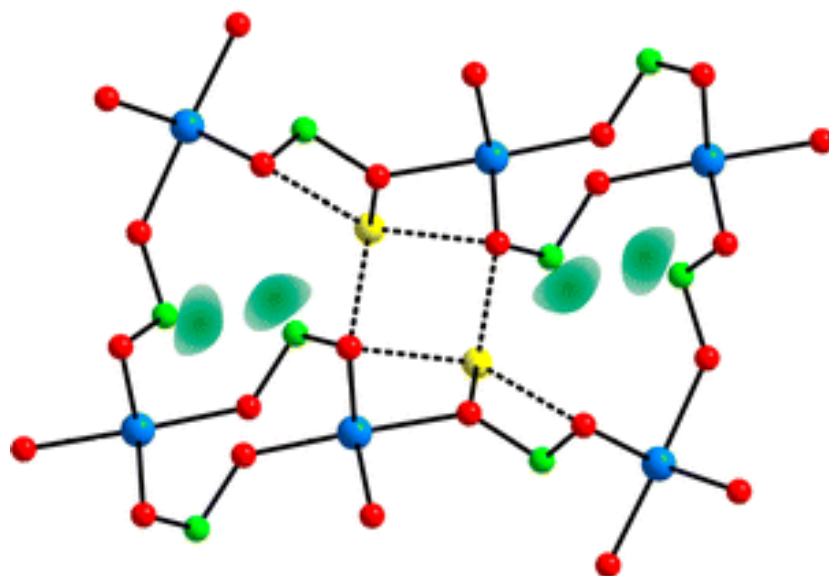


Fig. 1.13. Crystal lattice of 3D structure of $[\text{NaY}(\text{SeO}_3)_2]$, where blue color indicate Y; green color show Se; yellow color indicate Na and red color for O.

The complex is stable up to 570 °C. $[\text{NaY}(\text{SeO}_3)_2]$ compound crystallizes into a Non-Centro-Symmetric (NCS) space group and shows Non-Linear Optical (NLO) properties⁸⁷. This NCS $[\text{NaY}(\text{SeO}_3)_2]$ framework show that the compound has a similar Secondary-Harmonic-Generation (SHG) efficiency to that of $\text{NH}_4\text{H}_2\text{PO}_4$ (Fig 1.14). The further structural analysis suggests the observed SHG is due to a net moment originating from the lone pair of electron on Se^{4+} .

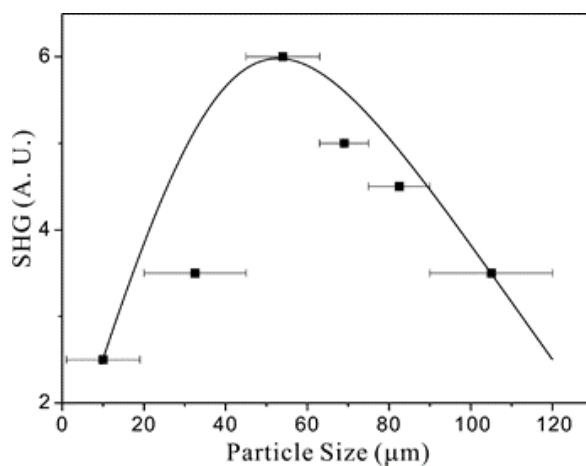


Fig 1.14. Type 1 phase matching curve for NCS $[\text{NaY}(\text{SeO}_3)_2]$.

1.5.4. Metal phosphites open-framework:

The phosphite anions have one oxygen atom less to the phosphate anions. The phosphite has pseudo-pyramidal geometry and occurs in two distinctive phases. Phosphorous in both the phase is stable which has the oxidation states +3 and +5. The phosphite is like phosphonate group where R-PO₃ where R is aryl or H. The phosphite can coordinate with three oxygen atoms leads to different structures formation than the phosphate, silicates, and zeolites.

Because of the lower coordination of phosphite results into numbers of low dimensional phases structures like 1D-chain and 2D-sheets. Harrison and coworker in 2001 use a pseudo-pyramidal phosphite unit HPO₃²⁻ group instead of phosphate with the Zn atom and reports the first organically templated zincophosphites framework^{88,89}. The covalent bond in P-H of phosphite is higher than the P-O-H in phosphate framework. In the phosphites framework, H is not acidic proton and hence does not take part in the H-bonding. Sometimes the analog of the phosphite and phosphate structures are same⁹⁰.

1.5.4.1. Zinc phosphite open-framework (C₄NH₁₂)₂[Zn₃(HPO₃)₄]:

The reported zinc phosphite (C₄NH₁₂)₂[Zn₃(HPO₃)₄] includes extra-large 24-ring channels (11 × 11 Å²), which is one of the biggest known channeled open-framework⁹¹. Surprisingly, this zinc phosphite is templated by the small n-butylamine molecule. The channels extend parallel to 8-membered ring channels along the *c*-axis and are engaged by the protonated amine (Fig. 1.15).

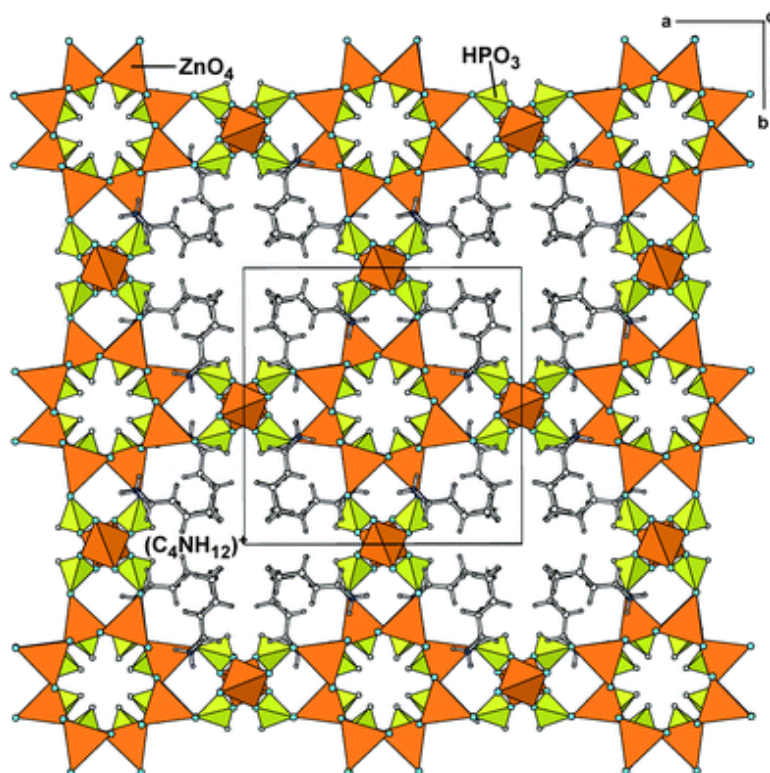


Fig. 1.15. Polyhedral view of sheets in the *ab*-plane of $(\text{C}_4\text{NH}_{12})_2[\text{Zn}_3(\text{HPO}_3)_4]$ showing the 24-membered ring channels present in this material.

1.5.4.2. Gallium phosphite open-framework (NTHU-15):

In 2016 wang and *et al.* synthesized the organically templated polyamine gallium phosphite $[\text{H}_6\text{PEHA}][(\text{GaOH})_9(\text{HPO}_3)_{12}]$ (NTHU-15) in hydrothermal condition⁹². The NTHU-15 has a three-dimensional framework with the 18-membered rings. The alternate arrangement of edge-shared bi-octahedral Ga (skew edge-sharing) center $\text{Ga}(\text{OH})_2\text{O}_4$ and pseudotetrahedral HPO_3 together forming 3D-inorganic framework, with a Ga/P ratio 3:4, having the formula $[(\text{GaOH})_9(\text{HPO}_3)_{12}]^{6-}$.

Each Ga1 dimers connected to two *cis* corners Ga2 octahedra. Further, each of the Ga2 octahedra interconnected with two Ga1 dimers by a skew edge. Therefore, it results in an infinite Ga–OH–Ga chains extending along the *c*-axis. The framework is neutralized with the protonated H_6PEHA template that lies in the cavity. Adsorption isotherms show that

NTHU-15 is a microporous system which has an average pore diameter of 5.6 Å and the surface areas for 15-PEHA (276 m²/g) (Fig 1.16).

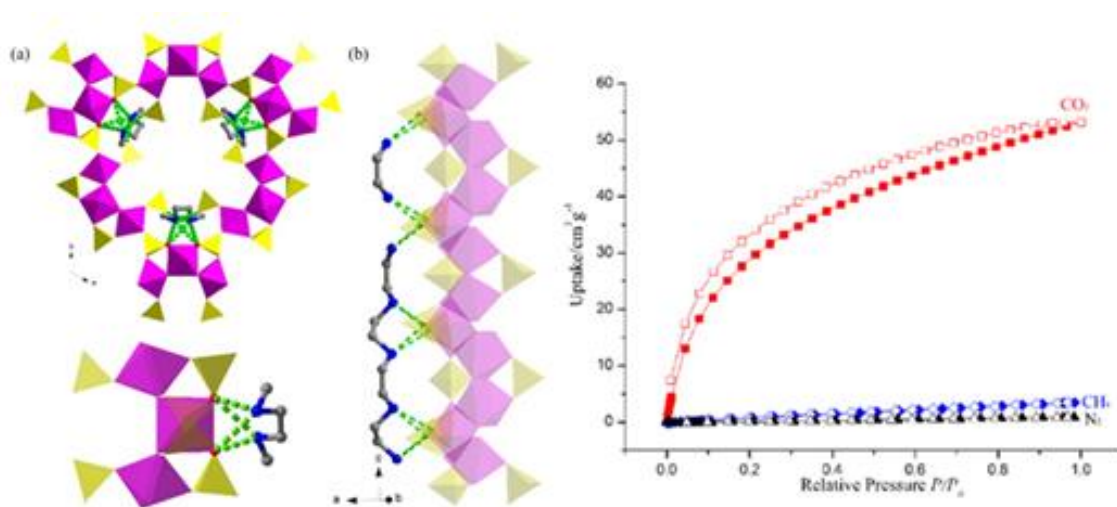


Fig. 1.16. (a) Polyhedral view of the three-dimensional [H₆PEHA][(GaOH)₉(HPO₃)₁₂](NTHU-15) showing the 18-membered ring channels present in this material and (b) Gas sorption isotherms of NTHU-15 of H₂, CO₂ (triangles), CH₄ (squares), and N₂ (circles) for 15-PEHA, adsorption curves measured at 77 K.

1.5.5. Metal hypophosphite open-framework:

The next family member of oxy phosphorous anion is hypophosphite. The hypophosphite is a similar structure to formate anion. In hypophosphite one less hydrogen atom present than the formate anions (Fig 1.17). The phosphorous has +1 oxidation states, the two hydrogen atoms are directly connected to the phosphorous atoms. The P–H bond lengths of *pseudo* tetrahedral H₂PO₂⁻ in the range of 1.27(5)–1.45(5) Å. The hypophosphite anion can bind with two/ three / four metal ions and forms thermally and chemically stable complexes of varying dimensionalities⁹³.

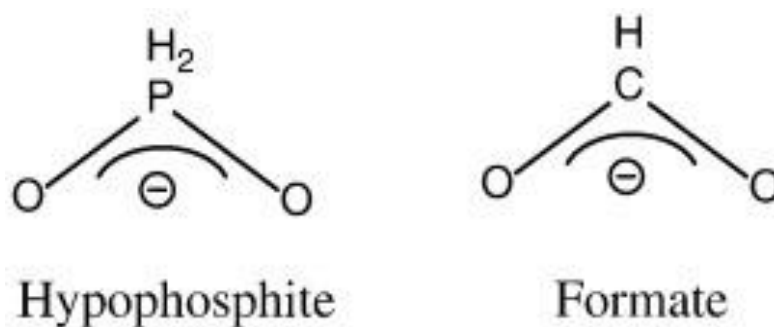


Fig. 1.17. Structures of hypophosphite and formate ligands.

1.5.5.1. Manganese hypophosphite open-framework:

Recently in 2015, Murugavel and his team member synthesized the $[\text{Mn}(\text{H}_2\text{PO}_2)_2]_n \cdot (\text{DMF})_{0.11}^{94}$. The distorted octahedral Mn(II) ions coordinate with the six oxygen atoms of six $[\text{H}_2\text{PO}_2]^-$ ligands and *vice-versa*, ligand molecule giving all its oxygen atoms to coordinates with three Mn(II) ions forms bridges Mn–O–Mn (edge sharing) and Mn–O–P–O–Mn and form a chain along [001] direction (Fig 1.18). The chains are interconnected and form the polymeric three-dimensional network containing hexagonal 1D channels with two DMF units which are squeezed. The complexes show antiferromagnetic nature with spin-orbital interaction $S = 5/2$, μ_B with $\theta = -9.9$ K.

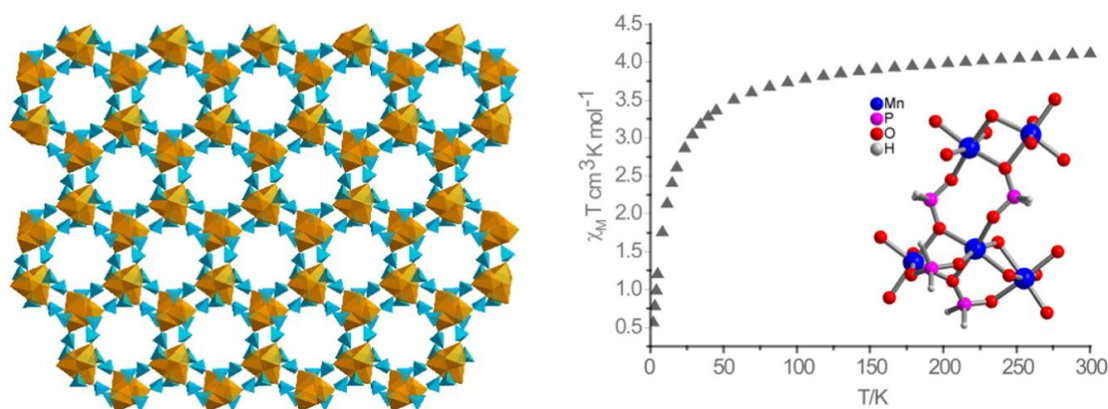


Fig. 1.18. Polyhedral view of the three-dimensional of $[\text{Mn}(\text{H}_2\text{PO}_2)_2]_n \cdot (\text{DMF})_{0.11}$, and temperature dependent magnetic susceptibility.

1.6. Metal carboxylates Frameworks

1.6.1. Carboxylate Ligands:

Carboxylic acids are also attractive as framework-forming reagents for the high acidity ($pK_a \sim 4$) that allows facile deprotonation. In the same way, the metal-carboxylate bond formation is reversible under relatively mild conditions, which presumably facilitates the formation of well-ordered, crystalline MOFs. Most of the carboxylate-based ligands are either commercially available, such as 1,4-benzenedicarboxylic acid (BDC) and 1,3,5-benzenetricarboxylate (BTC), or easily accessible through well-defined and high yielding synthetic pathways (Fig. 1.19).

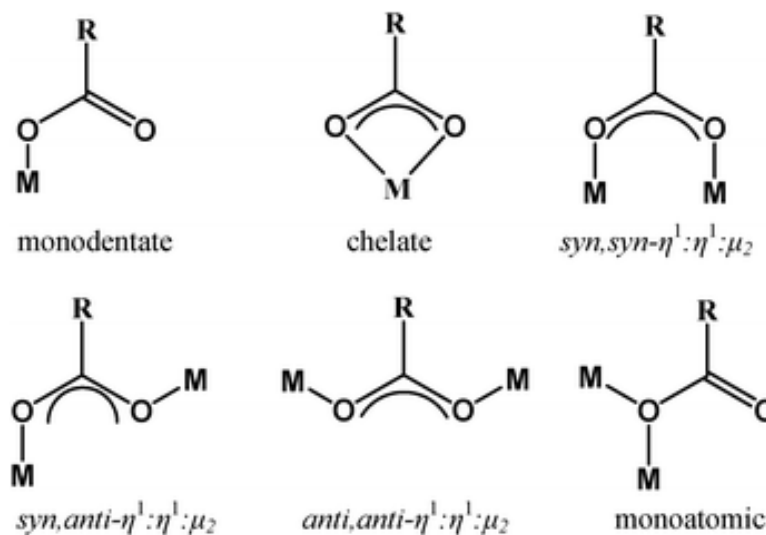


Fig. 1.19. The coordination modes of carboxylate, when the linking units are changed from dicarboxylates to tricarboxylates, the topology of the ligand is also changed from a two-point-linker to a three-point-linker, hence, the different networks will be resulted.

The negative charge of the deprotonated carboxylates is counter balanced by the positive charge of the metal center in a framework structure. This eliminates the need for counter ions to be present in the structural pores. Accessibility to the pores and favorable thermodynamics make carboxylic acids the most popular ligand choice^{95,96}.

1.6.2. Metal carboxylates frameworks:

Recently, Liu and co-worker have reported the solvothermal synthesis of $\{[\text{In}(\text{BTTB})_{2/3}(\text{OH})](\text{NMF})_5(\text{H}_2\text{O})_4\}_n$ (437-MOF) { where BTTB = 4,4',4''-[benzene-1,3,5-triyl-tris(oxy)]tribenzoic acid (Fig. 1.20a), NMF = *N*-methylformamide} in gram scale with a high yield⁹⁷. 437-MOF has a 3D coordination framework mesoporous with regular 1D hexagonal channels. The octahedral In(III) ions is connected with neighbor four oxygen atoms of four carboxylates anions and two $\mu\text{-OH}^-$ anions where the BTTB ligand is in deprotonated state and link to six In(III) ions. The adaptable BTTB ligand has a unique configuration of high symmetry, clearly, the $\pi\text{-}\pi$ stacking connections occur between the parallel benzene centres of the BTTB ligands (centroid distance 3.635 Å) to form a 1D organic supramolecular array along the *c*-axis. The arrangement of such organic arrays and rod-shaped inorganic SBUs offers ascend to a 1D concave triangular prism that acts as a supramolecular building block (Fig 1.20).

The 3D framework of 437-MOF comprises of orderly hexagonal mesoporous channels of 32.3 Å extended along the *c*-axis. The bonding mode of the triangular prism knots of the BTTB ligands and the hexagonal knots of the In(III) ions forms in a 2-nodal 6-connected 3D $(3^3.4^6.5^6)_2(3^4.4^4.5^4.6^3)_3$ net. Although 6-connected networks are familiar in MOFs. Alternatively, this structure considered as a (3, 4)-connected $(4^2.6^3.8)_3(6^3)$ topological network constructed by 1D In–O SBUs and 3-connected BTTB ligands.

The 437-MOF is stable up to 400 °C and it remains most stable in cool water for weeks. The 437-MOF is mesoporous with a large stable 1D channel with BET surface area of 1576 $\text{m}^2 \text{g}^{-1}$ with 0.92 $\text{cm}^3 \text{g}^{-1}$ pore volume. Due to hydrophobic in nature 437-MOF needs to activate in boiling water. The activation shows a change in the N_2 isotherm and increases in surface area and porosity (2379 $\text{m}^2 \text{g}^{-1}$ /1.11 $\text{cm}^3 \text{g}^{-1}$). The CO_2 adsorption-desorption

isotherm shows two steps. The adsorbed CO₂ is not immediately released by reducing the pressure.

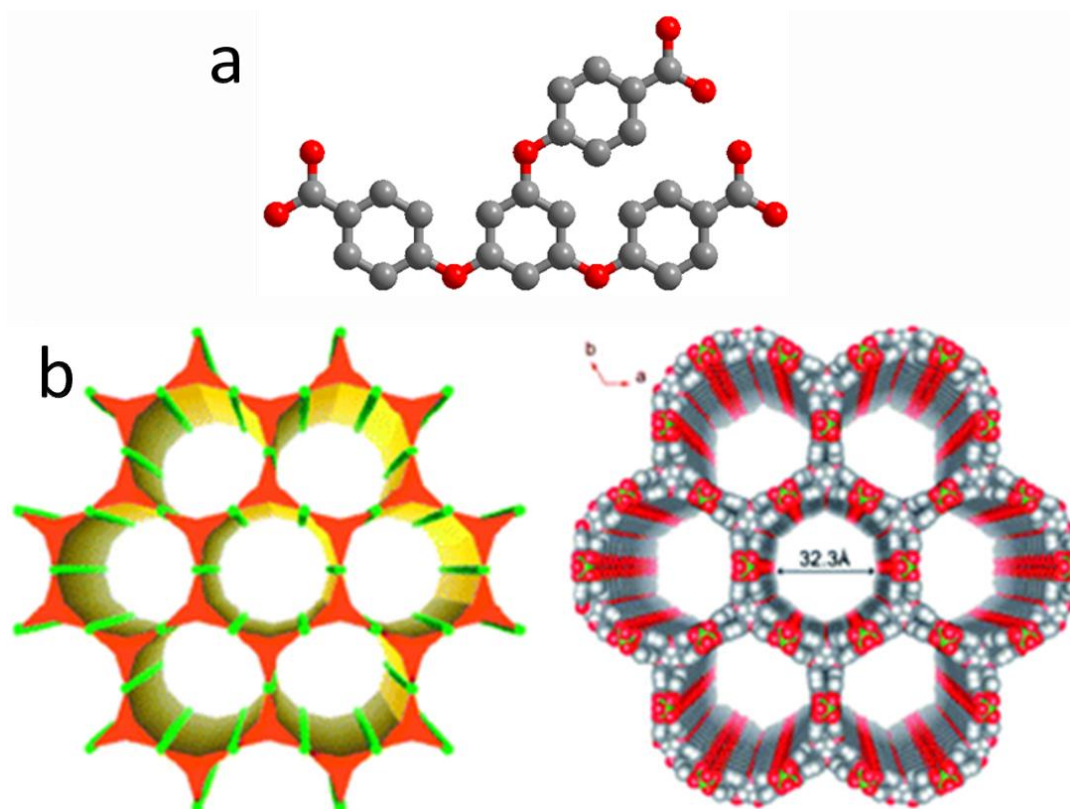


Fig. 1.20. Crystal structure of 437-MOF, (a) Ball and stick model of BTTB ligands and (b) Viewing direction of the 3-D framework and the space-filling model showing regular 1D hexagonal channels.

1.6.3. Hierarchy of structures in open-framework metal carboxylates:

Recent years, various open-framework metal oxalates synthesized and characterized successfully. A molecular zinc oxalate dimer has been found to change to a chain structure by warming in the presence of piperazine at 100 °C for 48h⁹⁸. A similar dimer provides a pseudo two-dimensional zinc oxalate and a three-dimensional zinc oxalate when heated at 165 and 180 °C separately amid the similar time period.

This demonstrates on heating with piperazine in an aqueous medium; dimensionality of the structure increases with increasing reaction temperature (Fig. 1.21). This change includes

hydrolysis and condensation, wherein the oxalate moiety is disposed of to construct the higher dimensional structures, joined by removal of water, on the increment of the reaction temperature. The dimensionality of the structure increases as the aggregate water content decreases, and this is joined by an increment in the number of zinc atoms connecting to the oxalate units (Zn/oxalate ratio).

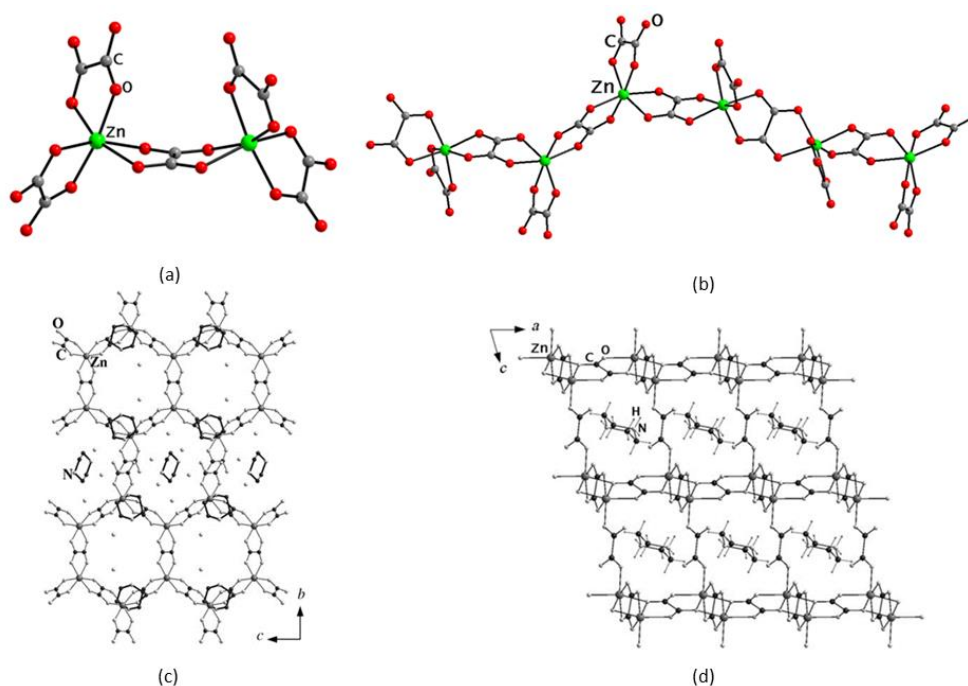


Fig. 1. 21. Transformation of a zinc oxalate dimer (a), to a linear chain (1D) structure (b), a pseudo two-dimensional structure with honeycomb apertures (c) and a 3-dimensional framework structure (d).

The successive formation of higher-dimensional structures of cobalt succinates with increment in temperatures has also been studied by Cheetam *et al.*⁹⁹ A nickel propionate dimer has been reported to change into a one-dimensional chain structure¹⁰⁰. The low-D to high-D changes is happened by a building-up process in solution, instead of a disintegration or reconstruction process. 1,4-benzenedicarboxylate also undergo a 1D to 3D transformation¹⁰¹.

1.7. Synthesis and characterization techniques of open-framework inorganic structures:

Generally, the open-framework materials are synthesized by solvothermal methods. Hydrothermal synthesis is used more frequently and is carried out under the sealed reaction container at 1 bar pressure and temperature more than 100 °C. Most of the reactant is hard to dissolve in the water and hardly dissociate and go in the solution as complex in hydrothermal condition.

The hydrothermal synthesis of open-framework materials is preferable over conventional synthetic techniques for; i) synthesis of compounds with elements in oxidation states that are hard to accomplish, ii) helpful for the preparation of “low-temperature phases” and iii) preparation of so-called metastable compounds¹⁰².

Where in the solvothermal methods, the reactions are carried out in a closed system at a temperature higher than the boiling point of the solvent used. The pressure automatically builds up inside the sealed reaction container and the temperature drastically increases. In addition to it, the reaction progress and the products form depends upon other experimental factors like volume percentage fill of the reaction container and any soft salts present.

Fig. 1.22 shows the pressure build-up inside the sealed reaction container with temperature for different volume percentage fill¹⁰³. The physical properties of water are being dependent on pressure and temperature. The viscosity of water diminishes with rising temperature, which flourishing the mobility of the diffused ions and molecules than at surrounding conditions. The dielectric constant of water is influenced by temperature and pressure and is impressively expanded at these

hydrothermal conditions. This increases the solvating capability of water under these circumstances, which permits the disintegration and mixing of the solid reagents to form an inhomogeneous gel in the initial phases of the reaction.

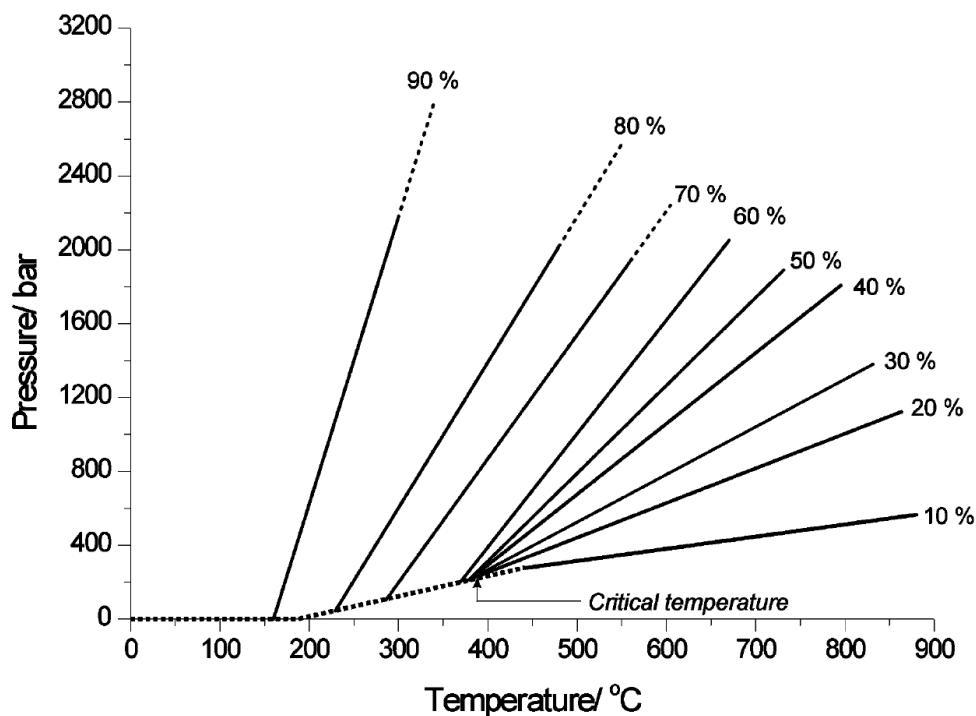


Fig. 1.22. Pressure as a function of temperature and percentage fill of water in a sealed vessel¹⁰³.

In hydrothermal synthesis, a huge number of reaction factors influence the pathway and kinetics of the reactions. The reaction factor includes time, temperature, pressure, type of initial reactants, starting concentration, pH, the inorganic or organic cations used, aging time of the gel, reaction cell fill volume and so forth. Variation of any of these parameters imparts an impact on several others in both direct and indirect ways. But the influence of these factors is not clearly understood.

It is observed that with an increment in reaction temperature, the inter-crystalline cage space decreases with a lower water content. Changing the reaction composition will

influence the nature of the final product constructed. However, it is not well established to tailor the arrangement of the final product by utilizing the desired proportion of the starting materials in the reaction. Subsequently, the molecular arrangement of the final product does not follow the general composition of the mixture.

The metastable phases of microporous materials are thermodynamically unstable. The arrangements of these metastable phases are controlled by both thermodynamic and kinetic factors. Hence, both temperature and time is an imperative variable in deciding the nature of products produced by the solvothermal synthesis. The different variables that influence the preparation of microporous materials have been plotted in the mid-nineties by Lobo *et al.* and furthermore as of late by O'Hare *et al.*^{53,104}

Autoclaves:

To endure the pressures associated with hydrothermal synthesis, the utilization of autoclaves is necessary. They aid to secure the reaction container. At first of these autoclaves were built of steel with the noble metal coating. Currently, *Teflon* container is used as reaction chamber¹⁰⁵. *Teflon* has a tendency to wind up noticeably and become porous with high pressure. So, only iso-statically treated potentially pore-free material (PTFE) can be utilized. Autoclaves with *Teflon* embeds are presently broadly utilized as digestion bombs and are commercially available (Fig. 1.23)¹⁰⁶. Quartz glass ampoules for hydrothermal examinations are additionally portrayed by Speed and Filice¹⁰⁵.



Fig. 1.23. (a) A schematic of TeflonTM-lined, stainless autoclave typically used in the laboratory and (b) The external view of the autoclave used for the synthesis described in this thesis with Teflon inserts¹⁰⁶.

1.7.1 Materials characterizations:

1.7.1.1 X-Ray diffraction:

The wavelength of X-Ray falls in the range of interplanar spacing in the crystal and hence get diffracted by the plane forming a diffraction pattern. Fig.1.24 illustrates the diffraction phenomena. The phenomenon of diffraction is explained by Bragg's equation.

$$n\lambda = 2d \sin\theta$$

where the d is interplanar spacing, θ is the Bragg's angle, λ is the wavelength of X-Rays and n is the order.

Powder X-ray diffraction is an effective non-destructive technique broadly utilized for qualitative and quantitative investigation of crystalline products. The phase content from the synthesis mixture is characterized by powder X-ray diffraction (PXRD). Crystalline solids show a characteristic XRD pattern, which is utilized as a 'fingerprint' for the phase identification. From the XRD structural analysis, the unit cell, the nature, and type of atoms and phase purity can be identified. The different pieces of information that can be acquired from the diverse features of the PXRD pattern are recorded in Table 1.2.

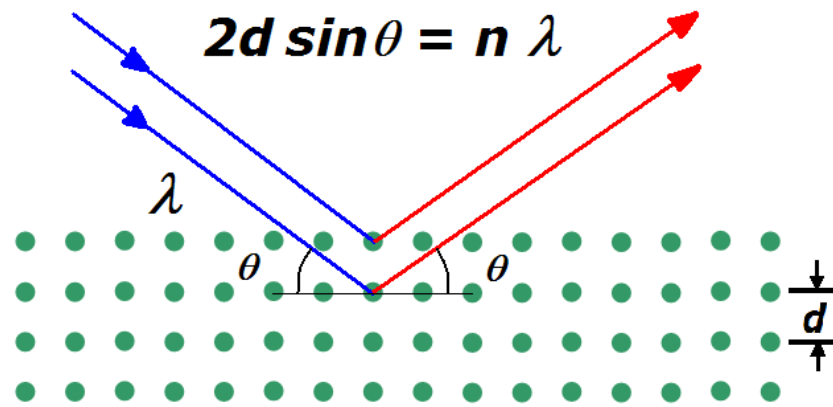


Fig 1.24. Diffraction of X-Ray by crystals.

Table 1.2. Information obtained from powder X-ray diffraction

Diffraction line parameter	Applications
Peak Position	Unit cell parameter refinement Pattern indexing Space group determination (from absent reflections) Qualitative phase identification
Intensity	Phase abundance Crystal structure analysis (whole pattern) Rietveld refinement (whole pattern) Search/match, quantitative phase identification Preferred orientation, texture analysis
Width/ breadth and shape	Microstructure (crystallite size, size distribution, lattice distortion, dislocations, microstrains etc.)

Single crystal X-ray diffraction:

The internal molecular structural information of single crystal materials can be derived from single crystal X-ray diffraction methods. It gives the information regarding the atoms, type, coordinates of atoms, coordination environment, its space arrangement, the symmetry of crystal space group, population of atoms (occupancies), anisotropic thermal parameters,

connectivity and the stereochemistry of the molecule, bond length and bond angle information and so on. Additionally, it enables to correlate between the properties detected for the material with its structure.

The X-ray data collection of crystal should have the criteria; (i) have a uniform internal structure (i.e. it must not be twinned or composed of microscopic sub-crystals. The existence of two different orientation of a lattice in one crystal is called twinning. The crystal should not be grossly fractured, bent or otherwise physically distorted. However, it need not have a uniform or neatly formed external surfaces) and (ii) it must be of average diffractive in size and shape (the preferred crystal size is 0.1-0.3 mm, but should not exceed 0.5 x 0.5 mm). An optical microscope is used to select the single crystal that satisfies above-mentioned properties prior to X-Ray data collection. It also helps in providing information regarding crystal morphology, size, shape, defects, color, and homogeneity.

1.7.1.2. Thermal analysis:

The thermal stability of open-framework materials is usually investigated by thermogravimetric analysis (TGA/DSC) (Fig. 1.25 and Fig. 1.26). The framework materials are heated in a steady heating rate under a flow of air or inert gas. The graph shows the stepwise weight loss measured with respect to rising in temperature. The weight loss shows the stepwise decomposition of the various constituent's species of framework materials present in the material. The residue left off can be utilized to verify the composition of the material with corroboration with powder X-ray diffraction technique.

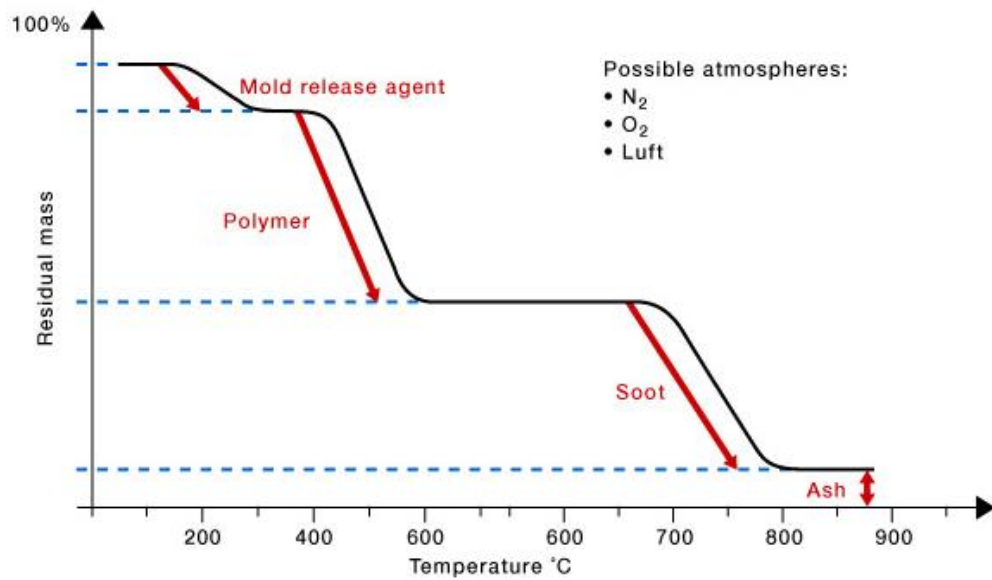


Fig.1.25. TGA profile diagram.

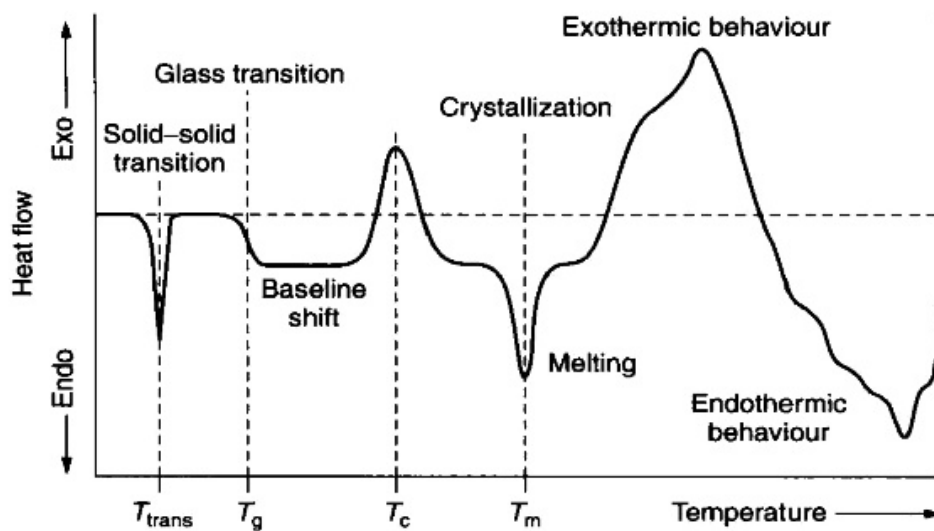


Fig. 1.26. DSC Profile diagram.

The thermal analysis of open-framework materials is also performed by differential calorimetry (DSC). The DSC measures the heat flow changes with rising temperature. The phase transition, glass transition temperature, crystallization, melting, exothermal and endothermal process are recorded as a peak in the thermogram (Fig 1.26).

Elemental Analysis:

The Elemental analysis can be performed by oxidative heating of microporous materials which provide the weight percentage of carbon, hydrogen, nitrogen and another element like halogen and sulfur. It provides the weight percentage of oxygen indirectly. It provides the compositional purity of the sample.

1.7.1.3. Gas adsorption study:

The free spaces or void or pore volume of open-framework materials can be investigated by adsorption isotherm. The adsorption isotherm study is performed by gases like N₂, CO₂, n-butane, alcohol, n-hexane, CH₄, H₂. The amount of gas molecule adsorbs by the materials tells us about the surface area and pore volumes. From the Adsorption-desorption isotherm curve, nature of pore surface in term of hydrophobicity, the hydrophilicity of materials can be derived.

1.7.1.4. Vibrating sample magnetometry (VSM):

VSM method gives helpful information on magnetic properties of materials. From these magnetic properties, one can derive information of the structure of materials, bonding pattern, energy level, oxidation state, connectivity of metal atoms and magnetic properties materials. In this method, the test sample is placed between the two poles of an electromagnet and attached to a high-frequency vibrating head (Fig 1.27). The magnetic moment of the sample is recorded with the variation of the magnetic field.

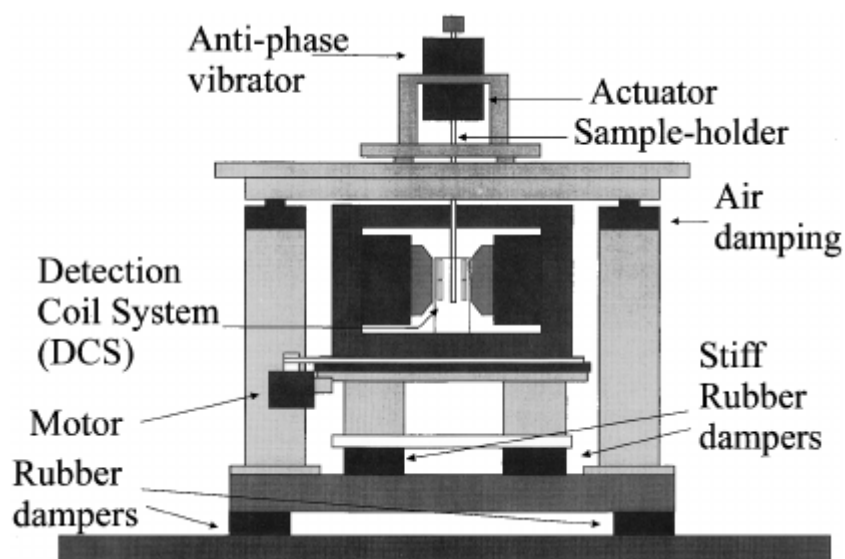


Fig. 1.27. Schematic diagram of VSM.

1.7.1.5. Fourier transfer infra-red spectroscopy:

Light in the IR region interacts with the vibration band in the molecule. When IR source light is passed on the sample, some light intensity absorbed by the sample vibration and some reflects. The functional groups have a finger-print vibrational band. So, FTIR spectroscopy is utilized in the identification of functional groups.

References:

- (1) Horcajada, P.; Chalati, T.; Serre, C.; Gillet, B.; Sebrie, C.; Baati, T.; Eubank, J. F.; Heurtaux, D.; Clayette, P.; Kreuz, C.; Chang, J.-S.; Hwang, Y. K.; Marsaud, V.; Bories, P.-N.; Cynober, L.; Gil, S.; Ferey, G.; Couvreur, P.; Gref, R. *Nat. Mater.* **2010**, *9*, 172.
- (2) Wu, M.-X.; Yang, Y.-W. *Adv. Mater.* **2017**, *29*, 1606134.
- (3) Li, R.-J.; Li, M.; Zhou, X.-P.; Li, D.; O'Keeffe, M. *Chem. Commun.* **2014**, *50*, 4047.
- (4) Xue, D.-X.; Belmabkhout, Y.; Shekhah, O.; Jiang, H.; Adil, K.; Cairns, A. J.; Eddaoudi, M. *J. Am. Chem. Soc.* **2015**, *137*, 5034.
- (5) Zhai, Q.-G.; Bu, X.; Mao, C.; Zhao, X.; Feng, P. *J. Am. Chem. Soc.* **2016**, *138*, 2524.
- (6) Bae, T.-H.; Lee, J. S.; Qiu, W.; Koros, W. J.; Jones, C. W.; Nair, S. *Angew. Chem. Int. Ed.* **2010**, *49*, 9863.
- (7) Chen, B.; Liang, C.; Yang, J.; Contreras, D. S.; Clancy, Y. L.; Lobkovsky, E. B.; Yaghi, O. M.; Dai, S. *Angew. Chem. Int. Ed.* **2006**, *118*, 1418.
- (8) Rodenas, T.; Luz, I.; Prieto, G.; Seoane, B.; Miro, H.; Corma, A.; Kapteijn, F.; Llabrés i Xamena, F. X.; Gascon, J. *Nat. Mater.* **2015**, *14*, 48.
- (9) Proch, S.; Herrmannsdörfer, J.; Kempe, R.; Kern, C.; Jess, A.; Seyfarth, L.; Senker, J. *Chem. Eur. J.* **2008**, *14*, 8204.
- (10) Sabo, M.; Henschel, A.; Frode, H.; Klemm, E.; Kaskel, S. *J. of Mater. Chem.* **2007**, *17*, 3827.
- (11) Lee, J.; Farha, O. K.; Roberts, J.; Scheidt, K. A.; Nguyen, S. T.; Hupp, J. T. *Chem. Soc. Rev.* **2009**, *38*, 1450.
- (12) Tiwari, R. K.; Behera, J. N. *Dalton Trans.* **2017**, *46*, 5911.

- (13) Sarkar, D.; Chandra Rao, P.; Aiyappa, H. B.; Kurungot, S.; Mandal, S.; Ramanujam, K.; Mandal, S. *RSC Adv.* **2016**, *6*, 37515.
- (14) Tian, Y.; Cong, J.; Shen, S.; Chai, Y.; Yan, L.; Wang, S.; Sun, Y. *Phys. Status Solidi* **2014**, *8*, 91.
- (15) Chen, Q.; Xue, W.; Lin, J.-B.; Wei, Y.-S.; Yin, Z.; Zeng, M.-H.; Kurmoo, M.; Chen, X.-M. *Chem. Eur. J.* **2016**, *22*, 12088.
- (16) Taylor, J. M.; Dawson, K. W.; Shimizu, G. K. H. *J. Am. Chem. Soc.* **2013**, *135*, 1193.
- (17) Umeyama, D.; Horike, S.; Inukai, M.; Itakura, T.; Kitagawa, S. *J. Am. Chem. Soc.* **2012**, *134*, 12780.
- (18) Sheberla, D.; Bachman, J. C.; Elias, J. S.; Sun, C.-J.; Shao-Horn, Y.; Dinca, M. *Nat. Mater.* **2017**, *16*, 220.
- (19) Sun, L.; Campbell, M. G.; Dincă, M. *Angew. Chem. Int. Ed.* **2016**, *55*, 3566.
- (20) Talin, A. A.; Centrone, A.; Ford, A. C.; Foster, M. E.; Stavila, V.; Haney, P.; Kinney, R. A.; Szalai, V.; El Gabaly, F.; Yoon, H. P.; Léonard, F.; Allendorf, M. D. *Science* **2013**, 1246738.
- (21) A. F. Cronstedt, K. *Vetenskaps, Akad. Handl. Stockholm*, **1756**, *17*, 120.
- (22) Cronstedt, A. F.; Schlenker, J. L.; Kuhl, G. *Akad. Handl. Stockholm*, **1756**, *17*, 123.
- (23) Damour, A. *Ann. Mines* **1840**, *17*, 191.
- (24) Friedel, G. *Bull. Soc. Fr. Minéral. Cristallogr* **1896**, *19*, 363.
- (25) Grandjean, F. C. R. *Seances Acad. Sci.* **1909**, *149*, 866.
- (26) Kim, M. J.; Jeong, M. S.; Kim, Y.; Seff, K. *Microporous, and Mesoporous Mater.* **1999**, *30*, 233.
- (27) Taylor, W.; Meek, C.; Jackson, W. Z. *Kristallogr.* **1933**, *84*, 373.
- (28) Taylor, W.; Jackson, R. Z. *Kristallogr.* **1933**, *86*, 53.

- (29) Barrer, R. M. *J. Chem. Soc.* **1948**, 127.
- (30) Morris, R. E.; Weigel, S. J. *Chem. Soc. Rev.* **1997**, 26, 309.
- (31) C. Baerlocher, W. M. Meier and D. H. Olson, eds., *Atlas of Zeolite Framework Types*, 5th Revised Edition (Elsevier, Amsterdam, 2001).
- (32) Price, G. D. *Geological Magazine* **2009**, 126, 446.
- (33) Weigel, O.; Steinhoff, E. *Z. Kristallogr.* **1925**, 61, 125.
- (34) Loewenstein, W. *Am. Mineral.* **1954**, 39, 92.
- (35) Estermann, M.; McCusker, L.; Baerlocher, C.; Merrouche, A.; Kessler, H. *Nature* **1991**, 352, 320.
- (36) Anderson, J.; Foger, K.; Mole, T.; Rajadhyaksha, R.; Sanders, J. *J. Catal.* **1979**, 58, 114.
- (37) Weisz, P. *Annu. Rev. Phys. Chem.* **1970**, 21, 175.
- (38) Csicsery, S. M. *Zeolites* **1984**, 4, 202.
- (39) E. G. Derouane, *Catalysis on The Energy Scene*, Kaliaguine, Mathay, eds., Elsevier, Amsterdam, 1984, 1.
- (40) Simmen, A.; McCusker, L.; Baerlocher, C.; Meier, W. *Zeolites* **1991**, 11, 654.
- (41) Bennett, J. M.; Kirchner, R. M. *Zeolites* **1992**, 12, 338.
- (42) Petrovic, I.; Navrotsky, A.; Davis, M. E.; Zones, S. I. *Chem. Mater.* **1993**, 5, 1805.
- (43) Henson, N. J.; Cheetham, A. K.; Gale, J. D. *Chem. Mater.* **1994**, 6, 1647.
- (44) Natarajan, S. V.; Rao, C. *J. Catal.* **2002**, 214.
- (45) Barrer, R.; Denny, P. *J. Chem. Soc. (Resumed)* **1961**, 971.
- (46) Kerr, G. T.; Kokotailo, G. T. *J. Am. Chem. Soc.* **1961**, 83, 4675.
- (47) Bibby, D.; Milestone, N.; Aldridge, L. *Nature* **1979**, 280, 664.

- (48) Meier, W.; Olson, D.; Baerlocher, C.; Butterworth-Heinemann, London: 1992.
- (49) Lii, K.-H.; Huang, Y.-F.; Zima, V.; Huang, C.-Y.; Lin, H.-M.; Jiang, Y.-C.; Liao, F.-L.; Wang, S.-L. *Chem. Mater.* **1998**, *10*, 2599.
- (50) Lok, B.; Cannan, T. R.; Messina, C. *Zeolites* **1983**, *3*, 282.
- (51) Parnham, E. R.; Wheatley, P. S.; Morris, R. E. *Chem. Commun.* **2006**, 380.
- (52) Cooper, E. R.; Andrews, C. D.; Wheatley, P. S.; Webb, P. B.; Wormald, P.; Morris, R. E. *Nature* **2004**, *430*, 1012.
- (53) Davis, M. E.; Lobo, R. F. *Chem. Mater.* **1992**, *4*, 756.
- (54) Zones, S.; Nakagawa, Y.; Yuen, L.-T.; Harris, T. *J. Am. Chem. Soc.* **1996**, *118*, 7558.
- (55) Li, J.; Yu, J.; Yan, W.; Xu, Y.; Xu, W.; Qiu, S.; Xu, R. *Chem. Mater.* **1999**, *11*, 2600.
- (56) Wilson, S. T.; Lok, B. M.; Messina, C. A.; Cannan, T. R.; Flanigen, E. M. *J. Am. Chem. Soc.* **1982**, *104*, 1146.
- (57) Wilson, S. T.; Lok, B. M.; Flanigen, E. M.; *Google Patents*: **1982**.
- (58) Chen, J.-S.; Pang, W.-Q.; Xu, R.-R. *Top. Catal.* **1999**, *9*, 93.
- (59) Davis, M. E.; Saldarriaga, C.; Montes, C.; Garces, J.; Crowdert, C. *Nature* **1988**, *331*, 698.
- (60) Kan, Q.; Glasser, F. P.; Xu, R. *J. Mater. Chem.* **1993**, *3*, 983.
- (61) Cavellec, M.; Riou, D.; Ninclaus, C.; Grenèche, J.-M.; Férey, G. *Zeolites* **1996**, *17*, 250.
- (62) Harrison, W. T.; Gier, T. E.; Stucky, G. D. *J. Mater. Chem.* **1991**, *1*, 153.
- (63) Feng, P.; Bu, X.; Tolbert, S. H.; Stucky, G. D. *J. Am. Chem. Soc.* **1997**, *119*, 2497.
- (64) Harrison, W. T.; Honnooman, L. *Angew. Chem. Int. Ed.* **1997**, *36*, 640.

- (65) Chen, J.; Natarajan, S.; Thomas, J. M.; Jones, R. H.; Hursthouse, M. B. *Angew. Chem. Int. Ed.* **1994**, *33*, 639.
- (66) Choudhury, A.; Neeraj, S.; Natarajan, S.; Rao, C. N. R. In *Adv. Chem. Ser.:* **2003**, p 489.
- (67) Natarajan, S.; Neeraj, S.; Choudhury, A.; Rao, C. N. R. *Inorg. chem.* **2000**, *39*, 1426.
- (68) Wang, M.; Luo, H.-B.; Liu, S.-X.; Zou, Y.; Tian, Z.-F.; Li, L.; Liu, J.-L.; Ren, X.-M. *Dalton Trans.* **2016**, *45*, 19466.
- (69) Wu, J.; Yan, Y.; Liu, B.; Wang, X.; Li, J.; Yu, J. *Chem. Commun.* **2013**, *49*, 4995.
- (70) Behera, J. N.; Rao, C. N. R. *Dalton Tran.* **2007**, 669.
- (71) Behera, J. N.; Bhattacharjee, J.; Horike, S.; Marri, S. R.; Dahiya, P. P. *RSC Adv.* **2014**, *4*, 50435.
- (72) Rao, C.; Behera, J.; Dan, M. *Chem. Soc. Rev.* **2006**, *35*, 375.
- (73) Morimoto, C. N.; Lingafelter, E. *Acta Crystallogr., Sect. B: Struct. Sci* **1970**, *26*, 335.
- (74) Choudhury, A.; Krishnamoorthy, J.; Rao, C. N. R. *Chem. Commun.* **2001**, 2610.
- (75) Nagaraja, C. M.; Behera, J. N.; Maji, T. K.; Pati, S. K.; Rao, C. N. R. *Dalton Trans.* **2010**, *39*, 6947.
- (76) Behera, J. N.; Rao, C. N. R. *J. Am. Chem. Soc.* **2006**, *128*, 9334.
- (77) Marri, S. R.; Kumar, J.; Panyarat, K.; Horike, S.; Behera, J. *Dalton Trans.* **2016**, *45*, 17792.
- (78) Ogiwara, N.; Inukai, M.; Itakura, T.; Horike, S.; Kitagawa, S. *Chem. Mater.* **2016**, *28*, 3968.
- (79) Halasyamani, P. S.; Poeppelmeier, K. R. *Chem. Mater.* **1998**, *10*, 2753.

- (80) Jin, G. B.; Skanthakumar, S.; Soderholm, L. *Inorg. Chem.* **2012**, *51*, 3220.
- (81) Behera, J. N.; Ayi, A. A.; Rao, C. N. R. *Chem. Commun.* **2004**, 968.
- (82) Porter, Y.; Bhuvanesh, N.; Halasyamani, P. S. *Inorg. chem.* **2001**, *40*, 1172.
- (83) Harrison, W. T.; Phillips, M. L.; Stanchfield, J.; Nenoff, T. M. *Angew. Chem. Int. Ed.* **2000**, *39*, 3808.
- (84) Choudhury, A.; Kumar, D.; Rao, C. N. R. *Angew. Chem. Int. Ed.* **2002**, *41*, 158.
- (85) Udayakumar, D.; Rao, C. *J. Mater. Chem.* **2003**, *13*, 1635.
- (86) Pasha, I.; Choudhury, A.; Rao, C. N. R. *Solid State Sci.* **2003**, *5*, 257.
- (87) Bang, S.-e.; Lee, D. W.; Ok, K. M. *Inorg. Chem.* **2014**, *53*, 4756.
- (88) Harrison, W. T. A.; Phillips, M. L. F.; Stanchfield, J.; Nenoff, T. M. *Inorg. Chem.* **2001**, *40*, 895.
- (89) Harrison, W. T. *J. Solid State Chem.* **2001**, *160*, 4.
- (90) Rojo, T.; Mesa, J. L.; Lago, J.; Bazan, B.; Pizarro, J. L.; Arriortua, M. I. *J. Mater. Chem.* **2009**, *19*, 3793.
- (91) Liang, J.; Li, J.; Yu, J.; Chen, P.; Fang, Q.; Sun, F.; Xu, R. *Angew. Chem. Int. Ed.* **2006**, *45*, 2546.
- (92) Sie, M.-J.; Lin, C.-H.; Wang, S.-L. *J. Am. Chem. Soc.* **2016**, *138*, 6719.
- (93) Lach, J.; Jeremies, A.; Lozan, V.; Loose, C.; Hahn, T.; Kortus, J.; Kersting, B. *Inorg. chem.* **2012**, *51*, 12380.
- (94) Bhat, G. A.; Vishnoi, P.; Gupta, S. K.; Murugavel, R. *Inorg. Chem. Commun.* **2015**, *59*, 84.
- (95) Yaghi, O.; Davis, C. E.; Li, G.; Li, H. *J. Am. Chem. Soc.* **1997**, *119*, 2861.
- (96) Tao, J.; Tong, M.-L.; Chen, X.-M. *J. Chem. Soc., Dalton Trans.* **2000**, 3669.
- (97) Du, M.; Chen, M.; Yang, X.-G.; Wen, J.; Wang, X.; Fang, S.-M.; Liu, C.-S. *J. Mater. Chem. A* **2014**, *2*, 9828.

- (98) Rao, C.; Natarajan, S.; Vaidhyanathan, R. *Angew. Chem. Int. Ed.* **2004**, *43*, 1466.
- (99) Oliver, S.; Kuperman, A.; Ozin, G. A. *Angew. Chem. Int. Ed.* **1998**, *37*, 46.
- (100) Dan, M.; Rao, C. *Angew. Chem. Int. Ed.* **2006**, *45*, 281.
- (101) Feng, P.; Bu, X.; Stucky, G. D. *Angew. Chem. Int. Ed.* **1995**, *34*, 1745.
- (102) Feng, S.; Xu, R. *Acc. Chem. Res.* **2001**, *34*, 239.
- (103) Rabenau, A. *Angew. Chem. Int. Ed.* **1985**, *24*, 1026.
- (104) Francis, R. J.; O'Hare, D.; Bhattacharyya, P.; Parr, J.; Ross, A. T.; Slawin, A. M.; Cotton, F. A.; Lin, C.; Murillo, C. A.; Scudder, M. *J. Chem. Soc., Dalton Trans* **1998**, 3133, 3148.
- (105) Herdtweck, E. *Z. Anorg. Allg. Chem.* **1983**, *501*, 131.
- (106) Davis, M. I.; Rubio, J. B.; Douhéret, G. *Thermochim. acta* **1995**, *259*, 177.

Chapter 2

ORGANICALLY-TEMPLATED/ CO-ORDINATED OPEN-FRAMEWORK

METAL SULFITES

Abstract	55
2.1. Introduction	55
2.2. Experimental section	59
2.2.1. Materials and methods	59
2.2.2. Syntheses of compounds 1-10	60
2.2.3 Characterization	62
2.2.3.1. Single crystal structure determination	62
2.2.3.2 Elemental analysis	63
2.3. Results and Discussion	64
2.3.1. Structural analysis of [(C₃H₁₀N)₂][Zn(SO₃)₂], 1	64
2.3.2. Structural analysis of [C₃H₁₂N₂][Zn(SO₃)₂], 2	67
2.3.3. Structural analysis of [C₄H₁₄N₂][Zn(SO₃)₂], 3	69
2.3.4. Structural analysis of [C₆H₁₈N₂][Zn(SO₃)₂], 4	71
2.3.5. Structural analysis of [C₄H₁₂N₂][Zn(SO₃)₂].H₂O, 5	75
2.3.6. Structural analysis of [C₄H₁₂N₂][Mn(SO₃)₂(H₂O)₂].2H₂O, 6	78
2.3.7. Structural analysis of [(C₃N₂H₁₀)₂NaCo(SO₃)₂(H₂O)₂].H₂O, 7	80
2.3.8. Structural analysis of [(C₆N₄H₁₈)Zn₃(SO₃)₃], 8	85
2.3.9. Structural analysis of [C₂H₁₀N₂][Zn₃(SO₃)₄], 9	88
2.3.10. Structural analysis of [CN₃H₆]₂[Zn(SO₃)₂], 10	92
2.3.10.1. Adsorption properties of [CN₃H₆]₂[Zn(SO₃)₂], 10	96
2.3.10.2. DSC analysis of [CN₃H₆]₂[Zn(SO₃)₂], 10	97
2.3.10.3. Dielectric constant analysis of [CN₃H₆]₂[Zn(SO₃)₂], 10	98

2.4. Thermal analysis	99
2.4.1. Thermogravimetric analysis of $[\text{CN}_3\text{H}_6]_2[\text{Zn}(\text{SO}_3)_2]$, 10	99
2.4.2. Temperature dependent PXRD analysis of $[\text{CN}_3\text{H}_6]_2[\text{Zn}(\text{SO}_3)_2]$, 10	101
2.5. Conclusions	102
References	104
Appendix	107
Summary	117

Abstract

*In this chapter, we are exploring sulfur based three-connected sulfite anions as secondary building units for generating open-framework materials and representing the ten organically templated metal sulfites namely $[(C_3H_{10}N)_2][Zn(SO_3)_2]$, **1**, $[C_3H_{12}N_2][Zn(SO_3)_2]$, **2**, $[C_4H_{14}N_2][Zn(SO_3)_2]$, **3**, $[C_6H_{18}N_2][Zn(SO_3)_2]$, **4**, $[C_4H_{12}N_2][Zn(SO_3)_2] \cdot (H_2O)$, **5**, $[C_4H_{12}N_2][Mn(SO_3)_2(H_2O)_2] \cdot 2H_2O$, **6**, $[(C_3N_2H_{10})_2NaCo(SO_3)_2(H_2O)_2] \cdot H_2O$, **7**, $[(C_6N_4H_{18})Zn_3(SO_3)_3]$, **8**, $[C_2H_{10}N_2][Zn_3(SO_3)_4]$, **9** and $(CN_3H_6)_2[Zn(SO_3)_2]$, **10** are synthesized under the hydrothermal condition, whereas these compounds demonstrate linear chain, coordination polymer, a layered and a three-dimensional framework by using various amine templates. These materials have been synthesized in a mild hydrothermal conditions and characterized by complimentary techniques such as single crystal X-ray diffraction (SCXRD), fourier transform infrared spectroscopy (FTIR), powder X-ray diffraction (PXRD) and thermogravimetric analysis (TGA). The compounds **1-6** show organically templated 1D linear metal sulfite structure, compounds **7** and **8** show the amine coordinated metal sulfite a layered structure, compound **9** has organically templated zinc sulfite which has a layered structure whereas compound **10** showing the organically templated a three-dimensional zinc-sulfite structure with diamondoid network. In compound **7**, the in-situ Co(II) oxidized to Co(III) during the reaction period.*

2.1 Introduction:

The crystalline microporous open-framework materials are extensively studied owing to their vast structural diversity and interesting application in catalysis, magnetism, gas separation and gas storage etc¹. The open-framework materials are of inorganic materials with permanent regular voids (size range 5-20 Å) and frequently known as molecular sieves or microporous materials. Zeolites or zeotypes open-frameworks belong to crystalline

aluminium silicate structure and composed of TO_4 tetrahedral (T = Si, Al) building unit with common oxygen atoms which connects the neighbouring tetrahedral building units.

The aluminium silicates open-framework materials are expanded to a vast research area by utilising various primary building units (PBUs) of structures having tetrahedral anions like phosphates, sulfates, selenates and tellurates etc²⁻⁷. These groups belong to group 14, 15 and 16 oxyanions showing the interesting novel topological structure and its applications⁸. One oxygen atom less from the tetrahedral unit i.e. the oxyanions of three-connected pyramidal primary building unit (PBUs) like phosphite, selenite, tellurites are additionally providing interesting structures with interesting properties⁹⁻¹¹.

CLO and JDF-20 zeolites have been formed from three-connected inorganic building unit (PBU like phosphite). They are low-density framework (11.1 T per 1000) with large pore size framework¹¹. The various three-connected PBUs like SnO_3^{4-} , SO_3^{2-} , SeO_3^{2-} , TeO_3^{2-} , and HPO_3^{2-} have pyramidal skeleton whereas three-connected BO_3^{3-} and CO_3^{2-} units are planar. The HPO_3^{2-} , SeO_3^{2-} and SnO_3^{4-} buildings units are more explored and their applications have been studied¹².

The formation of BO_3^{3-} unit is difficult as BO_4^{5-} associated cluster unit's formation is more favorable¹³⁻¹⁵. More studies based on CO_3^{2-} , phosphite anions and SeO_3^{2-} inorganic building units are well explored¹⁶⁻¹⁹. In phosphite anions, P exists in +3 and +5 oxidation states and both are stable at high temperatures. In the pyramidal selenite, the lone pair of electrons of Se(IV) is stereochemically active and control the non-centrosymmetric structure formation²⁰. The crystallization of metal selenite complex in polar (non-centrosymmetric) space group and provide physical properties like non-linear optical phenomenon for a second harmonic generation(SHG)^{20,21}.

The low reduction potential of Selenate (Se^{+6})/ Selenite (Se^{+4}) couple causes a Se^{+6} reduction to Se^{+4} and metallic Se (E_0 is 0.03 V). This limits the synthesis of amine-templated metal selenite open-framework at high temperature²². The structure of pyramidal sulfite anions is similar to pyramidal selenite. The sulfite based open-framework is less explored due to the high oxidation potential of sulfite (S^{+4})/ sulfate (S^{+6}) (E_0 is 0.119 V). The sulfite gets converted into sulfate under an acidic and hydrothermal condition at high temperature, hence the sulfate anions frameworks are extensively studied^{23,24}.

The trigonal pyramidal sulfite is a mild base and reducing agent as well as structure directing agent. The S in sulfite has +4 oxidation state and it has stereochemically active a lone pair of electrons. The lone pair of electrons is act like a structure directing agent. The metal-sulfite complexes crystallization in polar (non-centrosymmetric) space group and shows non-linear optical second harmonic generation (SHG)²⁵. Due to the similar structure of sulfite, selenite and tellurites anions, the metal frameworks are similar in structures²⁵. Aside from sulfur coordination, sulfite anions additionally provide more numbers of oxygen atoms for metal coordination, therefore it exhibits a various range of coordination modes which can be utilized to synthesize metal-sulfite compounds as shown in Fig. 2.1²⁶. Thus, investigation of the metal-sulfite coordination compounds opens up a new path for production of sulfite-based inorganic open-framework materials with interesting properties.

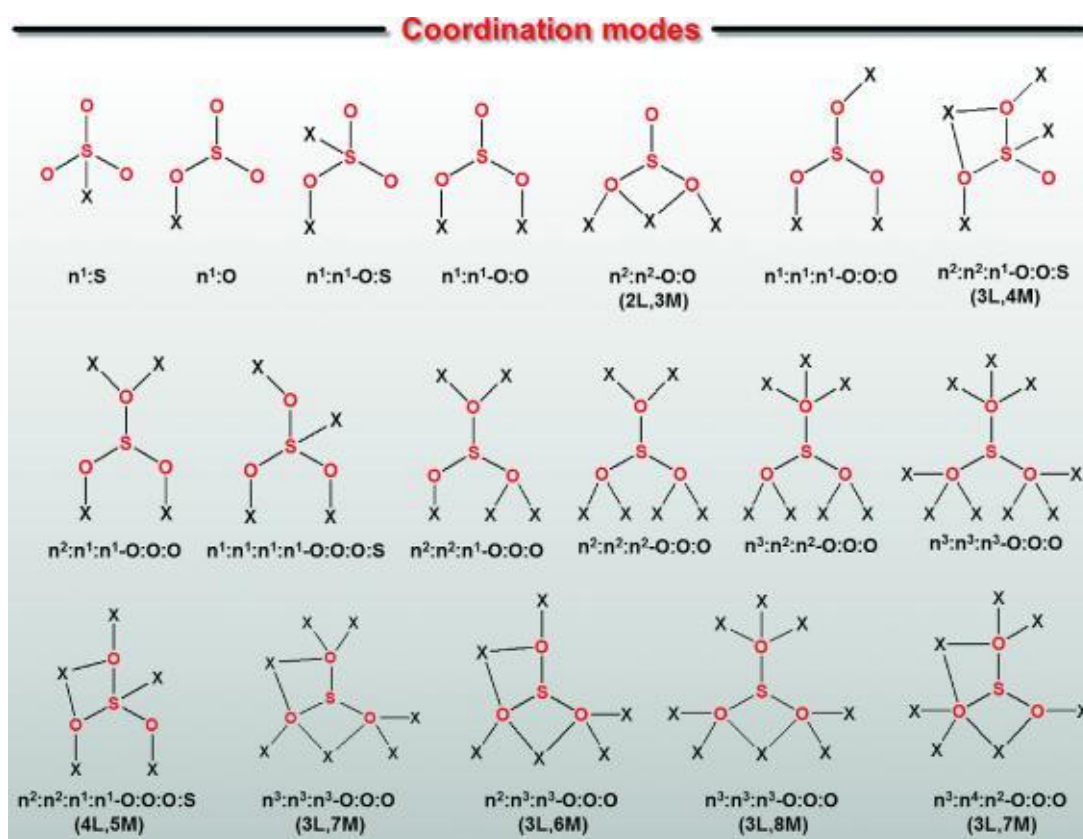


Fig. 2.1. The schematic representation of the observed coordination modes for the sulfite anion, where X is the transition metal and/or alkali metal.

In this work, we have explored sulfur based open-framework materials. In this system, S of sulfite is connected to three metal ions through oxygen atoms and form the PBUs. The ten organically templated metal-sulfite open-framework namely $[(C_3H_{10}N)_2][Zn(SO_3)_2]$, **1**, $[C_3H_{12}N_2][Zn(SO_3)_2]$, **2**, $[C_4H_{14}N_2][Zn(SO_3)_2]$, **3**, $[C_6H_{18}N_2][Zn(SO_3)_2]$, **4**, $[C_4H_{12}N_2][Zn(SO_3)_2] \cdot (H_2O)$, **5**, $[C_4H_{12}N_2][Mn(SO_3)_2(H_2O)_2] \cdot 2H_2O$, **6**, $[(C_3N_2H_{10})_2NaCo(SO_3)_2(H_2O)_2] \cdot H_2O$, **7**, $[(C_6N_4H_{18})Zn_3(SO_3)_3]$, **8**, $[C_2H_{10}N_2][Zn_3(SO_3)_4]$, **9** and $[CN_3H_6]_2[Zn(SO_3)_2]$, **10** are synthesized under hydrothermal condition. The compounds **1-6** shows organically templated 1D linear metal-sulfites open-framework. Compounds **7** and **8** show the amine coordinated metal-sulfite a layered structure. The compound **9** has organically templated zinc-sulfite open-framework with a layered structure, whereas compound **10** display the organically templated zinc-sulfite three-

dimensional structure with a diamondoid network. In compound **7**, the in-situ Co(II) oxidized to Co(III) during the reaction period²⁷.

2.2. Experimental section

2.2.1. Materials and methods:

Zinc (II) acetate dihydrate ($\text{Zn(OAc)}_2 \cdot 2\text{H}_2\text{O}$, 99.5%), Co (II) acetate tetrahydrate ($\text{Co(OAc)}_2 \cdot 4\text{H}_2\text{O}$, 99.5%), Manganese (II) acetate tetrahydrate ($\text{Mn(OAc)}_2 \cdot 4\text{H}_2\text{O}$, 99.5%); 1, 3-diaminopropane (DAP, 98%); 1, 4-diaminobutane (DAB, 98%); hexamethylenediamine (HMDA, 97%); piperazine (PIP, 98%); *tris*-(2-aminoethyl) amine (TAEA, 98%); ethylenediamine (EN, 97%); were purchased from Sigma-Aldrich. Guanidine carbonate (GC, 99%). Sodium disulfite ($\text{Na}_2\text{S}_2\text{O}_5$, 98%) were purchased from Merck, PA= *n*-propylamine was purchased from spectrochem.

All the compounds **1-10** were characterized by X-ray Diffraction (XRD), fourier transform infrared spectroscopy (FTIR) and thermogravimetric analysis (TGA). The XRD data were collected using a Bruker D8 advance X-ray powder diffractometer using *CuK α* radiation ($\lambda = 1.5418 \text{ \AA}$), radiation in the range of $5^\circ < 2\theta < 55^\circ$. The step size used was 0.02° and exposure time 1 s for each step and the voltage and current were used 40 kV and 40 mA. IR spectra were recorded on a 'Perkin Elmer FTIR spectrometer' equipped with an attenuated total reflectance accessory. The sample was mixed with KBr and pressed. The pressed samples were scanned in the spectral region of $400 - 4000 \text{ cm}^{-1}$ with a resolution of 4 cm^{-1} . Thermogravimetric analyses (TGA) were carried out using a Discovery TGA by TA Instruments-Waters Lab at a heating rate of $10 \text{ }^\circ\text{C}/\text{min}$ under constant nitrogen gas flow. Differential scanning calorimetry was performed using a Mettler Toledo with version 5.1 Stare software. Aluminium crucibles with lids were used to hold samples of known

weight (5 mg) for DSC analysis. The data were collected from -120 °C to 475 °C at a heating rate of 10° C/min constant argon gas flow.

2.2.2 Syntheses of compounds 1-10:

The amine templated metal sulfites compounds **1-10** were synthesized under hydrothermal method at mild condition utilizing a mixture containing a metal salt, organic amine, and sodium disulfite and sodium bisulfite as the source of sulfite anions. In general, compound **1** was synthesized by a mixture of zinc acetate dihydrate (0.219 g), sodium disulfite (0.380 g) and *n*-propylamine (0.224 mL) were dissolved in distilled water (3.0 mL) under constant stirring. The reaction mixture was stirred for 25 minutes at room temperature to get a homogeneous solution. Finally, the reaction mixture having molar compositions of $\text{Zn}(\text{OAc})_2/3.0 \text{ Na}_2\text{S}_2\text{O}_5/n\text{-PA}/155 \text{ H}_2\text{O}$ were transferred and sealed in a 15 mL polypropylene bottle, which heated at 100 °C. Initially, the pH of the reaction mixture was approximately 6.0 which remained almost the same during the reaction period. After 72 h the reaction mixture was cooled to ambient temperature naturally, the few colorless single crystals were obtained at the bottom of the bottle due to less yield, where the other important characterization of compound **1** was unable to perform. The other organically templated zinc sulfite compounds **2-9** were synthesized by following similar reaction condition as described for compound **1** with the addition of the different organic amine and sulfite source and the details for the respective reaction parameter are employed are listed in Table 2.1. For the synthesis of compound **10**, zinc acetate dihydrate (0.220 g) was dissolved in 3.0 mL distilled water (3 mL) and sodium disulfite (0.389 g) was added under constant stirring. Finally, guanidine carbonate (0.300 g) was added to the reaction mixture. The reaction mixture was stirred for an additional 30 minutes. The resulting reaction mixture having pH 6 was transferred to a 15 mL polypropylene bottle with the molar compositions of $\text{Zn}(\text{OAc})_2/3.0 \text{ Na}_2\text{S}_2\text{O}_5/1.66 \text{ GC}/155 \text{ H}_2\text{O}$ was sealed and heated at 75°C

for 24 h. After slow cooling of the reaction mixture to room temperature, resulting in transparent crystals with 62% yield.

Table 2.1. Synthetic conditions and molar ratios for the preparation of compounds 1-10.

	Starting composition (in mM) [#]	T [°C]	T [h]	p H	Formula	Yield (%)
1	Zn(OAc) ₂ .2H ₂ O:3.0 Na ₂ S ₂ O ₅ :4.0 PA:155 H ₂ O	100	72	6	[(C ₃ H ₁₀ N) ₂][Zn(SO ₃) ₂]	2-3%
2	Zn(OAc) ₂ .2H ₂ O:2.0 Na ₂ S ₂ O ₅ :1.0 DAP:155 H ₂ O	90	72	6	[C ₃ H ₁₂ N ₂][Zn(SO ₃) ₂]	70
3	Zn(OAc) ₂ .2H ₂ O:2.0 Na ₂ S ₂ O ₅ :1.0 DAB:155 H ₂ O	90	72	6	[C ₄ H ₁₄ N ₂][Zn(SO ₃) ₂]	68
4	Zn(OAc) ₂ .2H ₂ O:2.0 Na ₂ S ₂ O ₅ :1.0 HMDA:155 H ₂ O	90	72	6	[C ₆ H ₁₈ N ₂][Zn(SO ₃) ₂]	56
5	Zn(OAc) ₂ .2H ₂ O:2.0 Na ₂ S ₂ O ₅ :2.56 PIP:155 H ₂ O	75	24	6	[C ₄ H ₁₂ N ₂][Zn(SO ₃) ₂].H ₂ O	65
6	Mn(OAc) ₂ .4H ₂ O:3.0 Na ₂ S ₂ O ₅ :2.0 PIP:155 H ₂ O	100	120	6	[C ₄ H ₁₂ N ₂][Mn(SO ₃) ₂ (H ₂ O) ₂].2H ₂ O	62

7	Co(OAc) ₂ .4H ₂ O:2.0 Na ₂ S ₂ O ₅ :2.0 DAP:155 H ₂ O	75	72	8	[(C ₃ N ₂ H ₁₀) ₂ NaCo(SO ₃) ₂ (H ₂ O) ₂]. H ₂ O	61
8	Zn(OAc) ₂ .2H ₂ O:2.0 Na ₂ S ₂ O ₅ :1.0 TAEA:155 H ₂ O	85	72	8	[(C ₆ N ₄ H ₁₈)Zn ₃ (SO ₃) ₃]	68
9	Zn(OAc) ₂ .2H ₂ O:2.0 Na ₂ S ₂ O ₅ :1.0 EN:155 H ₂ O	90	72	6	[C ₂ H ₁₀ N ₂][Zn ₃ (SO ₃) ₄]	56
10	Zn(OAc) ₂ .2H ₂ O:2.0 Na ₂ S ₂ O ₅ :1.66 GC:155 H ₂ O	75	24	5	[CN ₃ H ₆] ₂ [Zn(SO ₃) ₂]	62

#PA= *n*-propylamine; DAP = 1, 3-diaminopropane; DAB = 1, 4-diaminobutane; HMDA = hexamethylenediamine; PIP = piperazine; TAEA = *tris*-(2-aminoethyl) amine; EN = ethylenediamine; GC = guanidine carbonate.

2.2.3. Characterization:

2.2.3.1. Single crystal structure determination:

A suitable single crystals of compounds **1-10** were carefully selected under a polarizing microscope and mounted at the tip of the thin glass fiber for X-ray diffraction data collection. Structures were solved by the direct method using SHELXTL and refined on F^2 by a full-matrix least-squares technique using the SHELXS-97 program package²⁸. An empirical absorption correction based on symmetry-equivalent reflections was applied using SADABS²⁹. The graphics programs DIAMOND³⁰ and ORTEP³¹ were used to draw the structures^{32,33}. The non-hydrogen atoms were refined anisotropically. In the refinement, hydrogen atoms were treated as riding atoms using the SHELXL default parameters.

Details of crystal structure refinement parameters for compounds **1-10** are given in Table 2.2 (Appendix-1). And the H-bonding interaction and other short interactions are provided in Table 2.4 (Appendix-1).

2.2.3.2 Elemental Analysis

Anal for $[\text{C}_3\text{H}_{12}\text{N}_2][\text{Zn}(\text{SO}_3)_2]$, **2**; Calc: C, 11.94; H, 4.01; N, 9.29; S, 21.26 % Found: C, 11.85; H, 4.05; N, 9.11; S, 21.17 %; Anal for $[\text{C}_4\text{H}_{14}\text{N}_2][\text{Zn}(\text{SO}_3)_2]$, **3**; Calc: C, 15.22; H, 4.47; N, 8.87; S, 20.31 % Found: C, 15.11; H, 4.59; N, 8.73; S, 20.23 %; Anal for $[\text{C}_6\text{H}_{18}\text{N}_2][\text{Zn}(\text{SO}_3)_2]$, **4**; Calc: C, 20.96; H, 5.28; N, 8.15; S, 18.66 % Found: C, 20.92; H, 5.25; N, 8.20; S, 18.58 %; Anal for $[\text{C}_4\text{H}_{12}\text{N}_2][\text{Zn}(\text{SO}_3)_2]\cdot\text{H}_2\text{O}$, **5**; Calc: C, 14.48; H, 4.25; N, 8.45; S, 19.33 % Found: C, 14.42; H, 4.30; N, 8.42; S, 19.23 %; Anal for $[\text{C}_4\text{H}_{12}\text{N}_2][\text{Mn}(\text{SO}_3)_2(\text{H}_2\text{O})_2]\cdot 2\text{H}_2\text{O}$, **6**; Calc: C, 12.80; H, 5.37; N, 7.46; S, 17.09 % Found: C, 12.72; H, 5.42; N, 7.50; S, 17.01 %; Anal for $[(\text{C}_3\text{N}_2\text{H}_{10})_2\text{NaCo}(\text{SO}_3)_2(\text{H}_2\text{O})_2]\cdot\text{H}_2\text{O}$ **7**; Calc: C, 16.22; H, 5.90; N, 12.61; S, 14.43 % Found: C, 16.18; H, 5.96; N, 12.57; S, 14.40 %; Anal. For $[(\text{C}_6\text{N}_4\text{H}_{18})\text{Zn}_3(\text{SO}_3)_3]$, **8**; Calc: C, 12.37; H, 3.11; N, 9.62; S, 16.51% Found: C, 12.32; H, 3.16; N, 9.58; S, 16.48 %; anal. for $(\text{NH}_3\text{CH}_2\text{CH}_2\text{NH}_3)[\text{Zn}_3(\text{SO}_3)_4]$, **9**; Calc: C, 4.15; H, 1.74; N, 4.84; S, 22.17 % Found: C, 4.21; H, 1.68; N, 4.80; S, 22.09 %; anal. $(\text{CN}_3\text{H}_6)_2[\text{Zn}(\text{SO}_3)_2]$, **10**; Calc: C, 6.95; H, 3.50; N, 24.31; S, 18.55 % Found: C, 6.88; H, 3.58; N, 24.21; S, 18.69 %.

FTIR (KBr, cm^{-1}) for compound **2**: 3431 br, 2924 m, 1638 s, 1532 m, 1478 s, 1413 s, 1221 s, 1144 b, 992 s, 968 s, 932 s, 884 s, 643 m, 490 m; for compound **3**: 3332 br, 2945 m, 1645 s, 1523 m, 1160 b, 960 s, 928 s, 616 m, 512 m; for compound **4**: 3323 br, 3018 m, 1616 s, 1472 m, 1112 b, 932 s, 875 s, 618 m, 512 m; for compound **5**: 3354 br, 3030 m, 1595 s, 14770 m, 1096 b, 969 s, 904 s, 618 m, 489 m; for compound **6**: 3258 br, 3020 m, 1628 s, 1458 m, 1096 b, 961 s, 910s, 636 m, 496 m; for compound **7**: 3406 br, 2985 m, 1595 s,

1467 m, 1237 s, 1030 s, 965 m, 934m, 621 m, 473 m; for compound **8**: 3424br, 2997m, 1580 s, 1472 m, 1086 b, 969 s, 932s, 623 m, 486 m; for compound **9**: 3307 br, 3012 m, 2920 m, 1635 m, 1530 m, 1385 w, 1145 s, 990-960 m, 925 s, 880 s, 645 m, 610 m, 530 m, 475 m; for compound **10**: 3430 br, 3185 s, 2791 w, 1670 s, 1117 m, 1045 s, 908 s, 834 s, 660 m, 620 m, 515 m.

2.3. Results and discussion

Metal sulfites open-framework were successfully synthesized under the mild hydrothermal method in low temperature (temperature range 70 to 100 °C). By using different metal acetate, sulfite, and different organic amine, we have synthesized 10 metal sulfite open-framework materials. Metal sulfite compounds **1-6** have a 1D chain, compounds **7-9** have a layered structure and compound **10** has 3D diamondoid network structure.

2.3.1. Structural analysis of $[(C_3H_{10}N)_2][Zn(SO_3)_2]$, **1**:

The single crystal (SCXRD) data analysis of compound **1** reveals that the colorless crystals of compound **1** crystallize in the achiral *Pbcn* space group having an orthorhombic crystal system which features a one-dimensional chain structure. The ORTEP diagram showing the molecular unit in Fig. 2.2, the asymmetric unit of compound **1** contain 9 non-hydrogen atoms which include one Zn(II) atoms with half occupancy, one SO_3^{2-} anion and one protonated propylamine. The anionic framework was neutralized by protonated propylamine cations. The crystal structure refinement parameters for compounds **1-10** are given in Table 2.2. The Zn(II) atoms show a four-coordinated distorted tetrahedral geometry and the surrounding environments of Zn(II) atoms is constituted by the four oxygen atoms shared with four different sulfite anions (Zn-O1 = 1.9445(12) Å; Zn-O2 = 1.9683(12) Å and corresponding symmetry equivalents). The average bond length of Zn-O

is 1.9564 Å which are within the normal range as accounted in the literature for other similar Zn-compounds³⁴. The selected bond lengths are given in Table 2.3 (Appendix-1).

The crystal lattice of compound **1** is shown in Fig. 2.2b, the ZnO₄ tetrahedrons are connected with two O-S-O bridges of two SO₃²⁻ anions through vertices sharing, which shows the formation of infinite 1D chain extending along the crystallographic *c*-axis. The SO₃²⁻ anion is providing its two oxygen atoms for bonding with Zn atoms in the fashion of μ^2 - η^1 : η^1 -O:O coordination mode. Hence, the Zn(II) ions coordinated with sulfite anion, which results in the formation of interlinked dimeric Zn₂S₂ unit (the bridging oxygen atoms are ruled out) to create a 1D chain running down along the *c*-axis (Fig. 2.2c). The two adjacent Zn atoms are separated by a distance within the [Zn(SO₃)]_∞ chain is 3.8735(1) Å.

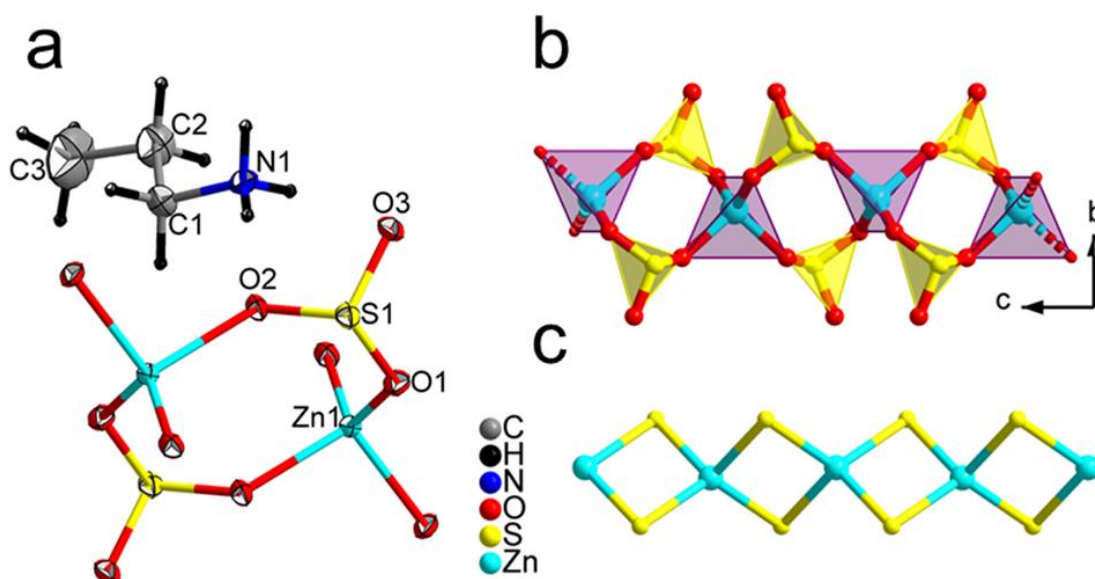


Fig. 2.2. (a) ORTEP diagram of compound **1** at 25% ellipsoidal probability level where asymmetric unit atoms were labeled, (b) Formation of the 1D chain due to zinc sulfite coordination (part of the lattice is omitted for clarity) and (c) Interconnected Zn₂S₂ dimeric units to generate 1D chain (the oxygen atom were ignored).

In the lattice of compound **1**, the protonated amines are situated in the anionic interchain space which acts as an organic template and additionally balances the charge required for neutralization of anionic framework in the crystal lattice (Fig. 2.3a). The two 1D chains are separated with distance 8.72 Å along the *b*-axis (Zn···Zn interchain) and the interplanar distance between two consisting Zn(II) ions along the *a*-axis is 11.08 Å, which additionally demonstrates in the unit cell parameters of compound **1**.

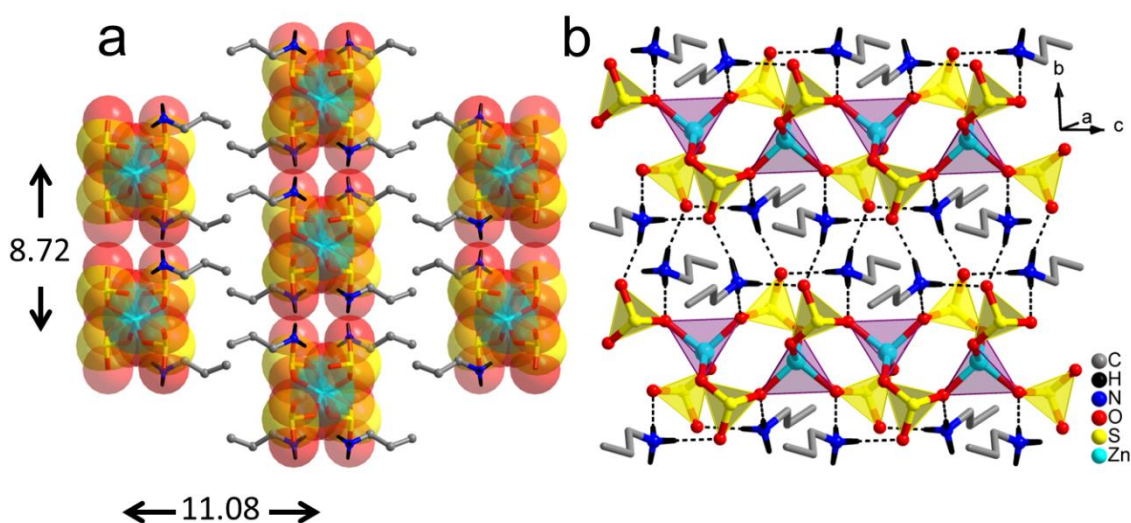


Fig. 2.3. (a) Crystal lattice of compound **1** as observed along the *c*-axis showing the interchain space where the [Zn(SO₃)]_∞ chain in the space-filling model and (b) A layered structure as a result of H-bonding interaction (shown with fragmented bonds and hydrogen on carbon are omitted).

The H-bonding interactions are enhanced by the protonated amine, which interlinks the chains along the *b*-axis, which extends the lattice in the *bc*-plane prompting an H-bonded layered structure (Fig. 2.3b). Interestingly, in the sulfite anions, all the S-O bond distances are unequal and one of the S1-O3 bond distance is 1.484 Å which indicates the double bond character for O3 oxygen atom which in-turn recommends an uneven electron distribution. The non-bonding oxygen atoms O3 takes part in strong bifurcated H-bonding by

simultaneously acting as an acceptor for N1-H1A and N1-H1C hydrogen atoms with $d_{\text{N1-H1A}\cdots\text{O3}} = 1.932(16)$ and $d_{\text{N1-H1C}\cdots\text{O3}} = 1.91(2)$ Å respectively, which are provided by two different protonated amines. The organic appendage of amine is located in between the H-bonded layers along the *a*-axis. The third hydrogen atom is engaged in an H-bonding interaction with the O2 oxygen atom of the sulfite anion, the H-bonding distance of $d_{\text{N1-H1B}\cdots\text{O2}}$ is 1.97(2) Å which further provide the stability to the lattice. The complete list of various H-bonding interactions is given in Table 2.4 (Appendix 1).

After having access to crystal structure with a mono amine, we wished to incorporate *bis*-substituted amine into the crystal lattice and studied its influence on the crystal lattice. We employed acyclic as well as cyclic amines for this purpose.

2.3.2. Structural analysis of [C₃H₁₂N₂][Zn(SO₃)₂], **2**:

The SCXRD analysis of compound **2** reveals that the plate shape colorless crystals adopt achiral *Pbcm* space group in an orthorhombic crystal system, which featured 1D chain structure and formulated as [C₃H₁₂N₂][Zn(SO₃)₂]. The asymmetric unit of compound **2** contains one 50% occupancy of Zn(II) ions, one sulfite anions, and half molecules of protonated 1,3-DAP units which collectively have 8 non-hydrogen atoms. In the part of the crystal structure of compound **2**, the central metal Zn(II) ions have a tetrahedral structure, which is composed of surrounding four oxygen atoms of sulfite anions through Zn-O-S linkage (Fig. 2.4a). In the zinc tetrahedron, the average Zn-O bond length is 1.9545 Å, whereas in pyramidal SO₃²⁻ anion, the average S-O bond length is 1.5311 Å and non-bonded S1-O2 bond distance is 1.5046 Å. All the bond lengths are in the normal range³⁴. The Zn atoms have +2 oxidation states as per bond valence sum calculations³⁵. The half molecules of protonated 1,3-DAP are occupied in the interchain space.

In the part of the crystal lattice of compound **2**, the strictly alternate arrangement of tetrahedron ZnO_4 and pyramidal SO_3^{2-} anions through vertices sharing (common oxygen atoms), which results in an infinite 1D chain running down through the crystallographic c -axis, similar trends are found in compound **1**. The SO_3^{2-} anion is shared its two oxygen atoms with Zn atoms with μ^2 - η^1 : η^1 -O:O coordination mode. Hence, the Zn(II) ions coordinated with sulfite anion, which results in the formation of interlinked Zn_2S_2 dimeric unit (the bridging oxygen atoms were omitted) to form a 1D-chain along c -axis as shown in Fig. 2.2c. The 1D chain trends similar to compound **1** and described in compound **1**.

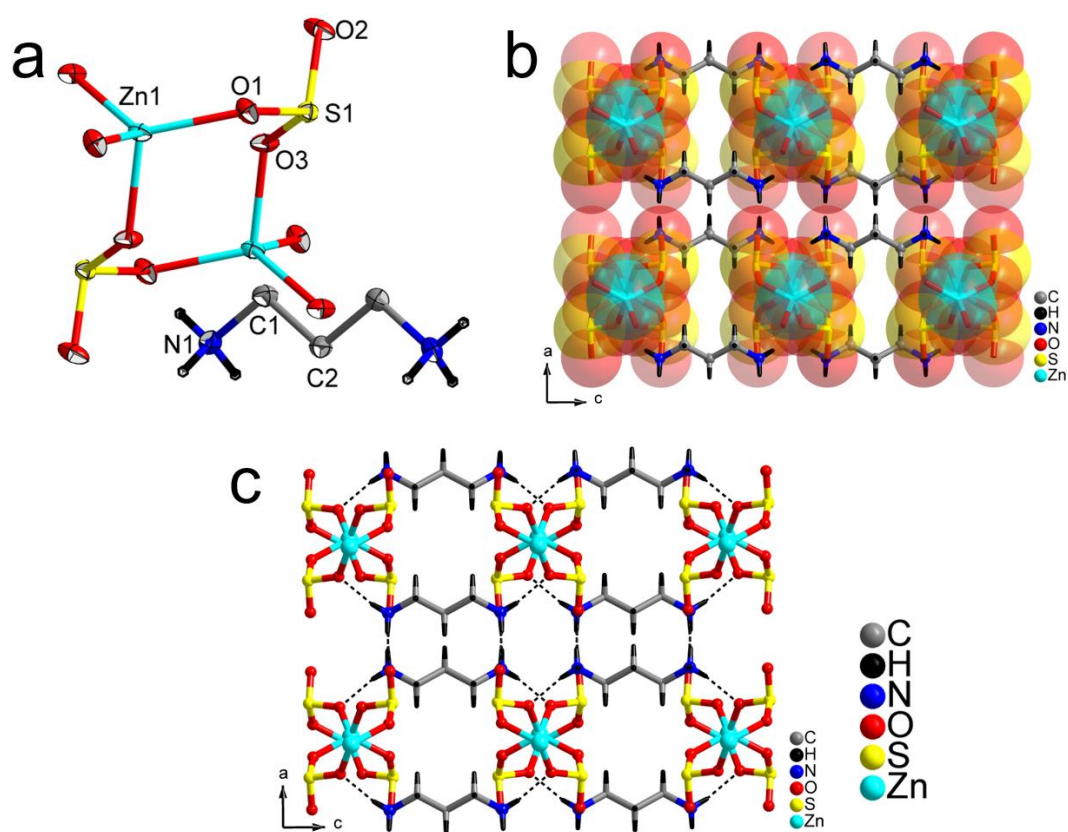


Fig. 2.4. (a) The molecular structure of compound **2** with unique atoms are labeled (ellipsoid probability is 25%), (b) Part of the crystal lattice of compound **2** viewed along b -axis (space fill model) compound **2** and (c) H-bonding pattern in compound **2**.

In the crystal lattice of compound **2**, the organic template 1,3-DAP is located in the space between the two Zinc sulfite chains (Fig. 2.4). The compound **2** gets extra stability from H-

bonding. The H-bonding are playing an important role in enhancing the dimensionality of the structure. The intricate H-bonding are involved in between all hydrogen atoms of protonated amine and the oxygen atoms of sulfite anions. The non-bonding oxygen atoms O2 of sulfite anions involved in the bifurcated intricate H-bonding (which provide strong interaction) with N1 of a terminal organic amine, which extends from both the ends and generates an infinite H-bonded three-dimensional network (Fig. 2.4c). The H-bond distance of $d_{N1-H1A...O2}$ 1.93(4) Å and $d_{N1-H1C...O2}$ 1.88(2) Å. Further, the bonded oxygen atoms of sulfite are involved in the H-bonding with hydrogen atoms of protonated amines. The H-bond distance is $d_{N1-H1B...O3}$ 1.97(3) Å. These H-bonding interactions make the lattice in orthogonal plane regard to 1D polymeric chain forming in an H-bonded 3D structure.

2.3.3 Structural analysis of [C₄H₁₄N₂][Zn(SO₃)₂], **3**:

The crystallographic analysis of a single crystal data reveals that the colorless crystals of compound **3** crystallized in centrosymmetrically *C2/c* space group in the monoclinic crystal system, which has formula [C₄H₁₄N₂][Zn(SO₃)₂], **3** and observed 1D polymeric chain. The repeating unit in the crystal lattice of compound **3** constitutes of 8 non-hydrogen atoms, where 5 atoms belong to the inorganic framework which are half occupied Zn(II) ion, one SO₃²⁻ anion and remaining 3 atoms belong to half molecules of protonated diaminobutane cations. The crystallographic distinct Zn atoms present at the centre of inversion, which shares its four oxygen atoms with neighboring four sulfite anions through Zn-O-S linkage (corner sharing) and provides tetrahedral arrangement around Zn(II) ions (Fig. 2.5). The Zn-O bond length in ZnO₄ is 1.9641 Å and 1.9383 Å, whereas in the pyramidal SO₃²⁻, S-O bond lengths are 1.5406 Å and 1.5214 Å and the non-bonded S1-O2 bond length is 1.50 Å. All the bond length are in the acceptable range³⁶. The protonated amine 1,4-diaminobutane occupied in the interchain space.

In the part of the crystal lattice of compound **3**, tetrahedron ZnO_4 and pyramidal SO_3^{2-} are successively arranged through corner sharing (common oxygen) linkage, which extend in crystallographic the c -axis, resulting in an infinite 1D chain, this is again similar to $[\text{ZnSO}_3]^{2-}$ chain in compound **1**. The SO_3^{2-} anion is coordinated with two Zn(II) ions through oxygen atoms in μ^2 - η^1 : η^1 -O:O trends of coordination mode. Hence, the Zn(II) ions coordinated with sulfite anions, which results in the formation of interlinked Zn_2S_2 dimeric unit (the bridging oxygen atoms were ruled out) to form a 1D chain along the c -axis as shown in Fig. 2.1c.

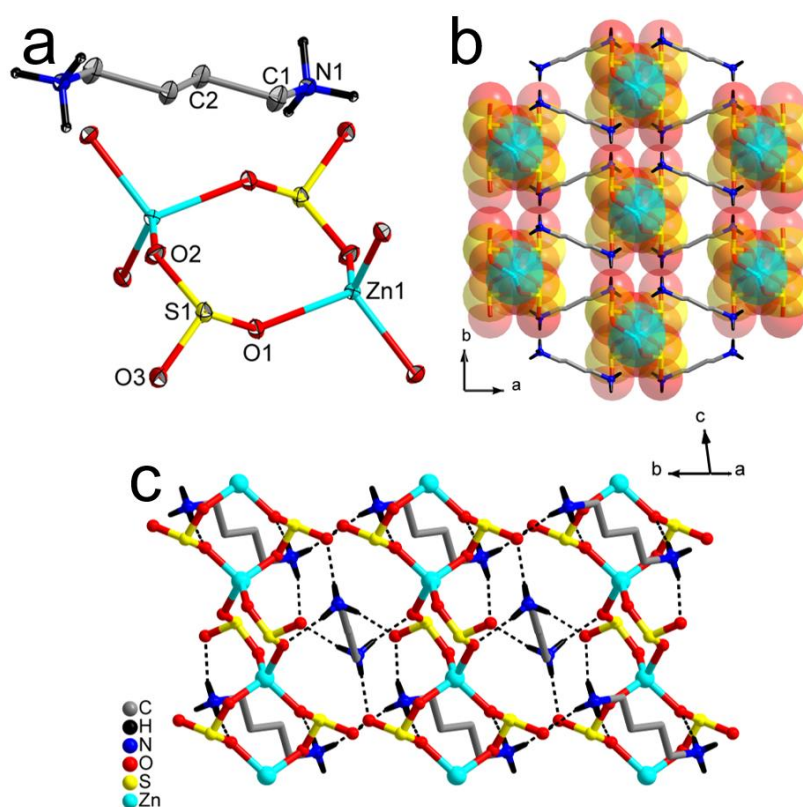


Fig. 2.5. (a) The molecular structure of compound **3** with unique atoms are labeled (ellipsoid probability is 25 %), (b) Part of the crystal lattice of compound **3** viewed along the c -axis (space fill model) compound **3** and (c) H-bonding pattern in compound **3**.

In the crystal lattice of compound **3** is shown in Fig. 2.5, the organic template 1,3-DAB is sited in the space between the two chains. The intricate H-bonding is playing an important

role in enhancing the dimensionality of the structure. Furthermore, H-bonding enhances the stability of the framework. The intricate H-bonding interactions are involved in between all hydrogen atoms of protonated amine and oxygen atoms of sulfite anions. The non-bonding oxygen atom O2 of sulfite anions involved in bifurcated intricate H-bonding (which provide strong interaction) with N1 of terminal organic amine, which extends from both the ends and generates an infinite H-bonded three-dimensional network (Fig. 2.5c). The H-bond distance of $d_{N1-H1B...O3}$ 1.94(3) Å and $d_{N1-H1C...O3}$ 1.90(4) Å. Further, the bonded oxygen atoms of sulfite are involved in the H-bonding with hydrogen atoms of protonated amines. The H-bond distance is $d_{N1-H1A...O1}$ 2.03(3) Å. These H-bonding interactions make the lattice in orthogonal plane regard to 1D polymeric chain forming in an H-bonded 3D-structure.

2.3.4. Structural analysis of $[C_6H_{18}N_2][Zn(SO_3)_2]$, **4**:

The crystallographic data analysis of compound **4** suggests that plate shape colorless crystal adopt the monoclinic crystal system with achiral $C2/c$ space group, the compound **4** show 1D polymeric chain and formulated as $[C_6H_{18}N_2][Zn(SO_3)_2]$, **4**. The asymmetric unit contains 9 non-hydrogen atoms, where 5 atoms from the inorganic framework which are one Zn(II) ion with half occupancy, one SO_3^{2-} anion and rest of 3 atoms from the extra-framework cations i.e. half-molecule of a protonated diaminohexane cation. In the crystal lattice of compound **4** is shown in Fig. 2.6. The independent Zn(II) ions have a tetrahedral structure, the coordination environment of Zn(II) ions is constituted of surrounding four oxygen atoms from four sulfite anions with Zn-O-S linkage (corner sharing). The Zn-O bond lengths in ZnO_4 are ranges from 1.9402-1.9623 Å, whereas in the SO_3^{2-} anions, the bonded S-O bond lengths are 1.5439 Å and 1.5187 Å and the non-bonded S1-O2 bond length is 1.4984 Å. All the bond lengths are in the normal range. The protonated amine 1,6-diaminohexane occupied in the space between two chains.

In the part of the crystal lattice, the pyramidal SO_3^{2-} and tetrahedron ZnO_4 are connected uniformly extends and running down along the crystallographic c -axis, which produced in an infinite 1D chain, this is again similar to $[\text{ZnSO}_3]^{2-}$ chain in compound **1**. The SO_3^{2-} anion is coordinated to two oxygen atoms of Zn atoms in μ^2 - η^1 : η^1 -O:O coordination mode. Hence, the Zn(II) ions coordinated with sulfite anion, which results in the formation of interlinked Zn_2S_2 dimeric unit (the bridging oxygen atoms are ruled out) to form a 1D chain along the c -axis (Fig. 2.1c). A similar trend is found in compound **1** and depicted in compound **1**.

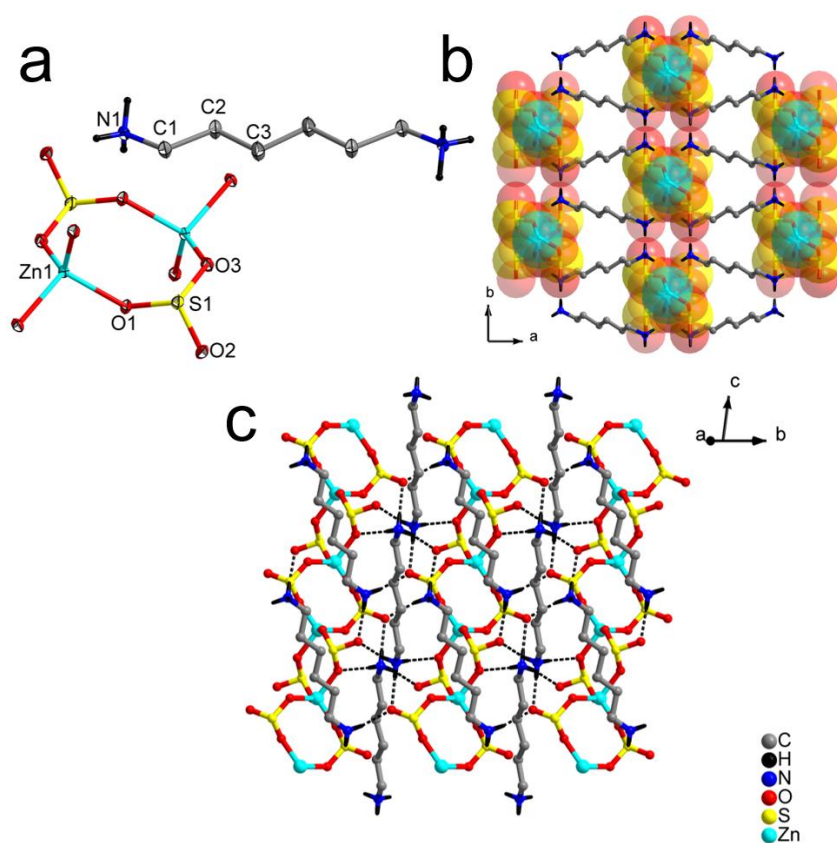


Fig. 2.6. (a) The molecular structure of compound **4** with unique atoms are labeled (ellipsoid probability is 25%), (b) Part of the crystal lattice of compound **4** viewed along the c -axis (space fill model) and (c) H-bonding pattern in compound **4**.

In the crystal lattice of compound **4** is shown in Fig. 2.6, the organic template 1,6-HMDA is located in the space between the two chains. Again the H-bonding are playing an

important role in the enhancing the dimensionality of the structure and it provides the stability to the framework. The intricate H-bonding interactions are involved in between the hydrogen atoms of protonated amine and oxygen atoms of sulfite anions. The non-bonding oxygen atom O2 of sulfite anion involved in bifurcated intricate H-bonding (which provide strong interaction) with N1 of a terminal organic amine, which extends from both the ends and generates an infinite H-bonded three-dimensional network (Fig. 2.6c). The H-bond distance of $d_{N1-H1B...O2}$ 1.90(3) Å and $d_{N1-H1C...O2}$ 1.95(3) Å. Further, the bonded oxygen atoms of sulfite anion involved in the H-bonding with the hydrogen atoms of protonated amines. The H-bond distance is $d_{N1-H1A...O1}$ 2.06(4) Å. These H-bonding interactions make the lattice in orthogonal plane regard to 1D polymeric chain forming in a 3D structure.

Collectively discussion of 2-4:

The analysis of compounds **2-4** reveals that there is an almost similar crystal packing structure are observed to change with respect to the diaminoalkane, which differs with one another in terms of the intervening methylene units, as the organic template and in all the amine groups are protonated. All the three compounds form a linear chain structure similar to compound **1**. As intended, the introducing the organic template with an increasing number of carbon atoms in between the diamine molecule (the intervening methylene units), causes the increase in the separation of 1D chain plane along the *b*-axis (for compound **2**) and along the *c*-axis (for compounds **3** and **4**). The interplanar distances increment takes place from 8.25 Å to 8.67 Å to 10.59 Å as the varying the template from propyl- to butyl- and finally to hexyldiamine Fig. 2.7 and 2.8.

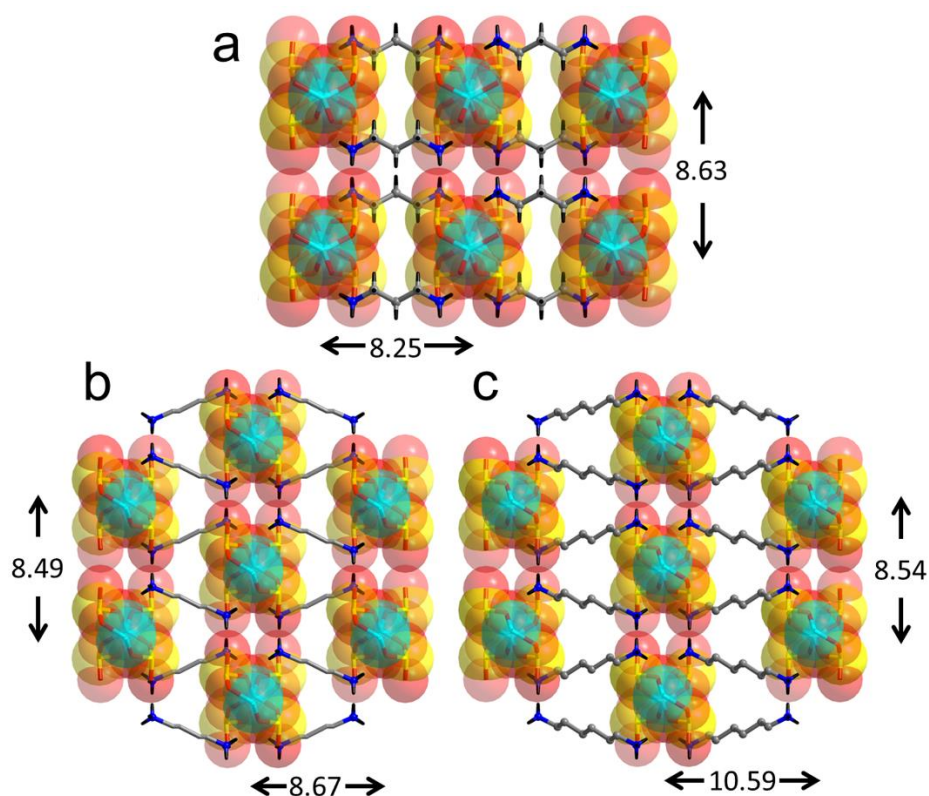


Fig. 2.7. Part of the crystal lattice of (a) compound **2** as viewed along the *b*-axis, (b) compound **3** as viewed along the *c*-axis and (c) compound **4** as viewed along the *c*-axis.

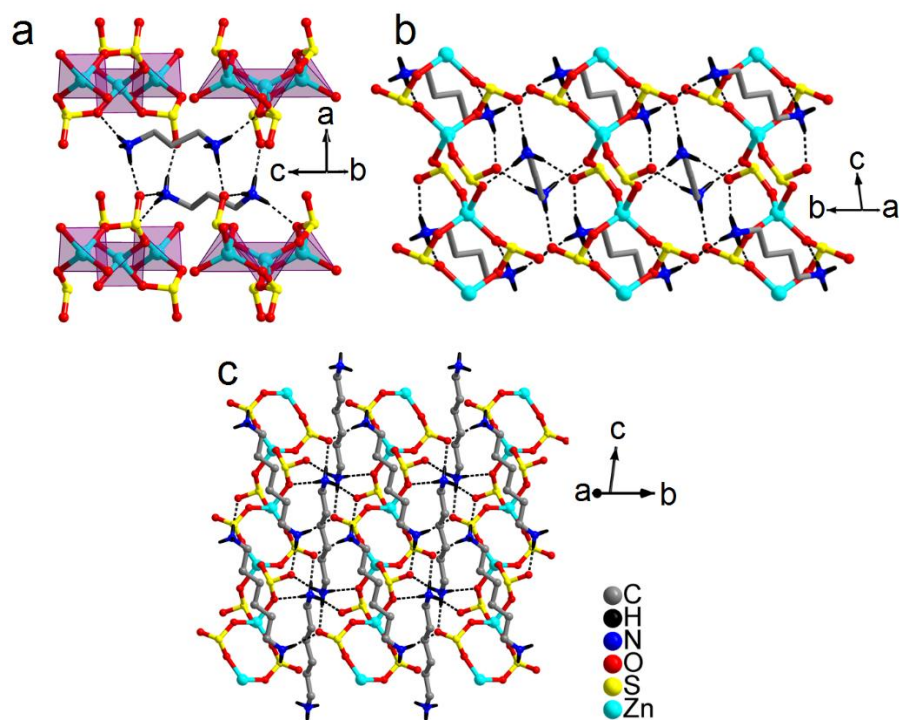


Fig. 2.8. An H-bonded 3D lattice of compounds (a) **2**, (b) **3** and (c) **4** (part of the lattice is omitted for clarity).

After accessing the crystal structure with an acyclic *bis*-substituted amine, we turned our attention towards *bis*-substituted cyclic amine. For this purpose, we employed piperazine as our organic template of choice under similar conditions as given in Table 3 and accessed compound **5**. The crystals of compound **6** were also obtained in this case to investigate the effect of metal Mn(II) ions over the lattice with interesting results.

2.3.5 Structural analysis of [C₄H₁₂N₂][Zn(SO₃)₂].H₂O, **5**:

The SCXRD analysis of compound **5** reveals that the colorless crystals of compound **5** adopt achiral *P*-1 space group in the triclinic crystal system with formula [C₄H₁₂N₂][Zn(SO₃)₂].H₂O and displayed 1D structure. The repeating unit of compound **5** contains 15 non-hydrogen atoms, where the inorganic framework form from one Zn(II) ion, two sulfite anions, and extra-framework have two halves of protonated piperazine moiety and one free water molecule which is shown in Fig. 2.9a. The asymmetric unit additionally has one trapped water molecule in the lattice as a solvent of crystallization. The crystallographically independent Zn(II) ions are coordinated with neighboring four oxygen atoms coming from four sulfite anions through Zn-O-S linkage and form a tetrahedral structure around Zn(II) ions. The Zn-O bond lengths in ZnO₄ are in the range of 1.945(2)-1.9798(19) Å. In the pyramidal SO₃²⁻ anions, the average coordinated S-O bond length is 1.5390 Å and the bond length of non-bonded S1-O2 and S2-O6 are 1.491 Å and 1.485 Å respectively, all the bond lengths are in the normal range. The two half-molecule of protonated piperazine and free water molecules are occupied by the interchain space.

In the part of crystal lattice of compound **5**, the alternate of arrangement of pyramidal SO₃²⁻ and tetrahedron ZnO₄ are connected through corner sharing, which shows the formation of one-dimensional chain, which extends and running down along the crystallographic *c*-axis. This is again similar [ZnSO₃]²⁻ chain in compounds **1-4** but the slight difference in position

of in non-bonded oxygen atoms, which are alternatively pointing away and towards. The SO_3^{2-} anion is connected with two oxygen atoms with Zn(II) ions in $\mu^2\text{-}\eta^1:\eta^1\text{-O:O}$ coordination mode. Hence, the Zn(II) ions coordinated with sulfite anion, which results in the formation of interlinked Zn_2S_2 dimeric unit (the bridging oxygen atoms are ruled out) to form a 1D chain along *c*-axis as shown in Fig. 2.1c. A similar trend is found and depicted in compound **1**.

The interplanar distance between 1D $[\text{ZnSO}_3]^{2-}$ chain is 7.59 Å along the *a*-axis (Fig. 2.10a). The intricate H-bonding interaction resulting in an H-bonded three-dimensional structure. Interestingly, the free water molecule interacts with the oxygen atoms of sulfite anions of the 1D chain. The H-bond distances are $d_{\text{O1w-H1w}\dots\text{O6}} = 2.16(3)$ Å and $d_{\text{O1w-H2w}\dots\text{O3}} = 2.01(5)$ Å, which results into an H-bonded layered structure in the *ac*-plane (Fig 2.11). Again, the protonated piperazine molecules connected to the oxygen atoms of sulfite anions of inorganic chain and a free water molecule to expand in the *ab*-plane. The piperazine and water molecules are a donor for H-bonding, hence, the free water molecules are involved in intricate quadrupole H-bonding interactions and generate an H-bonded 3D-structure containing metal-sulfite chains (Table 2.4).

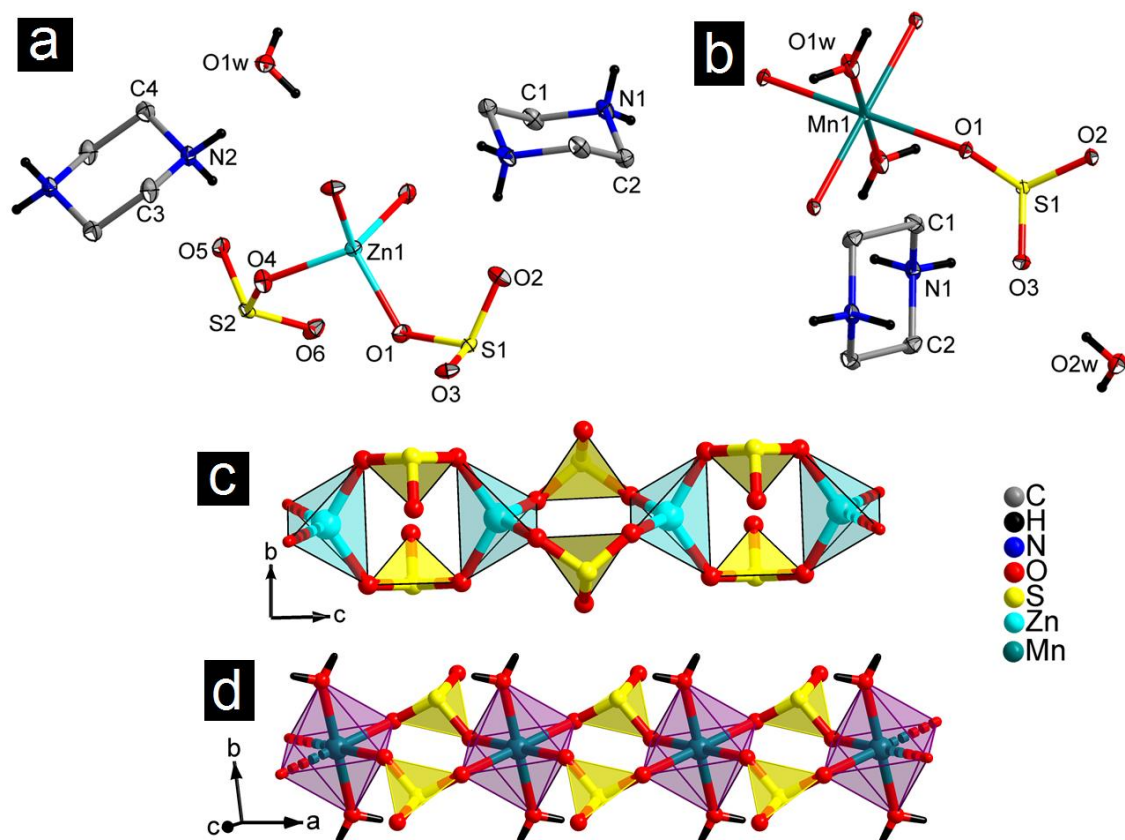


Fig. 2.9. The molecular structure of (a) compound **5** and (b) compound **6** at 25 % ellipsoid probability level (unique atoms are labeled); View of 1D structure with interconnected ZnO_4 tetrahedron for compound **5** (c) and MnO_6 octahedron for compound **6** (d).

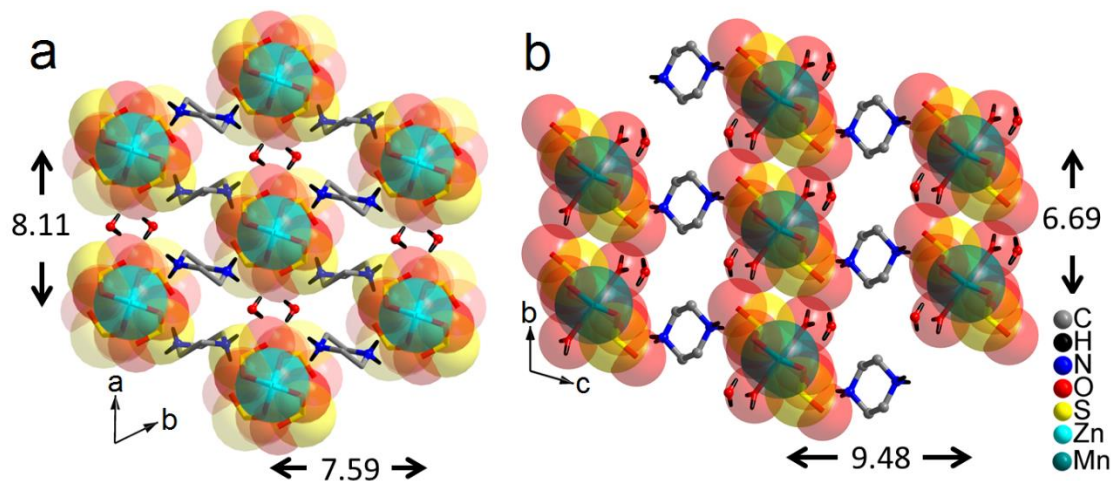


Fig. 2.10. Part of the crystal lattice of (a) compound **5** and (b) compound **6** showing the positions and orientations of water and protonated piperazine molecules.

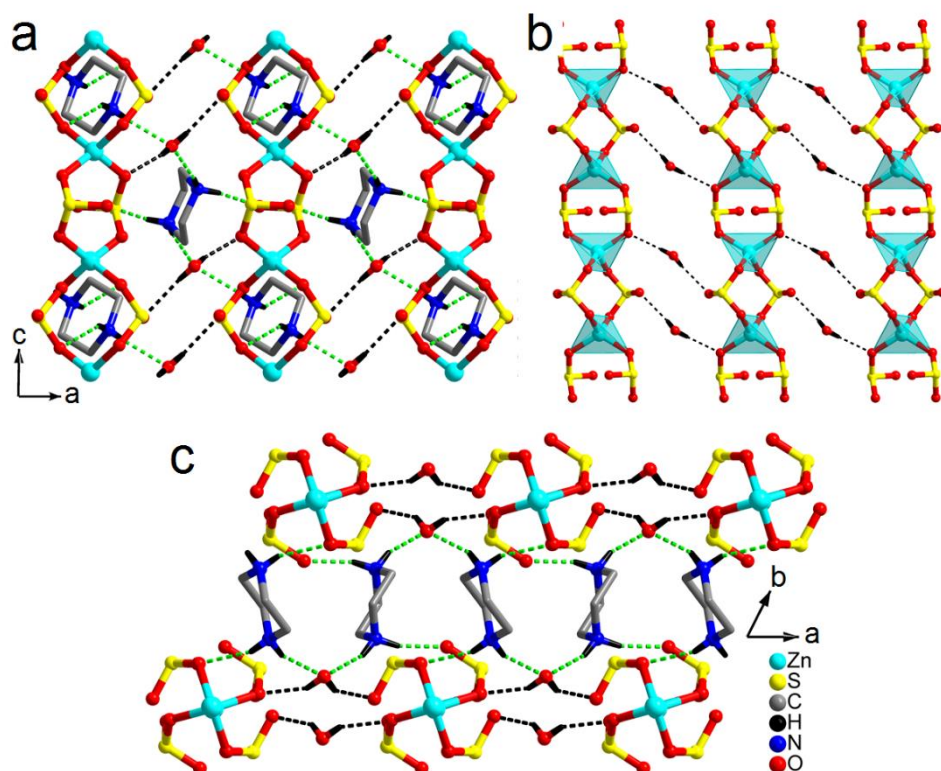


Fig. 2.11. (a) H-bonded lattice of compound **5**, (b) water molecule-mediated H-bonding in the lattice as viewed close to the *b*-axis and (c) involvement of piperazine molecules in the lattice as shown with green color fragmented bonds (H-bonds are represented with fragmented bonds).

2.3.6. Structural analysis of $[\text{C}_4\text{H}_{12}\text{N}_2][\text{Mn}(\text{SO}_3)_2(\text{H}_2\text{O})_2] \cdot 2\text{H}_2\text{O}$, **6**:

The molecular structure of compound **6** has been established by SCXRD, the data analysis suggested that the colorless crystal of compound **6** crystallizes in achiral *P*-1 space group with triclinic crystal system, which features an infinite one-dimensional polymeric chain and formulated as $[\text{C}_4\text{H}_{12}\text{N}_2][\text{Mn}(\text{SO}_3)_2(\text{H}_2\text{O})_2] \cdot 2\text{H}_2\text{O}$. The asymmetric unit of compound **6** contains one Mn(II) ions with 50% occupancy, one sulfite anions, half molecules of protonated piperazine cation, one aqua ligand and one free water molecule trapped in the lattice, have total 10 non-hydrogen atoms (Fig 2.9b). The central metal atom Mn(II) ions have octahedral geometry, which connected with four oxygen atoms of sulfite anions through corner sharing Mn-O-S linkage and occupies at the equilateral plane with average

Mn-O_{sulfite} bond length is 2.1955 Å and rest of two oxygen atoms of aqua ligand occupies the axial position Mn-O_{aqua} is 2.1861 Å³⁷. The bond valence sum calculations suggest that Mn atom in compound **6** is 2.023 which has +2 oxidation state of Mn ion³⁵.

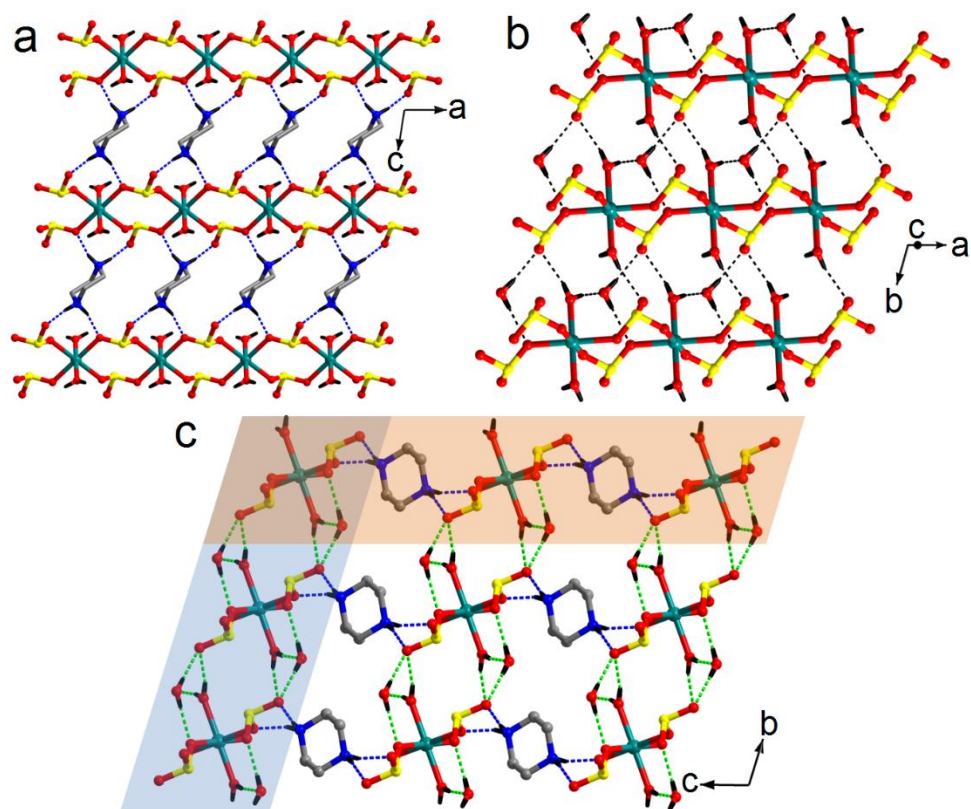


Fig. 2.12. (a) H-bonding in compound **6** through piperazine molecules giving an H-bonded 2D structure in the *ac*-plane; (b) A water molecule-mediated H-bonding in the lattice and (c) H-bonded lattice highlighting the extension through water and piperazine H-bonding as represented with a different color rectangle.

In the crystal lattice of compound **6**, the alternate arrangement of octahedra MnO₆ and pyramidal sulfite anions extend in the crystallographic *a*-axis and forms a 1D chain. As shown in Fig. 2.9d, the interchain space was occupied by the protonated piperazine molecules. The interplanar distance between [MnSO₃]²⁻ chain is 9.48 Å along the *a*-axis (Fig. 2.10b). The H-bonding interaction plays a vital role in compound **6** which enhance the stability and the formation of the H-bonded 3D structure which is shown in Fig. 2.12

and highlighted. The H-bonding interactions involved in between the protonated piperazine molecules and sulfite oxygen atoms of 1D chains (two 1D chains interconnected with piperazine) which extend the lattice in the *ac*-plane as shown in Fig. 2.12a. Additionally, the free lattice water molecule and the aqua ligands (Mn coordinated) interconnect the 1D-chain structures *via* H-bonding along the *b*-axis which further extend the lattice in the *ab*-plane (Fig. 2.12b, Table 2.4). Overall, these two types of intricate H-bonding interactions namely, N-H...O and O-H...O, along with metal-sulfite coordination, hence, forms an H-bonded 3D-structure which has been also highlighted in Fig. 2.12c with a different color rectangle, where the N-H...O interactions extend the lattice in *c*-direction, the H-bond distances are $d_{\text{N1-H1A}\cdots\text{O3}} = 1.89(3) \text{ \AA}$, and $d_{\text{N1-H1B}\cdots\text{O2}} = 1.85(2) \text{ \AA}$.

However, the organic template piperazine is same in compounds **5** and **6**, the distances vary significantly, which can be attributed to the different geometries adopted by the metal ions, the orientation of piperazine molecule and the trapped lattice water molecule.

The bond valence sum calculation value for Zn ion in case of compounds **1-5** is 2.023, 2.033, 2.052, 2.051 and 1.996 respectively which suggest +2 oxidation state of Zn atom in all five compounds.

2.3.7 Structural analysis of $[(\text{C}_3\text{N}_2\text{H}_{10})_2\text{NaCo}(\text{SO}_3)_2(\text{H}_2\text{O})_2]\cdot\text{H}_2\text{O}$, **7**:

The suitable rhombohedral shape orange color single crystals of compound **7** were an investigation by X-ray diffraction, the data reveals that the rhombohedral shape orange color crystal belongs to achiral monoclinic crystal system having $P2_1/c$ space group. The asymmetric unit of compound **7** contains two Co(III) ions with half occupancy 0.5, two SO_3^{2-} anions, two 1,3-diaminopropane units, one sodium ion, two aqua ligands and one trapped water molecule, which collectively contains 24 non-hydrogen atoms (Fig. 2.13). In

the compound **7**, the two crystallographically distinct Co(III) ions namely Co1 and Co2 are present at special position at the centre of inversion, each of Co(III) ions are connected with two sulfur atoms from two SO_3^{2-} anions located at the axial sites and four amino nitrogen atoms from the 1,3-diamino propane, which forms the equatorial plane, resulting into the octahedral structure. The bond length of Co1-S1 is 2.259(4) Å, and Co2-S2 is 2.273(4) Å. The two SO_3^{2-} anions and two 1,3-diaminopropane units coordinated to Co(III) ion in a chelate manner, and Co-N bond lengths are in the range between 1.978(1)-1.988(1) Å, which are in the normal bond length range³⁸.

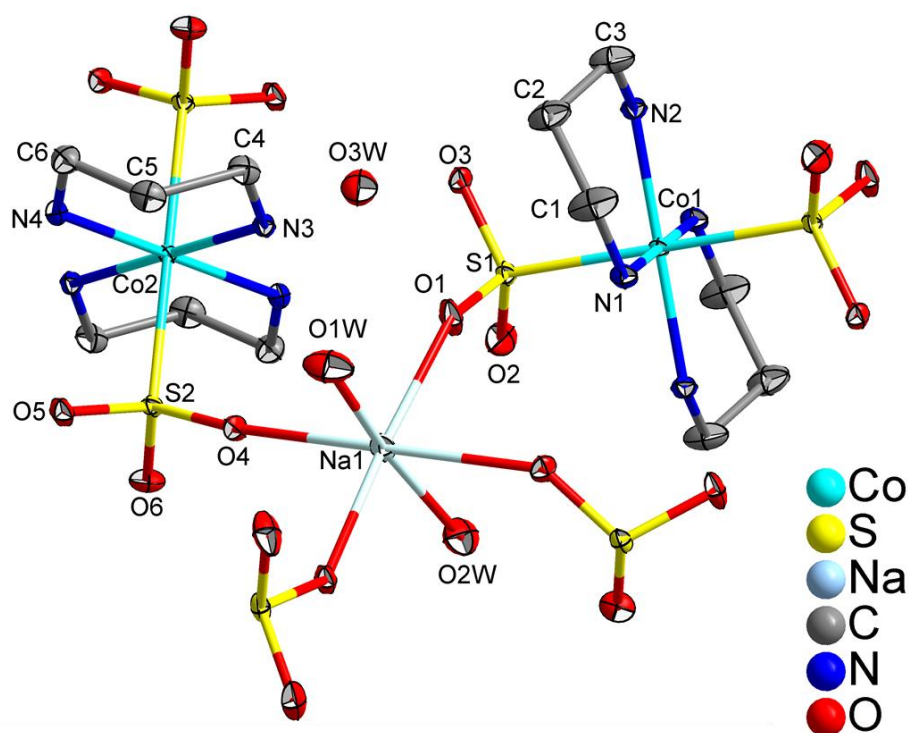


Fig. 2.13. The molecular unit of $[(\text{C}_3\text{N}_2\text{H}_{10})_2\text{NaCo}(\text{SO}_3)_2(\text{H}_2\text{O})_2]\cdot\text{H}_2\text{O}$, **7** where unique atoms are labeled.

One Na(I) ion present in the crystal lattice, which balances the electrical charge of the coordination network. The Na (I) ion has octahedral geometry, which is composed of four oxygen atoms from four different sulfite anions which situated at equatorial plane and two aqua ligands situated in the axial position. The Na-O bond lengths are in the range of

2.319(2)-2.563(2) Å which are in good agreement with the literature reports of similar compounds.^{23,39} The three water molecules were present in the crystal lattice, the two water molecules namely O1w and O2w are connected with Na(I) ion and the third water molecule (O3w) is trapped in the lattice (Fig. 2.15). Interestingly, the Co(II) ions are converted into Co(III) ions due to *in-situ* auto-oxidation²⁷. The bond valence sum calculations suggest that the Co present in +3 oxidation state and the value for Co1 is 3.3152, for Co2 is 3.3094 and for Na is 1.2245 again confirm the +1 oxidation state of Na ion⁴⁰.

In the crystal lattice of compound **7**, the Co metal centre coordinated with two bidentate amine ligands, which locates at the equatorial positions and remaining site of Co ions are connected with sulfur atoms of sulfite anions occupying the axial site, which further connected with Na(I) ion to form a layered structure.

In the part of crystal lattice of compound **7**, the Co(III) ions coordinated with SO_3^{2-} anions, these $[\text{Co}(\text{SO}_3)_2]^-$ units are bridged by Na(I) ion thorough SO_3^{2-} oxygen atoms to generate an infinite layered structure in the *bc*-plane, where each SO_3^{2-} anions are bonded with one Co(III) ion and two Na(I) ions (Fig. 2.14a) *via* $\eta^1:\eta^1:\eta^1\text{-O:O:S}$ coordination mode, respectively. The Co(III) ions are located on the corners of a perfect rectangle. The adjacent Co(III) ions are separated by 6.8966(1) Å along *b*-axis and 6.9774(1) Å along *c*-axis respectively. In the layer of compound **7**, the Co(III) ions are bonded with the sulfur atom of sulfite ion in *trans*-coordination fashion and produce a $[\text{Co}(\text{SO}_3)_2]^-$ unit which further interconnected with bridging Na(I) ion in almost orthogonal fashion and generate a two-dimensional structure as shown in Fig. 2.14b. The cobalt-sulfite compound under acidic pH were accounted for yet adverse to our results no oxidation to Co(III) and subsequent coordination to sulfur atom was observed⁴¹.

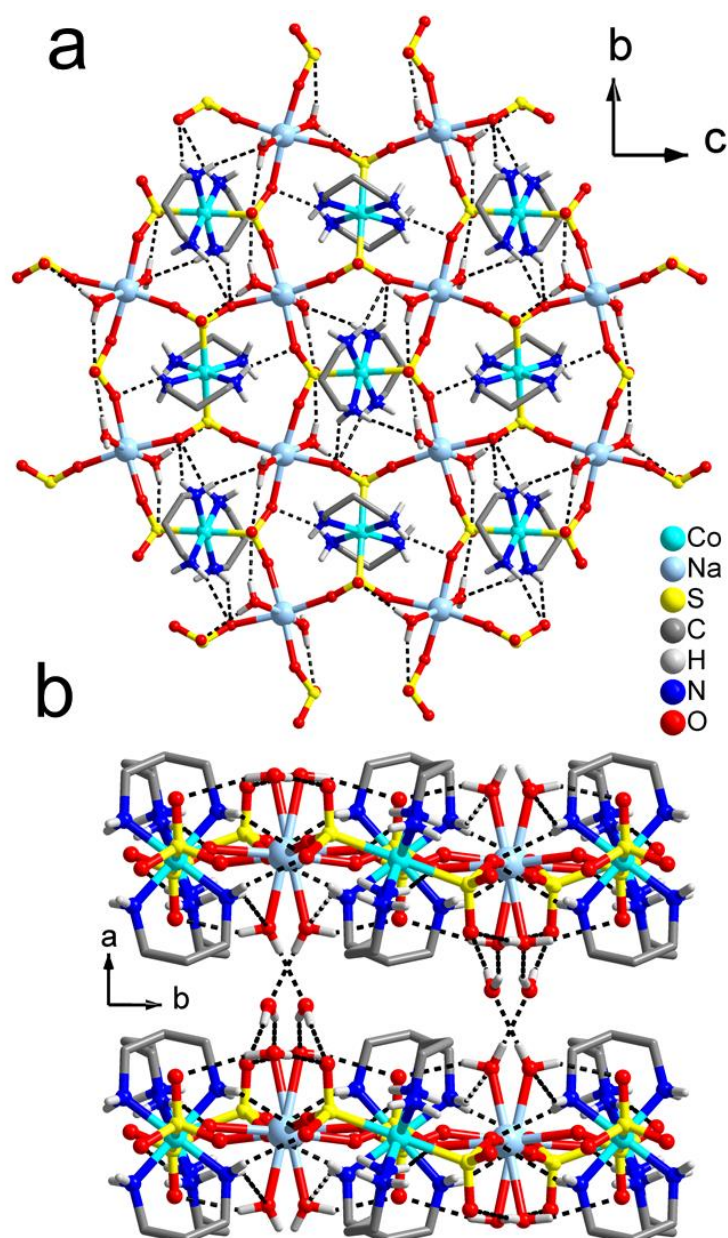


Fig. 2.14. (a) View of the two-dimensional layer of $[(C_3N_2H_{10})_2NaCo(SO_3)_2(H_2O)_2]$. H₂O, **7**, with H-bonding scheme (fragmented bonds) and (b) Interconnection of different layers via H-bonding as viewed along *c*-axis. Part of the crystal lattice has been omitted for clarity.

Even though the metal-sulfite coordination event in a 2D polymer in case of compound **7**, it is worth to present some important role in the complicated H-bonding interactions showed by amino groups of coordinated amine, aqua ligands and free water molecule trapped in the crystal lattice. In the crystal lattice of compound **7**, both the coordinated aqua ligands (O1w and O2w) show different H-bonding pattern. The O2w ligand donates both

of its hydrogen atoms for O2 ($d_{O2w-H2w2...O2} = 2.34(2) \text{ \AA}$) and O6 ($d_{O2w-H1w2...O6} = 2.17(3) \text{ \AA}$) oxygen atoms of sulfite anion present in the same layer (Fig. 2.15), which is non-bonding oxygen atoms.

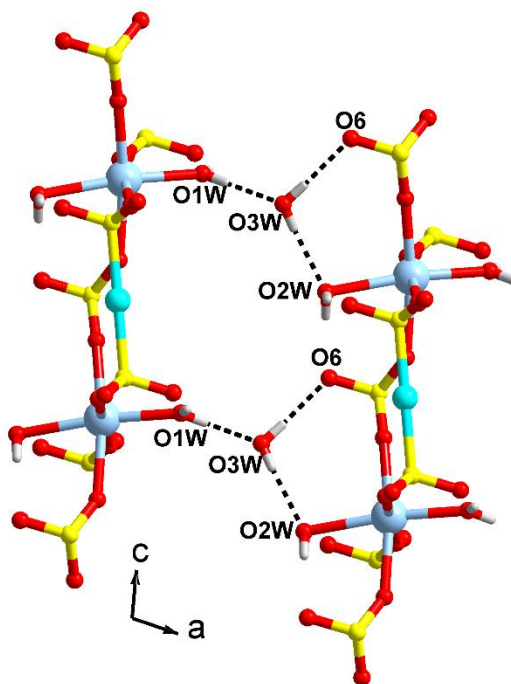


Fig. 2.15. Interconnection of different layers *via* H-bonding through water molecules in the $[(C_3N_2H_{10})_2NaCo(SO_3)_2(H_2O)_2] \cdot H_2O$, **7**.

In the crystal lattice of compound **7**, free water molecule O3w occupies in the interlayer space, which plays an important role in H-bonding interaction as shown in Fig. 2.14b. The trapped O3w molecule act as a bridge, which interconnects the two layers through strong H-bonding by simultaneously donate for O6 atom ($d_{O3w-H2w3...O6} = 2.00(2) \text{ \AA}$) of sulfite anion and O2w aqua ligand ($d_{O3w-H1w3...O2w} = 2.09(3) \text{ \AA}$) present in one layer and accept for O1w aqua ligand present in another layer ($d_{O1w-H1w1...O3w} = 1.979(19) \text{ \AA}$).

These H-bonding interaction results in the enhance in the dimensionality of the crystal lattice by extending it along the *a*-axis, finally generating an H-bonded 3D lattice⁴². The rest of the hydrogen atoms on O1w displays H-bonding with the O2 oxygen atoms of sulfite

anion ($d_{O1w-H2w1\cdots O2} = 2.15(2) \text{ \AA}$) of a similar layer. The amino groups additionally display significant H-bonding interactions inside the layer which further reinforces the crystal lattice of compound **7** (Table 2.4).

2.3.8. Structural analysis of $[(C_6N_4H_{18})Zn_3(SO_3)_3]$, **8**:

The molecular units are displayed in the Fig 2.16, the examination of the plate-shaped colorless crystals of compound **8** was performed on the SCXRD which suggest that compound **8** crystallizes in the centrosymmetrically triclinic crystal system and *P*-1 space group, which features a layered structure. The asymmetric unit is comprised of three Zn(II) ions, three sulfite anions, and one *tris*-(2-aminoethyl) amine molecule which collectively has 25 non-hydrogen atoms. In the molecular unit, it is clear that there are two crystallographically distinct Zn(II) ions are present in the lattice. Each Zn(II) ions namely Zn1 and Zn2 are bonded with surrounding four-four sulfite anions through common oxygen atom *via* corner sharing (Zn-O-S linkage) and forming distorted tetrahedral structures. Whereas the third Zn3 ions possess distorted trigonal bipyramidal geometry where the equatorial sites are occupied by terminal amino groups of *tris*-(2-aminoethyl) amine and the fifth site connected with sulfite oxygen atom namely O8 through corner sharing with Zn3-O8-S3 linkage. The average bond length for Zn-O are 1.925(7) Å for Zn1, 1.977(8) Å for Zn2. The bond distance of Zn3-O8 is 2.037(8) Å, and the average Zn3-N bond length is 2.057 Å, whereas the bond distance of Zn3-N1 is 2.262(9) Å which is slightly more than the remaining Zn3-N bond lengths which is comparable to the literature reports on other zinc-sulfite compounds, which is again in good agreement with literature reports⁴³. All the Zn-O and Zn-N bond lengths are in the acceptable range. The bond valence sum calculations for Zn1, Zn2 and Zn3 are 2.0713, 2.0734 and 2.1139 respectively, which further suggest the +2-oxidation state of Zn ions in compound **8**.

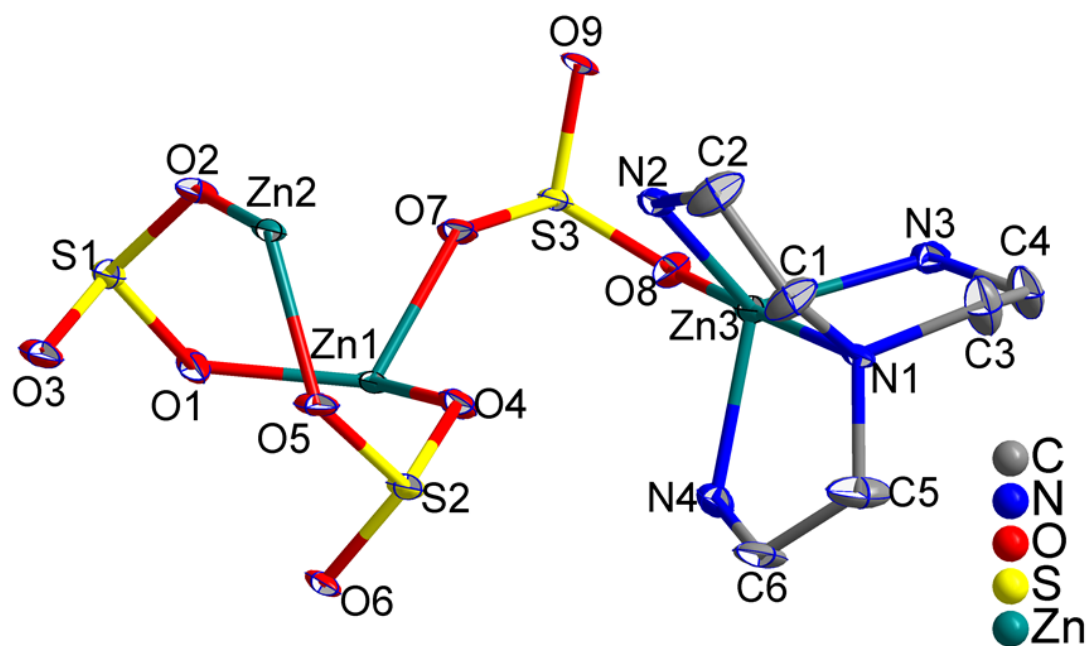


Fig. 2.16. Asymmetric unit of compound **8** where unique atoms are labeled.

In the crystal lattice, the compound **8** features a layered structure, which is composed of the alternate arrangement of the pyramidal SO_3^{2-} anions and tetrahedral Zn1, Zn2 ions, whereas the amine coordinated Zn3 ions, the coordinated organic amines are protruding outside the layer and located in the interlayer space (Fig. 2.17). As there are three different sulfite anions namely S1, S2 and S3 are present in the crystal lattice, the coordination engendered towards Zn(II) ions differ. The dimeric Zn_2S_2 unit (the bridging oxygen atoms are omitted for clarity) is formed by the coordination between two sulfite anions namely S1 and S2 with Zn1 and Zn2 ions, the adjacent Zn(II) ions are separated by a distance of 3.818 Å. These dimeric Zn_2S_2 units are further interconnected with the oxygen atom of sulfite anion to form a 1D chain running along the *a*-axis as highlighted with a grey color rectangle in Fig. 2.17a. Furthermore, sulfite anion S3 act as a bridge which connects two 1D chains and generate a layered structure in the *ac*-plane. The four sites of Zn3 ions connected with amine caps hence the extension of lattice limits to a layer (Fig. 2.17b). Thus, in the crystal lattice, each sulfite anion is coordinated with three Zn(II) ions in a fashion like $\eta^1\mu^3$ coordination mode as shown in Fig. 2.17c.

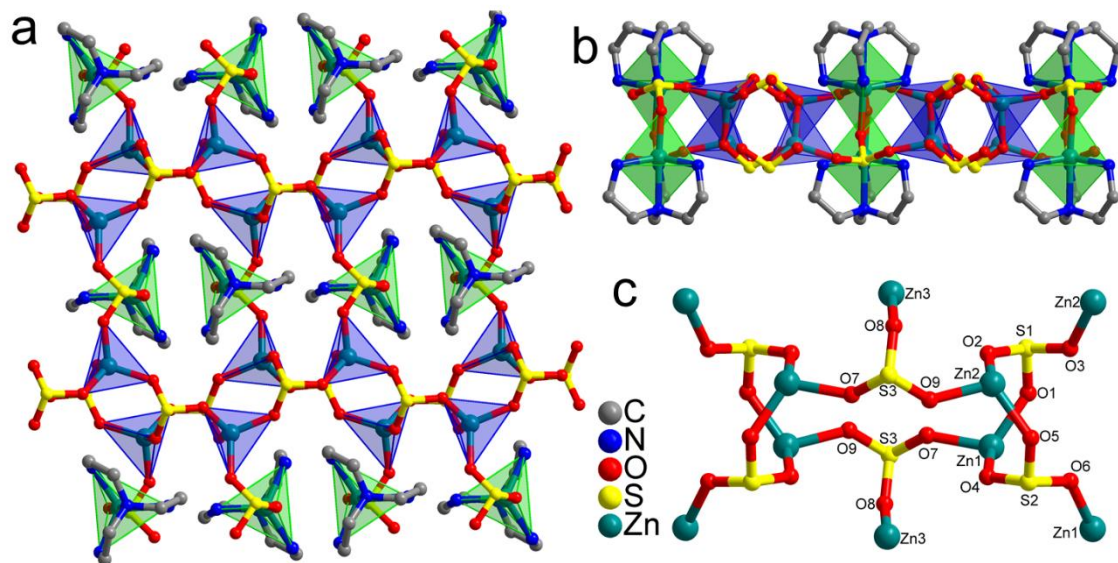


Fig. 2.17. (a) View of the layer in $[(C_6N_4H_{18})Zn_3(SO_3)_3]$, **8**, as viewed close to b -axis (green polyhedra represent the Zn_3 ions and blue polyhedra represent Zn_1 or Zn_2 ions, respectively), (b) View of the crystal lattice along the a -axis showing the position of coordinated organic amines and (c) Coordination of sulfite anions in the crystal lattice of compound **8**.

The crystal lattice of compound **8** is composed with two parallel hexagonal sheets (as differentiated with color code), which are alternately arranged and form 12 membered rings, thus the layer itself consists two sheets depending on the position of $Zn(II)$ ions. The separation of $Zn \cdots Zn$ distance ranging between 5.83-6.03 Å which resulting in a honeycomb structure as shown in Fig. 2.18a. The Zn_3 ions connected to the sulfite ions constructing the green sheet, which are roughly situated at the centre of the hexagonal honeycomb arrangement of the grey sheet and *vice-versa* (Fig. 2.18b).

The stability of compound **8** was enhanced by the H-bonding interaction shown by NH of the coordinated amino group and oxygen atoms of sulfite, and involved in bifurcated H-bonding, the H-bond distances ranges from 2.2-2.6 Å (Fig. 2.18b). Unfortunately, the H-bonding is restricted within the layer and unable to form higher dimensional structure.

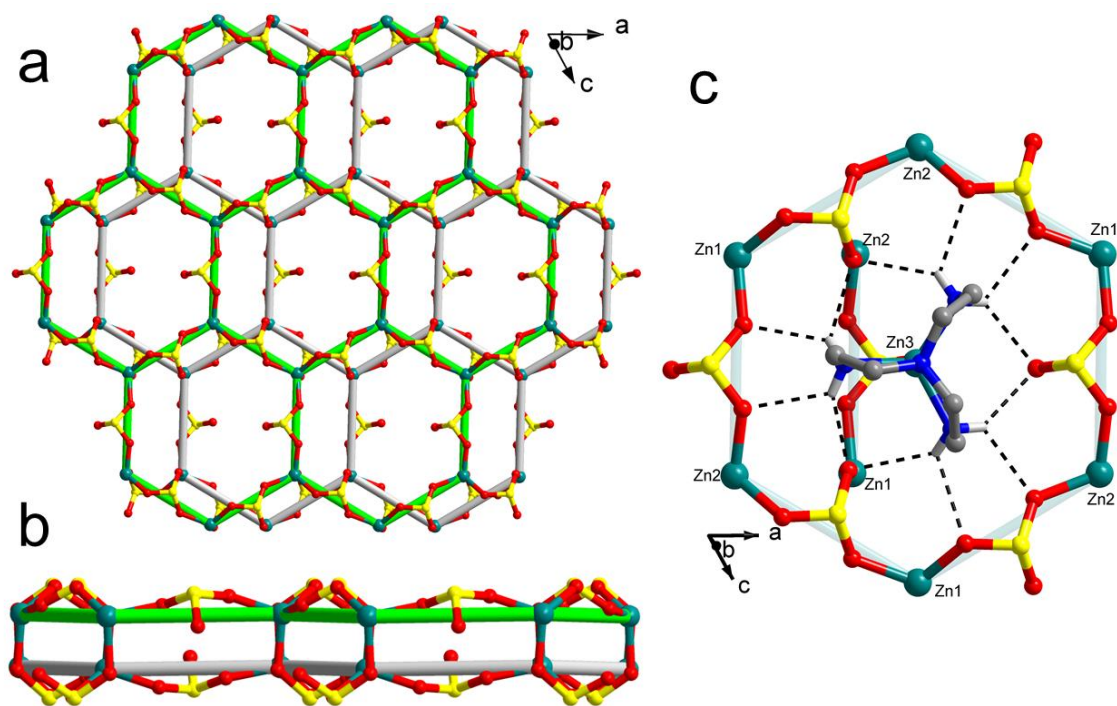


Fig. 2.18. (a) Interconnected sheets of honeycomb structure within a layer of $[(C_6N_4H_{18})Zn_3(SO_3)_3]$, **8**, composed of alternate Zn1 and Zn2 ions (b) Arrangement of two hexagonal sheet in the lattice and (c) Position of amine coordinated Zn3 ion in hexagonal space.

2.3.9. Structural analysis of $[C_2H_{10}N_2][Zn_3(SO_3)_4]$, **9**:

Hydrothermal reaction of $Zn(OAc)_2$ with sodium disulfite in presence of ethylenediamine afforded $[C_2H_{10}N_2][Zn_3(SO_3)_4]$, **9** as block shape single crystals. The molecular structure of compound **9** is shown in Fig. 2.19, which have been investigated by SCXRD data. The block shape crystals crystallize in achiral $C2/c$ space group in the monoclinic crystal system showing a layered structure and formulated as $(NH_3CH_2CH_2NH_3)[Zn_3(SO_3)_4]$.

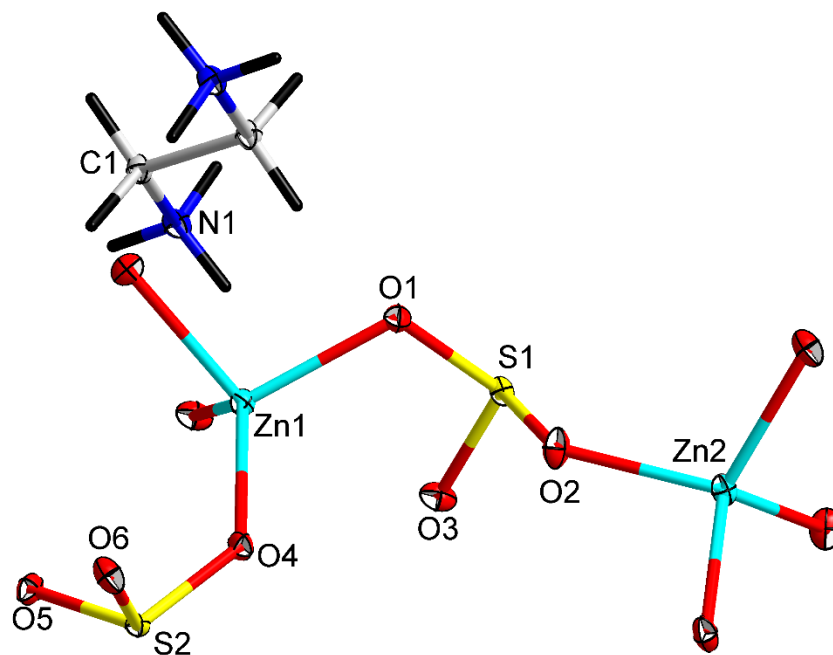


Fig. 2.19. Molecular structure of $[\text{C}_2\text{H}_{10}\text{N}_2][\text{Zn}_3(\text{SO}_3)_4]$, **9** where unique atoms are labeled.

The asymmetric unit of compound **9** constitutes 12 non-hydrogen atoms where 10 atoms having two Zn atoms and two sulfite anions from the inorganic framework and remaining 2 atoms from the extra-framework protonated amine molecule as shown in Fig. 2.19. There are two crystallographically independent Zn(II) ions present in the asymmetric unit, the Zn2 ions are present at the centre of inversion axis with half occupancy (Fig. 2.19). Each of the coordination spheres of Zn(II) ions is satisfied with neighboring sulfite anions and connected with four sulfite oxygen atoms, two oxygen atoms from $\text{S}(1)\text{O}_3^{2-}$ and another two oxygen atoms from $\text{S}(2)\text{O}_3^{2-}$ through corner sharing Zn-O-S linkages and forming tetrahedral structures. Each of the sulfite anions shares its all oxygen atoms with Zn(II) ions and coordination modes are in $\eta^1\mu^3$ -manner. The Zn-O bond lengths are in the normal range, which is 1.949-2.003 Å and S-O bond distances are in the ranges in between 1.523-1.5363 Å and are comparable to the literature reports^{43,39,44-46}. The crystal structure refinement parameters and a complete list of bond lengths and angles are given in Table 2.2 and 2.3 respectively (appendix).

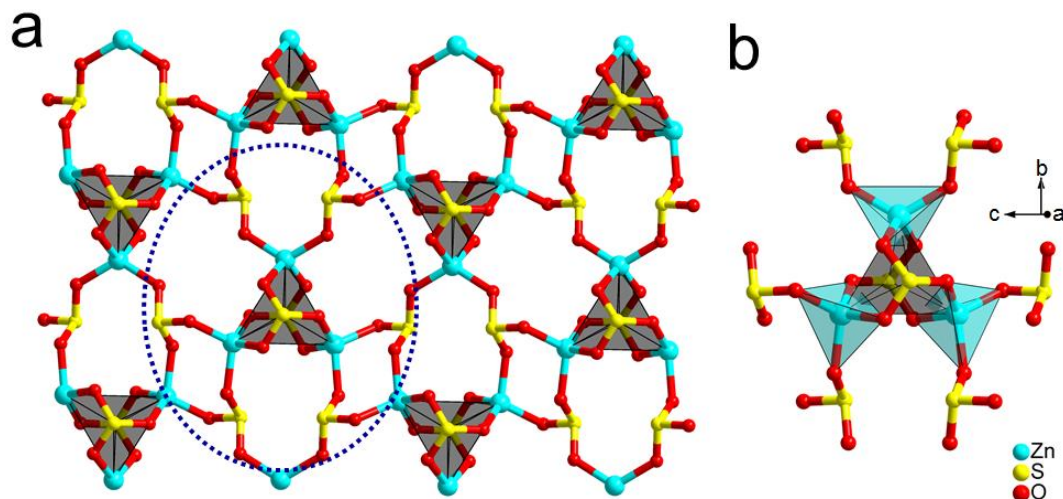


Fig. 2.20. (a) Crystal lattice of $[\text{C}_2\text{H}_{10}\text{N}_2][\text{Zn}_3(\text{SO}_3)_4]$, **9** showing an infinite anionic layer as viewed close to a -axis and (b) The arrangement of Zn(II) ions in a triangular node having $[\text{Zn}_3\text{S}_2\text{O}_{12}]^{10-}$ fragment capped by two sulfite groups as highlighted in (a).

In the crystal lattice, the pyramidal SO_3^{2-} and tetrahedra ZnO_4 are alternately arranged and resulting in the infinite layered structure in the bc -plane. The two $\text{S}(2)\text{O}_3^{2-}$ anions give its all oxygen atoms to coordinate with neighboring three Zn(II) ions in a way to make a sulfite capped triangular node $[\text{Zn}_3(\text{SO}_3)_2]$ (Fig. 2.20, grey polyhedra) where three adjoining ZnO_4 tetrahedra are interconnected. The sulfite capped triangular node $[\text{Zn}_3(\text{SO}_3)_2]$ are further extended with $\text{S}(1)\text{O}_3^{2-}$ anion to form a layer in bc -plane, which have the embedded 4, 6 and 8-membered ring system (excluding the intervening O atoms, Fig. 2.21).

The distorted tetrahedra ZnO_4 and pyramidal SO_3 anions are connected by their vertices through vertex-sharing linkage. Structure of compound **9** shows a similar kind of triangular node in guanidinium templated Zn-selenite system, nevertheless, the crystal lattice of compound **9** having embedded 4, 6 and 8 membered rings, whereas the crystal lattice is different in Zn-selenite system, which has only 12-membered rings⁴⁷.

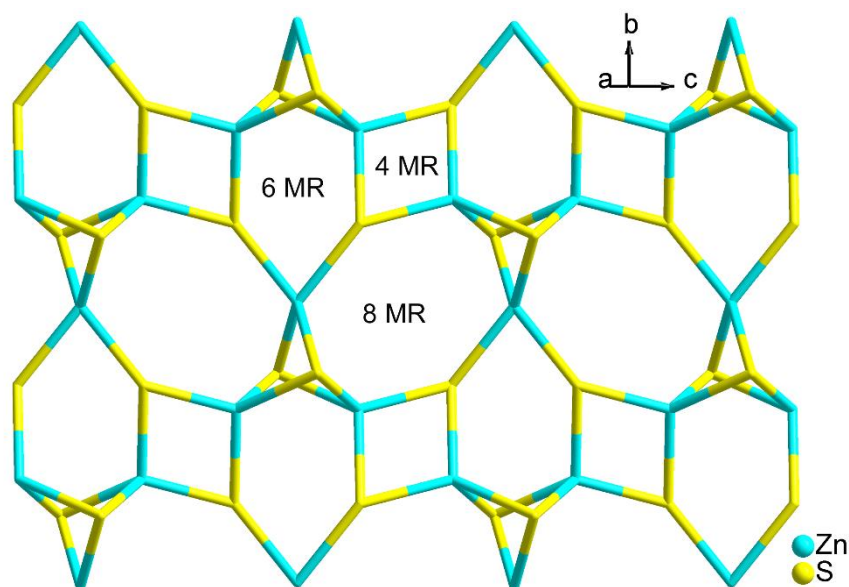


Fig. 2.21. (a) A layer structure of $[\text{C}_2\text{H}_{10}\text{N}_2][\text{Zn}_3(\text{SO}_3)_4]$, **9** with embedded 4, 6 and 8-membered rings (MR); excluding the oxygen atoms (ignoring the intervening sulfite oxygen atoms).

The protonated ethylenediamine molecules are occupying the interlamellar space, which balances the charge of the inorganic framework and it helps in the H-bonding. The H-bonding provides extra stability to the zinc-sulfite inorganic framework by the strong H-bonding interactions between the protonated ethylenediamine molecule and inorganic framework. Interestingly, the oxygen atoms of the triangular node of sulfite and hydrogen on the nitrogen atoms of ethylenediamine are involved in H-bonding. (Fig. 2.22). Hence, each triangular node acts as an acceptor to induce six H-bonding with $d_{\text{N1-H1A}\cdots\text{O6}} = 2.120$ Å; $d_{\text{N1-H1B}\cdots\text{O5}} = 2.049$ Å and $d_{\text{N1-H1C}\cdots\text{O4}} = 2.149$ Å and extends the lattice into the H-bonded three-dimensional network structure. Different H-bonding interactions for compound **9** are given in Table 2.4.

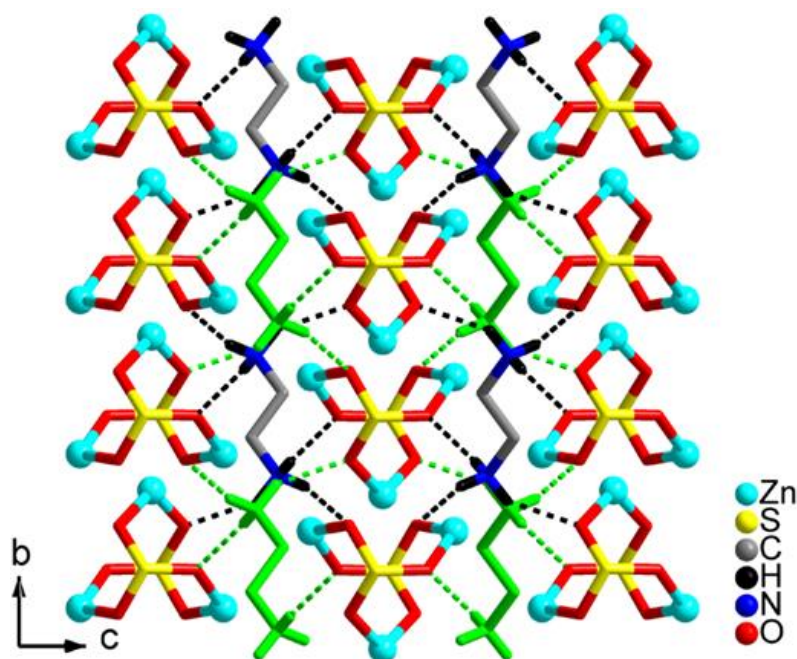


Fig. 2.22. Interconnection of a triangular node in compound **9** via H-bonding interaction shown with fragmented bonds (part of the lattice is omitted and protonated ethylenediamine is shown with a different color for clarity).

2.3.10. Structural analysis of $(\text{CN}_3\text{H}_6)_2[\text{Zn}(\text{SO}_3)_2]$, **10**:

Compound **10** was isolated under similar conditions when the organic template was changed to guanidine resulting a 3D network. The asymmetric unit of compound **10** is built up with 9 non-hydrogen atoms, the 5 atoms belong to the inorganic anionic framework (with 50% occupied Zn(II) ions are lying on two-fold rotational axis and one sulfite anions) and another 4 atoms are from a protonated guanidine molecule which belongs to extra-framework (guanidine) as shown in Fig. 2.23.

The central metal Zn(II) ions are connected with surrounding four SO_3^{2-} anions through corner sharing Zn-O-S linkage, which forms tetrahedral structure. In the SO_3^{2-} , the SO_3^{2-} shares its two oxygen atoms with Zn(II) ions in bidentate fashion, the other non-bonded oxygen atoms are comparatively shorter S-O bond length 1.478, the average S-O bond length is 1.518 Å, whereas the average bond distance of Zn-O is 1.951 Å which are in

normal range. The bond valence sum calculations suggest that Zn present in +2 oxidation states.

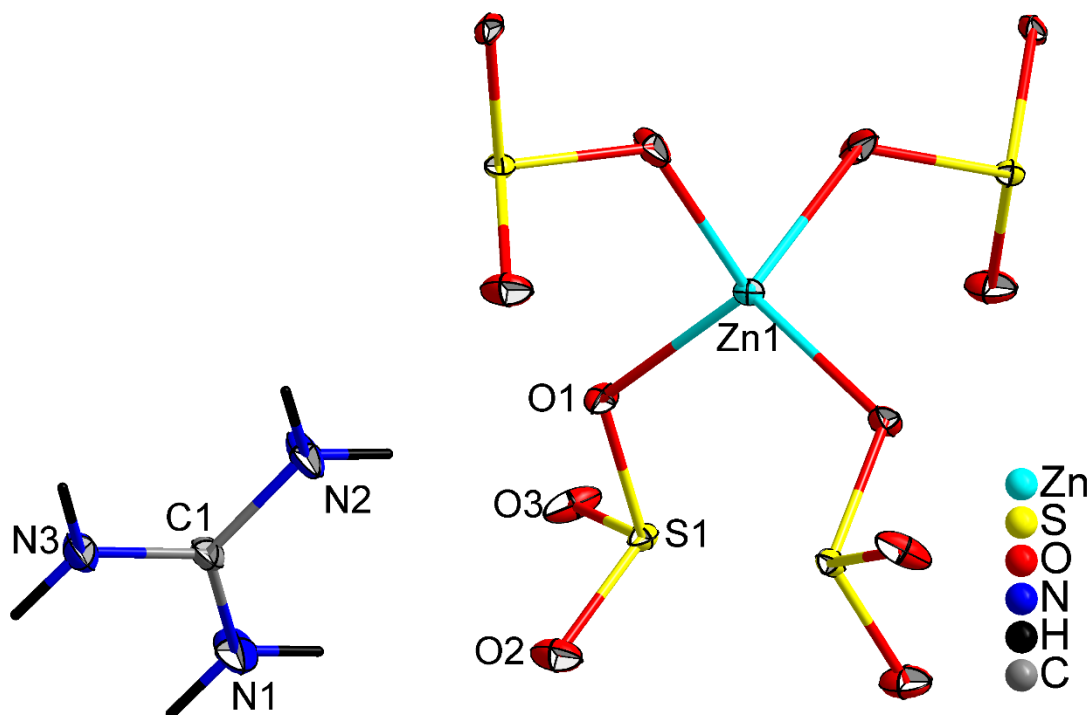


Fig. 2.23. Molecular unit of $[\text{CN}_3\text{H}_6]_2[\text{Zn}(\text{SO}_3)_2]$ **10**, where unique atoms are labeled.

In the part of the crystal lattice, the alternate arrangement of ZnO_4 tetrahedra and pyramidal SO_3^{2-} units giving rise to an infinite 3D network through Zn-O-S linkages. The alternate six ZnO_4 tetrahedra and six pyramidal SO_3^{2-} units are formed 12-membered ring system (Fig. 2.24a). The guanidinium cations are located in the center of each 12-membered ring system and forming H-bonding interactions between SO_3^{2-} oxygen and guanidinium nitrogen *via* strong $\text{N-H}\cdots\text{O}$ as shown in Fig. 2.24a. The H-bonding distance ranges between 2.07-2.28 Å. A similar observation has been reported for guanidine templated metal-selenite and metal-phosphite structures^{47,48}. Further compound **10** is found to be isostructural with the phosphate $[\text{CN}_3\text{H}_6]_2[\text{Zn}(\text{HPO}_4)_2]$, phosphite $[\text{CN}_3\text{H}_6]_2[\text{Zn}(\text{HPO}_3)_2]$ and sulfate $[\text{CN}_3\text{H}_6]_2[\text{Zn}(\text{SO}_4)_2]$ analogue hence, the present study further extends the series of guanidinium templated oxyanions⁴⁸⁻⁵⁰.

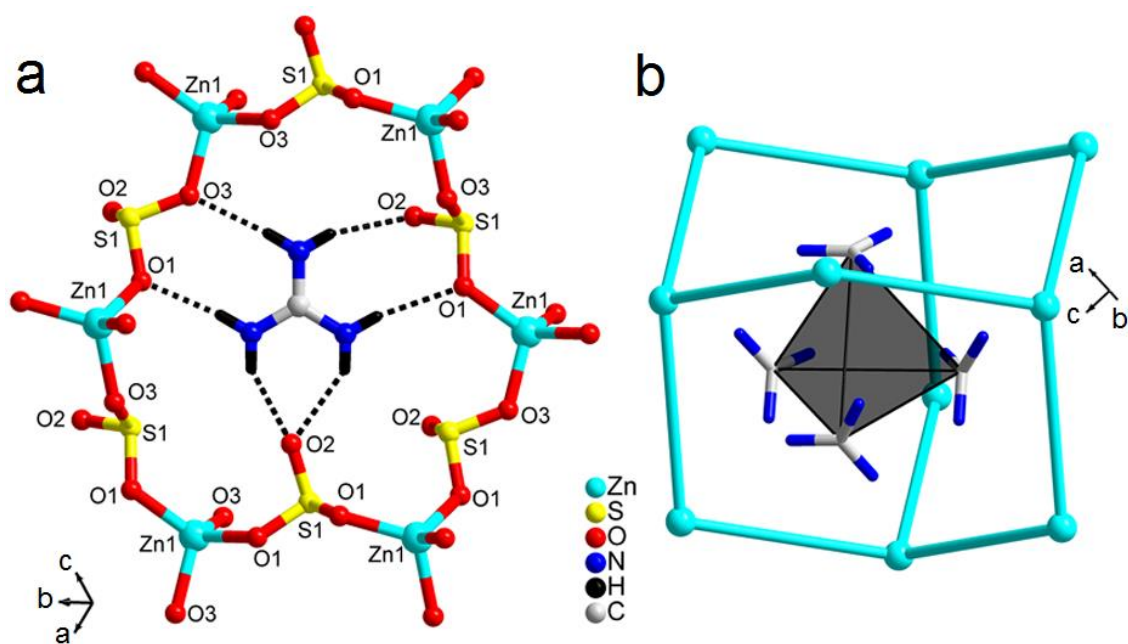


Fig. 2.24. (a) 12-membered ring with alternating ZnO₄ tetrahedra and SO₃ pyramids templated by guanidinium cation in [CN₃H₆]₂[Zn(SO₃)₂], **10**, H-bonding are shown with fragmented bonds and (b) Adamantane topology adopted by four 12-membered rings in the lattice of compound **10**, the position of guanidinium cation in a tetrahedral arrangement is also highlighted with grey color; Part of the lattice has been omitted for clarity).

The opposite Zn atoms are separated with ranges from 10.39–11.77 Å within the 12-membered ring. In the lattice, the 12-membered rings are appeared distorted adamantane like topology, as shown in Fig. 2.24b and Fig. 2.25. The guanidinium cation is sited in four 12-membered rings which are involved in the formation of the adamantane unit; which forms a distorted tetrahedral arrangement within the adamantane cavity (Fig. 2.24b).

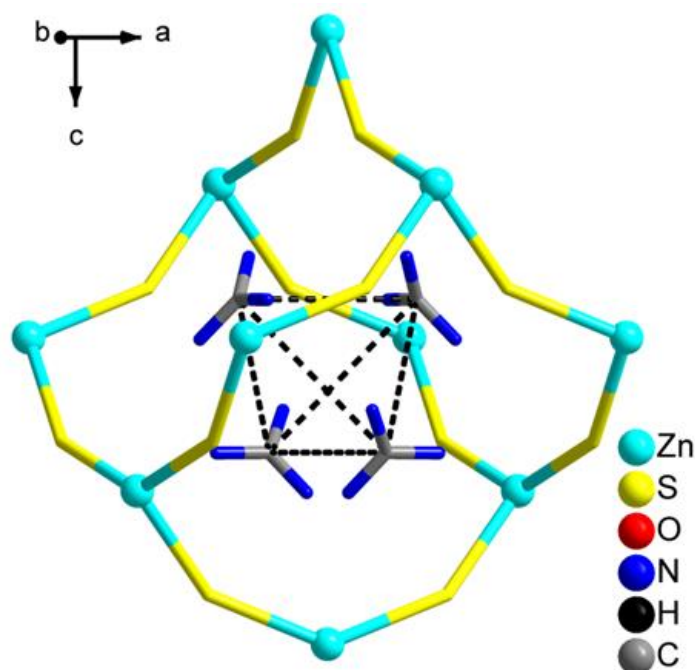


Fig. 2.25. 12-membered ring with Zn-S atoms in an adamantane topology in the compound **10**.

Part of the crystal lattice of compound **10** is constituted with the strictly alternating arrangement of SO_3 pyramids and ZnO_4 tetrahedra *via* vertex sharing. The guanidinium cations situated at almost center of each 12-membered ring which running forth and back in a type of distorted adamantane like topology to providing an infinite, anionic 3D-diamondoid network (Fig. 2.26a)¹⁰. Interestingly, in the crystal lattice, additionally the 12-membered ring system can be visualized as a helix running down along the *b*-axis having a pitch length of 12.12 Å where the guanidinium cations are located in the grooves, and the plane is indicating toward the helical axis as shown in Fig. 2.26b.

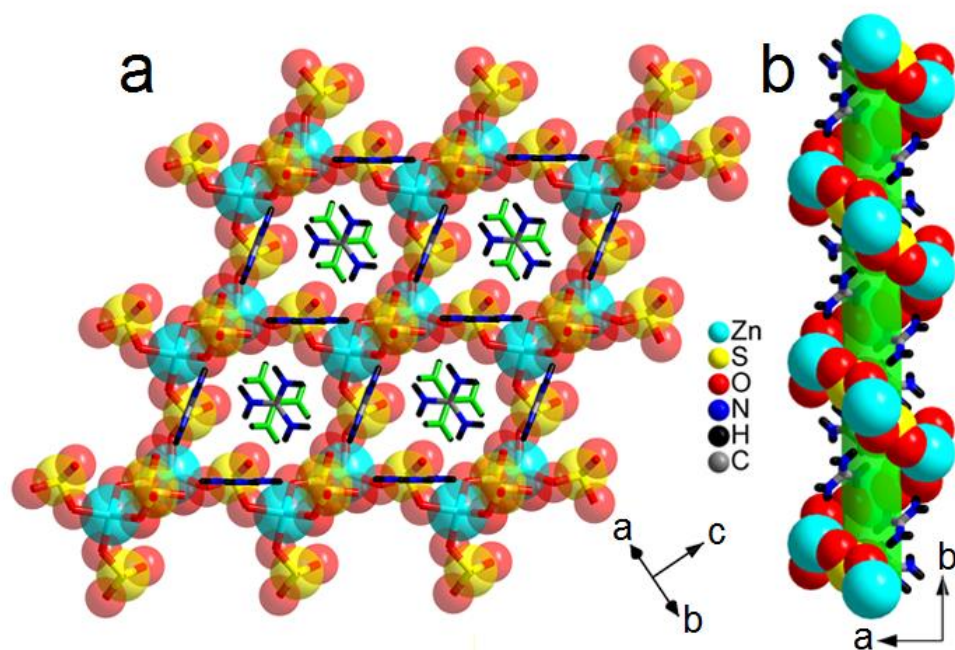


Fig. 2.26. (a) A 3D-Crystal lattice of compound **10** with guanidinium cations at the center of 12-MR window and (b) helical assembly observed in compound **10** (guanidinium cations in (a) are represented with different color for better visualization).

2.3.10.1. Adsorption properties of $[\text{CN}_3\text{H}_6]_2[\text{Zn}(\text{SO}_3)_2]$, **10**:

The compound **10** contains 12-membered ring systems, so additionally we investigated the gas sorption ability inclination for N_2 gas, it demonstrates the type-I adsorption curve. The presence of guanidinium cations in the center of the 12-membered ring causes strong H-bonding interactions, thus it shows the relatively lesser BET surface area than expected. The BET surface area was nearly $\approx 21 \text{ m}^2/\text{g}$ as shown in Fig. 2.27.

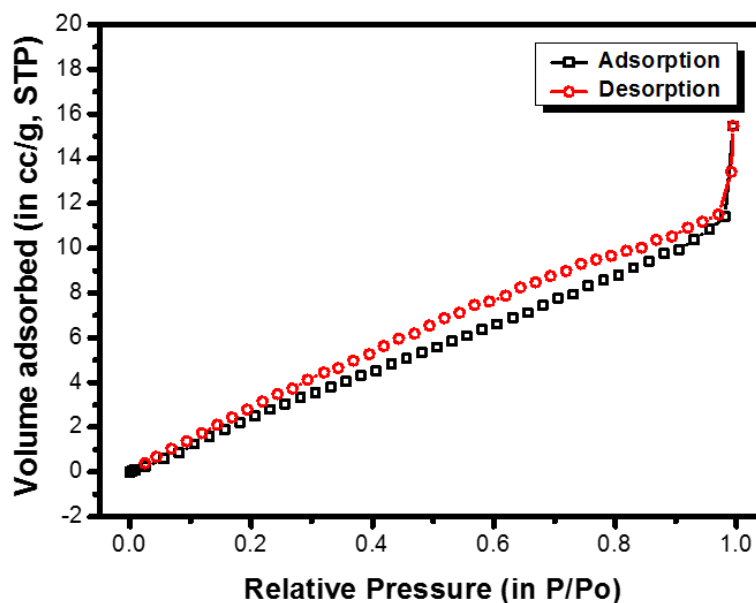


Fig. 2.27. Adsorption isotherms for N₂ on [CN₃H₆]₂[Zn(SO₃)₂], **10**.

2.3.10.2. DSC analysis of [CN₃H₆]₂[Zn(SO₃)₂], **10**:

DSC curve of compound **10** (Fig. 2.28), the phase transition for the compound **10** appear at 36.90 °C, however, in the curve, there was no significance heat change during temperature range of -80 to 30 °C. There are two glass transitions observed at 89.9 °C and 106.78 °C, respectively, and it again appeared followed by two melting curves at 118.66 °C and 164.51 °C, respectively.

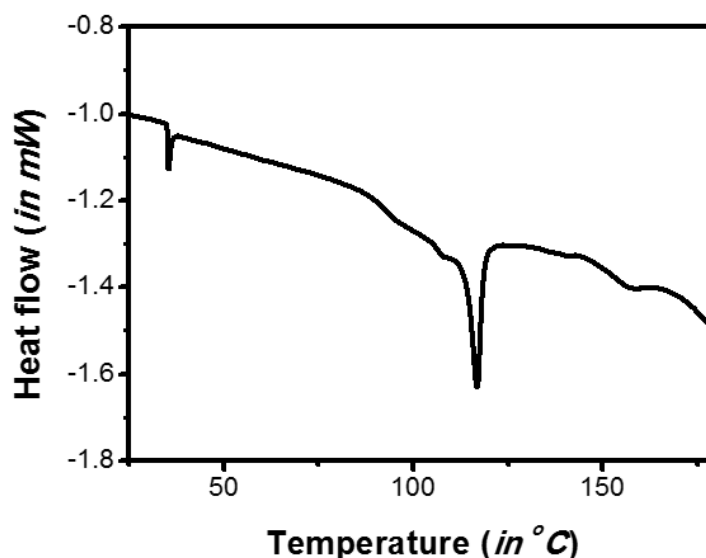


Fig. 2.28. (a) DSC profile diagram of compound **10**.

2.3.10.3. Dielectric constant analysis of $[\text{CN}_3\text{H}_6]_2[\text{Zn}(\text{SO}_3)_2]$, **10**:

The compound **10** crystallizes in NCS space group and belongs to a polar point group, the dielectric constant was performed with the temperature at different frequencies and *vice-versa*. The behavior was studied with the temperature at different frequencies (Fig 2.29a and 2.29b). The graph shows that at higher frequencies, dielectric constants rapidly drops and dielectric constant increases with increase in temperature. Furthermore, the frequency dependence graph of compound **10** was suggested that the dielectric constant rapidly decreases with an increase in frequency at a different temperature (Fig. 2.29b). These data recommend the dipole relaxation present in compound **10** at lower frequencies.

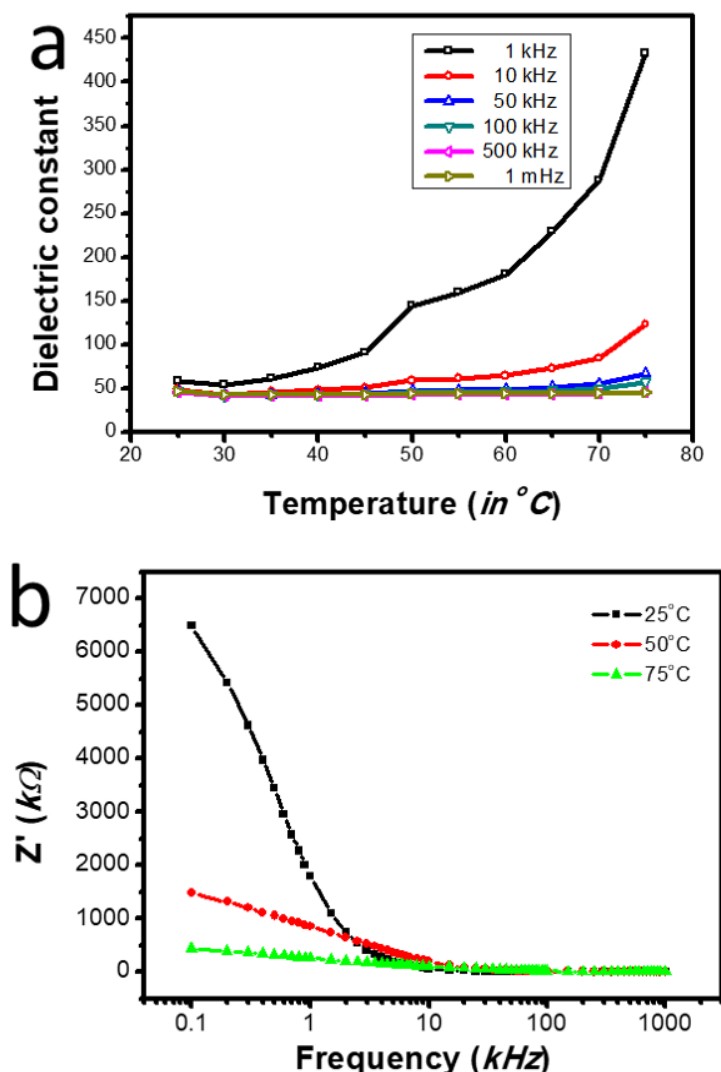


Fig. 2.29. (a) Dielectric constant profile of $[\text{CN}_3\text{H}_6]_2[\text{Zn}(\text{SO}_3)_2]$, **10** and (b) Dielectric constant (real part) vs. frequency profile of compound **10** at different temperatures.

2.4. Thermal analysis:

2.4.1. Thermogravimetric analysis:

The thermal stability of metal-sulfite framework was investigated by the TGA. The TGA analysis of compounds **2-10** was studied at a heating rate 10 °C/min under a constant flow of N₂ gas in the temperature range 30-700 °C (Fig. 2.30) utilizing a Discovery TGA by TA Instruments-Waters Lab. TGA graph of compound **2** suggest that compound **2** is stable up to 160 °C, after that, it shows multi-step decomposition. The compound **2** started to decompose in the temperature range 160-200 °C which accounts 31.3% (calc. 25.24%) weight loss due to the removal of the 1,3-diaminopropane moiety. Finally, the next step start disintegrates in the temperature range 240-400 °C, the weight loss due to the removal of SO₃ group observed 26.86 % (calc. 26.52%) weight loss.

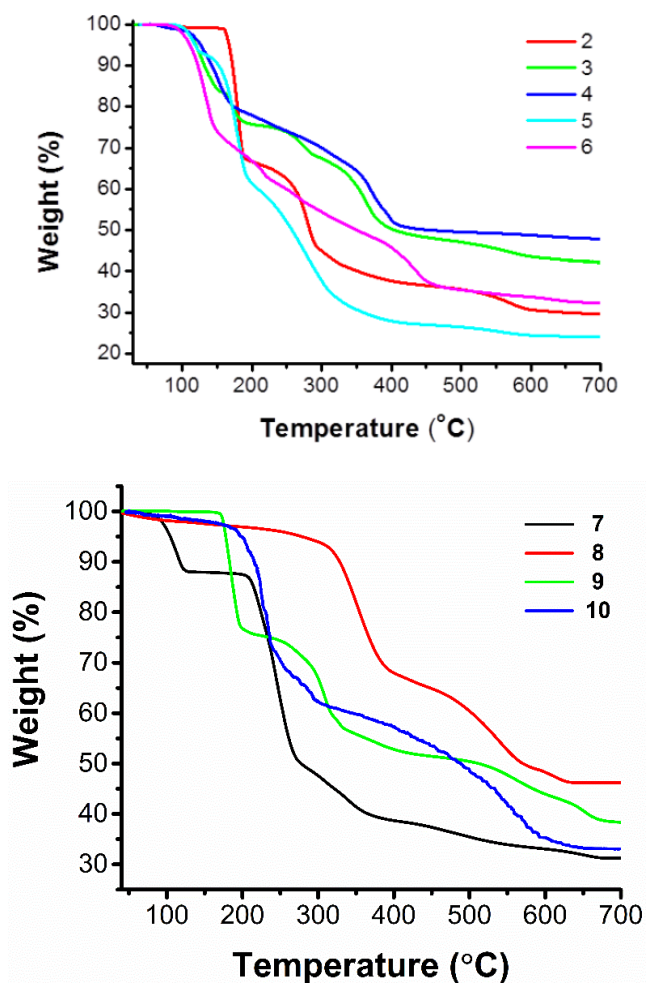


Fig. 2.30. Thermogravimetric analysis for compounds **2-10**.

Similarly, compound **3** undergoes two major disintegrate steps where the first step belongs to the degradation of template 1,4-diaminobutane moiety which accounts 24.14 % (calc. 28.51%) in the temperature range of 95-195 °C. In addition, the next weight loss due to the loss of sulfite in the temperature range of 290-390 °C which accounts 18.46 % (calc. 20.27 %) weight loss. In compound **4**, the TGA profile diagram shows that two-step weight loss, the first step weight loss belongs to the loss of templated amine (HMDA) in the temperature range of 110-200 °C (obs. = 34.53 %, calc. = 33.8%), the next weight loss corresponds to the decomposition of SO₃ in the range of 220-600 °C (obs. = 40.7%, calc. = 41.8 %).

In compound **5**, the curve shows that compound **5** undergoes a three-step weight loss, the first weight loss shows the dehydration of compound **5** in the temperature range of 85-135 °C (obs. = 6.0%, calc. = 5.8%), the second step weight loss belongs to removal of template amine molecules in the range 140-200 °C (obs. = 28.0%, calc. = 26.0 %), the disintegration of sulfite anions are in the range of 230-700 °C (obs. = 44.0 %, calc. 42.4%). In the case of compound **6**, the graph was continuously disintegrate with varying slopes was observed. The total 67.66 % weight loss observed between the temperature range of 100-700 °C, the observed weight loss is showing less weight loss from the collectively calculated weight loss of water, piperazine and SO₂ molecules i.e. 76.83 %. This is indicating the formation of Mn₃O₄ species along with MnO species as residual product and confirmed by the PXRD analysis of the calcined product. The residual product of compound **6** corresponds to MnO (PDF 01-077-2929) /Mn₃O₄ (PDF 01-080-0382) mixture. In compound **7**, the curve undergoes multi-step decomposition of the framework. The first step is involved in the dehydration of compound **7** in the temperature range of 75 to 140 °C which accounts 11.90 % (calc 12.15 %), with loss of water molecules. The second step takes place in 220 to 300 °C temperature range, the weight loss due to the disintegration of 1,3-diamino propane, which is found to be nearly 39.18 % (calc 38.48 %) weight loss. The weight loss of sulfite

group as sulfur dioxide molecule which accounts 19 % (18.00 %) weight loss in the temperature range of 400 to 600 °C. The residual product is identified as cobalt oxide (PDF-00-043-1004).

The TGA of compound **8** reveals that compound **8** disintegrate in two steps, the first step due to loss of *tris*-(2-ethylamino) amine ligand which accounts for 25.06 % weight loss (calc 25.94 %) in the temperature range of 200-300 °C. Additionally, compound **8** is thermally stable than the compounds **2-7** which is maybe the absence of water molecules in the crystal structure. Again, the disintegrates of compound **8** and results in ZnO as a residual product, the weight loss corresponds to a loss of sulfite ligands in the temperature range of 415-570 °C and accounts for 13.07 % (14.18 %) weight loss. TGA analyses of compound **9** (Fig. 2.30) suggests that it showed multi-step decomposition in the range of 165-670 °C leading to 60.4 % weight loss which can be accounted for the combined loss of ethylenediamine, and SO₃ (calc. 60.5%). Similarly, TGA curve of compound **10** is stable up to 180 °C and indicates the two-steps decay, the first step undergoes the removal of guanidinium moiety in the temperature range of 185-300 °C which found to be 34.5 % weight loss (calc. 34.76%). The second and final step is involved in the disintegration of SO₃ anions in the temperature range of 400-630 °C, which results in 23.39 % weight loss (calc. 23.14%). The PXRD analysis of the residual product of compounds **2-5** and compounds **8-10** correspond to the zinc oxide (PDF-01-075-0576).

2.4.2. Temperature-dependent PXRD analysis of [CN₃H₆]₂[Zn(SO₃)₂], **10:**

The PXRD analysis of all synthesized material is observed pure-phase of the compounds **2-10** framework structures (Appendix), which shows the compounds are in good agreement with simulated patterns. The temperature dependent PXRD analysis of compound **10** additionally indicates a similar result with the TGA result and shows the decomposition of

the framework above ≈ 180 °C (Fig. 2.31). In both the cases, the PXRD analysis of calcined samples showed characteristic peaks for ZnO (PDF-01-075-0576).

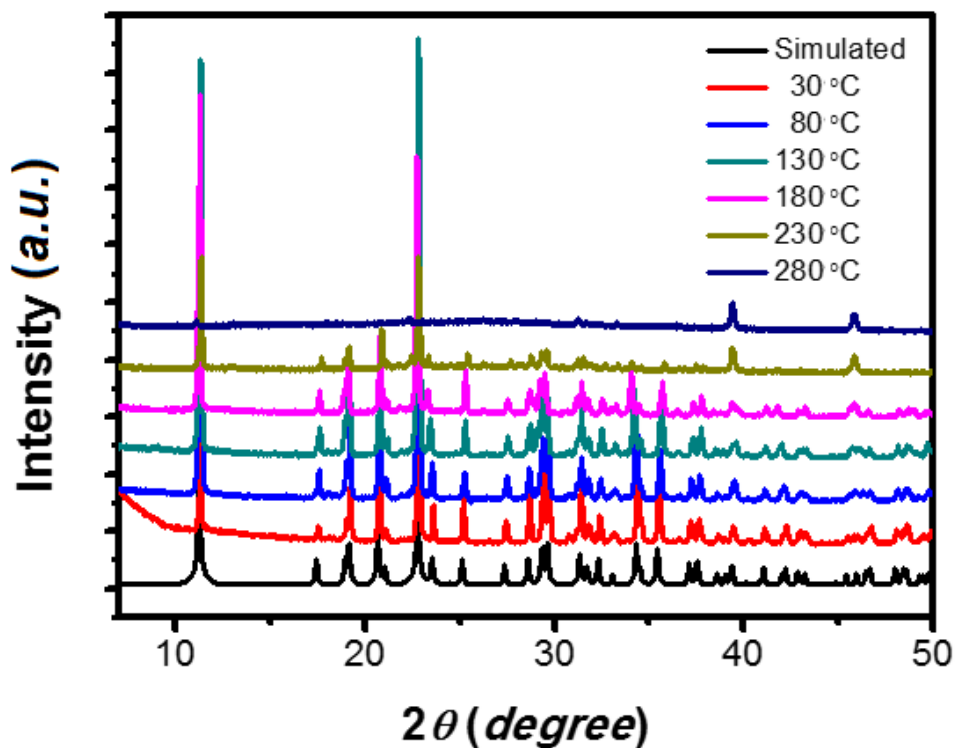


Fig. 2.31. Temperature-dependent PXRD pattern of $[\text{CN}_3\text{H}_6]_2[\text{Zn}(\text{SO}_3)_2]$, **10**.

2.5. Conclusions:

The 10 metal-sulfites open-framework are successfully synthesized, the sulfur based on three-connected sulfite anions as primary building units for generating open-framework materials and representing the ten organically templated metal-sulfites namely $[(\text{C}_3\text{H}_{10}\text{N})_2][\text{Zn}(\text{SO}_3)_2]$, **1**, $[\text{C}_3\text{H}_{12}\text{N}_2][\text{Zn}(\text{SO}_3)_2]$, **2**, $[\text{C}_4\text{H}_{14}\text{N}_2][\text{Zn}(\text{SO}_3)_2]$, **3**, $[\text{C}_6\text{H}_{18}\text{N}_2][\text{Zn}(\text{SO}_3)_2]$, **4**, $[\text{C}_4\text{H}_{12}\text{N}_2][\text{Zn}(\text{SO}_3)_2] \cdot (\text{H}_2\text{O})$, **5**, $[\text{C}_4\text{H}_{12}\text{N}_2][\text{Mn}(\text{SO}_3)_2(\text{H}_2\text{O})_2] \cdot 2\text{H}_2\text{O}$, **6**, $[(\text{C}_3\text{N}_2\text{H}_{10})_2\text{NaCo}(\text{SO}_3)_2(\text{H}_2\text{O})_2] \cdot \text{H}_2\text{O}$, **7**, $[(\text{C}_6\text{N}_4\text{H}_{18})\text{Zn}_3(\text{SO}_3)_3]$, **8**, $[\text{C}_2\text{H}_{10}\text{N}_2][\text{Zn}_3(\text{SO}_3)_4]$, **9** and $[\text{CN}_3\text{H}_6]_2[\text{Zn}(\text{SO}_3)_2]$, **10** are synthesized under hydrothermal condition. The compounds **1-6** shows organically templated 1D linear metal-sulfites open-framework, compounds **7** and **8** show the amine coordinated metal-sulfite a layered structure, compound **9** has organically templated 2D

metal-sulfite open-framework and compound **10** showing the organically templated three-dimensional metal-sulfite open-framework with diamondoid network. In compound **7**, the in-situ Co(II) oxidized to Co(III) during the reaction period. At slightly basic pH, the amine binds with the metal and form a coordinate metal polymer in case of compounds **7** and **8**. In compound **9**, the ethylenediamine templated a 2D structure, which is constituted of $Zn_3(SO_3)_2$ triangular nodes bonded by sulfite anion to give a layered structure with 4, 6 and 8-membered rings. In compound **10**, the guanidinium templated zinc-sulfite forms a 3D structure with embedded 12-membered rings which endorse a distorted adamantane topology. This result encourages its properties and novel structure and the sulfite ion can be usefully employed in designing new open-framework inorganic materials.

References

- (1) Natarajan, S.; Mandal, S. *Angew. Chem. Int. Ed.* **2008**, *47*, 4798.
- (2) Francis, R. J.; Jacobson, A. J. *Angew. Chem. Int. Ed.* **2001**, *40*, 2879.
- (3) Tasi, J.-M.; Tu, P.-T.; Chan, T.-S.; Lii, K.-H. *Inorg. Chem.* **2008**, *47*, 11223.
- (4) Murugavel, R.; Choudhury, A.; Walawalkar, M. G.; Pothiraja, R.; Rao, C. N. R. *Chem. Rev* **2008**, *108*, 3549.
- (5) Choudhury, A.; Krishnamoorthy, J.; Rao, C. N. R. *Chem. Commun.* **2001**, 2610.
- (6) Pasha, I.; Choudhury, A.; Rao, C. N. R. *J. Solid State Chem.* **2003**, *174*, 386.
- (7) Zhang, X.; Yao, J.; Jiang, X.; Fu, Y.; Lin, Z.; Zhang, G.; Wu, Y. *Dalton Trans.* **2015**, *44*, 15576.
- (8) Natarajan, S. V.; Rao, C. *Supramolecular organization and materials design* **2002**, 214.
- (9) Jing, X.-M.; Tan, Y.-B.; Xiao, L.-W.; Liu, Y.-L. *Inorg. Chem. Commun.* **2015**, *57*, 75.
- (10) Udayakumar, D.; Rao, C. *J. Mater. Chem.* **2003**, *13*, 1635.
- (11) Mao, J.-G.; Jiang, H.-L.; Kong, F. *Inorg. Chem.* **2008**, *47*, 8498.
- (12) Chang, H. Y.; Ok, K. M.; Kim, J. H.; Halasyamani, P. S.; Stoltzfus, M.; Woodward, P. *Inorg. Chem.* **2007**, *46*, 7005.
- (13) Lin, Z. E.; Yang, G. Y. *Eur. J. Inorg. Chem.* **2011**, *2011*, 3857.
- (14) Yu, H.; Wu, H.; Pan, S.; Wang, Y.; Yang, Z.; Su, X. *Inorg. Chem.* **2013**, *52*, 5359.
- (15) Wang, J.-H.; Wei, Q.; Cheng, J.-W.; He, H.; Yang, B.-F.; Yang, G.-Y. *Chem. Commun.* **2015**, *51*, 5066.
- (16) Harrison, W. T.; Phillips, M. L.; Nenoff, T. M.; MacLean, E. J.; Teat, S. J.; Maxwell, R. S. *J. Chem. Soc., Dalton Trans.* **2001**, 546.

- (17) Zhang, Y.; Huang, L.; Miao, H.; Wan, H. X.; Mei, H.; Liu, Y.; Xu, Y. *Chem. Eur. J.* **2015**, *21*, 3234.
- (18) Jin, G. B.; Skanthakumar, S.; Soderholm, L. *Inorg. Chem.* **2011**, *50*, 6297.
- (19) Tian, J.; Li, B.; Zhang, X.; Zhang, J. *CrystEngComm* **2014**, *16*, 1071.
- (20) Kong, F.; Sun, C.-F.; Yang, B.-P.; Mao, J.-G. In *Structure-Property Relationships in Non-Linear Optical Crystals I*; Springer: 2012, p 43.
- (21) Zhong, R.-L.; Xu, H.-L.; Li, Z.-R.; Su, Z.-M. *J. Phys. Chem. Lett.* **2015**, *6*, 612.
- (22) Rao, C.; Behera, J.; Dan, M. *Chem. Soc. Rev.* **2006**, *35*, 375.
- (23) Meyer, B. *Sulfur, energy, and environment*; Elsevier, 2013.
- (24) Zhang, D.; Lu, Y.; Zhu, D.; Xu, Y. *Inorg. Chem.* **2013**, *52*, 3253.
- (25) Manos, M. J.; Miras, H. N.; Tangoulis, V.; Woollins, J. D.; Slawin, A. M.; Kabanos, T. A. *Angew. Chem. Int. Ed.* **2003**, *42*, 425.
- (26) Miras, H. N.; Chilas, G. I.; Cronin, L.; Kabanos, T. A. *Eur. J. Inorg. Chem.* **2013**, *2013*, 1620.
- (27) Alipázaga, M. V.; Lowinsohn, D.; Bertotti, M.; Coichev, N. *Dalton Trans.* **2004**, 267.
- (28) Sheldrick, G. *Sheldrick, GM SHELXS-97, Program for X-ray Crystal Structure Solution* **1997**.
- (29) Sheldrick, G. *University of Göttingen, Göttingen, Germany* **1994**.
- (30) Pennington, W. T. *J. Appl. Crystallogr.* **1999**, *32*, 1028.
- (31) Farrugia, L. J. *J. Appl. Crystallogr.* **1997**, *30*, 565.
- (32) Pennington, W. T. *J. Appl. Crystallogr.* **1999**, *32*, 1028.
- (33) Farrugia, L. J. *J. Appl. Crystallogr.* **1997**, *30*, 565.
- (34) Rao, K. P.; Rao, C. *Inorg. Chem.* **2007**, *46*, 2511.
- (35) Brown, I. *Structure and bonding in crystals* **1981**, *2*, 1.

- (36) Nguyen, D.-T.; Chew, E.; Zhang, Q.; Choi, A.; Bu, X. *Inorg. Chem.* **2006**, *45*, 10722.
- (37) Rao, K. P.; Govindaraj, A.; Rao, C. *J. Solid State Chem.* **2007**, *180*, 3571.
- (38) Chilas, G. I.; Stylianou, M.; Kubicki, M.; Vaimakis, T.; Kögerler, P.; Keramidis, A. D.; Kabanos, T. A. *Inorg. Chem.* **2008**, *47*, 4451.
- (39) Rao, K. P.; Rao, C. N. R. *Inorg. Chem.* **2007**, *46*, 2511.
- (40) Palenik, G. J. *Inorg. Chem.* **1997**, *36*, 122.
- (41) Chilas, G. I.; Lalioti, N.; Vaimakis, T.; Kubicki, M.; Kabanos, T. *Dalton Trans.* **2010**, *39*, 8296.
- (42) D'vries, R.; de la Peña-O'Shea, V. *Cryst. Growth Des.* **2014**, *14*, 5227.
- (43) Austria, C.; Zhang, J.; Valle, H.; Zhang, Q.; Chew, E.; Nguyen, D.-T.; Gu, J.; Feng, P.; Bu, X. *Inorg. Chem.* **2007**, *46*, 6283.
- (44) Tiwari, R. K.; Kumar, J.; Behera, J. N. *RSC Adv.* **2015**, *5*, 78389.
- (45) Austria, C.; Zhang, J.; Valle, H.; Zhang, Q.; Chew, E.; Nguyen, D.-T.; Gu, J. Y.; Feng, P.; Bu, X. *Inorg. Chem.* **2007**, *46*, 6283.
- (46) Nguyen, D.-T.; Chew, E.; Zhang, Q.; Choi, A.; Bu, X. *Inorg. Chem.* **2006**, *45*, 10722.
- (47) Harrison, W. T.; Phillips, M. L.; Stanchfield, J.; Nenoff, T. M. *Angew. Chem. Int. Ed.* **2000**, *39*, 3808.
- (48) Harrison, W. T.; Phillips, M. L.; Nenoff, T. M. *J. Chem. Soc., Dalton Trans.* **2001**, 2459.
- (49) Morimoto, C. N.; Lingafelter, E. *Acta Crystallogr., Sect. C: Cryst. Struct. Commun.* **1970**, *26*, 335.
- (50) Harrison, W. T.; Phillips, M. L. *Chem. Mater.* **1997**, *9*, 1837.

Appendix

Table 2.2. Crystal structure refinement parameters for compounds 1-10.

Parameter	1	2	3
Formula	$[(C_3H_{10}N)_2][Zn(SO_3)_2]$	$[C_3H_{12}N_2][Zn(SO_3)_2]$	$[C_4H_{14}N_2][Zn(SO_3)_2]$
<i>Mr</i>	345.73	301.64	315.66
crystal system	Orthorhombic	Orthorhombic	Monoclinic
space group	<i>Pbcn</i>	<i>Pbcm</i>	<i>C2/c</i>
<i>a</i> /Å	22.1708(7)	8.6326(3)	17.3344(9)
<i>b</i> /Å	8.7244(2)	7.6916(3)	8.4890(3)
<i>c</i> /Å	7.7214(2)	16.5072(5)	8.1660(3)
α /°	90	90	90
β /°	90	90	106.855(5)
γ /°	90	90	90
<i>V</i> /Å ³	1493.53(7)	1096.05(7)	1150.02(8)
<i>Z</i>	4	4	4
ρ_{calc} (gcm ⁻³)	1.538	1.826	1.823
λ (MoK α) [Å]	0.71073	0.71073	0.71073
μ / mm ⁻¹ μ (cm ⁻¹)	1.939	2.628	2.509
θ range (deg)	3.61 to 30.50	3.42 to 30.53	3.49 to 28.71
reflections collected	12389	18464	8711
unique reflections [R(int)]	2278 [0.0294]	1732 [0.0859]	1482 [0.0522]
data/restraints/parameters	2278 / 1 / 91	1732 / 1 / 79	1482 / 0 / 81
GOF on <i>F</i> ²	1.038	1.002	1.064
<i>R</i> 1 and <i>R</i> 2 [<i>I</i> >2 σ (<i>I</i>)]	0.0282, 0.0622	0.0320, 0.0674	0.0301, 0.0701
<i>R</i> 1 and <i>R</i> 2 (all data)	0.0381, 0.0653	0.0517, 0.0737	0.0376, 0.0737
largest residual peaks (e.Å ⁻³)	0.266 and -0.296	0.397 and -0.340	0.339 and -0.479
CCDC no	1417645	1417646	1417647

Parameter	4	5	6
Formula	[C ₆ H ₁₈ N ₂][Zn(SO ₃) ₂]	[C ₄ H ₁₂ N ₂][Zn(SO ₃) ₂ . H ₂ O]	[C ₄ H ₁₂ N ₂][Mn(SO ₃) ₂ (H ₂ O) ₂ . 2H ₂ O]
<i>Mr</i>	343.71	331.66	375.28
crystal system	Monoclinic	Triclinic	Triclinic
space group	<i>C</i> 2/ <i>c</i>	<i>P</i> -1	<i>P</i> -1
<i>a</i> /Å	21.1872(13)	8.1135(2)	5.4228(3)
<i>b</i> /Å	8.5354(4)	8.4917(2)	6.6958(4)
<i>c</i> /Å	8.0784(4)	8.8022(3)	9.9304(5)
α /°	90	87.946(2)	104.871(3)
β /°	109.333(4)	88.256(3)	95.917(3)
γ /°	90	63.296(2)	99.602(3)
<i>V</i> /Å ³	1378.53(13)	541.35(2)	339.56(3)
<i>Z</i>	4	2	1
ρ_{calc} (gcm ⁻³)	1.656	2.035	1.835
λ (MoK α) [Å]	0.71073	0.71073	0.71073
μ /mm ⁻¹	2.100	2.677	1.327
μ (cm ⁻¹)			
θ range (deg)	3.48-30.57	2.32-30.56	2.15-30.49
reflections collected	12033	9824	5916
unique reflections [R(int)]	2113 [0.0419]	3316 [0.0552]	2028 [0.0284]
data/restraint s/ parameters	2113 / 0 / 90	3316 / 5 / 169	2028 / 3 / 112
GOF on <i>F</i> ²	1.069	0.992	1.066
<i>R</i> 1 and <i>R</i> 2 [<i>I</i> >2 σ (<i>I</i>)]	0.0310, 0.0781	0.0395, 0.0759	0.0313, 0.0778
<i>R</i> 1 and <i>R</i> 2 (all data)	0.0385, 0.0817	0.0624, 0.0837	0.0385, 0.0806
largest residual peaks (e.Å ⁻³)	0.439 and -0.517	0.450 and -0.502	0.367 and -0.685
CCDC no	1417648	1417649	1417650

Parameter	7	8	9	10
Formula	$[(C_3N_2H_{10})_2NaCo(SO_3)_2(H_2O)_2].H_2O$	$[(C_6N_4H_{18})Zn_3(SO_3)_3]$	$[C_2H_{10}N_2][Zn_3(SO_3)_4]$	$[CN_3H_6]_2[Zn(SO_3)_2]$
<i>Mr</i>	444.35	582.53	578.47	345.67
crystal system	Monoclinic	Triclinic	Monoclinic	Orthorhombic
space group	<i>P2₁/c</i>	<i>P-1</i>	<i>C 2/c</i>	<i>Fdd2</i>
<i>a</i> /Å	8.7984(2)	10.061(5)	13.7379(4)	14.4211(13)
<i>b</i> /Å	13.7933(2)	10.157(6)	8.3487(3)	12.1181(8)
<i>c</i> /Å	13.9548(3)	10.260(5)	13.0277(4)	14.0692(8)
α /°	90	70.753(11)	90	90
β /°	103.557(10)	61.288(10)	106.235(2)	90
γ /°	90	80.871(12)	90	90
<i>V</i> /Å ³	1646.35(5)	868.1(7)	1434.61(8)	2458.7(3)
<i>Z</i>	4	2	4	8
ρ_{calc} (gcm ⁻³)	1.793	2.229	2.678	1.868
λ (MoK α) [Å]	0.71073	0.71073	0.71073	0.71073
μ' mm ⁻¹ μ (cm ⁻¹)	1.372	4.522	5.623	2.365
θ range (deg)	2.11-30.04	2.12-25.50	2.89 to 30.52	2.63 to 27.52
reflections collected	26098	3226	13392	9404
unique reflections [<i>R</i> (int)]	4817 [0.0352]	3226 [0.000]	2195 [0.0331]	1109 [0.1040]
data/restraints/parameters	4817 / 13 / 267	3226 / 7 / 242	2195 / 0 / 117	1109 / 1 / 79
GOF on <i>F</i> ²	1.043	1.020	1.095	1.029
<i>R</i> 1 and <i>R</i> 2 [<i>I</i> >2 σ (<i>I</i>)]	0.0318, 0.0764	0.0681, 0.1627	0.0225, 0.0564	0.0380, 0.0669
<i>R</i> 1 and <i>R</i> 2 (all data)	0.0418, 0.0810	0.1226, 0.1966	0.0253, 0.0576	0.0531, 0.0723
largest residual peaks (e.Å ⁻³)	0.975 and -0.491	1.485 and -0.993	0.457 and -0.764	0.307 and -0.347
CCDC no	1407004	1407005	1424543	1424544

Table 2.3. Complete list of bond lengths [Å] and bond angles [°] for compounds 1-10.#

[(C₃H₁₀N)₂][Zn(SO₃)₂], 1					
Zn1-O1	1.9445(12)	O2-S1	1.5417(12)	C1-C2	1.499(4)
Zn1-O2 ⁱ	1.9683(11)	O3-S1	1.5034(13)	C2-C3	1.499(4)
O1-S1	1.5221(12)	C1-N1	1.469(3)		
[C₃H₁₂N₂][Zn(SO₃)₂], 2					
Zn1-O1	1.9403(15)	O2-S1	1.5046(18)	C1-N1	1.481(3)
Zn1-O3 ^{iv}	1.9687(15)	O3-S1	1.5408(15)	C1-C2	1.513(3)
O1-S1	1.5214(17)				
[C₄H₁₄N₂][Zn(SO₃)₂], 3					
Zn1-O1	1.9641(16)	O2-S1	1.5214(18)	C1-C2	1.497(3)
Zn1-O2 ^{viii}	1.9383(17)	O3-S1	1.500(2)	C2-C2 ^{ix}	1.509(5)
O1-S1	1.5406(17)	C1-N1	1.473(3)		
[C₆H₁₈N₂][Zn(SO₃)₂], 4					
Zn1-O1	1.9623(13)	O2-S1	1.4984(16)	C1-C2	1.501(3)
Zn1-O3 ^{ix}	1.9402(15)	O3-S1	1.5187(15)	C2-C3	1.508(3)
O1-S1	1.5439(14)	C1-N1	1.477(3)	C3-C3 ^{xi}	1.518(4)
[C₄H₁₂N₂][Zn(SO₃)₂].H₂O, 5					
Zn1-O1	1.945(2)	S1-O3	1.5463(19)	C3-N2	1.476(4)
Zn1-O3 ^{xiii}	1.968(2)	S2-O4	1.5462(19)	C4-N2	1.483(4)
Zn1-O4	1.9798(19)	S2-O5	1.5391(19)	C1-C2 ^{xv}	1.501(4)
Zn1-O5 ^{xiv}	1.9532(19)	S2-O6	1.485(2)	C3-C4 ^{xvi}	1.505(4)
S1-O1	1.5243(19)	C1-N1	1.481(4)		
S1-O2	1.491(2)	C2-N1	1.482(4)		

[C₄H₁₂N₂][Mn(SO₃)₂(H₂O)₂].2H₂O, 6					
Mn1-O1	2.1902(11)	O1-S1	1.5290(12)	C1-N1	1.483(3)
Mn1-O2 ^{xvii}	2.2008(12)	O2-S1	1.5344(12)	C2-N1	1.488(2)
Mn1-O1w	2.1861(15)	O3-S1	1.5365(13)	C1-C2 ^{xviii}	1.509(3)
[(C₃N₂H₁₀)₂NaCo(SO₃)₂(H₂O)₂].H₂O, 7					
Co1-N1	1.988(2)	Na1-O5 ^c	2.401(1)	C1-C2	1.479(3)
Co1-N2	1.978(2)	Na1-O1w	2.337(2)	C2-C3	1.475(3)
Co1-S1	2.259(4)	Na1-O2w	2.563(2)	C4-C5	1.508(3)
Co2-N3	1.971(1)	S1-O1	1.485(2)	C5-C6	1.510(3)
Co2-N4	1.987(2)	S1-O2	1.479(2)	C1-N1	1.472(3)
Co2-S2	2.273(4)	S1-O3	1.492(1)	C3-N2	1.476(3)
Na1-O1	2.319(2)	S2-O4	1.488(1)	C4-N3	1.480(2)
Na1-O3 ^b	2.379(1)	S2-O5	1.491(1)	C6-N4	1.485(2)
Na1-O4	2.389(1)	S2-O6	1.487(1)		
[(C₆N₄H₁₈)Zn₃(SO₃)₃], 8					
Zn1-O1	1.925(7)	Zn3-N3	2.058(10)	O9-S3	1.504(7)
Zn1-O4	1.977(8)	Zn3-N4	2.075(9)	C1-N1	1.428(14)
Zn1-O6 ^h	1.953(7)	O1-S1	1.508(7)	C1-C2	1.431(16)
Zn1-O7	1.939(7)	O2-S1	1.538(7)	C2-N2	1.428(16)
Zn2-O2	1.934(8)	O3-S1	1.513(8)	C3-C4	1.421(17)
Zn2-O3 ⁱ	1.962(7)	O4-S2	1.528(7)	C3-N1	1.453(14)
Zn2-O5	1.954(7)	O5-S2	1.501(7)	C4-N3	1.453(15)
Zn2-O9 ^j	1.936(7)	O6-S2	1.526(7)	C5-C6	1.404(16)
Zn3-O8	2.037(8)	O7-S3	1.506(8)	C5-N1	1.462(13)
Zn3-N1	2.262(9)	O8-S3	1.505(7)	C6-N4	1.445(14)

Zn3—N2	2.024(9)				
[C₂H₁₀N₂][Zn₃(SO₃)₄], 9					
Zn1—O1	1.9755(14)	Zn2—O6 ^c	1.9644(15)	S2—O5	1.5227(14)
Zn2—O2	1.9486(14)	S1—O1	1.5275(14)	S2—O6	1.5308(15)
Zn1—O3 ^a	1.9530(14)	S1—O2	1.5295(15)	C1—N1	1.485(2)
Zn1—O4	1.9596(14)	S1—O3	1.5330(15)	C1—C1 ^d	1.515(4)
Zn1—O5 ^b	2.0028(14)	S2—O4	1.5363(14)		
[CN₃H₆]₂[Zn(SO₃)₂], 10					
Zn1—O1	1.950(3)	S1—O2	1.478(4)	C1—N2	1.323(6)
Zn1—O3 ^g	1.952(3)	S1—O3	1.523(3)	C1—N3	1.319(7)
S1—O1	1.553(3)	C1—N1	1.301(7)		

#Symmetry elements (i) $-x+1, -y, -z+2$; (ii) $-x+1, y, -z+3/2$; (iii) $x, -y, z-1/2$; (iv) $-x+1, -y, -z+1$; (v) $x, -y+1/2, -z+1$; (vi) $-x+1, y+1/2, z$; (vii) $x, y, -z+3/2$; (viii) $x, -y, z+1/2$; (ix) $-x, -y, -z$; (x) $-x, y, -z+1/2$; (xi) $-x+1/2, -y-1/2, -z$; (xii) $-x-1/2, -y-1/2, -z-1$; (xiii) $-x, -y+1, -z+2$; (xiv) $-x, -y+1, -z+1$; (xv) $-x-1, -y+2, -z+2$; (xvi) $-x, -y, -z+1$; (xvii) $-x+1, -y+2, -z$; (xviii) $-x, -y+2, -z+1$; (xix) $-x, -y+2, -z$; (xx) $x-1, y, z$; and (xxi) $x+1, y, z$. : (a) $-x+1, y-1/2, -z-1/2$; (b) $x, -y+1/2, z-1/2$; (c) $-x, -y, -z+1$; (d) $-x-1, -y, -z+1$; (e) $-x, -y, -z$

Table 2.4. Hydrogen bonding table for compounds 1-10.#

D—H...A	Symmetry of A	D—H	H...A	D...A	∠D—H...A
[(C₃H₁₀N)₂][Zn(SO₃)₂], 1					
N1—H1A...O3		0.874(16)	1.932(16)	2.806(2)	179(2)
N1—H1B...O2	-x,y,1/2-z	0.85(2)	1.97(2)	2.819(2)	171(2)
N1—H1C...O3	x,-y,1/2+z	0.88(3)	1.91(2)	2.766(2)	166.0(18)
[C₃H₁₂N₂][Zn(SO₃)₂], 2					
N1—H1A...O2	1-x,1/2+y,z	0.87(4)	1.93(4)	2.798(3)	174(2)
N1—H1B...O3	1-x,1-y,-z	0.84(3)	1.97(3)	2.798(3)	169(2)
N1—H1C...O2	-1+x,y,z	0.874(19)	1.88(2)	2.750(3)	171(3)
[C₄H₁₄N₂][Zn(SO₃)₂], 3					
N1—H1A...O1	-x,y,1/2-z	0.86(3)	2.03(3)	2.884(3)	173(3)
N1—H1B...O3	x,y,1+z	0.88(3)	1.94(3)	2.788(3)	161(3)
N1—H1C...O3	x,1-y,1/2+z	0.88(3)	1.90(4)	2.768(3)	170(4)
[C₆H₁₈N₂][Zn(SO₃)₂], 4					
N1—H1A...O1	-x,y,1/2-z	0.83(3)	2.06(4)	2.876(2)	172(3)
N1—H1B...O2	x,1-y,-1/2+z	0.89(3)	1.90(3)	2.778(2)	169(3)
N1—H1C...O2	x,y,-1+z	0.84(3)	1.95(3)	2.785(2)	173(3)
[C₄H₁₂N₂][Zn(SO₃)₂].H₂O, 5					
N1—H1A...O2	-x,1-y,2-z	0.87(3)	1.87(3)	2.707(4)	163(4)
N1—H1B...O1w	1-x,1-y,1-z	0.84(3)	2.04(4)	2.838(4)	157(3)
N2—H2A...O1w		0.87(5)	2.00(5)	2.828(4)	158(5)
N2—H2B...O5		0.82(4)	2.43(4)	3.151(4)	147(3)
N2—H2B...O4	-x,1-y,1-z	0.82(4)	2.21(4)	2.885(4)	139(3)
O1w—H1w...O6	1-x,1-y,1-z	0.82(3)	2.16(3)	2.896(3)	150(3)
O1w—H2w...O3	-x,2-y,1-z	0.83(5)	2.01(5)	2.791(4)	155(4)
C1—H1D...O4		0.97	2.58	3.264(4)	127
C2—H2C...O3		0.97	2.57	3.421(4)	147
C3—H3A...O5	-x,2-y,1-z	0.97	2.59	3.372(5)	138
[C₄H₁₂N₂][Mn(SO₃)₂(H₂O)₂].2H₂O, 6					
N1—H1A...O3	x,1+y,z	0.89(2)	1.89(3)	2.767(2)	167(3)
N1—H1B...O2	-1+x,1+y,z	0.90(2)	1.85(2)	2.714(2)	160(2)
O1w—H1w1...O2w	-1+x,y,z	0.85(3)	1.87(3)	2.714(2)	171(3)
O1w—H1w2...O3	x,1+y,z	0.83(3)	2.05(3)	2.858(2)	166(3)
O2w—H2w1...O3	x,1+y,z	0.81(3)	1.98(3)	2.780(2)	172(3)
O2w—H2w2...O1		0.81(3)	2.00(3)	2.810(2)	177(2)
C2—H2A...O2w	1-x,1-y,1-z	0.97	2.55	3.350(3)	140
C2—H2B...O2w	-1+x,y,z	0.97	2.37	3.228(3)	147
[(C₃N₂H₁₀)₂NaCo(SO₃)₂(H₂O)₂].H₂O, 7					
N1—H1B...O1	1-x, -y, -z	0.83(3)	2.29(3)	2.855(2)	125(2)
N1—H1B...O5	1-x, -y, -z	0.83(3)	2.22(3)	2.946(2)	146(3)
N2—H2A...O3	1-x, -y, -z	0.85(3)	2.22(3)	2.866(2)	133(2)
N2—H2A...O4	x, 1/2-y, -1/2+z	0.85(3)	2.50(3)	3.085(2)	127(2)
N3—H3A...O1		0.84(2)	2.41(2)	2.934(2)	121(2)
N3—H3A...O4		0.84(2)	2.16(3)	2.870(2)	142(2)
N3—H3B...O3		0.84(3)	2.19(3)	3.005(2)	163(2)

N4—H4B...O5	$x, \frac{1}{2}-y, \frac{1}{2}+z$	0.86(3)	2.09(3)	2.821(2)	142(2)
O1w—H1w1...O3w	$1+x, y, z$	0.787(19)	1.979(19)	2.763(3)	175(2)
O1w—H2w1...O2	$1-x, \frac{1}{2}+y, \frac{1}{2}-z$	0.85(2)	2.15(2)	2.931(3)	152(3)
O2w—H1w2...O6	$x, \frac{1}{2}-y, -\frac{1}{2}+z$	0.84(2)	2.17(3)	2.986(3)	164(2)
O2w—H2w2...O2		0.84(2)	2.34(2)	3.136(3)	159(3)
O3w—H1w3...O2w		0.78(3)	2.09(3)	2.846(3)	164(4)
O3w—H2w3...O6		0.81(2)	2.00(2)	2.814(2)	174(3)
C3—H3B...O2		0.97	2.55	3.188(3)	123
C4—H4A...O6	$1-x, -y, 1-z$	0.97	2.53	3.182(2)	125
[(C₆N₄H₁₈)Zn₃(SO₃)₃], 8					
N2—H2A...O2	$-x, -y, -z$	0.85(11)	2.54(11)	3.008(11)	115(11)
N2—H2A...O7	$-x, -y, -z$	0.85(11)	2.33(14)	3.015(14)	138(11)
N2—H2B...O4		0.85	2.27	3.031(10)	150
N2—H2B...O9	$-x, -y, -z$	0.85	2.57	3.079(14)	120
N3—H3A...O6	$1-x, -y, -z$	0.86(8)	2.40(9)	3.057(14)	134(8)
N3—H3B...O5	$1+x, y, -1+z$	0.81(10)	2.50(11)	3.089(13)	131(11)
N3—H3B...O2	$-x, -y, -z$	0.81(10)	2.57(14)	3.158(16)	131(11)
N4—H4A...O4		0.88	2.38	3.125(14)	143
N4—H4B...O3	$-x, -y, 1-z$	0.86(10)	2.35(10)	3.049(13)	139(7)
C4—H4D...O5	$1+x, y, -1+z$	0.97	2.48	3.188(15)	130
[C₂H₁₀N₂][Zn₃(SO₃)₄], 9					
N1—H1A...O1	$\frac{1}{2}+x, -\frac{1}{2}+y, z$	0.88(4)	2.43(4)	3.016(2)	125(3)
N1—H1A...O6	$\frac{1}{2}-x, -\frac{1}{2}+y, \frac{1}{2}-z$	0.88(4)	2.12(4)	2.884(2)	145(3)
N1—H1B...O5	$-x, -y, -z$	0.92(3)	2.04(3)	2.936(2)	164(2)
N1—H1C...O4	$\frac{1}{2}-x, \frac{1}{2}-y, -z$	0.90(3)	2.15(3)	2.981(2)	154(2)
C1—H1E...O4		0.97	2.59	3.337(3)	133
[CN₃H₆]₂[Zn(SO₃)₂], 10					
N1—H1A...O3		0.86	2.13	2.984(7)	174
N1—H1B...O2	$\frac{1}{4}+x, \frac{3}{4}-y, -\frac{1}{4}+z$	0.86	2.20	2.987(7)	152
N2—H2A...O1	$\frac{1}{4}+x, \frac{3}{4}-y, -\frac{1}{4}+z$	0.86	2.27	3.114(6)	168
N2—H2B...O2	$-x, \frac{1}{2}-y, -\frac{1}{2}+z$	0.86	2.28	3.008(7)	143
N3—H3A...O1		0.86	2.07	2.928(6)	173
N3—H3B...O2	$-x, \frac{1}{2}-y, -\frac{1}{2}+z$	0.86	2.17	2.928(6)	147

Where 'D' is donor and 'A' is acceptor, the bond lengths are in (Å) and angles are in (°).

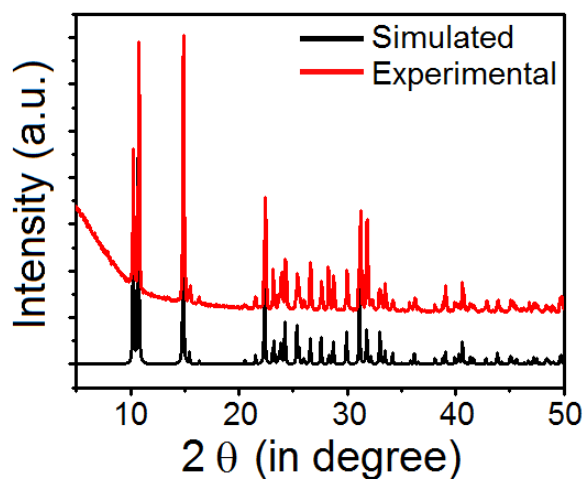


Fig. 2.32. The PXRD pattern of the complex $[\text{C}_3\text{H}_{12}\text{N}_2][\text{Zn}(\text{SO}_3)_2]$, **2** showing the phase purity of as-synthesized material.

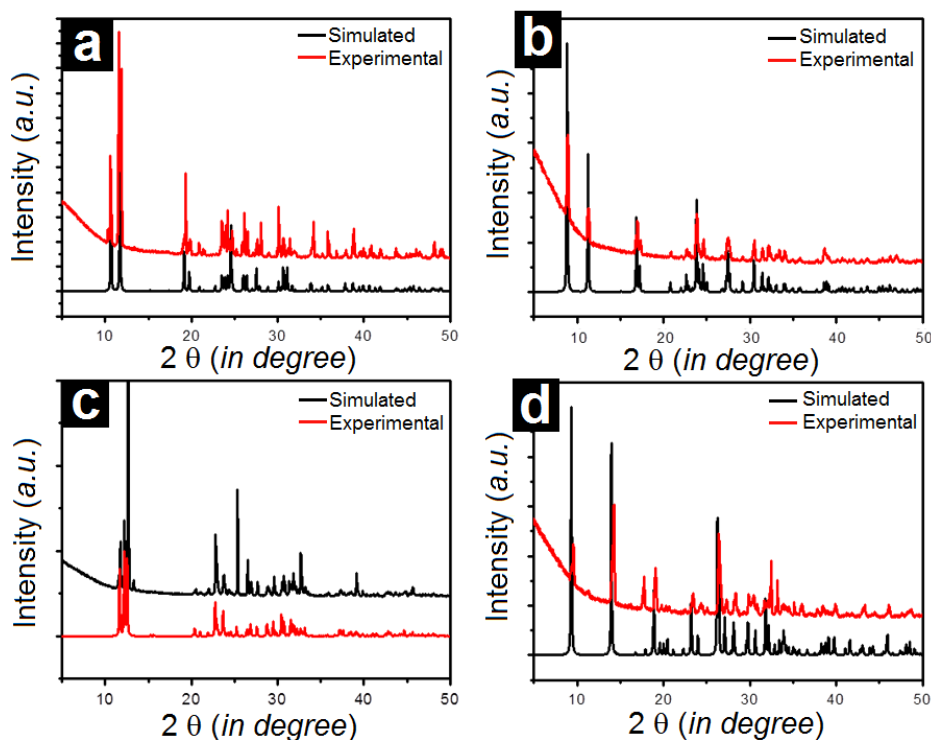


Figure 2.33. PXRD pattern for (a) $[\text{C}_4\text{H}_{14}\text{N}_2][\text{Zn}(\text{SO}_3)_2]$, **3**; (b) $[\text{C}_6\text{H}_{18}\text{N}_2][\text{Zn}(\text{SO}_3)_2]$, **4**; (c) $[\text{C}_4\text{H}_{12}\text{N}_2][\text{Zn}(\text{SO}_3)_2] \cdot \text{H}_2\text{O}$, **5** and (d) $[\text{C}_4\text{H}_{12}\text{N}_2][\text{Mn}(\text{SO}_3)_2(\text{H}_2\text{O})_2] \cdot 2\text{H}_2\text{O}$, **6**.

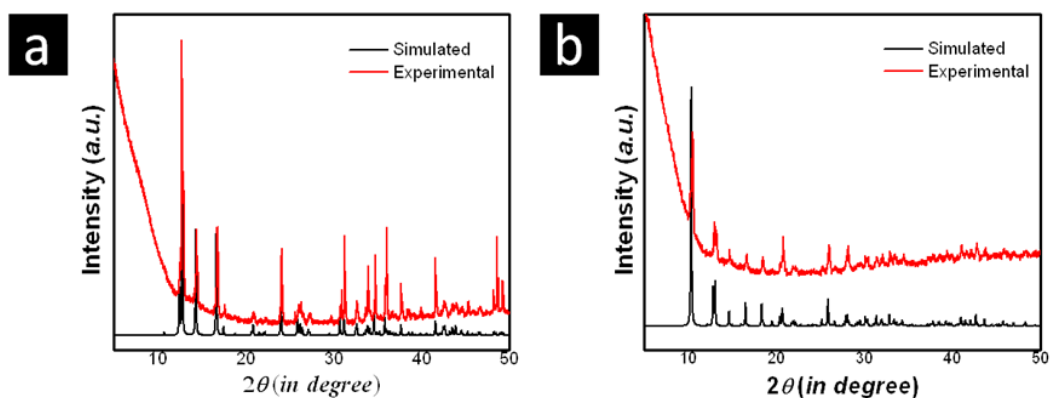


Fig. 2.34. PXR D pattern for (a) $[(C_3N_2H_{10})_2NaCo(SO_3)_2(H_2O)_2] \cdot H_2O$, **7** and (b) $[(C_6N_4H_{18})Zn_3(SO_3)_3]$, **8**.

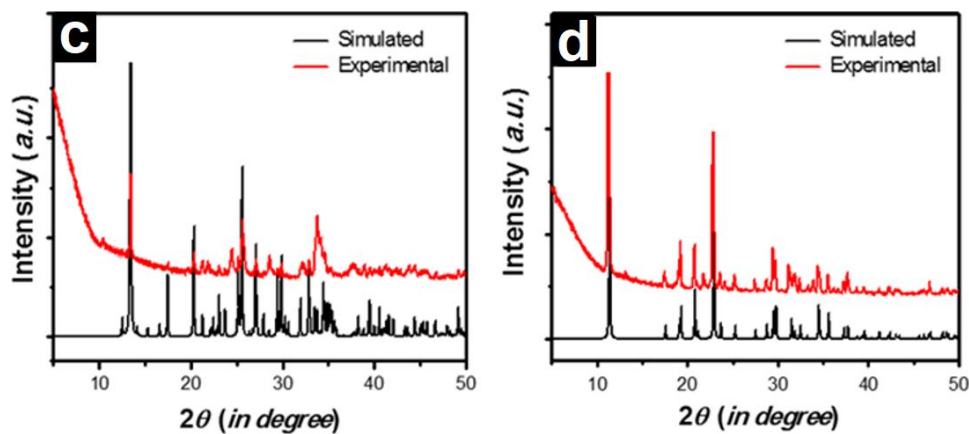
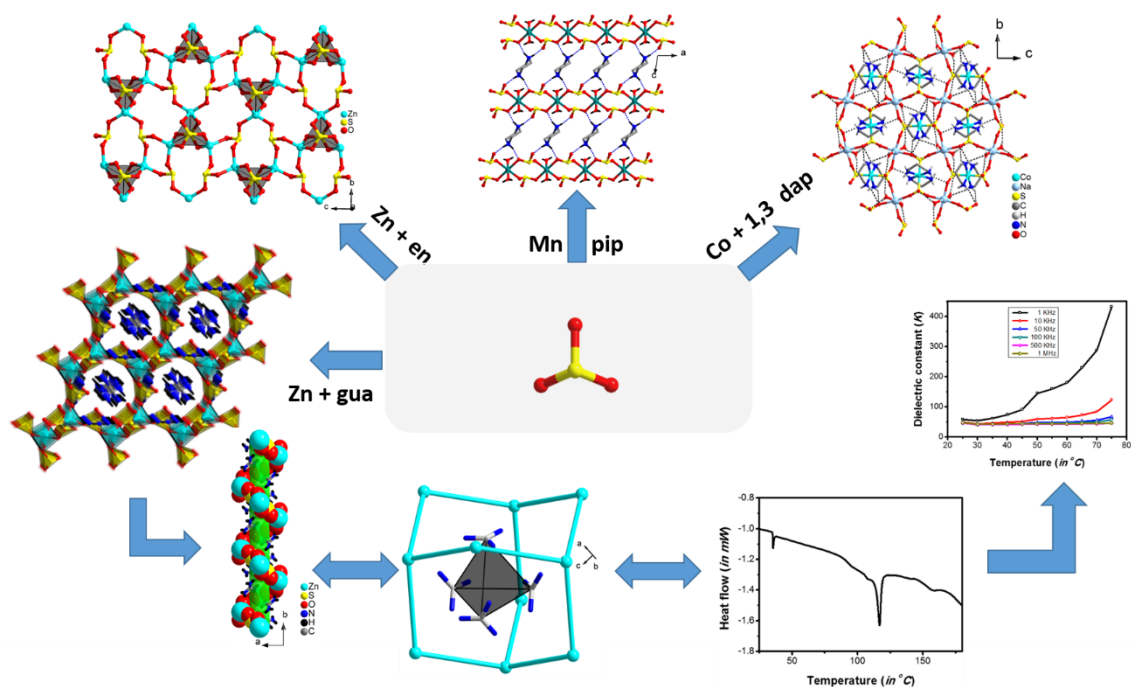


Fig. 2.35. PXR D pattern for (a) $[C_2H_{10}N_2][Zn_3(SO_3)_4]$, **9** and (b) $[CN_3H_6]_2[Zn(SO_3)_2]$, **10**.

Summary of Chapter



Chapter 3

OPEN-FRAMEWORK METAL SULFITE-OXALATE MATERIALS

Abstracts	121
3.1. Introduction	122
3.2. Experimental section	123
3.2.1. Materials and methods	123
3.2.2. Syntheses of compounds 11-15	124
3.2.3. Characterization	126
3.2.3.1. Single crystal structure determination	126
3.2.3.2. Elemental analysis	127
3.3. Results and Discussion	127
3.3.1. Structural analysis of $[\text{Zn}_2(\text{SO}_3)_2(\text{C}_2\text{O}_4)_{0.5}(\text{C}_6\text{N}_2\text{H}_{13})] \cdot (\text{H}_2\text{O})_2$, 11	127
3.3.2. Structural analysis of $[\text{C}_4\text{N}_2\text{H}_{12}]_{0.5}[\text{Zn}_2(\text{SO}_3)_2(\text{C}_2\text{O}_4)_{0.5}(\text{H}_2\text{O})_2]$, 12	130
3.3.3. Structural analysis of $[\text{C}_4\text{N}_2\text{H}_{12}][\text{Cd}_2(\text{SO}_3)_2(\text{C}_2\text{O}_4)(\text{H}_2\text{O})] \cdot \text{H}_2\text{O}$, 13	134
3.3.3.1. Dipole moment calculation for compounds 11-13	138
3.3.4. Structural analysis of $[\text{Na}_2\text{Mn}_2(\text{C}_2\text{O}_4)(\text{SO}_3)_2(\text{H}_2\text{O})_2]$, 14	139
3.3.4.1. Magnetic properties of $[\text{Na}_2\text{Mn}_2(\text{C}_2\text{O}_4)(\text{SO}_3)_2(\text{H}_2\text{O})_2]$, 14	143
3.3.5. Structural analysis of $[\text{NaEu}(\text{C}_2\text{O}_4)(\text{SO}_3)(\text{H}_2\text{O})_3]$, 15	144
3.3.5.1. Photoluminescence study of $[\text{NaEu}(\text{C}_2\text{O}_4)(\text{SO}_3)(\text{H}_2\text{O})_3]$, 15	147
3.4. Thermal analysis	148
3.4.1. Thermogravimetric analysis	148
3.4.2. Differential scanning calorimetry	151
3.5. Conclusions	152
References	153

Appendix	155
Summary	161

Abstract

*This chapter contains, the crystallographic signatures and characterization of five metal sulfite-oxalate inorganic-organic hybrid open-framework materials, namely $[Zn_2(SO_3)_2(C_2O_4)_{0.5}(C_6N_2H_{13})] \cdot (H_2O)_2$, **11**, $[C_4N_2H_{12}]_{0.5}[Zn_2(SO_3)_2(C_2O_4)_{0.5}(H_2O)_2]$, **12**, $[C_4N_2H_{12}][Cd_2(SO_3)_2(C_2O_4)(H_2O)] \cdot H_2O$, **13**, $[Na_2Mn_2(C_2O_4)(SO_3)_2(H_2O)_2]$, **14** and $[NaEu(C_2O_4)(SO_3)(H_2O)_3]$, **15** which demonstrates a layered and 3D structures with different organic templates. These materials have been synthesized in a mild hydrothermal conditions and characterized by techniques such as single crystal X-ray diffraction, dipole moment calculations, fourier transform infrared spectroscopy, powder X-ray diffraction (PXRD), thermogravimetric analysis (TGA) and differential scanning calorimeter (DSC). The common characteristics for compound **11** and compound **12** are the interconnection of surrounded zinc-sulfite chains via oxalate anions in the framework. In compound **13**, cadmium-oxalate chains are interconnected through sulfite anions, whereas in compound **14**, the manganese sulfite layers are interconnected via oxalate anions. In the compound **15**, europium oxalate sheets are interconnected with europium sulfite chain. The coordination geometries of metal (II) ions vary significantly with a ladder-like layered structure in compound **11**, a 3D framework in compound **12**, whereas a layered structure with one-dimensional channel incorporated in compound **13**, while 3D framework and honeycomb-like structures in case of compound **14** (with aqua bridged Sodium oxalate chain) and compound **15** (aqua bridged Sodium oxalate embedded 3D network). The observed structures can also be partly attributed to the influence exerted by the presence of a different structure directing agents (SDA) in the lattice. The dipole moments for metal polyhedral in compound **11-13** were calculated from bond valence sum calculations and are 2.39 D for Zn(1)O₄N polyhedra and 1.66 D for Zn(2)O₄ polyhedra in compound **11**, 24.90 D for Zn(1)O₆ and 29.52 D for Zn(2)O₄ in compound **12** and 5.82 D for Cd(1)O₇ and 2.90 D for Cd(2)O₆ in compound **13**. The magnetic properties of compound **14** show*

antiferromagnetic interactions between the metal centers and compound 15 show good photoluminescence properties.

3.1. Introduction:

The inclusion of oxalate anion in phosphate, selenite, and sulfate-based open-framework materials changes the crystallographic signatures of the crystal lattice¹⁻⁹. The hybrid materials such as oxalate-phosphate, oxalate-phosphite, oxalate-selenate, oxalate-selenite and oxalate-sulfate have some additional type of structural unit. The metal phosphate, metal phosphite or metal sulfate, the metal sulfite has a chain or a sheet-like structures¹⁰. Here the oxalate moiety acts as a bridging ligand which connects the two chains or layers and forms the three-dimensional network^{11,12}. Metal sulfite-oxalate materials are less explored, due to the easy oxidation of sulfite to sulfate¹³. Hence, it is important to explore hybrid materials based on sulfite and oxalate anions. The stereochemically active lone pair electrons of S(IV) ion influences the coordination geometry and can provide new structures with interesting applications.

We have explored the organically templated metal sulfite open-framework. Metal-sulfites show low dimensional (a linear metal-sulfites and a layered metal-sulfite) structure. We use the oxalate as an organic linker which may bind the chains or layers and provide a three-dimensional framework. This chapter contains, five inorganic-organic hybrid open-framework materials with metal-sulfite-oxalate backbone. These compounds have been formulated as $[\text{Zn}_2(\text{SO}_3)_2(\text{C}_2\text{O}_4)_{0.5}(\text{C}_6\text{N}_2\text{H}_{13})] \cdot (\text{H}_2\text{O})_2$, **11**, $[\text{C}_4\text{N}_2\text{H}_{12}]_{0.5}[\text{Zn}_2(\text{SO}_3)_2(\text{C}_2\text{O}_4)_{0.5}(\text{H}_2\text{O})_2]$, **12**, $[\text{C}_4\text{N}_2\text{H}_{12}][\text{Cd}_2(\text{SO}_3)_2(\text{C}_2\text{O}_4)(\text{H}_2\text{O})] \cdot \text{H}_2\text{O}$, **13**, $[\text{Na}_2\text{Mn}_2(\text{C}_2\text{O}_4)(\text{SO}_3)_2(\text{H}_2\text{O})_2]$, **14** and $[\text{NaEu}(\text{C}_2\text{O}_4)(\text{SO}_3)(\text{H}_2\text{O})_3]$, **15**. We have employed organic template DABCO (1,4-diazabicyclo[2.2.2]octane), piperazine and guanidinium carbonate as a structure directing agents (SDA) and they also play a key role in influencing

and stabilizing the crystal structure by providing charge balance and H-bonding interactions with the framework oxygen atoms.

3.2 Experimental section

3.2.1 Materials and methods:

Zinc (II) acetate dihydrate ($\text{Zn}(\text{OAc})_2 \cdot 2\text{H}_2\text{O}$, 99.5%), Cadmium (II) acetate hydrate ($\text{Cd}(\text{OAc})_2 \cdot x\text{H}_2\text{O}$, 99.5%), Europium (III) acetate hydrate ($\text{Eu}(\text{OAc})_3 \cdot x\text{H}_2\text{O}$, 99.5%), 1,4-diazabicyclo[2.2.2]octane (DABCO, 98%) and piperazine (PIP, 98%); were purchased from Sigma-Aldrich. Sodium bisulfite (NaHSO_3 , 99%), Zinc oxalate (ZnC_2O_4 , 98%) and Manganese oxalate dihydrate ($\text{MnC}_2\text{O}_4 \cdot 2\text{H}_2\text{O}$, 98%) Guanidine carbonate (GC, 99%). Sodium disulfite ($\text{Na}_2\text{S}_2\text{O}_5$, 98%) and oxalic acid (98%) were purchased from Merck.

All the compounds **11-15** were characterized by X-ray Diffraction (XRD), Fourier transform infrared spectroscopy (FTIR) and thermogravimetric analysis (TGA). The XRD data were collected using a Bruker D8 advance X-ray powder diffractometer using $\text{CuK}\alpha$ radiation ($\lambda = 1.5418 \text{ \AA}$), radiation in the range of $5^\circ < 2\theta < 55^\circ$. The step size used was 0.02° and exposure time 1 s for each step and the voltage and current used were 40 kV and 40 mA. IR spectra were recorded on a 'Perkin Elmer FTIR spectrometer' equipped with an attenuated total reflectance accessory. The sample was mixed with KBr and pressed. The pressed samples were scanned in the spectral region of $400 - 4000 \text{ cm}^{-1}$ with a resolution of 4 cm^{-1} . Thermogravimetric analyses (TGA) were carried out using a Discovery TGA by TA Instruments-Waters Lab at a heating rate of $10 \text{ }^\circ\text{C}/\text{min}$ under constant nitrogen gas flow. Differential scanning calorimetry was performed using a Mettler Toledo with version 5.1 Stare software. Aluminium crucibles with lids were used to hold samples of known weight (5 mg) for DSC analysis. The data were collected from $-120 \text{ }^\circ\text{C}$ to $475 \text{ }^\circ\text{C}$ at a heating rate of $10^\circ \text{ C}/\text{min}$ constant argon gas flow. The bond valence sums for different

metal ions in **14** and **15** were calculated by considering $r_o(\text{Mn-O}) = 1.790(\text{\AA})$ and $r_o(\text{Eu-O}) = 2.074(\text{\AA})$ ¹⁴.

3.2.2 Syntheses of compounds 11-15:

The amine templated metal sulfite-oxalate compounds **11-15** were synthesized under hydrothermal method at mild condition utilizing a mixture of a metal salt, oxalic acid, organic amine and sodium disulfite and sodium bisulfite as the source of sulfite anions. In general, compound **11** was synthesized by a mixture of zinc acetate dihydrate (0.219 g) was dissolved in distilled water (3.0 mL), and sodium hydrogen sulfite (0.208 mg) and oxalic acid dihydrate (0.126 mg) were added followed by the addition of DABCO (0.285 mg) under constant stirring. The reaction mixture was stirred for 25 minutes at room temperature to make a homogeneous solution. Finally, the reaction mixture was transferred to a 15 mL polypropylene bottle, sealed and heated at 110 °C for 72 h. Initially, the pH of the reaction mixture was approximately 6.0 which remained almost same during the reaction period. After 72 h the reaction mixture was slowly cooled to ambient temperature. The colorless single crystals were obtained at the bottom of the bottle. The other organically templated/ coordinate metal sulfite-oxalate framework compounds **12-14** were synthesized by following similar reaction condition as described for compound **11** with the addition of the different organic amine, oxalic acid, and sulfite source. The details for the respective reaction parameter are employed are listed in Table 3.1.

For the synthesis of compound **15**, Europium acetate hydrate (0.165 g) was dispersed in 3.0 mL distilled water and sodium bisulfite (0.156 g) and oxalic acid (95 mg) was added under constant stirring. Finally, guanidinium carbonate (90 mg) was added to the reaction mixture. The reaction mixture was stirred for an additional 30 minutes. The resulting reaction mixture having pH 6 was transferred to 7 mL autoclave with the molar compositions of

Eu(OAc)₃.xH₂O/3.0 NaHSO₃/1.5 Ox/ GC/300 H₂O was sealed and heated at 115°C for 144 h. After slow cooling of the reaction mixture to room temperature, resulting in transparent crystals with 62% yield.

Table 3.1. Synthetic conditions and molar ratios for the preparation of 11-15#

	Starting composition (in mM) [#]	T[° C]	t[h]	p H	Formula	Yield (%)
11	Zn(OAc) ₂ .2H ₂ O: 2 Na ₂ S ₂ O ₅ : 0.4 OA: 2.5 DABCO:155 H ₂ O	110	72	6	[Zn ₂ (SO ₃) ₂ (C ₂ O ₄) _{0.5} (HDABC O)].(H ₂ O) ₂	78
12	Zn(C ₂ O ₄):3 NaHSO ₃ : 2 PIP:155 H ₂ O	115	48	6	[H ₂ PIP] _{0.5} [Zn ₂ (SO ₃) ₂ (C ₂ O ₄) _{0.5} (H ₂ O) ₂]	72
13	Cd(OAc) ₂ .2H ₂ O:2 NaHSO ₃ :1 OA:2.0 PIP:110 H ₂ O	110	48	6	[H ₂ PIP][Cd ₂ (SO ₃) ₂ (C ₂ O ₄)(H ₂ O)].H ₂ O	51
14	Mn(C ₂ O ₄).2H ₂ O:3.0 NaHSO ₃ :2.0 PIP:155 H ₂ O	115	48	6	[Na ₂ Mn ₂ (C ₂ O ₄)(SO ₃) ₂ (H ₂ O) ₂]	70
15	Eu(OAc) ₂ .xH ₂ O:3.0 NaHSO ₃ :1.5 OA:1.0 GC:300 H ₂ O	115	144	5	[NaEu(C ₂ O ₄)(SO ₃)(H ₂ O) ₃]	63

[#]OA = Oxalic acid; DABCO = 1,4-diazabicyclo[2.2.2]octane; PIP = piperazine; GC = guanidinium carbonate.

3.2.3. Characterization

3.2.3.1. Single-Crystal Structure Determination:

A suitable single crystal of compounds **11-15** was carefully selected under a polarizing microscope and mounted at the tip of the thin glass fiber using cyanoacrylate (super glue) adhesive. Single crystal structure determination by X-ray diffraction was performed on a Bruker AXS-KAPPA Apex II diffractometer equipped with a normal focus, 2.4 kW sealed-tube X-ray source (Mo-K α radiation, $\lambda = 0.71073$ Å) operating at 50 kV and 30 mA. Structures were solved by the direct method using SHELXTL and refined on F^2 by a full-matrix least-squares technique using the SHELXS-97 program package¹⁵. An empirical absorption correction based on symmetry-equivalent reflections was applied using SADABS¹⁶. The graphic programs DIAMOND and ORTEP were used to draw the structures^{17,18}. Non-hydrogen atoms were refined anisotropically. In the refinement, hydrogen atoms were treated as riding atoms using the SHELXL default parameters.

In the case of compound **11**, water hydrogen atoms were not located on Fourier map, and it is present as isolated oxygen atom which is also reflected in the check-cif report of compound **11** having associated 'A' level alert, however, in the refinement the hydrogen atoms were added. In the case of compound **12**, the water hydrogen is located on Fourier map. Also, the piperazine molecule is having the conformational disorder and constrain was applied to fix N-C distances, further, the H-bonding interactions were well established for its protonated nitrogen atom. In case of compound **13**, the lattice water molecule was disordered at two places namely O2wa and O2wb with occupancy of 59.66 and 40.34 % respectively which was solved by PART instruction. Details of crystal structure refinement parameters for compounds **11-15** are given in Table 3.2. (Appendix) whereas the H-bonding interaction and other short interactions are given in Table 3.4 (Appendix).

3.2.3.2. Elemental analysis:

Anal. for $[\text{Zn}_2(\text{SO}_3)_2(\text{C}_2\text{O}_4)_{0.5}(\text{C}_6\text{N}_2\text{H}_{13})] \cdot (\text{H}_2\text{O})_2$, **11**, Calc: C, 17.37; H, 3.54; N, 5.79; S, 13.25 % Found: C, 17.32; H, 3.51; N, 5.74; S, 13.22 %; Anal. For $[\text{C}_4\text{N}_2\text{H}_{12}]_{0.5}[\text{Zn}_2(\text{SO}_3)_2(\text{C}_2\text{O}_4)_{0.5}(\text{H}_2\text{O})_2]$, **12**, Calc: C, 8.68; H, 2.43; N, 3.37; S, 15.45 % Found: C, 8.57; H, 2.39; N, 3.34; S, 15.33 %; Anal. For $[\text{C}_4\text{N}_2\text{H}_{12}][\text{Cd}_2(\text{SO}_3)_2(\text{C}_2\text{O}_4)(\text{H}_2\text{O})] \cdot \text{H}_2\text{O}$, **13**, Calc: C, 12.07; H, 2.70; N, 4.69; S, 10.74 % Found: C, 12.01; H, 2.61; N, 4.57; S, 10.62 %; Anal. For $[\text{Na}_2\text{Mn}_2(\text{C}_2\text{O}_4)(\text{SO}_3)_2(\text{H}_2\text{O})_2]$, **14**, Calc: C, 5.46; H, 0.92; S, 14.57% Found: C, 5.34; H, 0.86; N, S, 14.65 %; Anal. For $[\text{NaEu}(\text{C}_2\text{O}_4)(\text{SO}_3)(\text{H}_2\text{O})_3]$, **15**, Calc: C, 6.05; H, 1.52; S, 8.08 % Found: C, 6.11; H, 1.42; S, 7.93 %.

FTIR (KBr, cm^{-1}) for compound **11**: 3431 br, 2924 m, 1638 s, 1532 m, 1478 s, 1413 s, 1221 s, 1144 b, 992 s, 968 s, 932 s, 884 s, 643 m, 490 m; for compound **12**: 3332 br, 2945 m, 1645 s, 1523 m, 1160 b, 960 s, 928 s, 616 m, 512 m; for compound **13**: 3323 br, 3018 m, 1616 s, 1472 m, 1112 b, 932 s, 875 s, 618 m, 512 m; for compound **14**: 3354 br, 3030 m, 1595 s, 14770 m, 1096 b, 969 s, 904 s, 618 m, 489 m; for compound **15**: 3258 br, 3020 m, 1628 s, 1458 m, 1096 b, 961 s, 910s, 636 m, 496 m.

3.3. Results and Discussion:

Compounds **11-15** were synthesized in hydrothermal conditions at 110-115 °C, by employing different organic templates like DABCO, piperazine and guanidinium carbonate and different metal source which gave a 2D and the three-dimensional structures.

3.3.1. Structural analysis of $[\text{Zn}_2(\text{SO}_3)_2(\text{C}_2\text{O}_4)_{0.5}(\text{C}_6\text{N}_2\text{H}_{13})] \cdot (\text{H}_2\text{O})_2$, **11:**

The SCXRD analysis of compound **11** reveals that colorless crystals are crystallized in the monoclinic crystal system with $P2_1/c$ space group and featuring a layered structure. The

unique unit is composed of 23 non-hydrogen atoms, the 21 atoms belong to a neutral framework which forms a layered structure along with two free lattice water molecules. The asymmetric unit has two crystallographic unique Zn(II) ions which were neutralized by two sulfite anions. The lattice contains a half unit of oxalate anion which is neutralized by mono protonated DABCO cations. The DABCO is further coordinated to one of the Zn(II) ions through another nitrogen atom (Fig. 3.1a).

The two crystallographically distinct Zn(II) ions have two different coordination environments. The Zn1 atoms connected with two oxygen atoms of sulfite anions with monodentate coordination mode through vertex sharing, two oxygen atoms of oxalate anions in chelate fashion and nitrogen of mono protonated DABCO unit and form a penta-coordinated structure around Zn1 ion. The bond length of Zn-N is 2.160(14) Å which is typical of similar coordination. The other Zn2 has a tetrahedral geometry. The coordination sphere of Zn2 is constituted with four sulfite anions in mono-dentate fashion. The average bond length of Zn-O is 1.992 Å and the average S-O bond length is 1.512 Å which is in the normal range and reported in the literature¹⁹. Selected bond lengths are given in Table 3.3 (Appendix).

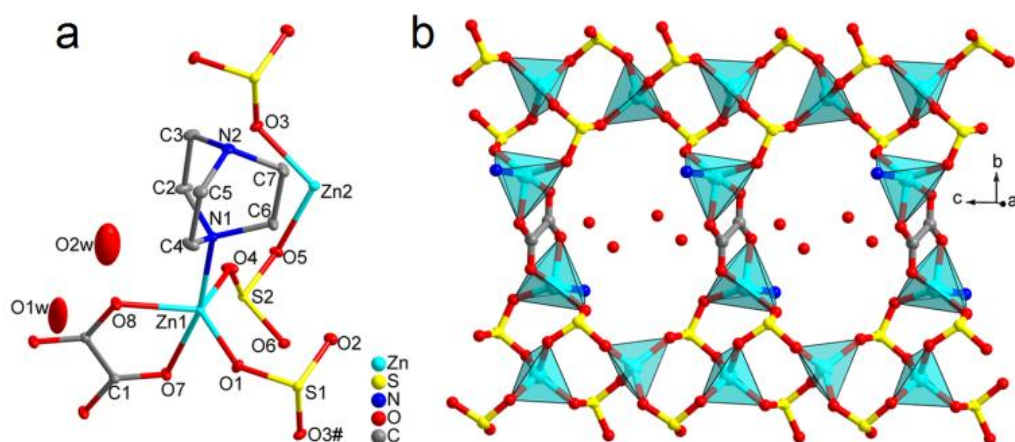


Fig. 3.1. (a) Asymmetric unit of $[\text{Zn}_2(\text{SO}_3)_2(\text{C}_2\text{O}_4)_{0.5}(\text{C}_6\text{N}_2\text{H}_{13})] \cdot (\text{H}_2\text{O})_2$, **11** at 20% ellipsoidal probability where unique atoms were labelled and (b) Part of 2D-crystal lattice

of $[\text{Zn}_2(\text{SO}_3)_2(\text{C}_2\text{O}_4)_{0.5}(\text{C}_6\text{N}_2\text{H}_{13})] \cdot (\text{H}_2\text{O})_2$, **11** highlighting $[\text{Zn}(\text{SO}_3)]_\infty$ 1D chains (N atom is coming from mono protonated DABCO cation has been partly removed for clarity).

The crystal lattice of compound **11** showing the construction of a layered structure (Fig. 3.1b). The layer itself is constituted of $[\text{Zn}(\text{SO}_3)]_\infty$ chain as highlighted in Fig. 3.1b. Within the chain, the tetrahedral Zn(II) ion is connected with four sulfite anions forming a ZnO_4 tetrahedra unit as a result of $\mu^2\text{-}\eta^1\text{:}\eta^1\text{-O:O}$ coordination manner from SO_3^{2-} anion.

These ZnO_4 tetrahedra units are interconnected by their vertices by two O–S–O bridges of two SO_3^{2-} anions to give rise to a 1D chain which runs along the crystallographic *c*-axis similar to compound **1** which is discussed in the previous chapter in linear metal sulfites chain²². However, in this case, the nearest $\text{Zn}\cdots\text{Zn}$ separation within $[\text{Zn}(\text{SO}_3)]_\infty$ chain is 4.0393(5) Å which is comparable to the previous report. The remaining oxygen atoms of the sulfite anion is further connected with other Zn(II) ions (namely Zn1) the along *b*-axis, therefore, each sulfite anions are finally shown $\mu^3\text{-}\eta^1$ coordination fashion. In addition, these Zn1 ions are interconnected *via* oxalate anions which act as a bridge between two Zn1 centres and extend the lattice along *b*-axis to generate a layered structure. In the layer, six Zn(II) ions, four sulfite anions, and two oxalate anions get together and form a 12-membered ring and the coordinated organic amine namely, the DABCO units are pointing outwards and present in between the layers.

The protonated end of coordinated DABCO cation is implicated in bifurcated interlayer H-bonding $\text{N}2\text{-H}2\cdots\text{O}6^i$ ($d_{\text{H}\cdots\text{O}} = 2.18$ Å) and $\text{N}2\text{-H}2\cdots\text{O}7^i$ ($d_{\text{H}\cdots\text{O}} = 2.32$ Å), where $i = -1+x$, y , $-1+z$, along *a*-axis which further stabilizes the lattice (Fig. 3.2). The lattice water molecules are also located in between the layers.

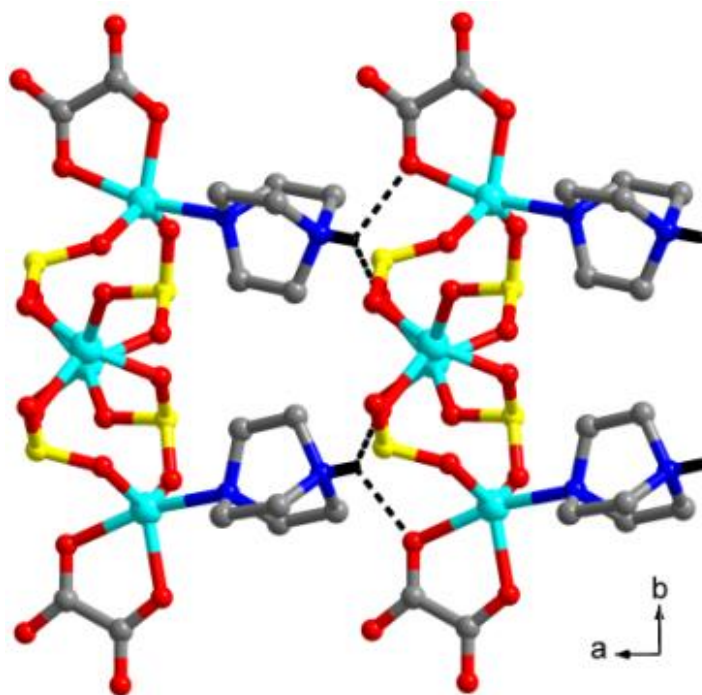


Fig. 3.2. Bifurcated H-bonding interaction in $[\text{Zn}_2(\text{SO}_3)_2(\text{C}_2\text{O}_4)_{0.5}(\text{C}_6\text{N}_2\text{H}_{13})] \cdot (\text{H}_2\text{O})_2$, **11**, through partially protonated DABCO cations.

3.3.2. Structural analysis of $[\text{C}_4\text{N}_2\text{H}_{12}]_{0.5}[\text{Zn}_2(\text{SO}_3)_2(\text{C}_2\text{O}_4)_{0.5}(\text{H}_2\text{O})_2]$, **12**:

The single crystal X-Ray diffraction data reveals that the plate-shaped colorless crystals of compound **12** crystallize in achiral $P4_2/mnm$ space group in tetragonal crystal system. The crystallographic analysis shows an infinite three-dimensional network of Zn(II) ions as a central atom with sulfite and oxalate as counter anions. The unique unit of compound **12** contains 10 non-hydrogen atoms, eight of which are involved in the formation of the inorganic framework and two atoms belong to organic templated piperazine. The asymmetric unit contains two crystallographically distinct Zn(II) ions with one-quarter occupancy which is counteracted by the presence of a half unit of the sulfite anion and a one-quarter unit of oxalate anion. The extra negative charge is further balanced by the presence of a one-quarter unit of protonated piperazine cation (Fig. 3.3).

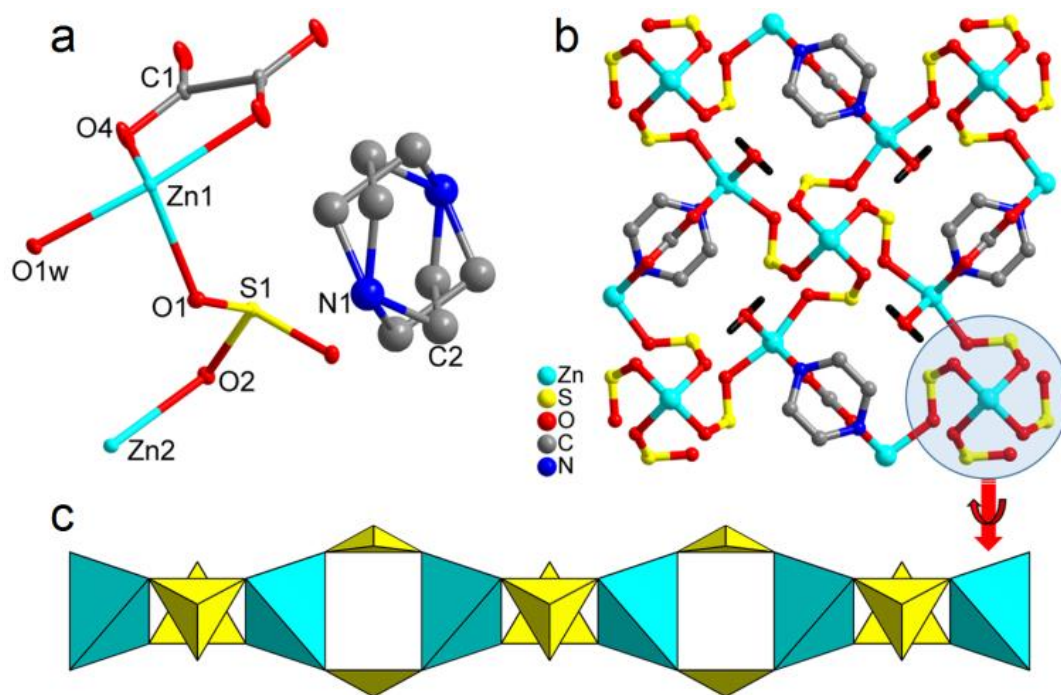


Fig. 3.3. (a) Asymmetric unit of $[C_4N_2H_{12}]_{0.5}[Zn_2(SO_3)_2(C_2O_4)_{0.5}(H_2O)_2]$, **12** at 25% ellipsoidal probability (unique atoms were labelled; disordered piperazine is also shown), (b) Part of the 3D-crystal lattice of $[C_4N_2H_{12}]_{0.5}[Zn_2(SO_3)_2(C_2O_4)_{0.5}(H_2O)_2]$, **12** as viewed along the *c*-axis and (c) Formation of $[Zn(SO_3)]_{\infty}$ chain along the *c*-axis which is highlighted in 'b' (as viewed close to the *b*-axis).

In the crystal lattice, the two crystallographically distinct Zn(II) ions have different coordination environment, where the Zn1 has octahedral geometry and Zn2 has tetrahedral geometry. The coordination sphere of Zn1 is consists of six oxygen atoms, two of which are shared by two sulfite anions, two are coming from oxalate anion (coordinated in chelate mode) and two aqua ligands, while the coordination sphere of Zn2 ion is composed of four oxygen atoms which are shared with four symmetries related sulfite anions. Therefore, the sulfite anion has $\mu^3-\eta^1$ coordination mode. All the Zn-O bond lengths are in good agreement with the reported literature (Table 3.3 Appendix)²².

In the part of the crystal lattice of compound **12**, the tetrahedron Zn(II) ions namely Zn2 and pyramidal sulfite anions share their vertices to lead to a twisted 1D chain of Zn_2S_2

(excluding the intervening O atoms) running along the crystallographic *c*-axis with a closest Zn···Zn distance of 4.458 Å as shown in Fig. 3.3b and 3.3c. These chains are interconnected through the coordination of the remaining oxygen atoms of sulfite anion towards the octahedral Zn1 ions to generate a 3D lattice (Fig. 3.4a).

Moreover, the interchain connectivity is strengthened by the bridging capability of oxalate anions which is tessellated between two Zn1 ions as shown in Fig. 3.4b. The possibility of oxalate anions to direct the crystal lattice structure due to the bridging of Zn(II) ions along the protonated piperazine cation cannot be ruled out.

Interestingly, compound **12** shows remarkable similarity with the previously reported $[\text{Zn}_4(\text{C}_6\text{H}_{12}\text{N}_2)(\text{SO}_3)_4(\text{H}_2\text{O})_4]$ structure which is devoid of oxalate moiety and piperazine template²³. Also, the DABCO molecule which was used as amine acts as a bridging ligand coordinating to the Zn(II) ions through both of its nitrogen. Notably, the oxalate moiety in case of compound **12** effectively takes over the role of DABCO molecule as described above and the additional negative charge of oxalate anion is neutralized by the presence of protonated piperazine cation.

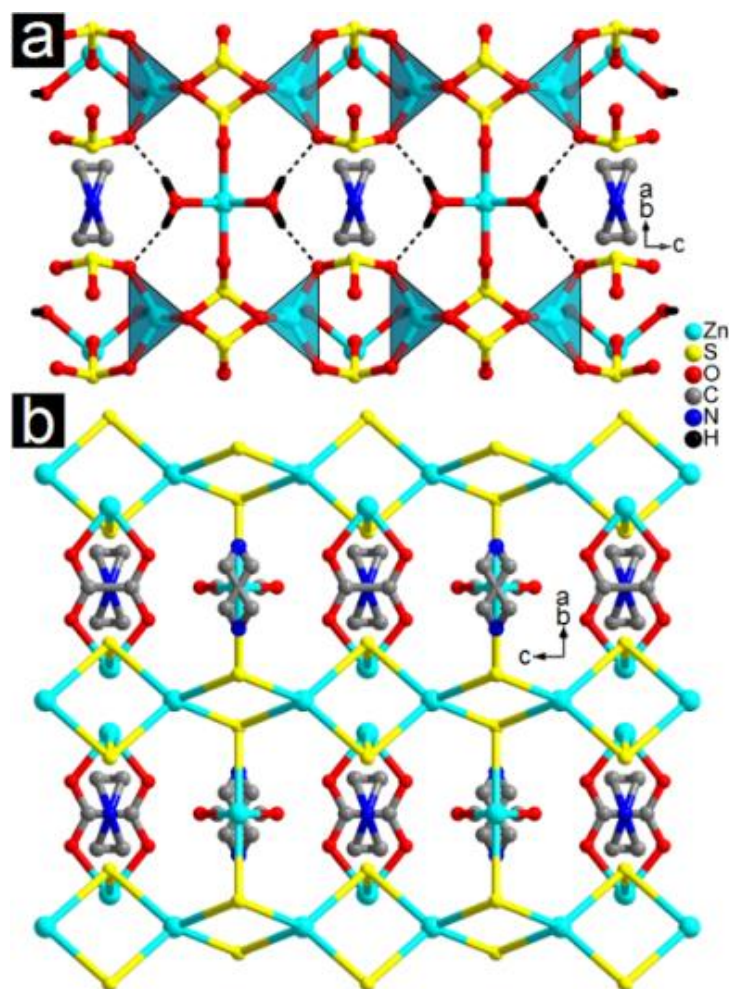


Fig. 3.4. A 3D-Crystal lattice of $[\text{C}_4\text{N}_2\text{H}_{12}]_{0.5}[\text{Zn}_2(\text{SO}_3)_2(\text{C}_2\text{O}_4)_{0.5}(\text{H}_2\text{O})_2]$, **12**, showing interconnection of Zn_2S_2 chains (excluding the intervening O atoms) running along c -axis (a) *via* Zn-sulfite coordination and (b) *via* Zn-oxalate coordination (H-bonding through aqua ligand is also shown with fragmented bonds along crystallographic position of disordered protonated piperazine cation).

The infinite 3D network of compound **12** consists of 12 membered rings (MRs) composed of six zinc ions and six sulfite anions when viewed along the diagonal of the ab -plane (Fig. 3.5). It also has 10-membered rings which are formed by five Zn(II) ions, four sulfite anions, and one oxalate anion when viewed along the c -axis as can be seen in Fig. 3.3b. Further strength of the crystal lattice comes from the H-bonding interaction displayed by protonated piperazine cation towards oxalate oxygen atom with $d_{\text{N1-H1A}\cdots\text{O3}} = 2.28 \text{ \AA}$ (symmetry of O3 = $y, x, 1-z$; Fig. 3.5) and by coordinated aqua ligands towards one of the

sulfite oxygen atoms with $d_{O1w-H1w...O2} = 2.00 \text{ \AA}$ (symmetry of O2 = $1/2+y, 1/2-x, 1/2-z$;

Fig. 3.4a).

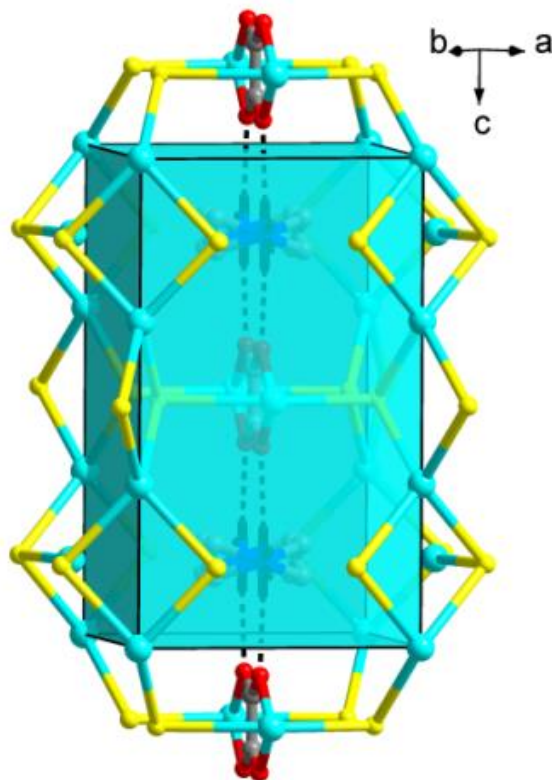


Fig. 3.5. H-bonding interaction in case of $[C_4N_2H_{12}]_{0.5}[Zn_2(SO_3)_2(C_2O_4)_{0.5}(H_2O)_2]$, **12** between protonated piperazine and oxalate oxygen atoms (black fragmented bonds), 12-membered rings are also visible.

3.3.3. Structural analysis of $[C_4N_2H_{12}][Cd_2(SO_3)_2(C_2O_4)(H_2O)].H_2O$, **13**:

Colorless crystals of compound **13** crystallize in a triclinic crystal system having $P-1$ space group and showed a two-dimensional structure. The asymmetric unit of compound **13** (Fig. 3.6) consists of 24 non-hydrogen atoms, where 17 atoms constitute the inorganic framework and 7 atoms belong to the organic template with one lattice water molecule. The inorganic framework consists of two crystallographically unique Cd(II) ions, two sulfite anions, one oxalate anion and one aqua ligand. The charge of the anionic framework is balanced by the presence of half unit of two unique protonated piperazine cations.

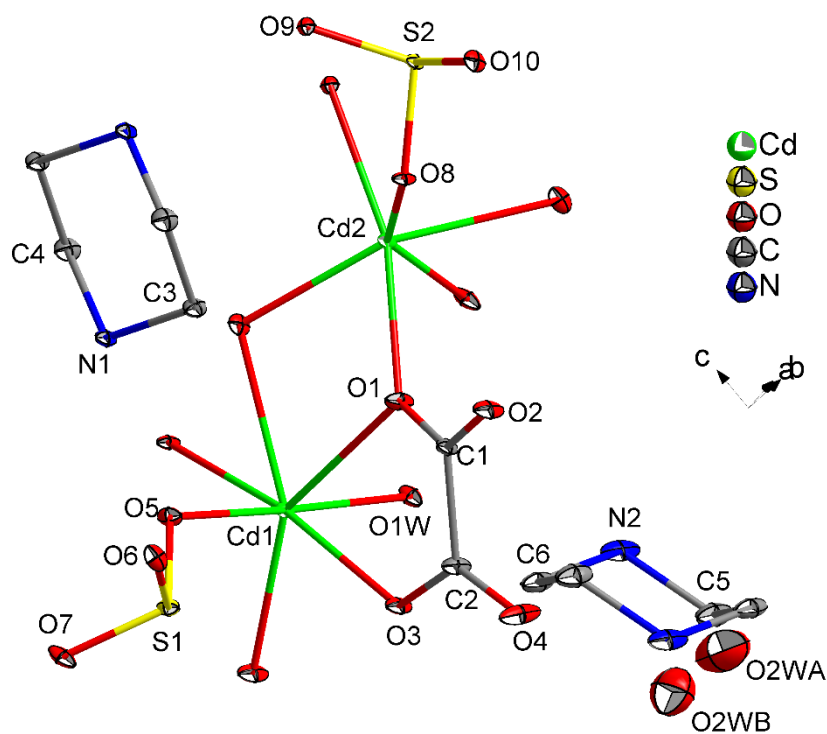


Fig. 3.6. The asymmetric unit of $[\text{C}_4\text{N}_2\text{H}_{12}][\text{Cd}_2(\text{SO}_3)_2(\text{C}_2\text{O}_4)(\text{H}_2\text{O})].(\text{H}_2\text{O})$, **13** with 15% ellipsoidal probability.

The two Cd(II) ions have distinct crystallographic environments where the coordination atmosphere of Cd1 ion is composed of seven oxygen atoms contributed by two sulfite anions, two oxalate anions, and one aqua ligand. The S(1)O₃ is coordinated in a monodentate fashion and S(2)O₃ provide its two oxygen atoms in a chelate manner to the Cd1 ions resulting in a pentagonal bipyramidal geometry. The Cd2 ion has a distorted octahedral geometry and the oxygen atoms are contributed by four different sulfite anions and one oxalate anion where S(1)O₃ anion gives two of its oxygen towards the Cd2 centre. Thus, both unique pyramidal sulfite anions give all of its oxygen atoms to the Cd(II) ions with significantly different coordination mode; where S(1)O₃ coordinates two Cd(II) ions in a $\mu^2\text{-}\eta^1\text{:}\eta^1\text{-O:O:O}$ manner and S(2)O₃ coordinates four Cd(II) ions in a $\mu^4\text{-}\eta^1\text{:}\eta^2\text{:}\eta^2\text{-O:O:O}$ manner. The selected Cd-O bond lengths are given in Table 3.2 which are within the range as reported for other Cd-O bonds²⁴.

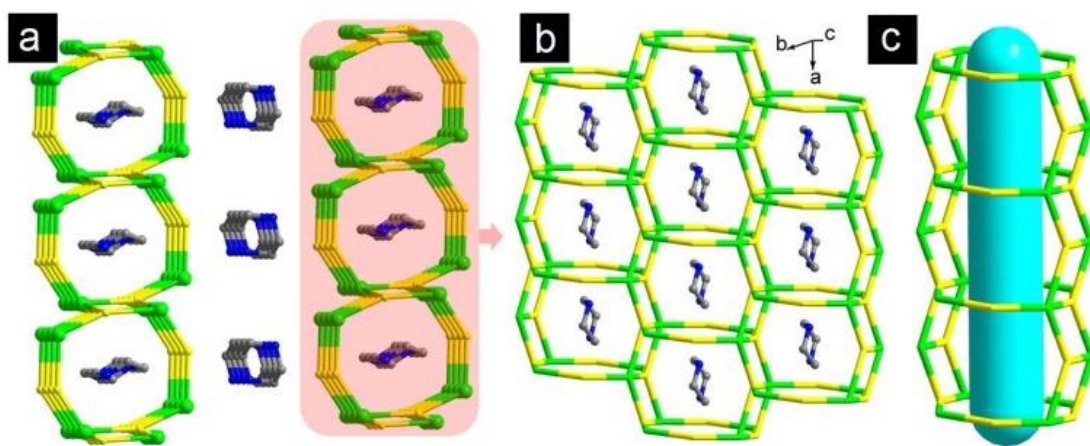


Fig. 3.7. (a) Part of crystal lattice of the $[\text{C}_4\text{N}_2\text{H}_{12}][\text{Cd}_2(\text{SO}_3)_2(\text{C}_2\text{O}_4)(\text{H}_2\text{O})]\cdot\text{H}_2\text{O}$, **13** as viewed close to a -axis, (b) The layered structure in case of compound **13** in the ab -plane and (c) Embedded 1D channel along the a -axis having 8 and 4-membered rings within the layers (The oxygen atoms have been omitted for clarity, S = yellow, Cd = green, N = blue and C = grey).

The crystal lattice of compound **13** is shown in Fig. 3.7, which clearly shows the presence of a layered structure with embedded one-dimensional channels consist of 8-membered (Cd_4S_4) and 4-membered (Cd_2S_2) rings (excluding the intervening oxygen atoms). The interlayer space is occupied by a protonated piperazine molecule which interconnects the two layers by H-bonding interactions. Interestingly, crystallographically different protonated piperazine molecules occupy the cavity of the one-dimensional channel (Fig. 3.7a and 3.7b). Each channel is composed of four similar sets of edge-sharing $\text{Cd}(1)\text{O}_7$ and $\text{Cd}(2)\text{O}_6$ polyhedra which are interconnected through one of the vertices resulting in a Cd-oxalate chain along the a -axis (Fig. 3.8). Two such chains are further linked *via* $\text{S}(2)\text{O}_3^{2-}$ coordination which leads to a ribbon-like structure along the a -axis as shown in Fig. 3.8b. These ribbons are further connected *via* $\text{S}(1)\text{O}_3^{2-}$ anions along the b -axis to give one-dimensional channel.

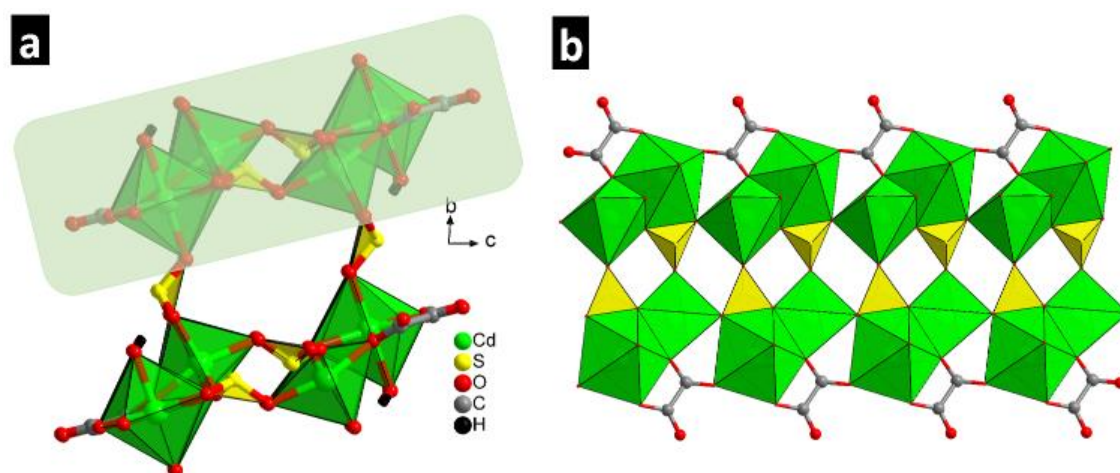


Fig. 3.8. (a) Four sets of $\text{CdO}_{6/7}$ polyhedrons for the construction of 1D channel as a result of sulfite and oxalate coordination in compound **13** and (b) Part of the 1D channel highlighted in 'a' shows formation of ribbon structure in compound **13**.

The other lattice stabilizing interaction is strong H-bonding engendered by protonated piperazine cations and lattice water molecules towards sulfite and oxalate oxygen atoms. The H-bonding interactions shown by piperazine moieties situated inside the 1D channel further reinforces the channel structure whereas the protonated piperazine cations situated in between the layers and interconnects the inorganic frameworks, thus resulting in an increase in the crystal lattice dimensionality (Fig. 3.9). Various H-bonding interactions are given in Table 3.4.

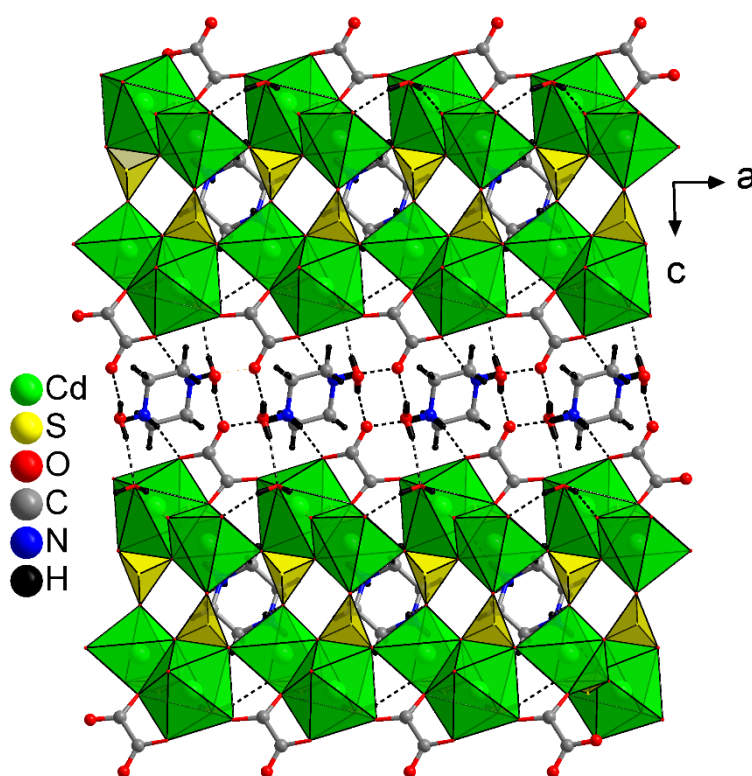


Fig. 3.9. H-bonding pattern in $[\text{C}_4\text{N}_2\text{H}_{12}][\text{Cd}_2(\text{SO}_3)_2(\text{C}_2\text{O}_4)(\text{H}_2\text{O})]\cdot\text{H}_2\text{O}$, **13**.

3.3.3.1. Dipole moment calculations for compounds 11-13:

In the crystal lattice, the dipole-dipole interactions are a common phenomenon. This dipole-dipole interaction occurs between two neighboring polar species which can be repulsive (+/+, -/-) or attractive (+/-). In the crystal lattice, the dipole moment of species is nullified by neighboring species. The compounds contain multiple polar groups which counteract each other. The dipole moment calculations are required to determine net dipole moment and the electrostatic dipole-dipole interaction between the molecules. The magnitude and direction of the dipole moment can be determined by applying bond-valence sum calculations by the bond length and bond angle of polyhedron species²⁵.

The local dipole moment of compounds **11-13** was calculated (from the Debye equation $\mu = neR$, where the dipole moment μ is in Debye (10^{-18} esu cm), R is the distance between two charge species, e is the charge on the species in -4.8×10^{-10} esu and n is the total number

of electrons) to understand the odd coordination environment of SO_3^{2-} anion due to the presence of lone pair of electrons over S(IV) in sulfite anions^{25,26}. Using a similar approach as described for metal oxyfluorides²⁵, the average dipole moments of the local sulfite anion is approximately 18.32 Debye (D) (S1) and 17.42 D (S2) for compound **11**, 16.55 D (S1) for compound **12** and 16.63 D (S1) and 16.53 D (S2) for compound **13**. Sulfite based compounds show net dipole moment of S1 is 17.64 D & S2 is 23.80 D for compound **11**, 33.19 D for compound **12** and S1 and S2 are 21.24 D & 20.88 D respectively for compound **13** as per the calculation reported by Poeppelmeier *et al.* with an atomic valence of S on +4 and O is -1.37²⁶. Further, the net dipole moment of metal polyhedra in compounds **11-13** are 2.39 D for Zn(1)O₄N polyhedra and 1.66 D for Zn(2)O₄ polyhedra in compound **11**, 24.90 D for Zn(1)O₆ and 29.52 D for Zn(2)O₄ in compound **12** and 5.82 D for Cd(1)O₇ and 2.90 D for Cd(2)O₆ in compound **13**.

3.3.4. Structural analysis of $[\text{Na}_2\text{Mn}_2(\text{C}_2\text{O}_4)(\text{SO}_3)_2(\text{H}_2\text{O})_2]$ **14**:

The reaction between manganese oxalate and sodium bisulfite in presence of piperazine under hydrothermal condition results a block shape colorless crystal of $[\text{Na}_2\text{Mn}_2(\text{C}_2\text{O}_4)(\text{SO}_3)_2(\text{H}_2\text{O})_2]$, **14**. The single crystal X-ray analysis reveals that compound **14** crystallizes in the monoclinic crystal system with a $C2/c$ space group. The asymmetric unit of compound **14** contains one manganese ion, one sodium ion, one sulfite anion, a half moiety of oxalate anion and one aqua ligand (10 non-hydrogen atoms) as shown in Fig. 3.10. The crystallographic independent central Mn(II) ion has octahedral geometry and surrounded by the four neighboring sulfite anions *via* Mn-O-S and Mn-O-Mn linkage with the average bond length of Mn-O is 2.2026 Å and the S-O bond length is 1.5337 Å. The Mn atoms coordinate oxo-bridge with trifurcated oxygen atom O4 and form the edge-sharing structure. The separation between two Mn(II) ions is 3.4907(3) Å.

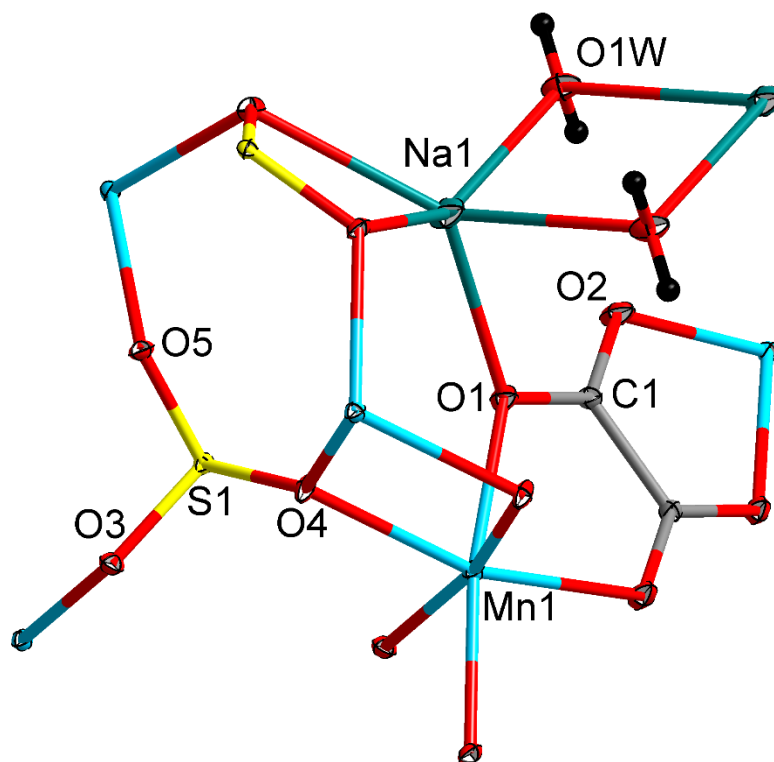


Fig. 3.10. The Molecular unit of $[\text{Na}_2\text{Mn}_2(\text{C}_2\text{O}_4)(\text{SO}_3)_2(\text{H}_2\text{O})_2]$, **14** with 25% ellipsoidal probability (unique atoms were labeled).

For understanding the packing, in the crystal lattice of compound **14**, it consists of the alternating MnO_4 tetrahedron and SO_3 trigonal pyramids linked through their corner to form the layer structure in the bc -plane with 4-member rings as shown in the Fig. 3.11a. In the crystal lattice, SO_3^{2-} anion provides its all oxygen atoms towards the Mn atom and coordinate in $\eta^1\mu^3$ -manner as shown in Fig. 3.11a. The organic oxalate anion moiety connects the two Mn(II) ions to form a chain along a -axis (Fig. 3.11b). Further, the oxalate anions are acting as a bridge and connect the two manganese-sulfite layers in the a -axis, forming a honeycomb-like structure and results in an infinite 3D network as shown in Fig. 3.11c.

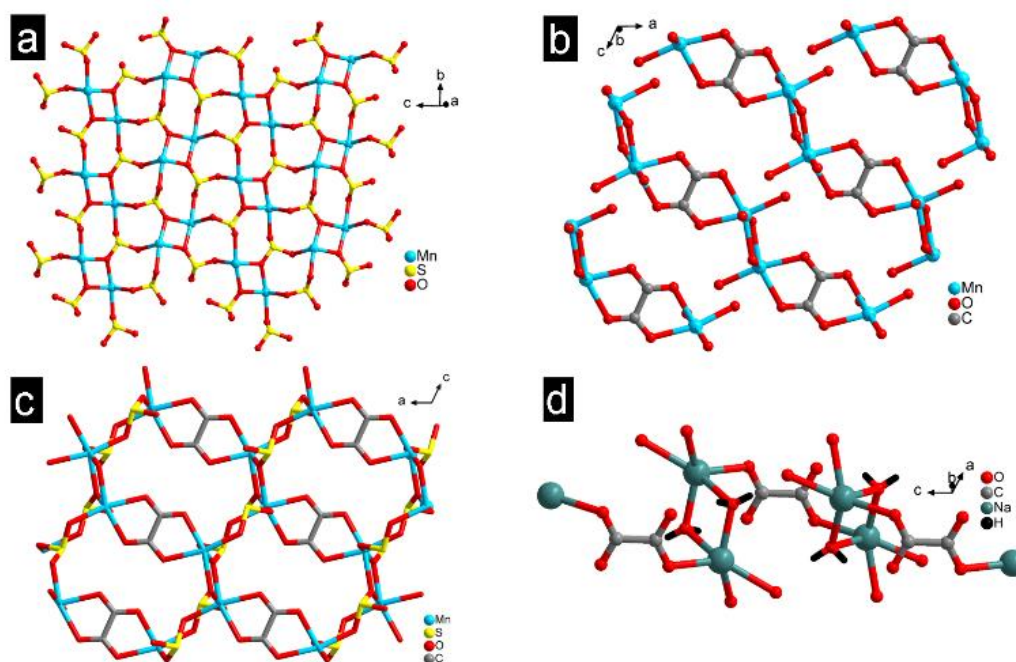


Fig. 3.11. (a) MnSO_3 layer of $[\text{Na}_2\text{Mn}_2(\text{C}_2\text{O}_4)(\text{SO}_3)_2(\text{H}_2\text{O})_2]$, **14**, in the bc -plane, (b) the arrangement of Mn-oxalate chain along a -axis (c) 3D honeycomb structure of compound **14** and (d) Na-oxalate chain along c -axis $[\text{Na}_2\text{Mn}_2(\text{C}_2\text{O}_4)(\text{SO}_3)_2(\text{H}_2\text{O})_2]$, **14**.

Sodium ions bonded with the oxalate anions to form the sodium oxalate infinite chain along c -axis (Fig. 3.11d). The Na ion sits in the center of the cavity which has two roles (a) to provide extra stability (Fig. 3.12) and (b) charge balancing and provide higher dimensional structure. The two sodium ions connected to each other through bridging aqua ligand. The hydrogen atoms of the aqua ligands form a strong H-bond with the oxygen atoms of sulfite and oxalate rendering stability to the structure. The penta-coordinated sodium ions surrounded by the five oxygen atoms, two from one sulfite anion, two from bridging aqua ligand (bridge between two Na ions) and one from oxalate anion as shown in Fig. 3.12 and 3.13a. The H-bonding in compound **14** provide the extra stability of the molecule, formed between water and the surrounding sulfite and oxalate oxygen atoms. The H-bond lengths are $d_{\text{O1W-H1W1}\cdots\text{O3}} = 2.02(4) \text{ \AA}$ and $d_{\text{O1W-H2W1}\cdots\text{O2}} = 2.15(3) \text{ \AA}$ as shown in Fig. 3.13b. The bond valence sum calculations of compound **14** gave +2 oxidation state of Mn and +1 oxidation state for Na.

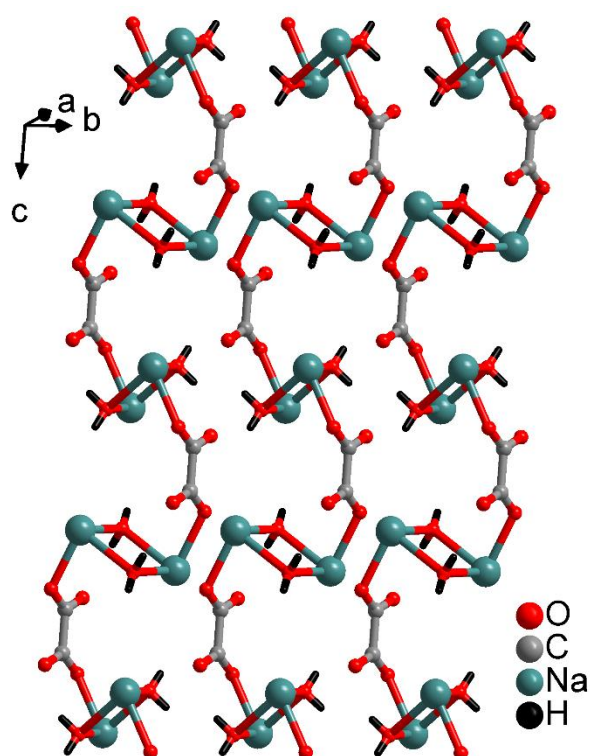


Fig. 3.12. Na oxalate chain along the *c*-axis in $[\text{Na}_2\text{Mn}_2(\text{C}_2\text{O}_4)(\text{SO}_3)_2(\text{H}_2\text{O})_2]$, **14**.

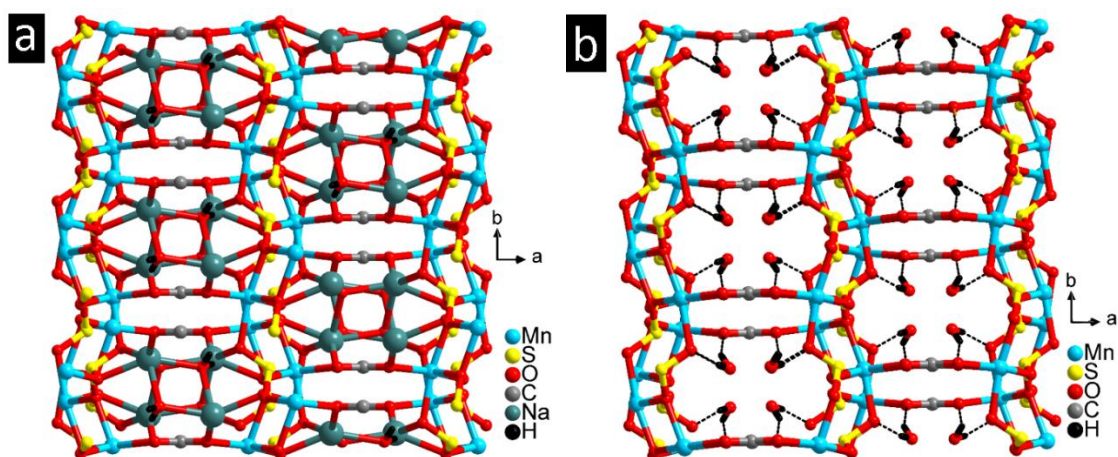


Fig. 3.13. (a) The crystal lattice of $[\text{Na}_2\text{Mn}_2(\text{C}_2\text{O}_4)(\text{SO}_3)_2(\text{H}_2\text{O})_2]$, **14** showing an infinite anionic 3D network and (b) H-bonding pattern in compound **14** (Na is omitted for the clarity).

3.3.4.1. Magnetic properties of $[\text{Na}_2\text{Mn}_2(\text{C}_2\text{O}_4)(\text{SO}_3)_2(\text{H}_2\text{O})_2]$ **14**:

Fig. 3.14 show the temperature dependence magnetic susceptibility (χ) and the $\chi_m T$ data of compound **14** recorded at 1000 Oe external magnetic field. At the high-temperature inverse susceptibility data follows the Curie-Weiss law and give a Weiss temperature of -16 K, which suggests that the exchange interaction between Mn is antiferromagnetic. The effective magnetic moment of Mn is $5.88 \mu_B$, almost close to the spin only $S = 5/2$ value of $5.92 \mu_B$, since there is a negligible orbital contribution to the moment and is comparable to that of manganese (II) compounds reported in the literature^{27,28}. The $\chi_m T$ of compound **14** at 300 K is $4.2 \text{ emu mol}^{-1} \text{ K}$. As the temperature decreases to 5 K, the value of $\chi_m T$ is also decreased to reach a minimum value of $0.55 \text{ emu mol}^{-1} \text{ K}$ at 5 K.

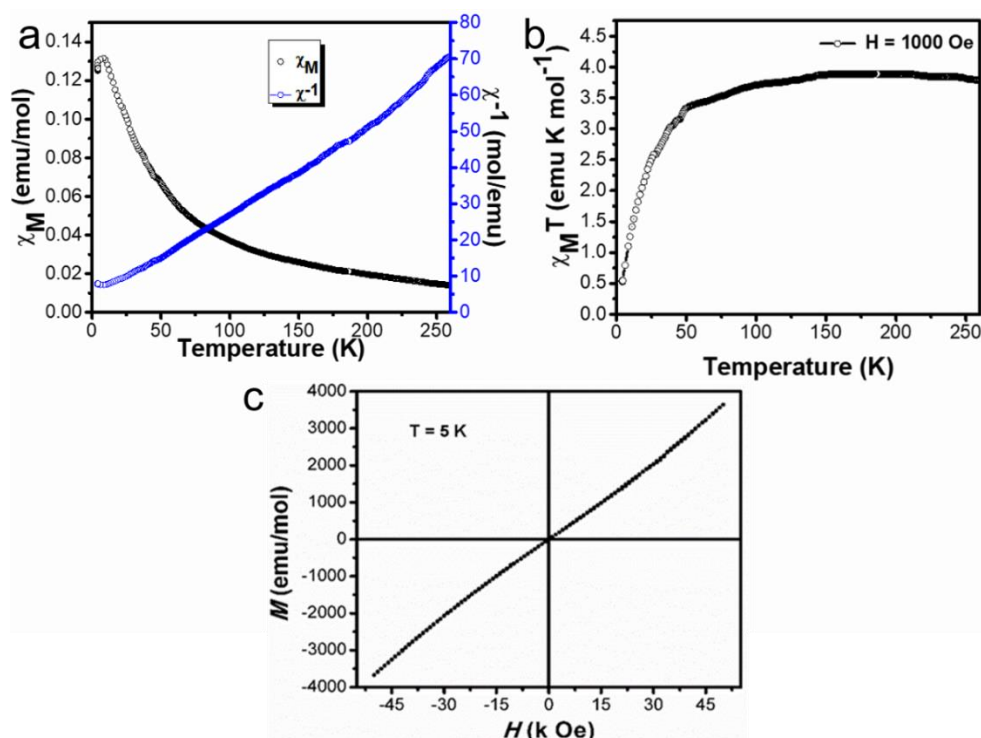


Fig. 3.14. (a) Temperature dependence graph of magnetic susceptibility and inverse susceptibility of compound **14** at 1000 Oe, (b) Temperature dependent $\chi_m T$ plot of compound **14** and (c) M-H cycle of compound **14** at 5 K.

The M-H curves (M = magnetization, H = applied field) at 5 K (Fig. 3.14c) do not show hysteresis but show linear field dependence magnetization. This behavior suggests that the material is essentially a paramagnetic behaviour with antiferromagnetic interactions exhibiting only short-range order.

3.3.5. Structural analysis of [NaEu(C₂O₄)(SO₃)(H₂O)₃], **15**:

[NaEu(C₂O₄)(SO₃)(H₂O)₃], **15** were isolated in similar conditions as that of compound **14** by using europium acetate in place of manganese oxalate and guanidine carbonate instead of piperazine. Colourless block shape crystals of compound **15** were formed and show triclinic crystal system with centrosymmetric *P*-1 space group. The asymmetric unit has 15 non-hydrogen atoms (one Eu, one Na, one SO₃, two half oxalates, and three aqua ligands with full occupancy). In the lattice, central atom Eu(III) ion is nona-coordinated to neighboring three sulfite anions through Eu-O-S linkages (edge corner sharing), two oxalates and one aqua ligand. The Eu-O bond length ranges from 2.3559–2.5210 Å and S-O bond distances in between 1.5176-1.5549 Å. Here O(2), O(4) and O(6) are trifurcately coordinated to the metal (Eu and Na ions), sulfur and carbon atom as shown in Fig. 3.15.

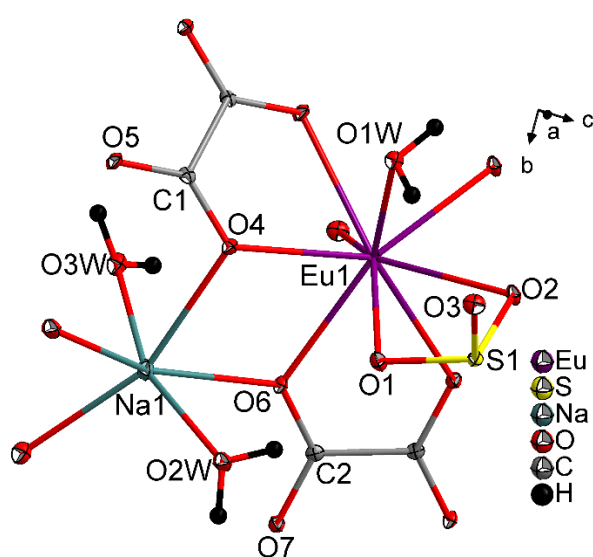


Fig. 3.15. The asymmetric unit of [NaEu(C₂O₄)(SO₃)(H₂O)₃], **15** with 45% ellipsoidal probability (the unique atoms are labeled).

The two Eu atom connected with each other by the edge-sharing through the oxalate oxygen atom. The other cation Na has distorted octahedral geometry binds to four neighbouring aqua ligand (Fig. 3.16) that connects another Na ion with edge-sharing through O2w and O3w to form the Na-O-Na bridge chain. The SO_3^{2-} anion gives all the three oxygen atom towards the Eu(III) ions and coordinates in $\eta^1\mu^3$ -manner. The Eu atom present in +3 oxidation state and the Na has +1 oxidation state which are calculated from the bond valence sum calculations.

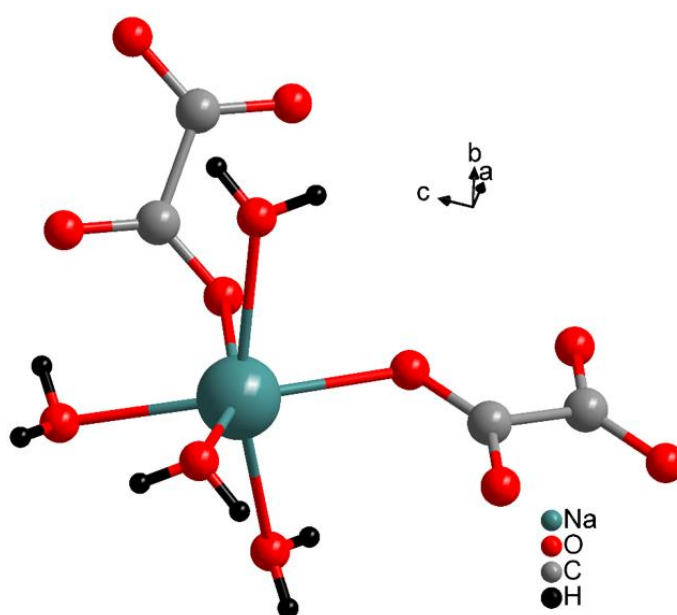


Fig. 3.16. Distorted octahedral geometry of Na ion in $[\text{NaEu}(\text{C}_2\text{O}_4)(\text{SO}_3)(\text{H}_2\text{O})_3]$, **15**.

The crystal lattice of compound **15** is packed in such a way that alternate arrangement of EuO_9 and SO_3^{2-} polyhedra forms an infinite one-dimensional ladder like a chain along a -axis (Fig. 3.17a), containing 4-membered rings formed by the two Eu(III) ions and two sulfite anions. EuO_9 and oxalate anion forms the honeycomb-like layered structure in the bc -plane (Fig. 3.17b). The honeycomb structure contains 6 Eu ions and 4 oxalate anions and forms 10-membered rings. The EuSO_3 chain acts as a bridge and connects two europium oxalate layers and form a three-dimensional network as shown in Fig. 3.17f. The coordination of Na ion and oxalate, itself form a 3D network, the aqua bridged Na ion being

extended along [100] to form an infinite 1D chain along *a*-axis. The oxalate anions connects two aqua bridged Na chain in *b* and *c*-axes as shown in Fig. 3.17c and 3.17d respectively.

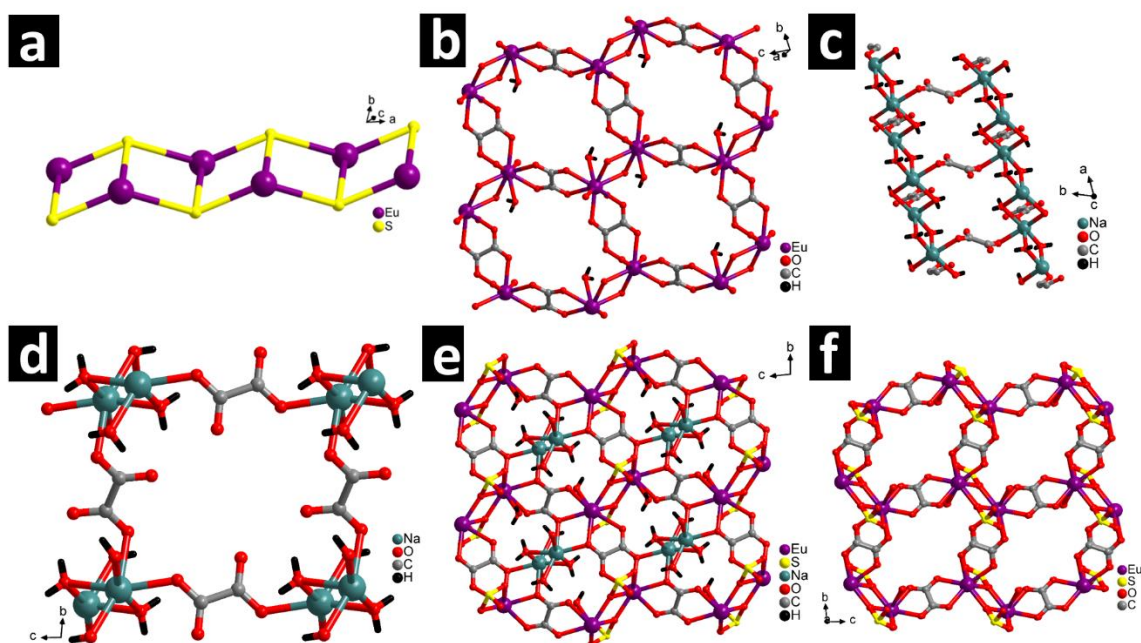


Fig. 3.17. (a) 1D Europium-sulfite chain in $[\text{NaEu}(\text{C}_2\text{O}_4)(\text{SO}_3)(\text{H}_2\text{O})_3]$, **15** with 4-membered rings window, (b) Eu-oxalate honeycomb structure in compound **15** (c and d) Aqua bridge Na-oxalate 3D network, (e) The 3D crystal lattice of compound **15**, and (f) The honeycomb structure of compound **15** where the aqua bridge Na ions are omitted.

In overall structure, the two honeycomb layers were connected by Eu-sulfite chain and form a 3D network and aqua bridged Na ion is situated in the centre of the honeycomb cavity (Fig. 3.17e). In the honeycomb ring, the bridged Na atom present in the centre of the ring provides extra stability and maintains the electrical charge of the framework (Fig. 3.17d). The compound **15** shows strong H-bonding interactions within the molecule from water and neighbour oxygen atom of sulfite, oxalate and water molecule and form six H-bonding with $d_{\text{O1W-H1W1}\cdots\text{O7}} = 1.96(3) \text{ \AA}$ (1-x,1-y,1-z), $d_{\text{O2W-H1W2}\cdots\text{O1}} = 2.07(3) \text{ \AA}$, $d_{\text{O3W-H1W3}\cdots\text{O1W}}$

$= 2.01(3) \text{ \AA}$ $(1-x, 1-y, -z)$, $d_{O1W-H2W1...O3} = 2.07(4) \text{ \AA}$, $d_{O2W-H2W2...O5} = 1.980(18) \text{ \AA}$ $(x, 1+y, z)$, $d_{O3W-H2W3...O1} = 2.30(3) \text{ \AA}$ $(-1+x, y, z)$ with the symmetric notation (Fig. 3.18).

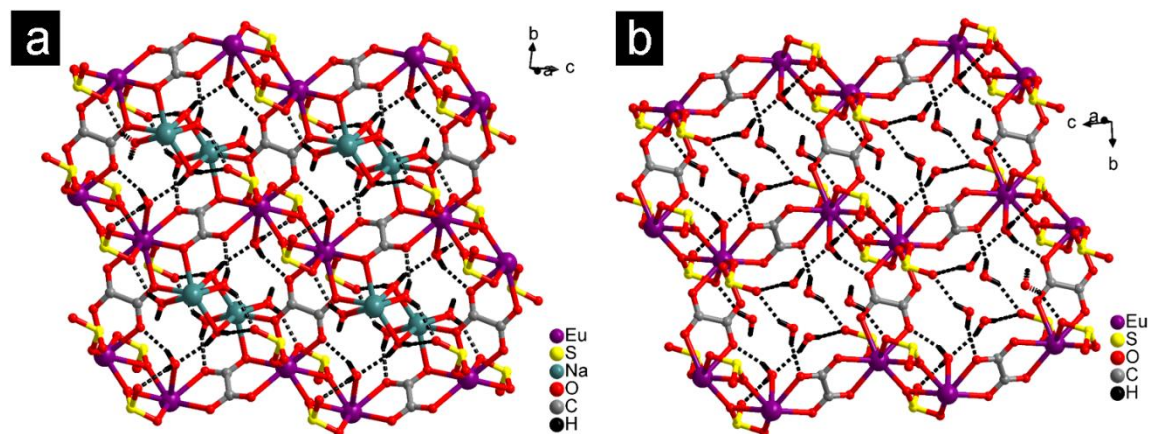


Fig. 3.18. (a) H-bonding pattern of $[\text{NaEu}(\text{C}_2\text{O}_4)(\text{SO}_3)(\text{H}_2\text{O})_3]$, **15** and (b) H-bonding pattern of $[\text{NaEu}(\text{C}_2\text{O}_4)(\text{SO}_3)(\text{H}_2\text{O})_3]$, **15** where Na ions are deleted for clarity.

3.3.5.1. Photoluminescence study of $[\text{NaEu}(\text{C}_2\text{O}_4)(\text{SO}_3)(\text{H}_2\text{O})_3]$, **15**:

The photoluminescence emission spectra (PL) of compound **15** upon excitation at 395 nm (Fig. 3.19). The lanthanide materials were showing weak fluorescence emission in that case organic ligand or chromophore (combined with lanthanide metal) were irradiated with ultraviolet radiation, the ligand get absorbs the radiation which transfer the energy to the lanthanide metal and the photoluminescence properties of Eu ions get enhance. This phenomenon is an antenna effect. The energy transition takes place from $^5\text{D}_0$ level of oxalate anions. It shows four expected peaks for the $^5\text{D}_0 \rightarrow ^7\text{F}_j$ transitions and is assigned to $^5\text{D}_0 \rightarrow ^7\text{F}_1$ (592 nm), $^5\text{D}_0 \rightarrow ^7\text{F}_2$ (618 nm), $^5\text{D}_0 \rightarrow ^7\text{F}_3$ (656 nm) and $^5\text{D}_0 \rightarrow ^7\text{F}_4$ (692 nm) as shown in Fig. 3.19. It emits sharp intense red emission band at 616 nm, which is its characteristic emission due to the electron dipole transition ($^5\text{D}_0 \rightarrow ^7\text{F}_2$) of central Eu (III) ion and is very sensitive to the coordination environment of the Eu(III) ion. The two transitions $^5\text{D}_0 \rightarrow ^7\text{F}_1$ and $^5\text{D}_0 \rightarrow ^7\text{F}_3$ are a magnetic dipole transition, which is independent of their local environment. The intensity of $^5\text{D}_0 \rightarrow ^7\text{F}_1$ transition varies with the field strength

of ligands acting on the Eu(III) ions. On the other hand, two ${}^5D_0 \rightarrow {}^7F_2$ and ${}^5D_0 \rightarrow {}^7F_4$ transitions are electric dipole transition and depends on their local environment. The high-intensity transition (${}^5D_0 \rightarrow {}^7F_2$) for the bright red emission is due to high polarity around the Eu(III) ions indicating strong coordination interactions between the ligands (SO_3 , Oxalate) and the metal ions.

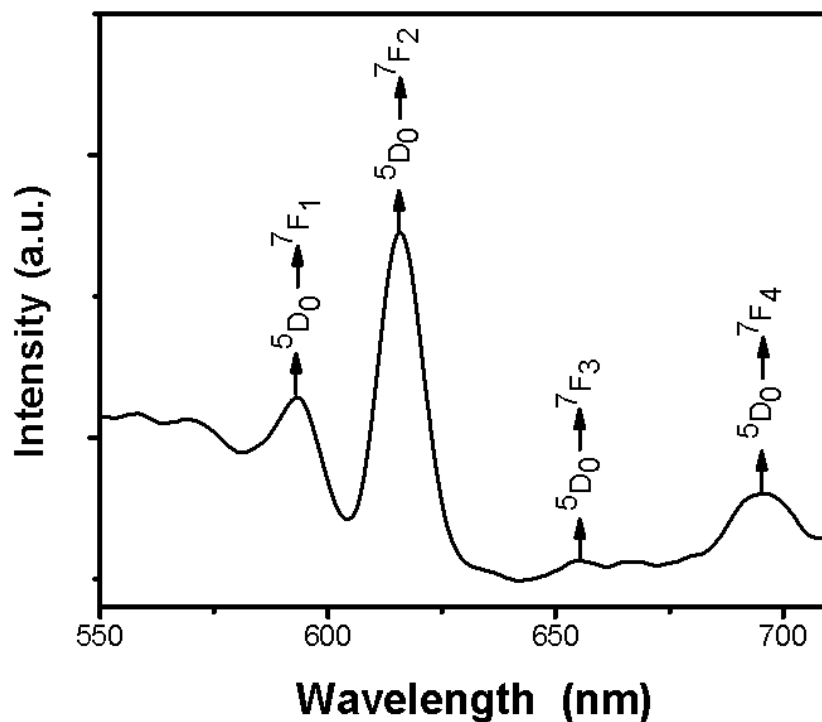


Fig. 3.19. Photoluminescence emission spectrum of $[NaEu(C_2O_4)(SO_3)(H_2O)_3]$, **15** at room temperature.

3.4. Thermal analysis

3.4.1. Thermogravimetric analysis:

Thermal stability of compounds **11-15** was investigated by thermogravimetric analysis which was carried out in an inert atmosphere of N_2 gas flow at a heating rate of $10\text{ }^\circ\text{C min}^{-1}$ up to a temperature of $750\text{ }^\circ\text{C}$ and is given in Fig. 3.20.

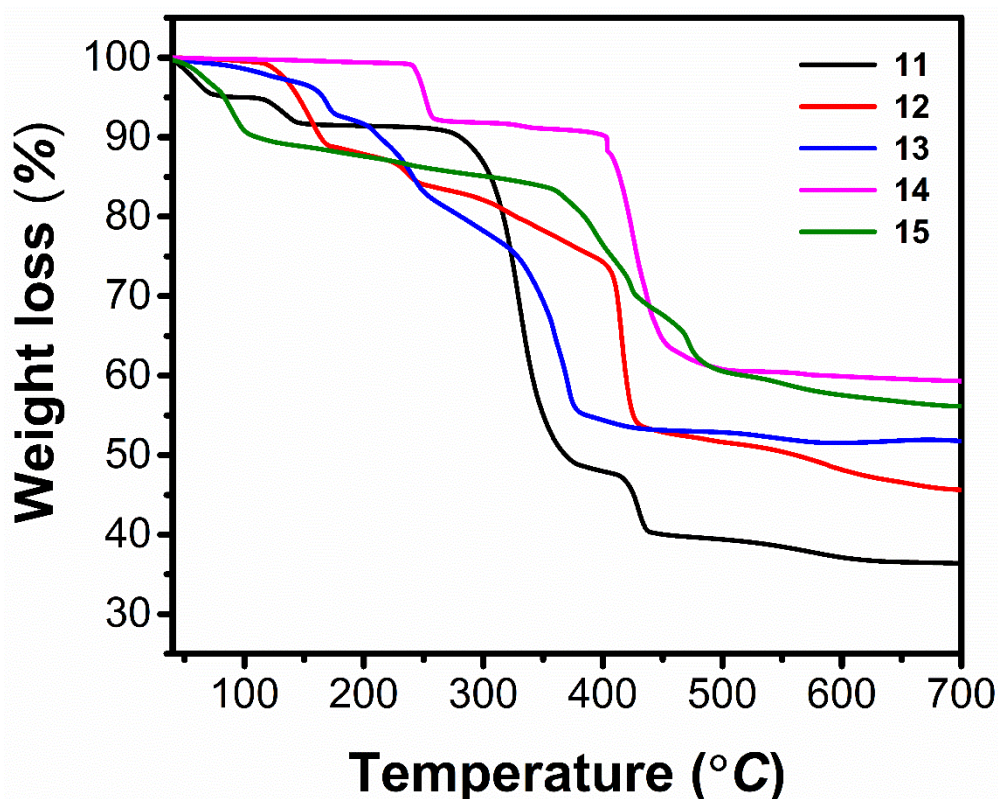


Fig. 3.20. TGA profile diagram for compounds 11-15.

Compound **11** shows multi-steps decomposition, in the first step, the lattice water molecules are removed in the temperature range of 30-140 °C which accounts for 7.94% weight loss (calc 7.43%). The second step (decomposition) takes place in the temperature range of 270-380 °C which corresponds to the loss of DABCO and two molecules of sulfur dioxide (obs = 41.94%; calc = 43.47% weight loss). In the final step, CO₂ gas is removed in the temperature range of 410-440 °C which accounts for 6.44% weight loss (calc 4.54%). From the TGA curve of compound **12**, it clearly shows continuous multi-steps weight loss, however, compound **12** is stable up to 120 °C. It loses its aqua ligand in the temperature range of 120-160 °C (obs = 9.05%; calc 8.67%) and piperazine unit in the temperature range of 180-385 °C which accounts for 13.25% (calc 13.97%) weight loss. In the next step, a sharp decomposition in the temperature range of 400-445 °C is observed which is probably due to the loss of SO₃ moiety which corresponds to 20.45% (calc 19.27%) weight loss. Finally, removal of CO₂ gas (obs 5.05%; calc 5.30% weight loss) was observed in the

temperature range of 545-700 °C. The PXRD analysis of post-calcined product indicates the formation of ZnO (PDF-01-075-0576) as an end product in both the cases.

In the case of compound **13**, a total of 52 % was observed which can be attributed to the loss of water, piperazine, SO₃, and CO₂ moiety. The first step involves the loss of water molecules in the temperature range 60-150 °C (obs. 5.84 %, calcd 6.02 %). The second step involves the decomposition of piperazine molecules in the temperature range of 190-270 °C (obs. 13.48 %, calcd. 14.73 %). The next step is the removal of SO₃ in the range of 290-360 °C (obs. 24.79 %, calcd 26.79 %) followed by the removal of CO₂ in the range 390-700 °C (obs. 8.24 %, calcd 9.37 %). The PXRD pattern of the post-calcined product indicates the formation of cadmium oxide (COD-2016-1011096). Compound **14** is stable up to 250 °C and then it undergoes two-steps decomposition. The first weight loss is due to the water molecules which are bonded to Na atom, remove as water vapor and shows 7.95% (calc 8.18%) in the temperature range of 250-270 °C. The second weight loss corresponds to the loss of SO₂ and CO₂ in the range 400-600 °C (obs. 32.4 %, calcd 33.4 %). The PXRD pattern of the sample heated to 1000 °C was identified as a mixture of Mn₃O₄ (PDF-01-070-9110) and MnO (PDF-01-077-2929). Similarly, the TGA profile curve of compound **15** showed decomposition which accounts a total of 44.56% weight loss. The complex start decomposing due to the loss of water in the temperature range 60-110 °C (obs. 10.68 %, calcd 13.22 %). It involves slow decomposition in the range 350-600 °C (obs. 29.7 %, calcd 31.2 %) which could be accounted for the loss of SO₂ and CO₂. The calcined product after 700 °C was identified by the PXRD peak as Europium oxide (PDF-00-032-0380).²⁹

3.4.2. Differential scanning calorimetry

DSC data of compounds **11-15** were performed with the Mettler Toledo instrument under a flow of argon gas, in the temperature range of -120 to 400 °C with the heating rate of 10 °C/min as shown in Fig. 3.21. The DSC curve shows the heat absorption resulting in a decrease in the heat flow, which indicates both the melting due to the removal of water/aqua ligand and the next series of a decrease in curve shows decomposition of the compounds. The DSC curves corroborated TGA observations which show the melting around 120 °C for compound **11**, 250 °C for compound **12** and 174 °C for compound **13** as shown in Fig. 3.21. Compound **14** shows the endothermic behavior and melted at 260 °C. Compound **15** shows evaporation of water molecule in the range 90-120 °C followed by continuous decomposition of the compound and finally the removal of SO₂ above 400 °C. DSC data corroborate the TGA data.

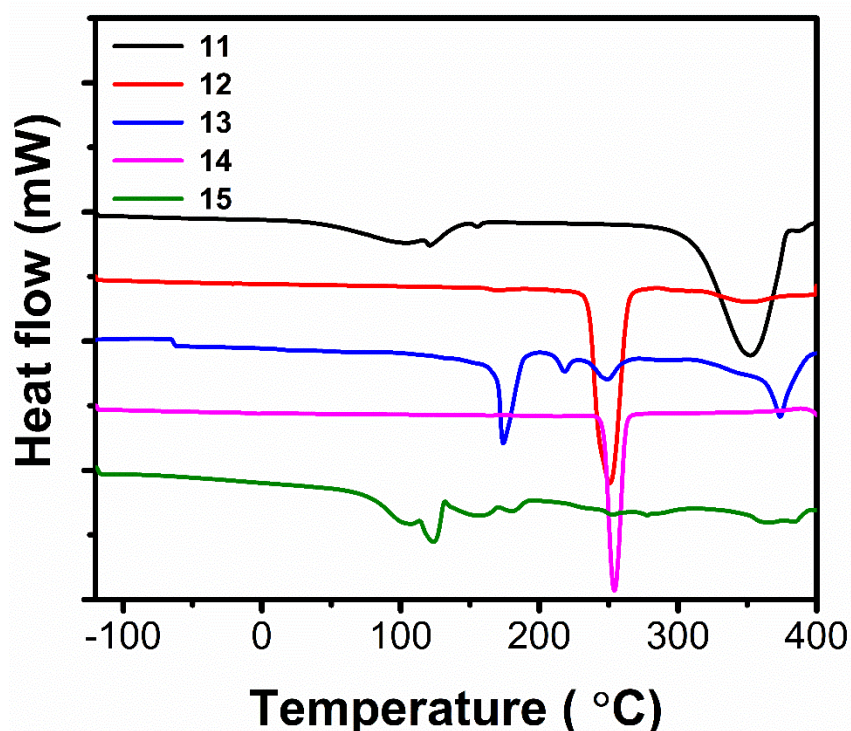


Fig. 3.21. DSC spectra of compounds 11-15.

3.5. Conclusions:

Amine templated five metal-sulfite-oxalate open-framework materials with metal ions (Zn(II) Cd(II), Mn(II) and Eu(III) ion) namely $[\text{Zn}_2(\text{SO}_3)_2(\text{C}_2\text{O}_4)_{0.5}(\text{C}_6\text{N}_2\text{H}_{13})] \cdot (\text{H}_2\text{O})_2$, **11**, $[\text{C}_4\text{N}_2\text{H}_{12}]_{0.5}[\text{Zn}_2(\text{SO}_3)_2(\text{C}_2\text{O}_4)_{0.5}(\text{H}_2\text{O})_2]$, **12**, $[\text{C}_4\text{N}_2\text{H}_{12}][\text{Cd}_2(\text{SO}_3)_2(\text{C}_2\text{O}_4)(\text{H}_2\text{O})] \cdot (\text{H}_2\text{O})$ **13**, $[\text{Na}_2\text{Mn}_2(\text{C}_2\text{O}_4)(\text{SO}_3)_2(\text{H}_2\text{O})_2]$, **14** and $[\text{NaEu}(\text{C}_2\text{O}_4)(\text{SO}_3)(\text{H}_2\text{O})_3]$, **15** have been successfully synthesized and characterized by complementary techniques which show a two and three dimensional structures. These compounds serve as the organically templated inorganic-organic hybrid materials involving sulfite and oxalate anions. Here, the role of oxalate anions to generate solids with increased dimensionality and the role of SDAs to dictate the structural outcome has been re-established. We believe that a similar approach can be extended for the realization of more aesthetically pleasing structures with possible applications by varying SDAs and metal ions. Both compounds **14** and **15** possess a honeycomb structure along with the presence of the aqua bridged Na ions that gives the extra stability to the framework.

References

- (1) Davis, M. E. *Nature* **2002**, *417*, 813.
- (2) Wang, K.; Luo, D.; Xu, D.; Guo, F.; Liu, L.; Lin, Z. *Dalton Trans.* **2014**, *43*, 13476.
- (3) Li, L.; Yu, R.; Wang, D.; Lai, X.; Mao, D.; Yang, M. *Inorg. Chem. Commun.* **2010**, *13*, 831.
- (4) Luan, L.; Yang, M.; Bian, Y.; Lin, Z.; Huang, H. *Dalton Trans.* **2015**, *44*, 13485.
- (5) Kedarnath, K.; Choudhury, A.; Natarajan, S. *J. Solid State Chem.* **2000**, *150*, 324.
- (6) Liu, L.; Luo, D.; Li, D.; Lin, Z. *Dalton Trans.* **2014**, *43*, 7695.
- (7) Zhou, G.; Yang, Y.; Fan, R.; Liu, X.; Wang, Q.; Wang, F. *Solid State Sci.* **2010**, *12*, 873.
- (8) Medrish, I.; Peresypkina, E.; Virovets, A.; Serezhkina, L. *Russ. J. Coord. Chem.* **2008**, *34*, 629.
- (9) Tang, Q.; Liu, Y.; Liu, S.; He, D.; Miao, J.; Wang, X.; Yang, G.; Shi, Z.; Zheng, Z. *J. Am. Chem. Soc.* **2014**, *136*, 12444.
- (10) Xu, X.-Y.; Chen, Q.-C.; Yu, Y.-D.; Huang, X.-C. *Inorg. Chem.* **2015**, *55*, 75.
- (11) An, C.; Feng, X.; Zhao, N.; Liu, P.; Wang, T.; Lian, Z. *J. Cluster Sci.* **2015**, *26*, 889.
- (12) Xu, J.; Yao, X.-Q.; Huang, L.-F.; Li, Y.-Z.; Zheng, H.-G. *CrystEngComm* **2011**, *13*, 857.
- (13) Meyer, B. *Sulfur, energy, and environment*; Elsevier, 2013.
- (14) Brown, I. D.; Altermatt, D. *Acta Crystallogr., Sect. B: Struct. Sci* **1985**, *41*, 244.

- (15) Herbst-Irmer, R.; Sheldrick, G. M. *Acta Crystallogr., Sect. B: Struct. Sci* **1998**, *54*, 443.
- (16) Sheldrick, G. *University of Göttingen, Göttingen, Germany* **1994**.
- (17) Pennington, W. T. *J. Appl. Crystallogr.* **1999**, *32*, 1028.
- (18) Farrugia, L. J. *J. Appl. Crystallogr* **1997**, *30*, 565.
- (19) Austria, C.; Zhang, J.; Valle, H.; Zhang, Q.; Chew, E.; Nguyen, D.-T.; Gu, J. Y.; Feng, P.; Bu, X. *Inorg. Chem.* **2007**, *46*, 6283.
- (20) Austria, C.; Zhang, J.; Valle, H.; Zhang, Q.; Chew, E.; Nguyen, D.-T.; Gu, J. Y.; Feng, P.; Bu, X. *Inorg. Chem.* **2007**, *46*, 6283.
- (21) Nguyen, D.-T.; Chew, E.; Zhang, Q.; Choi, A.; Bu, X. *Inorg. Chem.* **2006**, *45*, 10722.
- (22) Tiwari, R. K.; Kumar, J.; Behera, J. N. *RSC Adv.* **2015**, *5*, 78389.
- (23) Rao, K. P.; Rao, C. N. R. *Inorg. Chem.* **2007**, *46*, 2511.
- (24) Wu, P.; Liu, Y.; Liu, Y.; Wang, J.; Li, Y.; Liu, W.; Wang, J. *Inorg. Chem.* **2015**, *54*, 11046.
- (25) Maggard, P. A.; Nault, T. S.; Stern, C. L.; Poeppelmeier, K. R. *J. Solid State Chem.* **2003**, *175*, 27.
- (26) Izumi, H. K.; Kirsch, J. E.; Stern, C. L.; Poeppelmeier, K. R. *Inorg. Chem.* **2005**, *44*, 884.
- (27) Lethbridge, Z. A.; Smith, M. J.; Tiwary, S. K.; Harrison, A.; Lightfoot, P. *Inorg. Chem.* **2004**, *43*, 11.
- (28) Lethbridge, Z. A.; Congreve, A. F.; Esslemont, E.; Slawin, A. M.; Lightfoot, P. *J. Solid State Chem.* **2003**, *172*, 212.
- (29) Wickleder, M. S. *Chem. Rev.* **2002**, *102*, 2011.

Table 3.2. Crystal structure refinement parameters for compounds 11-15.

Parameter	11	12	13
Formula	[Zn ₂ (SO ₃) ₂ (C ₂ O ₄) _{0.5} (C ₆ N ₂ H ₁₃)] · (H ₂ O) ₂	[C ₄ N ₂ H ₁₂] _{0.5} [Zn ₂ (SO ₃) ₂ (C ₂ O ₄) _{0.5} (H ₂ O) ₂]	[C ₄ N ₂ H ₁₂] [Cd ₂ (SO ₃) ₂ (C ₂ O ₄)(H ₂ O)] H ₂ O
<i>Mr</i>	484.09	414.98	597.13
crystal system	Monoclinic	Tetragonal	Triclinic
space group	<i>P</i> 2 ₁ / <i>c</i>	<i>P</i> 4 ₂ / <i>mm</i>	<i>P</i> -1
<i>a</i> /Å	8.618(7)	11.091(2)	6.223(2)
<i>b</i> /Å	23.506(2)	11.091(2)	8.039(3)
<i>c</i> /Å	8.044(7)	8.915(1)	16.729(6)
α /°	90	90	86.11(2)
β /°	114.13(4)	90	87.14(3)
γ /°	90	90	71.78(2)
<i>V</i> /Å ³	1487.1(2)	1096.6(6)	792.97(5)
<i>Z</i>	4	4	2
ρ_{calc} (gcm ⁻³)	2.162	2.513	2.501
λ (MoK α) [Å]	0.71073	0.71073	0.71073
μ / mm ⁻¹ μ (cm ⁻¹)	3.561	4.804	3.009
θ range (deg)	2.59 to 30.54	2.60 to 30.46	2.67 to 30.57
reflections collected	25327	7590	15470
unique reflections [<i>R</i> (int)]	4524 [0.0361]	934 [0.0496]	4824 [0.0408]
data/restraints/ parameters	4524 / 0 / 209	934 / 1 / 61	4824 / 12 / 235
GOF on <i>F</i> ²	1.046	1.130	1.036
<i>R</i> 1 and <i>R</i> 2 [<i>I</i> > 2 σ (<i>I</i>)]	0.0254, 0.0627	0.0464, 0.0839	0.0364, 0.0893
<i>R</i> 1 and <i>R</i> 2 (all data)	0.0317, 0.0649	0.0584, 0.0878	0.0449, 0.0938
largest residual peaks (e.Å ⁻³)	0.587 and -0.573	1.421 and -1.340	2.259 and -1.320
CCDC no	1431807	1431808	1531878

	14	15
Empirical formula	[Na ₂ Mn ₂ (C ₂ O ₄)(SO ₃) ₂ (H ₂ O) ₂]	[NaEu(C ₂ O ₄)(SO ₃)(H ₂ O) ₃]
<i>Mr</i>	220.02	397.08
crystal system	Monoclinic	Triclinic
space group	<i>C2/c</i>	<i>P-1</i>
<i>a</i> /Å	17.1457(4)	6.2787(3)
<i>b</i> /Å	6.3087(2)	8.4948(4)
<i>c</i> /Å	11.5051(4)	9.4543(4)
α /°	90	89.165(3)
β /°	115.424(2)	72.524(2)
γ /°	90	69.150(2)
Volume/ Å ³	1123.95(6)	447.07(4)
<i>Z</i>	8	2
<i>D_x</i> /Mg m ⁻³	2.600	2.950
μ / mm ⁻¹	2.759	7.337
θ range for data collection/ °	2.63 to 30.48	3.62 to 30.52
Reflections collected	9221	7972
unique reflections	1701	2689
R(int)	0.0379	0.0215
Data / restraints / parameters	1701 / 1 / 100	2689 / 9 / 161
<i>R</i> 1 and <i>R</i> 2 [<i>I</i> >2 σ (<i>I</i>)]	0.0236, 0.0550	0.0162, 0.0371
<i>R</i> 1 and <i>R</i> 2 (all data)	0.0248, 0.0554	0.0170, 0.0375
Goodness-of-fit on <i>F</i> ²	1.161	1.081
Largest peak and hole/e.Å ⁻³	0.593 and 0.314	- 1.310 and -1.293
CCDC no	1431805	1431806

Table 3.3 Selected bond lengths for compounds 11-15.

[Zn₂(SO₃)₂(C₂O₄)_{0.5}(C₆N₂H₁₃)]·(H₂O)₂, 11					
Zn1-O1	1.9766(14)	Zn1-O8	2.0528(14)	Zn2-O3	1.9795(14)
Zn1-O4	1.9791(14)	Zn1-N1	2.1601(14)	Zn2-O5	1.9451(13)
Zn1-O7	2.1461(13)	Zn2-O2	1.9406(14)	Zn2-O6	1.9772(14)
[C₄N₂H₁₂]_{0.5}[Zn₂(SO₃)₂(C₂O₄)_{0.5}(H₂O)₂], 12					
Zn1-O1	2.056(4)	Zn2-O2	1.978(3)	Zn1-O3	2.128(4)
Zn1-O1w	2.081(4)				
[C₄N₂H₁₂][Cd₂(SO₃)₂(C₂O₄)(H₂O)]·H₂O, 13					
Cd1-O1	2.481(3)	Cd1-O10	2.481(3)	Cd2-O8	2.261(3)
Cd1-O2	2.336(3)	Cd1-O1w	2.313(3)	Cd2-O9	2.268(3)
Cd1-O3	2.292(3)	Cd2-O1	2.284(3)	Cd2-O10	2.279(3)
Cd1-O5	2.255(3)	Cd2-O6	2.335(3)		
Cd1-O8	2.383(3)	Cd2-O7	2.317(3)		
[Na₂Mn₂(C₂O₄)(SO₃)₂(H₂O)₂], 14					
Mn1-O1	2.2181(13)	Mn1-O1b	2.1797(12)	Mn1-O2a	2.1535(12)
Mn1-O3c	2.2129(12)	Mn1-O4	2.2299(13)	Mn1-O5d	2.2183(14)
Na1-O2e	2.3589(15)	Na1-O3e	2.5146(15)	Na1-O4	2.3410(16)
Na1-O5g	2.9900(19)	Na1-O1W	2.3171(18)	Na1-O1Wf	2.507(2)
[NaEu(C₂O₄)(SO₃)(H₂O)₃], 15					
Eu1-O1	2.4269(16)	Eu1-O2	2.5210(15)	Eu1-O2k	2.3655(15)
Eu1-O3j	2.3559(16)	Eu1-O4	2.4361(16)	Eu1-O5l	2.4662(17)
Eu1-O6	2.4980(15)	Eu1-O7m	2.4879(16)	Eu1-O1W	2.6458(16)
Na1-O4	2.3933(17)	Na1-O6	2.3065(18)	Na1-O2W	2.395(2)
Na1-O2Wn	2.323(2)	Na1-O3Wo	2.3743(19)	Na1-O3W	2.478(2)

Table 3.4. Hydrogen bonding table for compounds 11-15.#

D—H···A	Symmetry of A	D—H	H···A	D—A	∠D—H···A
[Zn₂(SO₃)₂(C₂O₄)_{0.5}(C₆N₂H₁₃)]·(H₂O)₂, 11					
N2—H2···O6	-1+x,y,-1+z	0.91	2.18	2.908(2)	136
N2—H2···O7	-1+x,y,-1+z	0.91	2.32	2.917(2)	123
C2—H2B···O4		0.97	2.54	3.108(3)	117
C6—H6A···O2	x,1/2-y,-1/2+z	0.97	2.40	3.304(3)	155
C6—H6B···O2		0.97	2.57	3.201(3)	123
[C₄N₂H₁₂]_{0.5} [Zn₂(SO₃)₂(C₂O₄)_{0.5}(H₂O)₂], 12					
N1—H1A···O3	y,x,1-z	0.90	2.28	3.146(5)	161
O1W—H1W···O2	1/2+y,1/2-x,1/2-z	0.78(6)	2.00(5)	2.767(5)	172(6)
C2—H2A···O1W	1/2-x,-1/2+y,1/2-z	0.97	2.49	2.879(12)	104
C2—H2B···O3		0.97	2.24	3.023(12)	137
[C₄N₂H₁₂][Cd₂(SO₃)₂(C₂O₄)(H₂O)]·(H₂O), 13					
O2WA—H2WA···O1W	2-x,-y,1-z	0.85	2.15	2.997(13)	171
N1—H1A···O9	2-x,1-y,-z	0.89	2	2.812(4)	150
N1—H1B···O5		0.89	1.91	2.777(4)	164
O2WA—H2WB···O4		0.85	2.06	2.901(12)	168
N2—H2A···O3	-1+x,y,z	0.89	1.88	2.751(5)	166
N2—H2B···O2	-1+x,y,z	0.89	2.52	3.009(5)	116
N2—H2B···O4		0.89	1.86	2.689(5)	154
O1W—H1WA···O6	1+x,-1+y,z	0.83(5)	1.91(6)	2.728(4)	167(6)
O1W—H1WB···O7	x,-1+y,z	0.83(6)	1.88(6)	2.672(4)	161(6)
C3—H3A···O8	-1+x,y,z	0.97	2.52	3.429(5)	156
C3—H3B···O7	-1+x,y,z	0.97	2.56	3.334(5)	137
C4—H4A···O5	2-x,1-y,-z	0.97	2.55	3.372(6)	142
C4—H4B···O10		0.97	2.56	3.295(6)	133
C6—H6A···O4	1-x,1-y,1-z	0.97	2.45	3.370(6)	158

[Na₂Mn₂(C₂O₄)(SO₃)₂(H₂O)₂], 14					
O1W—H1W1···O3	-x,y,1/2-z	0.82(4)	2.02(4)	2.829(2)	168(3)
O1W—H2W1···O2	-x,2-y,-z	0.81(2)	2.15(3)	2.856(2)	146(3)
[NaEu(C₂O₄)(SO₃)(H₂O)₃], 15					
O1W—H1W1···O7	1-x,1-y,1-z	0.81(3)	1.96(3)	2.738(2)	162(3)
O2W—H1W2···O1		0.81(3)	2.07(3)	2.813(2)	153(3)
O3W—H1W3···O1W	1-x,1-y,-z	0.82(3)	2.01(3)	2.795(2)	158(3)
O1W—H2W1···O3		0.82(4)	2.07(4)	2.856(3)	159(3)
O2W—H2W2···O5	x,1+y,z	0.82(2)	1.980(18)	2.741(2)	155(3)
O3W—H2W3···O1	-1+x,y,z	0.81(3)	2.30(3)	3.107(3)	170(4)

#Where 'D' is a donor and 'A' is acceptor, the bond lengths are in (Å) and angles are in (°).

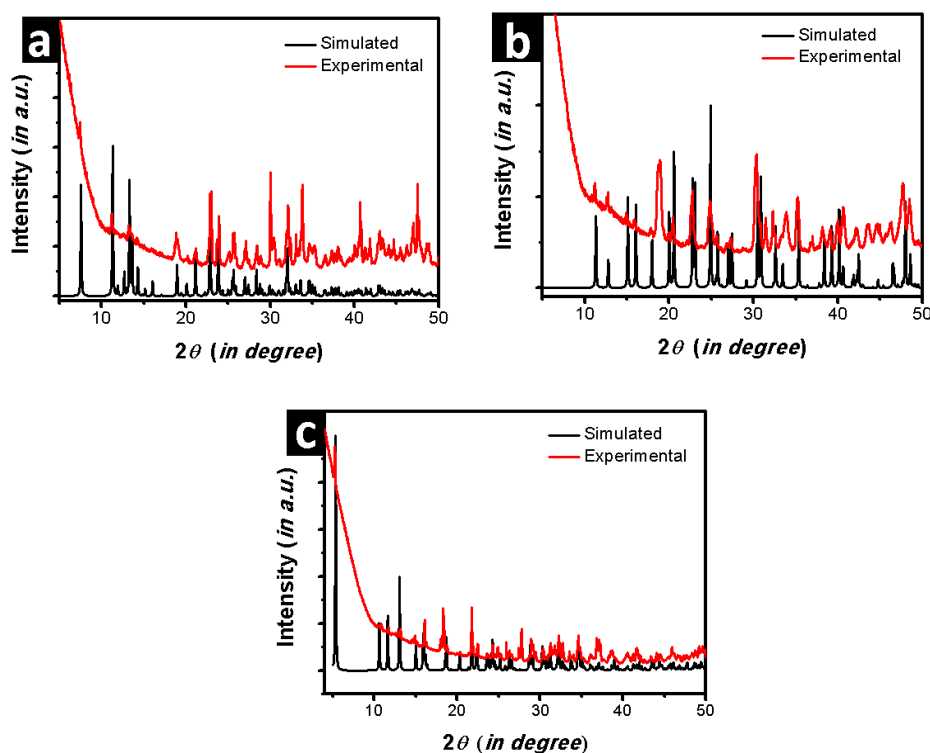


Fig. 3.23. PXRD pattern for (a) $[\text{Zn}_2(\text{SO}_3)_2(\text{C}_2\text{O}_4)_{0.5}(\text{C}_6\text{N}_2\text{H}_{13})] \cdot (\text{H}_2\text{O})_2$, **11**, (b) $[\text{C}_4\text{N}_2\text{H}_{12}]_{0.5}[\text{Zn}_2(\text{SO}_3)_2(\text{C}_2\text{O}_4)_{0.5}(\text{H}_2\text{O})_2]$, **12**, and (c) $[\text{C}_4\text{N}_2\text{H}_{12}][\text{Cd}_2(\text{SO}_3)_2(\text{C}_2\text{O}_4)(\text{H}_2\text{O})] \cdot (\text{H}_2\text{O})$ **13**.

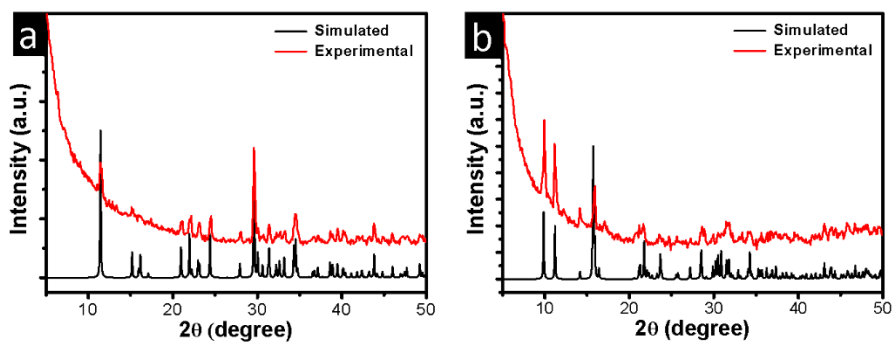
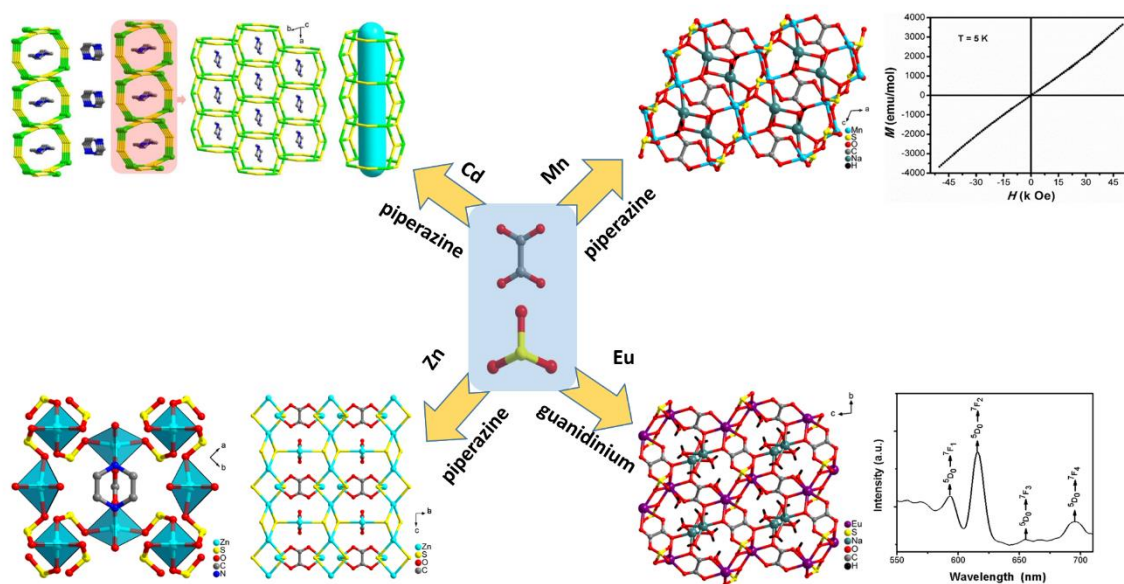


Fig. 3.24. PXRD pattern for (a) $[\text{Na}_2\text{Mn}_2(\text{C}_2\text{O}_4)(\text{SO}_3)_2(\text{H}_2\text{O})_2]$, **14** and (b) $[\text{NaEu}(\text{C}_2\text{O}_4)(\text{SO}_3)(\text{H}_2\text{O})_3]$, **15**.

Summary of Chapter 3



Chapter 4

METAL TRIHYDROXY-BENZENE-TRISULFONATE FRAMEWORK MATERIALS

Abstracts	165
4.1. Introduction	165
4.1.1. Mechanism of Proton-conduction	166
4.1.2 [Na₃(THBTS)] ligand	167
4.2. Experimental section	168
4.2.1. Materials and methods	168
4.2.2. Syntheses of compounds 16-19	168
4.2.3. Characterization	170
4.2.3.1. Single-Crystal Structure Determination	170
4.2.3.2. Elemental Analysis	171
4.3. Results and discussion	171
4.3.1. Structural analysis of [(C₃N₆H₆)(C₃N₆H₇)₃(C₆H₃O₉S₃).(H₂O)₄], 16	171
4.3.2. Structural analysis of [Na₂(C₆H₃O₃S₃)(CN₃H₆)(H₂O)].(H₂O), 17	174
4.3.3. Structural analysis of [K₃(C₆H₃O₉S₃)(H₂O)₃], 18	177
4.3.4. Structural analysis of [C₄N₂H₁₃]₂[Cd₂(C₆H₃O₃S₃)(H₂O)₂].(H₂O), 19	181
4.4. Thermal analysis	184
4.4.1. Thermogravimetric analysis	184
4.5. Conclusions	186
References	187
Appendix	189
Summary	193

Abstract

Four compounds have successfully been self-assembled using trihydroxy-benzenetrisulfonate (THBTS) and different counter cations under a mild condition at room temperature. The synthesized compounds are: $[(C_3N_6H_6)(C_3N_6H_7)_3(C_6H_3O_9S_3).(H_2O)_4]$, **16**, $[Na_2(C_6H_3O_3S_3)(CN_3H_6)(H_2O)].(H_2O)$, **17**, $[K_3(C_6H_3O_9S_3)(H_2O)_3]$, **18** and $[C_4N_2H_{13}]_2[Cd_2(C_6H_3O_3S_3)_2(H_2O)_2].(H_2O)$, **19**. These four compounds were characterized with single crystal X-Ray diffraction (SCXRD), powder X-Ray diffraction (PXRD) and thermogravimetry analysis (TGA). The compound **16** featured H-bonded 3D structure with helix structure between water and THBTS ligand system, compound **17** shows a layered structure with the tetrahedral arrangement at para-position of THBTS ligand. Compound **18** shows an ordered three-dimensional framework with one-dimensional water chain and compound **19** has the one-dimensional chain structure.

4.1 Introduction:

In recent days, crystalline ordered Metal-organic frameworks (MOFs) have attracted more attention in the field of proton conducting materials. The potential application includes hydrogen fuel cells and storage energy and convert when it required¹⁻⁶. MOF ordered structures are interesting due to the tunable pore size and distributions that allows the proton conduction. The proton conduction is through the functional groups and the protic species present inside the voids. Most of the PC-MOF show conductivity ($>10^{-3} \text{ S cm}^{-1}$) in presence of high relative humidity (RH > 90%, is the highest reported conductivity)⁷⁻⁹.

Fuel cells (FCs) produces electrical energy from the electro-chemical break down of a fuel¹⁰. In a fuel cell, oxygen gas supplied to the cathode and hydrogen gas passed through the anode electrode. Hydrogen gives up an electrons in the conducting electrolyte and gets deposited on the electrode. The electron moves toward cathode through the periphery circuit, and reduces the oxygen. At the cathode interface, oxygen reacts with proton and

produces water. Overall the hydrogen and oxygen react and produces water and electricity¹¹. FCs are interesting as a renewable energy source. Advantages include; environment-friendly, low weight, more efficiency and high energy per unit weight¹². Hydrogen is the most common and powerful fuel source. The other fuels source are hydronium, methanol, dimethylamine, and other fuels etc.

All the PC-MOFs are categorized into three classes; (a) low temperature^{8,13}, (b) intermediate temperature¹⁴ and (c) high-temperature PC-MOFs.¹⁵ (a) low-temperature (water-assisted) PC-MOFs operates at low temperature (20–80 °C) and is controlled by the presence of water and/or H-bonding interactions with water, (b) intermediate temperature PC-MOFs are anhydrous and water-mediated proton-conducting MOFs and (c) high-temperature (anhydrous) PC-MOFs works at intermediate temperatures (100–250 °C) by replacing water with amphiprotic organic molecules. The aim of the following sections is to discuss the recent progress in MOF-based materials with respect to their proton-conducting behaviors.

4.1.1. Mechanism of Proton-conduction:

In a MOF based proton conductor, conduction basically works on the two-major principle; Grotthuss mechanism/ proton-hopping mechanism and Vehicular mechanism¹⁶⁻¹⁸. Both of the mechanisms are differentiated on the basis of AC impedance activation energies. In Grotthuss mechanism the protons are moving in an infinite network structure through the H-bonding network between nitrogen and oxygen atoms. Grotthuss mechanism suggests a reorientation of surrounding water molecules leading the formation of a continuous path for the migration of protons along the H-bonding. The other proposed mechanism is a vehicular mechanism in which H₂O and NH₃ are treated as a proton carrier vehicle. The

hydrogen ions diffuse from higher concentration to lower concentration through H_3O^+ and NH_4^+ , whereas the deprotonated H_2O and NH_3 are moving in the opposite direction.

The phosphonate has three oxygen atoms and its chelation with metal ions results in multidimensional frameworks^{4,19}. Some of the phosphonate oxygen atoms are available for H-bonding in metal phosphonate frameworks which is used in proton conduction. The sulfonate groups are very much similar to phosphonate having three oxygen atoms bonded to sulfur. However, the metal sulfonate is less explored than the metal phosphonate^{20,21}. This is due to the weak interaction between metal ions and sulfonate anions that does not support a well-defined metal-sulfonate framework. Sulfonate groups are easily soluble in water and cannot displace the solvent molecules from the coordination sphere of the metal ions leading to amorphous structure formation²².

4.1.2 [Na_3 (THBTS)]; THBTS³⁻ = 2, 4, 6-trihydroxy-1, 3, 5-benzenetrisulfonate] ligand:

In this work, we have used trihydroxy-benzene-trisulfonate based ligands¹⁵. The metal can coordinate sulfonate oxygen atoms to provide multifunctional and multi-dimensional structures. The phenolic oxygen atoms of ligands provide architectural diversity and robustness to the framework through bonding with metals²²⁻²⁴. The advantages in using these types of ligands are to provide the pathway for proton conduction. In these ligands, the sulfonate and phenolic oxygen atoms provide the pathway for the proton conduction.

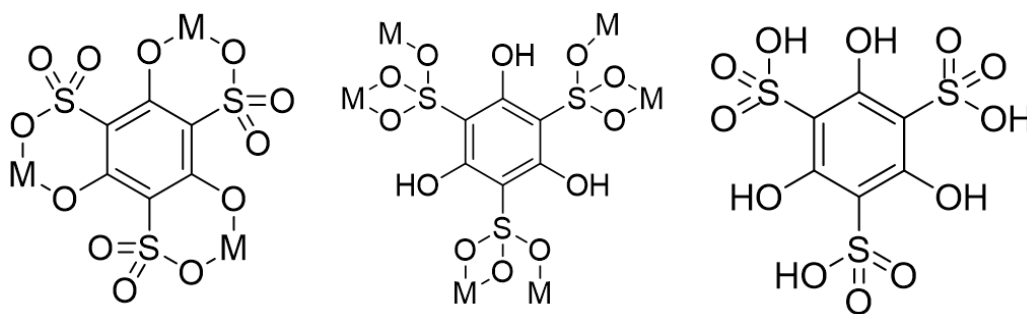


Fig. 4.1. Coordination mode of THBTS³⁻ ligand with metals.

4.2 Experimental section

4.2.1 Materials and methods:

Cadmium nitrate hexahydrate ($\text{Cd}(\text{NO}_3)_2 \cdot 6\text{H}_2\text{O}$, 99.5%), Chlorosulfonic acid (ClSO_3H , 99.5%), were purchased from Sigma-Aldrich. Dimethyl carbonate (98%), Sodium bicarbonate (NaHCO_3 , 98%), Potassium bicarbonate (KHCO_3 , 98%), were purchased from Hi-Media. The Phloroglucinol ($\text{C}_6\text{H}_6\text{O}_3$, 99%), Acetone were purchased from Spectrochem. All the chemicals were used without further purification.

All the compounds **16-19** were characterized by X-ray Diffraction (XRD), Fourier transform infrared spectroscopy (FTIR) and thermogravimetric analysis (TGA). The XRD data were collected using a Bruker D8 advance X-ray powder diffractometer using $\text{CuK}\alpha$ radiation ($\lambda = 1.5418 \text{ \AA}$), radiation in the range of $5^\circ < 2\theta < 55^\circ$. The step size used was 0.02° and exposure time 1 s for each step and the voltage and current used were 40 kV and 40 mA. Infrared spectra were recorded on a 'Perkin Elmer FTIR spectrometer' equipped with an attenuated total reflectance accessory. The sample were mixed with KBr and pressed. The pressed samples were scanned in the spectral region of $400 - 4000 \text{ cm}^{-1}$ with a resolution of 4 cm^{-1} . Thermogravimetric analyses (TGA) were carried out using a Discovery TGA by TA Instruments-Waters Lab at a heating rate of $5 \text{ }^\circ\text{C}/\text{min}$ under constant flow of nitrogen gas.

4.2.2 Synthesis:

4.2.2.1 Synthesis of $\text{Na}_3(\text{THBTS})$ ligand:

$\text{Na}_3(\text{THBTS})$ ligand was first synthesized by a similar process reported earlier¹⁵. 8g of anhydrous phloroglucinol was added to dry dimethyl carbonate in argon atmosphere resulted in a yellow solution. The solution slowly cooled to the $0 \text{ }^\circ\text{C}$, following the dropwise addition of 12.43 mL of chlorosulfonic with vigorous stirring in the 2 minute time period.

The solution slowly turned into an orange colored solution. Then it was heated back to room temperature followed by constant stirring for another 24 h. The solvent was evaporated in a rotary evaporator leaving a brown viscous liquid. The brown liquid was dissolved in water and neutralized with sodium bicarbonate. Then the white thick precipitated was obtained by the addition of acetone to the neutralized aqueous solution. The product was isolated by vacuum filtration.

4.2.2.2 Synthesis of compound 16:

86 mg of Na₃(THBTS) ligand (0.20 mmol) and 13 mg of melamine (0.10 mmol) were dissolved in 2.0 mL water and 1.0 mL methanol solvent mixture. The reaction mixture was transferred in a 15 mL polypropylene bottle and kept at room temperature without disturbance. The block shape crystal was obtained at the bottom after slow evaporation of the solvent mixture. (Yield 40% with respect to Na₃L ligand).

4.2.2.3 Synthesis of compound 17:

86 mg of Na₃(THBTS) ligand (0.20 mmol) and 18 mg of guanidine hydrochloride (0.20 mmol) were dissolved in the 2.0 mL water and 1.0 mL methanol solution. The reaction mixture was left at room temperature for slow solvent evaporation for a time period of 2 weeks. The colorless plate shape crystals were formed at the bottom of the reaction container (Yield 30% with respect to Na₃L ligand).

4.2.2.4 Synthesis of compound 18:

Compound **18** was synthesized under similar condition to the alpha phase of Na₃(THBTS) ligand. The Anhydrous phloroglucinol 2.0 g was dissolved in 30 mL dimethyl carbonate. The yellow reaction mixture was cooled to 0 °C under argon gas. Then chlorosulfonic acid (3.1 mL) was added dropwise with vigorous stirring lead to an orange color solution

formation. The reaction mixture was slowly heated to room temperature followed by stirring for 24 h in argon atmosphere. A brown color oil was collected after solvent evaporation using a rotary evaporator. The brown oil was dissolved in the water and pH was adjusted to 2.0 using potassium bicarbonate. Addition of acetone 200 mL resulted in a thick white precipitate. The precipitate was collected through vacuum filtration. The compound was dissolved in the mixture of 2.0 mL water and 1.0 mL methanol solution. The slow evaporation of solvent at room temperature resulted in the rod shape colorless crystals (Yield 60% with respect to phloroglucinol ligand).

4.2.2.5 Synthesis of compound 19:

43 mg of Na₃(THBTS) ligand (0.20 mmol), 54 mg Cadmium nitrate hexahydrate (0.20 mmol) and 68 mg of DABCO (0.20 mmol) were taken in the polypropylene bottle and were dissolved in the 2.0 mL water and 1ml methanol solution. The colorless block shape crystals were obtained after the slow evaporation of solvent mixture at room temperature (Yield 30% with respect to Na₃L ligand).

4.2.3 Characterisation

4.2.3.1 Single-Crystal Structure Determination:

Suitable single crystals of compounds **16-19** were carefully selected under a polarizing microscope and mounted at the tip of the thin glass fiber for X-ray diffraction data collection. Structures were solved by the direct method using SHELXTL and refined on F^2 by a full-matrix least-squares technique using the SHELXL-2014²⁵ program's package. An empirical absorption correction based on symmetry-equivalent reflections was applied using SADABS.²⁶ The graphics programs DIAMOND²⁷ and ORTEP²⁸ were used to draw the structures. Non-hydrogen atoms were refined anisotropically. In the refinement, hydrogen atoms were treated as riding atoms using the SHELXL default parameters.

Details of crystal structure refinement parameters for compounds **16-19** are given in Table 4.1.

4.2.3.2. Elemental Analysis:

Anal for compound **16**; calc (found): C, 11.94 (11.85); H, 4.01 (4.05); N, 9.29 (9.11); S, 21.26 (21.17). Anal for compound **17**; calc (found): C, 15.22 (15.11); H, 4.47 (4.59); N, 8.87 (8.73); S, 20.31 (20.23). Anal for compound **18**; calc (found): C, 20.96 (20.92); H, 5.28 (5.25); N, 8.15 (8.20); S, 18.66 (18.58); Anal for compound **19**; calc (found): C, 14.48 (14.42); H, 4.25 (4.30); N, 8.45 (8.42); S, 19.33 (19.23).

4.3 Results and discussion:

The α -phase of the $\text{Na}_3(\text{THBTS})$ ligand was prepared at low temperature (room temperature). At high temperature, the α -phase of $\text{Na}_3(\text{THBTS})$ ligands is converted into β -phase of $\text{Na}_3(\text{THBTS})$ ¹⁵. Protic amines (melamine, guanidinium carbonate, imidazole 1, 2, 3-triazole) are used to support the framework structure to increase the proton conduction.

4.3.1 Crystallographic analysis of $[(\text{C}_3\text{N}_6\text{H}_6)(\text{C}_3\text{N}_6\text{H}_7)_3(\text{C}_6\text{H}_3\text{O}_9\text{S}_3)\cdot(\text{H}_2\text{O})_4]$, **16**:

$\text{Na}_3(\text{THBTS})$ ligand reacts with melamine in water-methanol solvent mixture resulted in 1:3 hydrated salt of compound **16**. The compound **16** was crystallized from the slow evaporation of reaction mixture containing $\text{Na}_3(\text{THBTS})$ ligand, melamine, water and methanol solution. The colourless plate shape crystals formed at the bottom of the container. The single crystal X-ray diffraction study suggests that compound **16** has an H-bonded three-dimensional organic framework. Crystallization of compound **16** takes place in the monoclinic $P2_1/n$ space group. The empirical molecular formula of compound **16** is derived from the SCXRD analysis as $[(\text{C}_3\text{N}_6\text{H}_6)(\text{C}_3\text{N}_6\text{H}_7)_3(\text{C}_6\text{H}_3\text{O}_9\text{S}_3)\cdot(\text{H}_2\text{O})_4]$. The asymmetric unit contains one $(\text{THBTS})^{3-}$ ligand, three protonated melamine units, one

melamine unit and four free water molecules trapped in the crystal. The asymmetric unit is shown in Fig. 4.2 where unique non-hydrogen atoms are labelled.

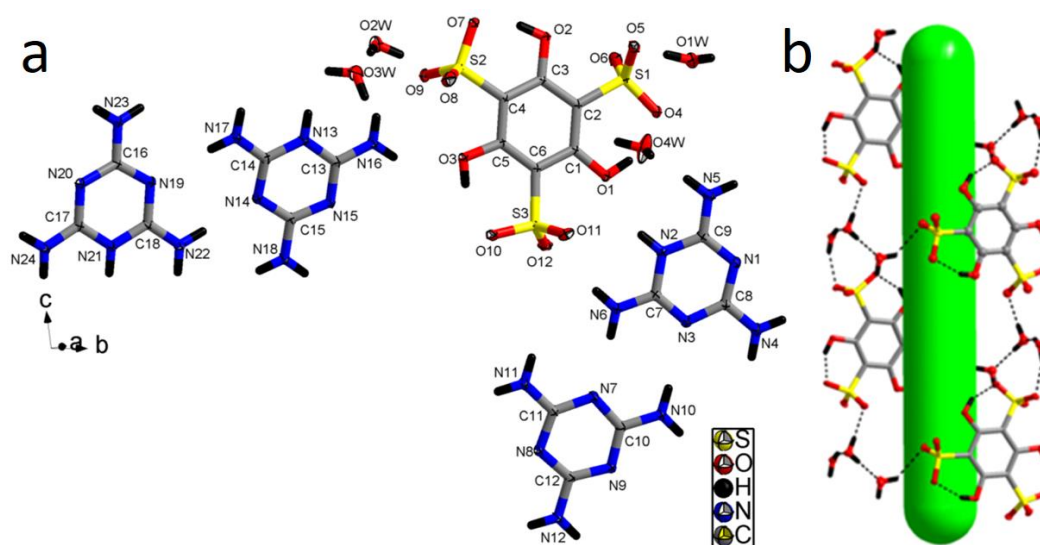


Fig. 4.2. (a) Asymmetric unit of compound **16** with ellipsoidal probability 15% and unique atoms are labelled and (b) H-Bonded helix structure of ligands and water molecules.

The deprotonated (THBTS)³⁻ ligand surrounded by three protonated melamine and neutralizes the molecules. The melamine nitrogen N2, N13, and N21 of core triazine are protonated and resulted in slight change in the bond lengths and bond angle of a normal melamine moiety. The unprotonated melamine and four water molecules are trapped in the crystal lattice. All the sulfonate group of (THBTS)³⁻ ligands are present in the same plane of benzene. All the bond lengths are in the normal range as reported²⁹. The core body of ligand i.e. benzene C-C bond length lies in between 1.390-1.408 Å which means that the pi electrons are symmetrically distributed on each carbon atom. The average C-S bond length is 1.768 Å, and S-O bond lengths are ranges in between 1.4366-1.4677 Å. In the core body of melamine, the average protonated N-C bond length is 1.364 Å and remaining N-C bond lengths are in between 1.315-1.354 Å. The core body of unprotonated melamine has N-C bond length of 1.333-1.352 Å. All the terminal C-NH₂ bond lengths are lying in the range of 1.311-1.342 Å.

The crystal lattice is stabilized by the H-bonding. The crystal lattice have of two types of H-bonding; 1) intramolecular H-bonding formed between phenolic oxygen atoms and oxygen atoms of sulfonate group of same ligand molecules and 2) intermolecular H-bonding existing between phenolic oxygen atoms, oxygen atoms of sulfonate group, lattice water molecules and melamine nitrogen atoms. The ligand itself is a hexagonally layered like structure in the *bc*-plane and connected with water molecules through H-bonding in the *a*-axis and forming an H-bonded one-dimensional channel (4 membered rings formed by the two water and two ligand molecules) in the *b*-axis direction (Fig. 4.3) and highlighted by the dotted black line. This one-dimensional channel has a helical structure and the helix is running down along *b*-axis. The pitch length is 12.11 Å, the H-bonding are in the ranges of 1.987-2.654 Å.

In the crystal lattice, the two protonated melamine units are also connected by other melamine units *via* H-bonding. This resulted in melamine-melamine sinusoidal waves like a melamine ribbon which is extended along *b*-axis involving an H-bonding (a pair of N-H...N) as shown in Fig.4.3 (highlighted by green color). These adjacent melamine tapes are further connected with the (THBTS)³⁻ ligands and a lattice water molecule in a head to head an H-bonded three-dimensional network. The H-bonding is present in between ligand hydroxyl oxygen atoms, oxygen atoms of sulfonate group, a lattice water molecule and nitrogen atoms of melamine unit.

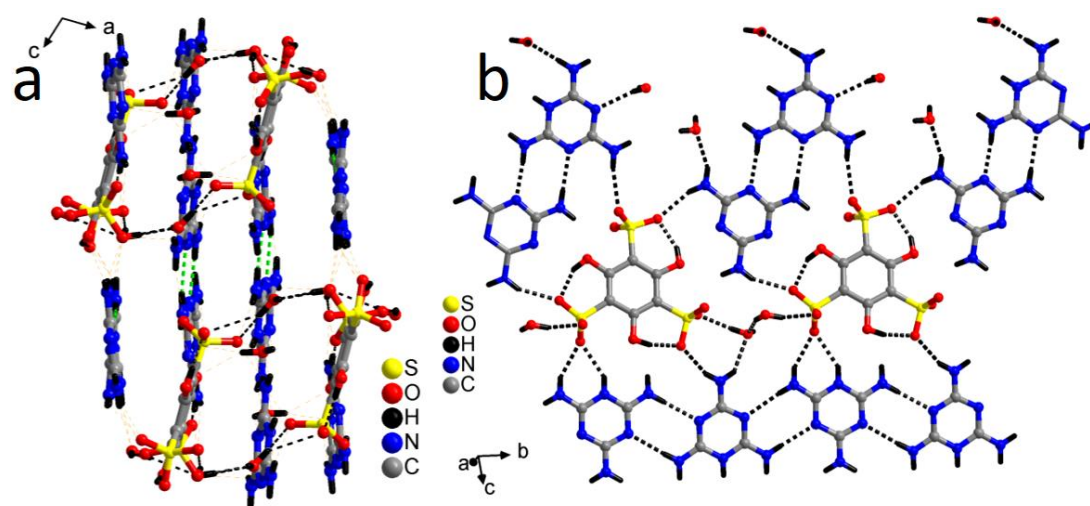


Fig. 4.3. (a and b) H-bonding pattern between (THBTS)³⁻ ligand water and melamine units.

4.3.2 Crystallographic analysis of [Na₂(C₆H₃O₃S₃)(CN₃H₆)(H₂O)].(H₂O), **17**:

The compound **17** was also synthesized under similar condition as compound **16** except melamine is replaced by the guanidinium hydrochloride. The colorless block shape crystals were obtained after evaporation of a mixture of solvents. The molecular formula of compound **17** is calculated as [Na₂(C₆H₃O₃S₃)(CN₃H₆)(H₂O)].(H₂O), from the single crystal X-Ray diffraction. Compound **17** having a layered structure and crystallizes in an orthorhombic system in *Cmca* space group.

The unique unit contains 2/3rd of the ligand unit, two half protonated guanidine units, two sodium ions (full and half occupied) and one water molecules trapped in the crystal lattice (Fig. 4.4). The lattice water molecules and one of the guanidine show thermal ellipsoids (disorder). The hexagonal sheet of ligand in *ac*-plane was coordinated with six sodium ions in *b*-axis and form a two-dimensional structure. In the Ligand C2, C3, O2, and S2 are present special C_{3v} symmetry position. The S1 of sulfonate has R-chiral centre. The two-distinct sodium ions have octahedral geometry. The Na1 ion is coordinated with four oxygen atoms of sulfonate group and two hydroxy oxygen atoms of all different ligands *via* edge sharing with adjacent Na2 ions. The Na2 ions surrounded by two oxygen atoms

of hydroxy and three oxygen atoms of a sulfonate group of ligands and it shared the aqua bridge with two Na2 ions and one Na1 ion *via* edge sharing. The sodium ions and oxygen atoms are separated by 2.453 Å which is in the normal range.

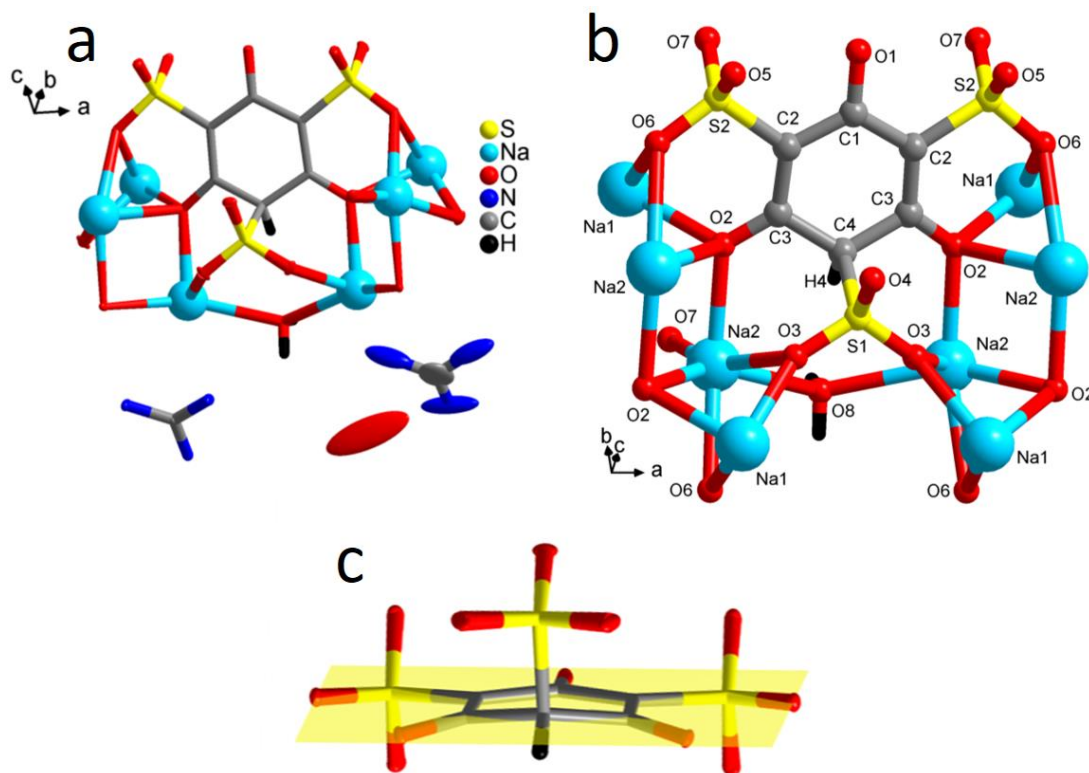


Fig. 4.4. (a) Molecular Structure of $[\text{Na}_2(\text{C}_6\text{H}_3\text{O}_3\text{S}_3)(\text{CN}_3\text{H}_6)(\text{H}_2\text{O})].(\text{H}_2\text{O})$, **17**, (b) Coordination mode of $(\text{THBTS})^{3-}$ ligand with surrounding Na ions and (c) A non-planar tetrahedral arrangement of $(\text{THBTS})^{3-}$ ligand in compound **17**.

Interestingly, in the presence of guanidine hydrochloride the hydrogen atom of O1 of the OH group of ligands, travel to its para-position of the same $(\text{THBTS})^{3-}$ ligand and forms the tetrahedral geometry at the para-position with carbon and losing its aromaticity (Fig. 4.4c). Due to this, the sulfonate group comes out of the $(\text{THBTS})^{3-}$ ligand plane. The bond angle between H-C-S1 is 104.23° . After removal of the hydrogen atom, C1-O1 bond length reduces to 1.267 Å from 1.351 Å. As discussed in the compound **16**, compound **17** is also stabilized by the pi-pi interaction between the two ligands and the distance is 3.5212 Å.

The O3 of S1 provides its oxygen atom for bonding with Na2 ions, whereas O4 of S1 doesn't take part in bonding. S2 present on symmetrical position and sharing O6 and O7 to form a bond with Na1 and Na2 ions, respectively, the O5 of S2 is nonbonding oxygen atom (Fig. 4.5).

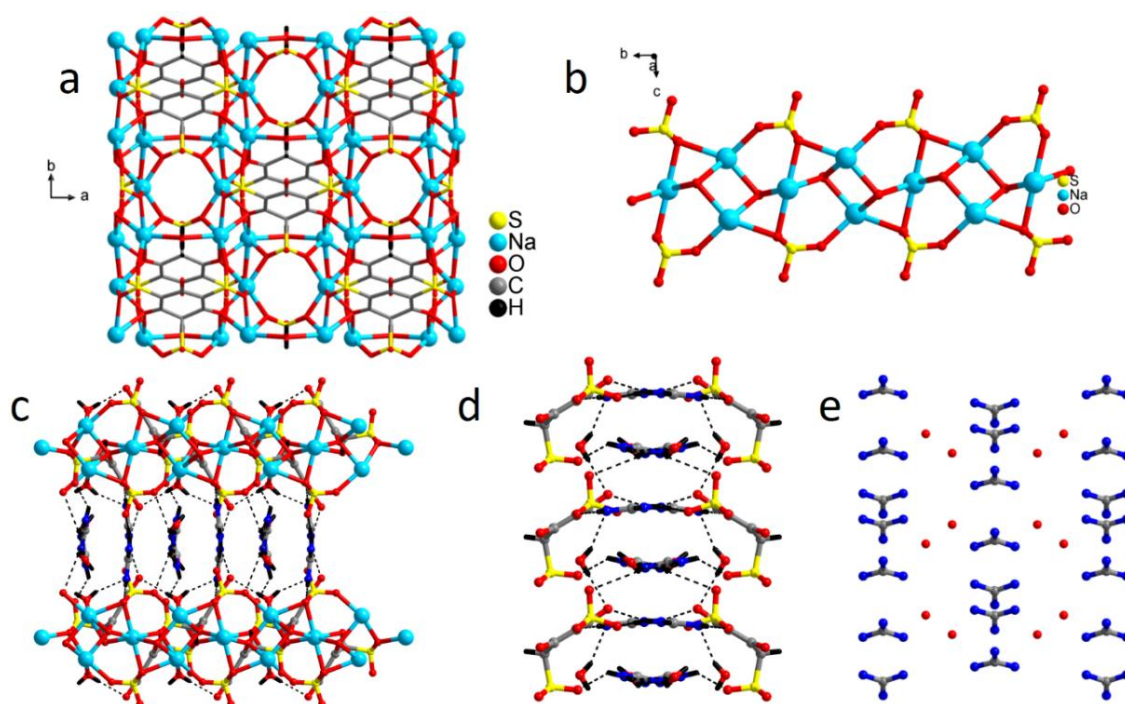


Fig. 4.5. (a) A single layer of $[\text{Na}_2(\text{C}_6\text{H}_3\text{O}_3\text{S}_3)(\text{CN}_3\text{H}_6)(\text{H}_2\text{O})].(\text{H}_2\text{O})$, **17**, (b) Infinite Na-sulfonate chain running along the *b*-axis, (c) H-bonding pattern in $[\text{Na}_2(\text{C}_6\text{H}_3\text{O}_3\text{S}_3)(\text{CN}_3\text{H}_6)(\text{H}_2\text{O})].(\text{H}_2\text{O})$, **17**, (d) H-bonding between (THBTS)³⁻ ligand, water and guanidinium and (e) Arrangement of guanidinium and water molecule.

All the sulfonate groups adopt $\mu^l-\eta^l:\eta^2:\eta^l$ and $\mu^l-\eta^l:\eta^l$ coordination modes to coordinate with four different sodium ions. The O3 of S1 and O6 of S2 is bifurcately bonded with Na1 and Na2 ions (Fig. 4.5). The hydroxy O2 presents its C_{2v} symmetry position which is trifurcated bonded with one Na1 and two Na2 ions. In the lattice, two sodium ions are placed in a special position, having one and a half occupancy with octahedral geometry. The Na1 is coordinated with four sulfonate anions (S2) and two hydroxy oxygen atoms

(O2). The Na1 ions act as a bridge which connects the two ligands along *a*-axis and Na2 chain octahedra along *b*-axis. The Na1 is sharing its all oxygen atoms with Na2 ions *via* edge sharing. The Na2 ions share its all oxygen atoms with Na2 and Na1 ions through edge sharing. The Na2 ion connected with three oxygen atoms of three sulfonate group, two hydroxy oxygen atoms, and one aqua bridge. The Na2 ions form oxido dimer with Na2 ion and this Na2 oxido dimer further connected with Na2 ions *via* the common aqua bridge and sulfonate oxygen atom (O3) and extended in *a*-axis forming a one-dimensional Na2 chain.

The protonated guanidine and free water molecules are situated in between the two layers. The two water molecules are separated by 3.102 Å and the guanidinium and water molecules are separated by 3.86 Å. Here, the H-bonding enhances the stability of the framework and it increases the dimensionality of the molecule and forms an H-bonded three-dimensional framework. The intralayer H-bonding are involved in between the oxygen atoms of sulfonate group and aqua bridge sodium ions. H-bonding also forms in between the nitrogen atoms of Guanidine and oxygen atoms of a water molecule extends along *c*-axis and form a one-dimensional ribbon. These ribbons connect the other two layers through H-bonding and form an H-bonded three-dimensional framework. All the H-bond ranges in between 1.94-2.65 Å.

4.3.3 Crystallographic analysis of $[K_3(C_6H_3O_9S_3)(H_2O)_3]$, **18**:

Replacing guanidine carbonate with K_2CO_3 we got a chiral three-dimensional framework with ordered structure. The single crystal X-ray analysis suggests that the crystal has an orthorhombic crystal system. The asymmetric unit of compound **18** contains two potassium and one $(THBTS)^{3-}$ ligand molecule and two water molecules (Fig 4.6). The bond lengths of K-O are ranges from 2.65 to 3.10 Å. The Potassium is loosely bonded and coordinated with 8 neighboring oxygen atoms. In the compound **18**, the water molecule itself forms a

water channel. The distance between the two sets of water molecules are 2.85 Å and 3.18 Å.

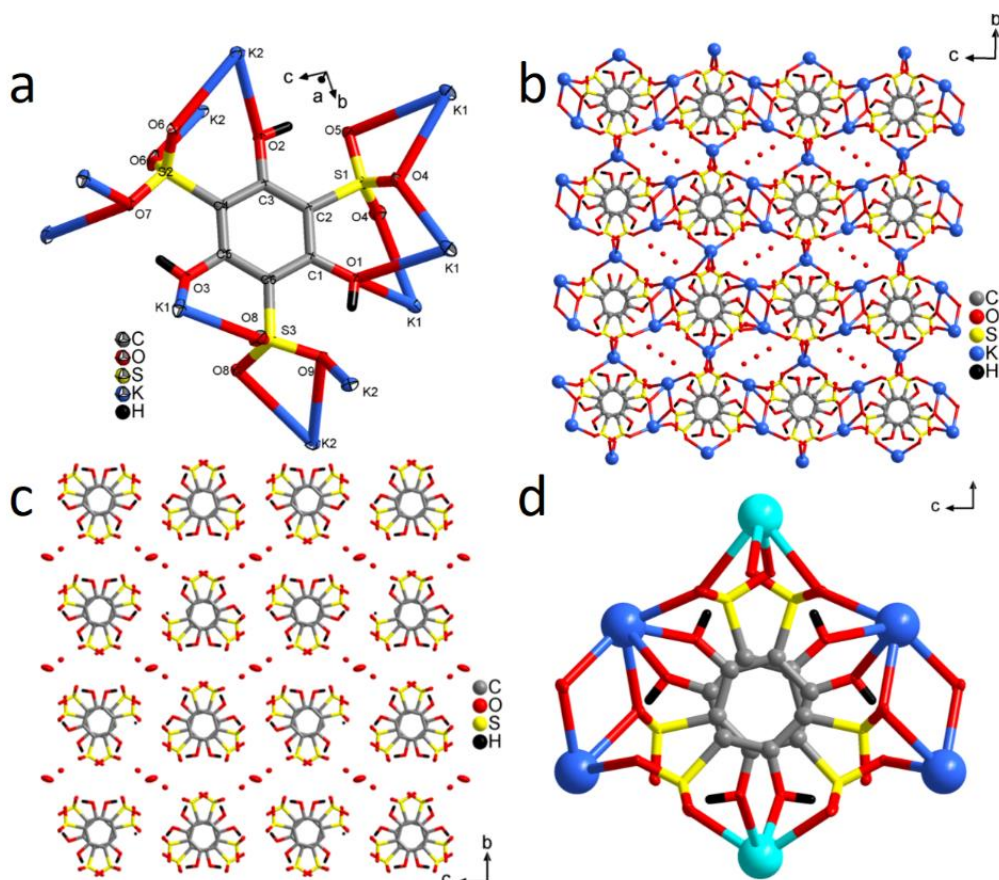


Fig. 4.6. (a) Asymmetric unit of $[\text{K}_3(\text{C}_6\text{H}_3\text{O}_9\text{S}_3)(\text{H}_2\text{O})_3]$, **18**, (b) Lattice diagram of $[\text{K}_3(\text{C}_6\text{H}_3\text{O}_9\text{S}_3)(\text{H}_2\text{O})_3]$, **18**, (c) A water channel in $[\text{K}_3(\text{C}_6\text{H}_3\text{O}_9\text{S}_3)(\text{H}_2\text{O})_3]$, **18** where potassium ions are omitted and (d) Coordination mode of potassium and $(\text{THBTS})^{3-}$ ligands along *a*-axis where K1 ions are blue and K2 ions in turquoise color.

In the compound **18**, the sulfonate ligands S2 and S3 are showing S and R chiral center. Within the ligand, all the sulfonate groups (S1, S2, S3) are present with half occupancy, which is neutralized by K1 half occupancy and K2 fully occupied (Fig. 4.6). Each potassium ions are surrounded by eight oxygen atoms (sulfonate oxygen atoms and phenolic oxygen atoms of the same $(\text{THBTS})^{3-}$ ligand). K1 ions surrounded with six oxygen atoms from the four sulfonate groups and two phenolic oxygen atoms of $(\text{THBTS})^{3-}$ ligands. Whereas K2 ions connected with its surrounding four oxygen atoms of four

sulfonate group, two phenolic oxygen atoms of (THBTS)³⁻ ligands and two water molecules. The bond lengths of K-O are in the range of 2.612-3.102 Å. The K-O bond lengths are longer as compared to the normal range, suggesting that the potassium ions are loosely bonded to oxygen atoms. The potassium atom has +1 oxidation state as per bond valence sum calculations.

In crystal lattice, the (THBTS)³⁻ ligand is having C_{3v} symmetry. It is in the *ab*-plane and is coordinated by K ions along *c*-axis and form a three-dimensional framework. In ligand, S1 provides its two oxygen atoms, which have a (special position O4) for bonding with K1 ion, whereas O5 is non-bonding. The O4 is bifurcately bonded with two K1 ions. The other sulfonate group S2 shares its all oxygen atoms with potassium ions. The two O6 of S2 bonded with two K2 ions and O7 of S2 is bifurcately coordinated with two K1 ions. In the S3 of a sulfonate group, all oxygen atoms are bonded with two K1 ions and two K3 ions and all the oxygen atoms are bifurcately bonded with potassium ions. The two O8 are bifurcately bonded with two K1 and two K2 ions, whereas O9 bifurcately bonded with two K2 ions. In other part of ligand, the phenolic oxygen O1, and O3 bifurcately bonded with K1 ions. The phenolic oxygen O2 of ligands are again bifurcately bonded with two K2 ions. The K ions are pointing outside of the ligand plane and coordinate with sulfonate oxygen and a phenolic oxygen atoms and extends, which results in a three-dimensional framework.

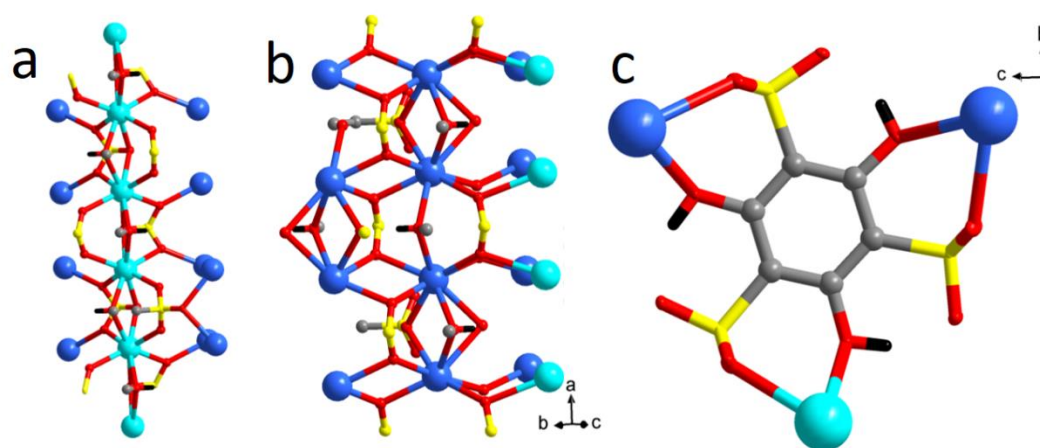


Fig. 4.7. (a) K2 chain in compound **18** running parallel to K1 chain, (b) K1 chain in compound **18** and (c) Potassium ions at equilateral triangle position in the compound **18**.

The two K1 are joined by the common bifurcately bonded O7 and phenolic O1 oxygen atoms and aqua bridge O1w oxygen atoms and forms two-membered rings with edge sharing linkage (K1-O7-K1 and K1-O1-K1). On opposite direction it forms 3-membered rings, these 3-membered rings are composed of common phenolic O3, two O8 of S3 via K1-O3-K1 linkage. The 4-membered rings composed with bifurcated O4 and O8 of S3 sulfonate group of (THBTS)³⁻ ligand. The alternate arrangement of 2 and 3-membered rings extends along *a*-axis and forms one-dimensional chain and runs parallel to K2 chain. The distance between two K1 ions in 2-membered rings is 4.2064 Å and in 3-membered rings is 4.6169 Å. The K1 chain further connected with the common O4 oxygen of S1 sulfonate and form 2-membered rings and separated with distance 4.4912 Å. These 2-membered rings further extend along *b*-axis and branched, one connects K1 through common O2w oxygen atoms and others connect K2 ions with O8 of S3 sulfonate. K2 ions are surrounded with two S2 and two S3 of sulfonate group and two phenolic O2 oxygen atoms. The two K2 ions shares its common oxygen O9 of S3 and phenolic O2 oxygen atoms and extend along *a*-axis and resulting chain through edge sharing. The K1-O are loosely bonded to each other. The potassium ions are coordinated with the two K2 ions are separated by a distance 4.4117 Å (Fig.4.7).

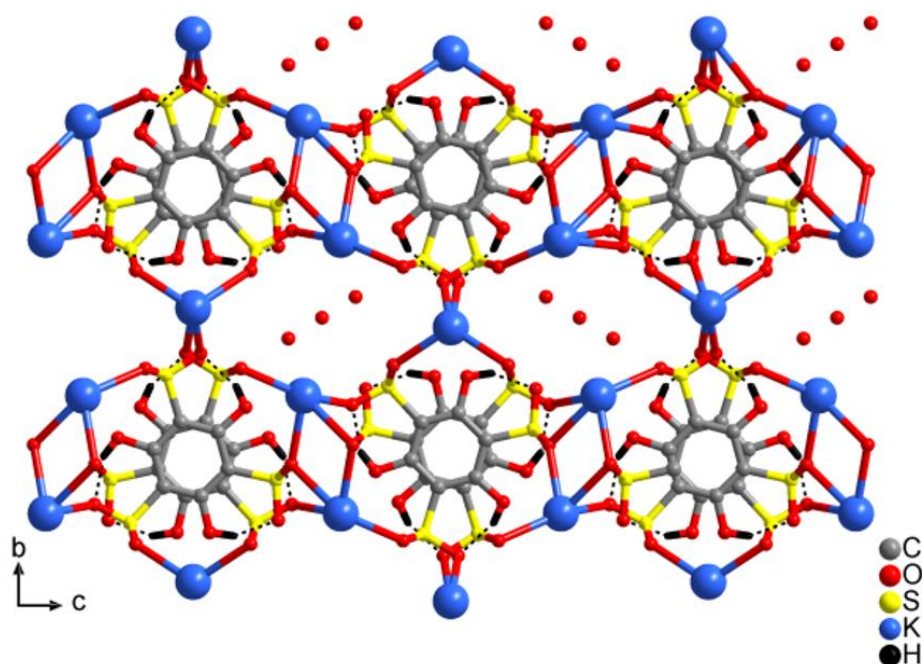


Fig.4.8. H-bonding pattern in $[K_3(C_6H_3O_9S_3)(H_2O)_3]$, **18**.

In the crystal lattice, two benzene rings of $(THBTs)^{3-}$ ligands are separated by distance 4.4154 Å. The K2 ion is situated at the hexagonal head and tail and distance between opposite K2 ions is 9.9348 Å, the single $(THBTs)^{3-}$ ligands are connected by two K1 and one K2 ion and separated by 7.8474-7.9824 Å. In the molecule K1 and K2 ions located at nearly equilateral triangle position along *a*-axis. The compound **18** is getting extra stability from H-bonding. The H-bonding in the $(THBTs)^{3-}$ ligands is involved in between the phenolic oxygen atoms and the oxygen atoms of sulfonate group which provides the stability to $(THBTs)^{3-}$ ligands. The inter H-bonding are formed in between phenolic oxygen, the sulfonate oxygen atom of $(THBTs)^{3-}$ ligands and a water molecule. The H-bonding ranges from 1.82-2.96 Å as shown in Fig. 4.8.

4.3.4 Crystallographic analysis of $[C_4N_2H_{13}]_2[Cd_2(C_6H_3O_3S_3)(H_2O)_2] \cdot (H_2O)$, **19**:

By introducing d^{10} metal (Cd) to $Na_3(THBTs)$ ligand, we got a one-dimensional chain. The compound **19** was synthesized from $Cd(NO_3)_2$ and 4 units of $Na_3(THBTs)$ ligand. The colorless crystals of compound **19** were synthesized by slow diffusion of water into

methanol. The colorless crystals of compound **19** have a monoclinic crystal system with achiral $P2_1/c$ space group. Compound **19** has an infinite one-dimensional structure as shown in Fig. 4.9. The asymmetric unit consists of two cadmium ions, one $(\text{THBTS})^{3-}$ ligand, one partially protonated DABCO, five aqua ligands and one water molecules are trapped inside the crystal lattice. There are two crystallographically distinct cadmium ions present in the crystal. The Cd1 has hepta-coordination and coordination sphere is satisfied by the surrounding $(\text{THBTS})^{3-}$ ligand through corner sharing linkage and aqua ligands. The Cd2 ions show octahedral geometry and coordinate similar to Cd1 ions except here only two aqua ligands coordinated.

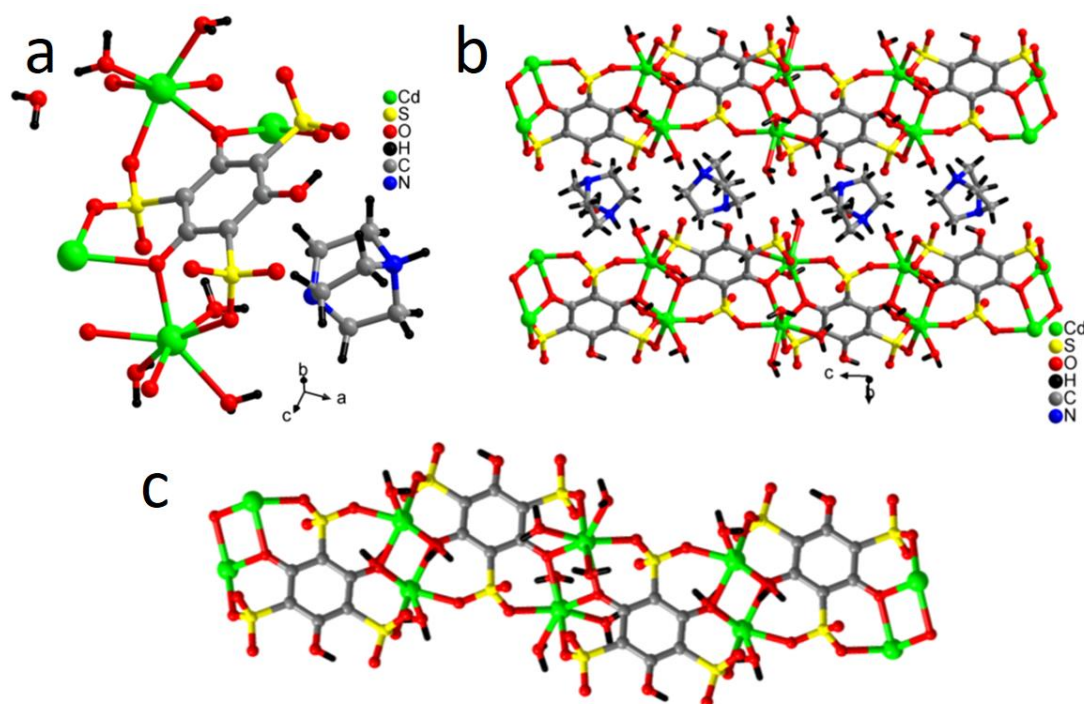


Fig. 4.9. (a) Asymmetric unit of $[\text{C}_4\text{N}_2\text{H}_{13}]_2[\text{Cd}_2(\text{C}_6\text{H}_3\text{O}_3\text{S}_3)(\text{H}_2\text{O})_2] \cdot (\text{H}_2\text{O})$, **19**, where unique atoms are labeled, (b) Lattice diagram of $[\text{C}_4\text{N}_2\text{H}_{13}]_2[\text{Cd}_2(\text{C}_6\text{H}_3\text{O}_3\text{S}_3)(\text{H}_2\text{O})_2] \cdot (\text{H}_2\text{O})$, **19** and (c) Cd chain running along c -axis in $[\text{C}_4\text{N}_2\text{H}_{13}]_2[\text{Cd}_2(\text{C}_6\text{H}_3\text{O}_3\text{S}_3)(\text{H}_2\text{O})_2] \cdot (\text{H}_2\text{O})$, **19**.

The two Cd1 ions connected to each other by the edge-sharing with common O10 of two different $(\text{THBTS})^{3-}$ ligands. The bond lengths of Cd1-O are ranges from 2.254-2.422 Å

which are in normal range. The O12 oxygen atom of (THBTS)³⁻ ligand is connected to two Cd²⁺ ions and shows edge sharing linkage. The Cd²⁺-O bond lengths are existing in the range of 2.21-2.303 Å and having in the normal range³⁰. The bond valence sum calculations suggested that Cd in +2 oxidation state. The (THBTS)³⁻ ligand is providing its all sulfonate oxygen atoms and two hydroxy oxygen atoms to the Cd(II) ions and forming a one-dimensional chain, whereas the phenolic oxygen atom namely O11 of (THBTS)³⁻ ligand remains non-bonded. The bond lengths of all the C-S_{sulfonate} is lying in between 1.743-1.781 Å and C-O_{hydroxy} is 1.31 Å.

In the crystal lattice, the hydroxy oxygen O1 bifurcately bonded with two Cd1 ions, whereas the other hydroxy O2 of same (THBTS)³⁻ ligand bifurcately coordinate with two Cd²⁺ ions. The phenolic oxygen atom of ligand remains as OH. The sulfonate oxygen atom namely O4 is coordinated with Cd1 ion and another sulfonate oxygen atoms namely O5 and O6 remain non-bonded. The other sulfonate group S2, the oxygen atoms namely O7 and O8 connected with Cd1 and Cd²⁺ ions through corner sharing, the oxygen atom O9 does not take part in bonding. The oxygen atom O10 of sulfonate S3 share its oxygen atoms to Cd²⁺ ions *via* corner sharing, the other two oxygen atoms namely O11 and O12 remain inactive.

The Cd1 ions surrounded with two sulfonate of two (THBTS)³⁻ ligands, three aqua ligands, and Cd1 ions share its common oxygen O1 of hydroxy oxygen atom with other Cd1 ions and form Cd1-O1-Cd1 edge sharing linkage. Cd²⁺ ions have coordination sphere fill with two sulfonates (THBTS)³⁻ ligands, two aqua ligands. Whereas the Cd²⁺ ions shares common hydroxy oxygen atom O2 and form Cd²⁺-O2-Cd²⁺ edge sharing dimer. The alternate arrangement of the hepta-coordinate Cd1 dimer, C_{3v} symmetry (THBTS)³⁻ ligand and octahedra Cd²⁺ dimer results into a one-dimensional chain which is running through c-axis.

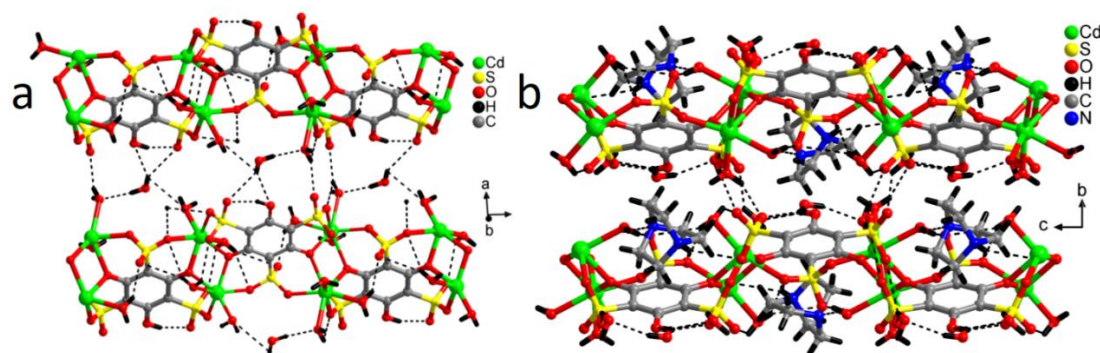


Fig. 4.10. (a and b) H-bonding pattern in $[C_4N_2H_{13}]_2[Cd_2(C_6H_3O_3S_3)(H_2O)_2] \cdot (H_2O)$, **19** from different viewing direction (in case of (a) DABCO units are omitted).

The organic template DABCO situated in the interchain space. The free water molecule is present in the space between two chains. The dimensionality of a compound **19** enhances from H-bonding and provide extra stability. The H-bonding involves in between sulfonate oxygen atoms, phenolic OH of $(THBTS)^{3-}$ ligand, and aqua ligands in the chain. Furthermore, the H-bonding involves in between the oxygen of free water molecule, the nitrogen atoms of DABCO and the oxygen atoms of chain and forms an infinite H-bonded three-dimensional framework. The H-bond distances ranges from 1.962- 2.68 Å (Fig. 4.10).

4.4. Thermal analysis

4.4.1. Thermogravimetric analysis:

The thermal stability of compounds **16-19** based on sulfonate ligand was carried out on Discovery TGA -TA Instrument by Waters at a heating rate of 10 °C/min under N_2 gas flow and shown in Fig. 4.11. The TGA graphs show that compound **16** show three-steps weight loss. The first step show slow, steady disintegration corresponds to dehydration of compound **16** until 325 °C which accounts 9.40%. The second step begins from 330 °C and shows a sudden drop to 420 °C which corresponds to melamine decomposition that accounts 43.23 %. The next step starts from 450 °C up to 880 °C and is due to the thermal disintegration of compound **16**. The residual products were black solid.

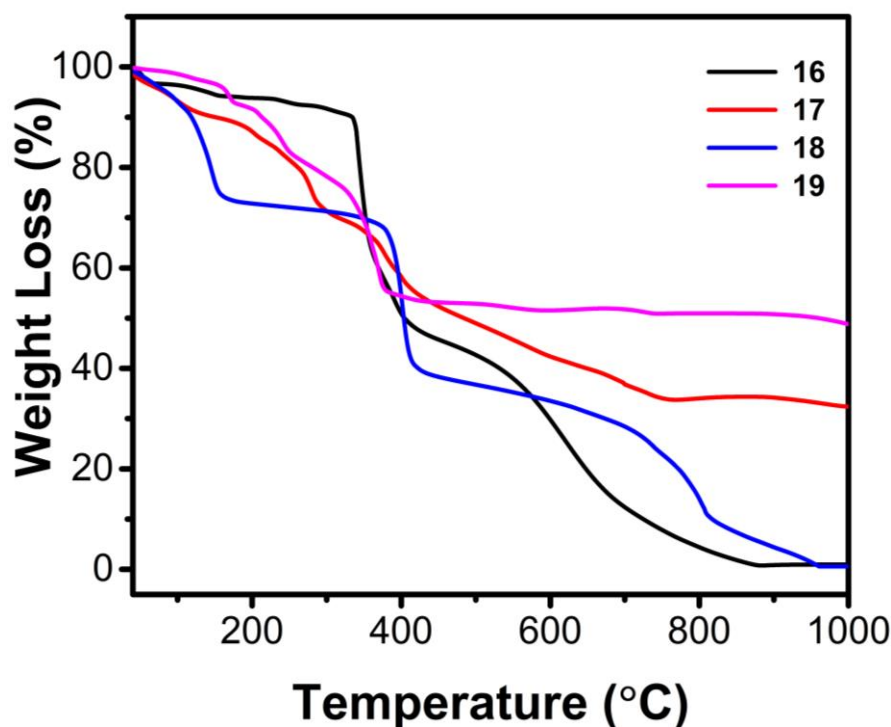


Fig. 4.11. TGA Profile diagram for compounds **16-19**.

The TGA curve of compound **17** shows multi-steps degradations; the first step in the range 40-90 °C correspond to removal of water molecules (8.82 %, weight loss), the second step shows weight loss due to loss of guanidinium (17.37 %, weight loss) in the temperature range of 180-290 °C and the next and final step corresponds to the thermal degradation of compound **17** in between 335 to 760 °C (34.63 %, weight loss). The Residual product analyzed by PXRD shows unidentified phase.

The TGA profile diagram of compound **18** suggests steady removal of water molecules up to 160 °C (26.31 %, weight loss). The next two weight losses correspond to the thermal degradation of compound **18** and potassium until 970°C (68%, weight loss). The residual product is black mass. TGA curve analysis of compound **19** shows steady continuous decomposition which corresponds to a collective loss of water DABCO and sulfonate ligands (48.34 %, weight loss) in the temperature range of 40-410 °C. The red color residual product was identified as cadmium oxide by PXRD.

4.5 Conclusion:

In conclusion, four sulfonate-based ligand compounds have been successfully synthesized at room temperature. All the compounds are with same core ligand, but different counter cations. Compound **16** formed an H-bonded three-dimensional framework. The structural arrangement between Na_3L and water molecules extend and form the helix structure. The compound **17** shows a layered structure with Na ions bonded with sulfonate and guanidinium cations present in the interlayer space. In compound **17**, the ligand lost its aromaticity at para-position with a tetrahedral arrangements. Compound **18** shows an ordered three-dimensional structure. The potassium is loosely bonded to surrounding oxygen atoms with water channel. The arrangement of ligand and potassium ions look like a nearly equilateral triangle. The Compounds **19** have one-dimensional chain structure. The partial protonated DABCO is located in the interchain space. These DABCO and water molecules provide the path for H-bonding between the coordinate chains which extends and forma an H-bonded three-dimensional framework.

References:

- (1) Ōkawa, H.; Shigematsu, A.; Sadakiyo, M.; Miyagawa, T.; Yoneda, K.; Ohba, M.; Kitagawa, H. *J. Am. Chem. Soc.* **2009**, *131*, 13516.
- (2) Ōkawa, H.; Sadakiyo, M.; Yamada, T.; Maesato, M.; Ohba, M.; Kitagawa, H. *J. Am. Chem. Soc.* **2013**, *135*, 2256.
- (3) Kundu, T.; Sahoo, S. C.; Banerjee, R. *Chem. Commun.* **2012**, *48*, 4998.
- (4) Taylor, J. M.; Mah, R. K.; Moudrakovski, I. L.; Ratcliffe, C. I.; Vaidhyanathan, R.; Shimizu, G. K. *J. Am. Chem. Soc.* **2010**, *132*, 14055.
- (5) Yamada, T.; Otsubo, K.; Makiura, R.; Kitagawa, H. *Chem. Soc. Rev.* **2013**, *42*, 6655.
- (6) Nguyen, N. T.; Furukawa, H.; Gándara, F.; Trickett, C. A.; Jeong, H. M.; Cordova, K. E.; Yaghi, O. M. *J. Am. Chem. Soc.* **2015**, *137*, 15394.
- (7) Bureekaew, S.; Horike, S.; Higuchi, M.; Mizuno, M.; Kawamura, T.; Tanaka, D.; Yanai, N.; Kitagawa, S. *Nat. Mater.* **2009**, *8*, 831.
- (8) Sadakiyo, M.; Yamada, T.; Kitagawa, H. *ChemPlusChem* **2016**, *81*, 691.
- (9) Zhai, Q. G.; Mao, C.; Zhao, X.; Lin, Q.; Bu, F.; Chen, X.; Bu, X.; Feng, P. *Angew. Chem. Int. Ed.* **2015**, *54*, 7886.
- (10) Hamrock, S. J.; Yandrasits, M. A. *J. Macromol. Sci., Polym. Rev.* **2006**, *46*, 219.
- (11) Meng, X.; Wang, H.-N.; Song, S.-Y.; Zhang, H.-J. *Chem. Soc. Rev.* **2017**, *46*, 464.
- (12) Kraytsberg, A.; Ein-Eli, Y. *Energy & Fuels* **2014**, *28*, 7303.
- (13) Nagarkar, S. S.; Unni, S. M.; Sharma, A.; Kurungot, S.; Ghosh, S. K. *Angew. Chem. Int. Ed.* **2014**, *53*, 2638.
- (14) Umeyama, D.; Horike, S.; Inukai, M.; Kitagawa, S. *J. Am. Chem. Soc.* **2013**, *135*, 11345.

- (15) Hurd, J. A.; Vaidhyanathan, R.; Thangadurai, V.; Ratcliffe, C. I.; Moudrakovski, I. L.; Shimizu, G. K. *Nat. Chem.* **2009**, *1*, 705.
- (16) Weppner, W.; Kreuer, K.; Rabenau, A. *Angew. Chem., Int. Ed. Engl* **1982**, *122*, 208.
- (17) Kreuer, K.-D. *Chem. Mater.* **1996**, *8*, 610.
- (18) Ramaswamy, P.; Wong, N. E.; Shimizu, G. K. *Chem. Soc. Rev.* **2014**, *43*, 5913.
- (19) Taylor, J. M.; Dawson, K. W.; Shimizu, G. K. *J. Am. Chem. Soc.* **2013**, *135*, 1193.
- (20) Clearfield, A. *Prog. Inorg. Chem.* **1998**, *47*, 371.
- (21) Gunderman, B. J.; Squattrito, P. J. *Inorg. Chem.* **1995**, *34*, 2399.
- (22) Shimizu, G. K.; Enright, G. D.; Ratcliffe, C. I.; Rego, G. S.; Reid, J. L.; Ripmeester, J. A. *Chem. Mater.* **1998**, *10*, 3282.
- (23) Guan, L.; Wang, Y. *J. Coord. Chem.* **2017**, *70*, 2520.
- (24) Côté, A. P.; Shimizu, G. K. *Chem. Commun.* **2001**, 251.
- (25) Sheldrick, G. *SADABS, SHELXS-2008, SHELXL-2014*; University of Göttingen: Göttingen, Germany, 2014.
- (26) Sheldrick, G. M. *SADABS Siemens Area Correction Absorption Program*; University of Göttingen, Göttingen, Germany, 1994.
- (27) Pennington, W. T. *J. Appl. Crystallogr.* **1999**, *32*, 1028.
- (28) Farrugia, L. J. *J. Appl. Crystallogr.* **1997**, *30*, 565.
- (29) Kim, S.; Dawson, K. W.; Gelfand, B. S.; Taylor, J. M.; Shimizu, G. K. *J. Am. Chem. Soc.* **2013**, *135*, 963.
- (30) An, C.; Feng, X.; Zhao, N.; Liu, P.; Wang, T.; Lian, Z. *J. Cluster Sci.* **2015**, *26*, 889.

Appendix

Table 4.1. Crystallographic table of compounds 16-19.

	16	17	18	19
Empirical formula	C ₁₈ H ₃₈ N ₂₄ O ₁₆ S ₃	C ₈ H ₁₃ N ₆ Na ₃ O ₁₅ S ₃	C ₆ H ₃ K ₃ O ₁₄ S ₃	C ₁₂ H ₂₆ Cd ₂ N ₂ O ₁₈ S ₃
Mr	942.90	598.39	512.56	807.33
crystal system	Monoclinic	Orthorhombic	Orthorhombic	Monoclinic
space group	<i>P2₁/n</i>	<i>Cmca</i>	<i>Cmca</i>	<i>P2₁/n</i>
<i>a</i> /Å	16.8237(6)	12.8318(9)	8.8233(4)	10.8593(13)
<i>b</i> /Å	12.2192(4)	12.1850(9)	19.8695(9)	15.2006(18)
<i>c</i> /Å	18.3904(7)	25.4468(18)	18.6688(4)	14.0240(2)
α /°	90	90	90	90
β /°	106.431(2)	90	90	93.166(9)
γ /°	90	90	90	90
Volume/ Å ³	3626.2(2)	3978(5)	3272.9(3)	2311.4(5)
Z	4	8	8	4
<i>D_x</i> /Mg m ⁻³	1.727	1.998	2.080	2.320
μ / mm ⁻¹	0.311	0.533	1.289	2.204
θ range for data collection/ °	2.027 to 25.50	2.44 to 25.499	2.05 to 29.617	3.54 to 24.495
Reflections collected	47594	18071	31193	20084
unique reflections	6740	1955	2438	3783
R(int)	0.0687	0.0542	0.0554	0.0998
Data / restraints / parameters	6740 / 0 / 556	1955 / 3 / 184	2438 / 0 / 466	3783 / 0 / 133
R1 and R2 [<i>I</i> >2 σ (<i>I</i>)]	0.0408, 0.1005	0.0463, 0.1167	0.0341, 0.1002	0.0989, 0.2606
R1 and R2 (all data)	0.0540, 0.1111	0.0548, 0.1232	0.0498, 0.1133	0.1005, 0.2724
Goodness-of-fit on <i>F</i> ²	1.028	1.102	1.043	1.136
Largest diff. peak and hole/e.Å ⁻³	0.619 and -0.425	1.00 and -0.970	0.46 and -0.53	0.23 and -0.15
CCDC no	1813876	1813877	1813878	1813879

Table 4.2. Selected bond length tables for compounds 16-19.

[(C₃N₆H₆)(C₃N₆H₇)₃(C₆H₃O₉S₃).(H₂O)₄], 16					
S1-O6	1.4505(18)	N3-C8	1.338(3)	N16-C13	1.316(3)
S1-O4	1.4518(17)	N4-C8	1.332(3)	N17-C14	1.313(3)
S1-O5	1.4569(18)	N5-C9	1.312(3)	N18-C15	1.317(3)
S1-C2	1.765(2)	N6-C7	1.312(3)	N19-C18	1.320(3)
S2-O8	1.4366(18)	N7-C11	1.342(3)	N19-C16	1.354(3)
S2-O9	1.4385(18)	N7-C10	1.352(3)	N20-C17	1.315(3)
S2-O7	1.4677(17)	N8-C11	1.337(3)	N20-C16	1.354(3)
S2-C4	1.770(2)	N8-C12	1.345(3)	N21-C17	1.367(3)
S3-O12	1.4370(17)	N9-C10	1.333(3)	N21-C18	1.368(3)
S3-O10	1.4532(18)	N9-C12	1.339(3)	O2-C3	1.351(3)
S3-O11	1.4622(18)	O1-C1	1.342(3)	S3-C6	1.771(2)
O3-C5	1.336(3)	N10-C10	1.335(3)	N22-C18	1.317(3)
N13-C14	1.362(3)	N11-C11	1.340(3)	N23-C16	1.311(3)
N1-C9	1.331(3)	N13-C13	1.364(3)	C1-C6	1.407(3)
N1-C8	1.345(3)	N13-H13	0.8600	C2-C3	1.408(3)
N15-C13	1.324(3)	N12-C12	1.342(3)	N24-C17	1.319(3)
N3-C7	1.324(3)	N15-C15	1.352(3)	C1-C2	1.399(3)
N2-C9	1.360(3)	N14-C14	1.321(3)	C3-C4	1.390(3)
N2-C7	1.363(3)	N14-C15	1.352(3)	C4-C5	1.403(3)
C5-C6	1.399(3)				
[Na₂(C₆H₃O₃S₃)(CN₃H₆)(H₂O)](H₂O), 17					
Na1-O1	2.257(2)	Na1-O3	2.435(2)	Na1-O6	2.347(2)
Na2-O1	2.369(3)	Na2-O1W	2.5772(18)	Na2-O4	2.337(2)
Na2-O3	2.520(2)	Na2-O6	2.440(2)	Na2-61	2.400(2)
[K₃(C₆H₃O₉S₃)(H₂O)₃], 18					
K1-O1W	3.002(3)	K1-O2W	3.006(4)	K1-O3	3.0463(16)
K1-O4	2.7571(19)	K1-O5	3.2422(19)	K1-O7	2.7665(16)
K1-O8	2.6983(19)	K2-O2	2.9031(15)	K2-O6	2.688(2)
K2-O8	2.9656(19)	K2-O8	2.966(2)	K2-O9	2.7653(14)
[C₄N₂H₁₃]₂[Cd₂(C₆H₃O₃S₃)(H₂O)₂].(H₂O), 19					
Cd1-O7	2.253(11)	Cd1-O1	2.401(11)	Cd1-O4	2.312(12)
Cd1-O1W	2.284(12)	Cd1-O2W	2.438(13)	Cd1-O3W	2.372(13)
Cd1-O3	2.2276(15)	Cd2-O5	2.277(12)	Cd2-O5	2.222(12)
Cd2-OD	2.264(12)	Cd2-O8	2.288(13)	Cd2-O4W	2.294(14)
Cd2-OO5W	2.220(15)				

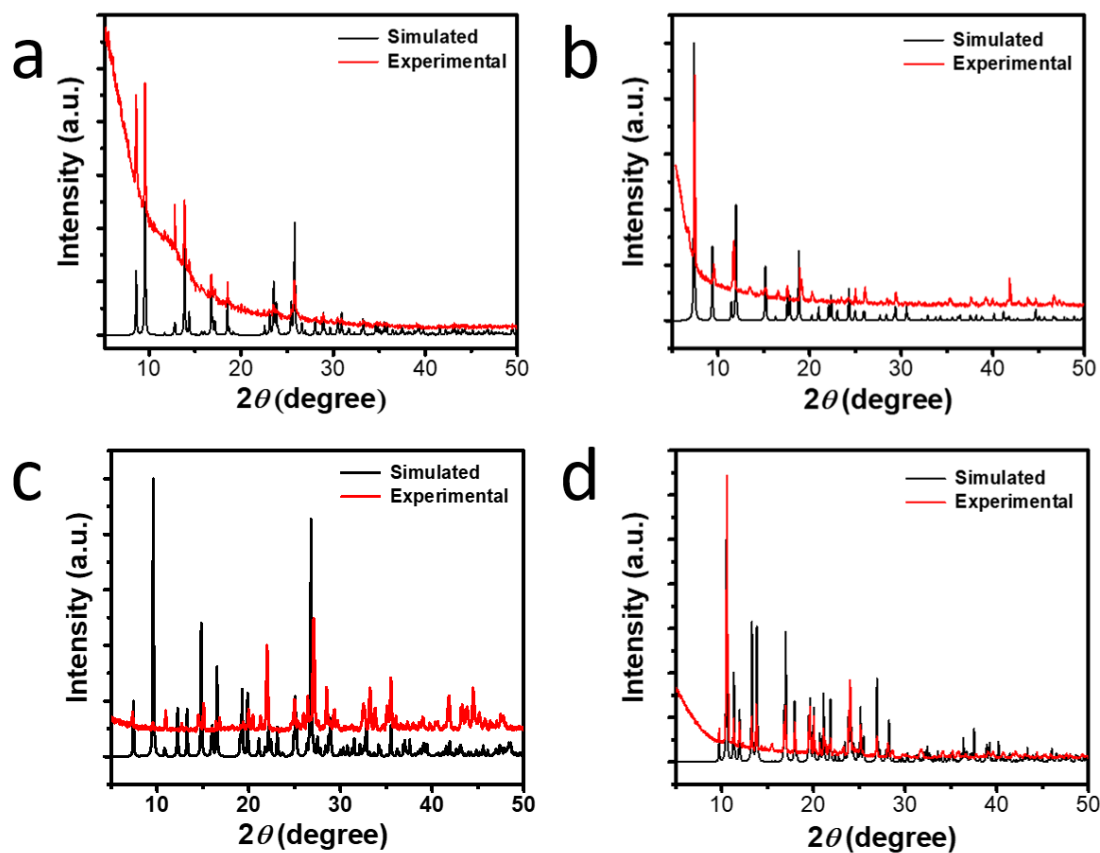
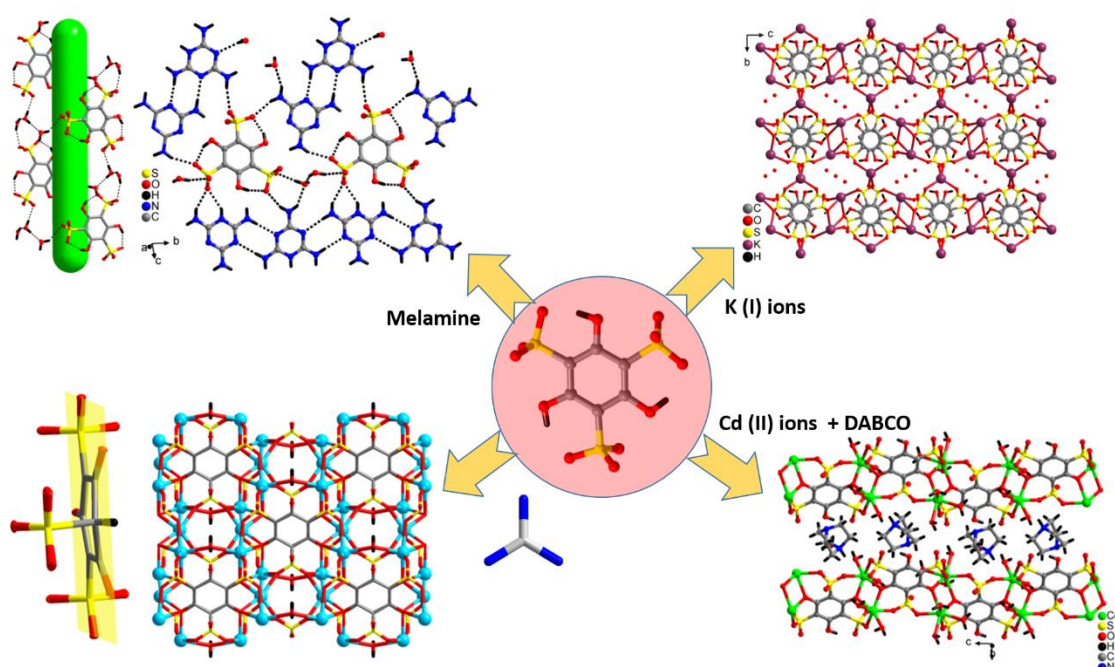


Fig. 4.12. PXRD pattern of the compounds (a) $[(C_3N_6H_6)(C_3N_6H_7)_3(C_6H_3O_9S_3) \cdot (H_2O)_4]$, **16**, (b) $[Na_2(C_6H_3O_3S_3)(CN_3H_6)(H_2O)](H_2O)$, **17**, (c) $[K_3(C_6H_3O_9S_3)(H_2O)_3]$, **18** and (d) $[C_4N_2H_{13}]_2[Cd_2(C_6H_3O_3S_3)(H_2O)_2] \cdot (H_2O)$, **19** showing the phase purity of as-synthesized material.

Summary of chapter 4



Chapter 5

INORGANIC-ORGANIC HYBRID MATERIALS BASED ON BTC-IMIDAZOLE (Im) AND BTC-BENZIMIDAZOLE (BIm) LIGANDS

Abstracts	197
5.1. Introduction	197
5.2. Experimental section	199
5.2.1. Materials and methods	199
5.2.2. Syntheses of compounds 20-25	200
5.2.3. Characterization	201
5.2.3.1. Single crystal structure determination	201
5.2.3.2. Elemental analysis	202
5.3. Results and discussion	202
5.3.1. Structural analysis of [Co₆(formate)₆(BTC)₆(Im)₆], 20	202
5.3.1.1. Magnetic properties of [Co₆(formate)₆(BTC)₆(Im)₆], 20	205
5.3.2. Structural analysis of [(CH₃)₂NH₂][Cu(BTC)₃(Im)], 21	206
5.3.3. Structural analysis of [Zn₂(HBTC)₂((Im)(H₂O))], 22	209
5.3.4. Structural analysis of [Co₄(BTC)₃(BIm)₆][solvent], 23	213
5.3.5. Structural analysis of [Cu₃(BTC)₂(BIm)₆][solvent], 24	216
5.3.6. Structural analysis of [(CH₃CH₂)₂NH₂][Zn(BTC)(BIm)].(H₂O) 25	218
5.3.6.1. Dielectric measurement of [(CH₃CH₂)₂NH₂][Zn(BTC)(BIm)].(H₂O) 25	220
5.4. Thermal analysis	221
5.4.1. Thermogravimetric analysis	221
5.5. Conclusions	223
References	225

Appendix	228
Summary	233

Abstract

Six novel Metal-BTC-Im and Metal-BTC-Benzimidazole based coordination polymers with different topologies namely, $[Co_6(\text{formate})_6(\text{BTC})_6(\text{Im})_6]$, **20**, a layered structure; $[(CH_3)_2NH_2][Cu(\text{BTC})(\text{Im})]$, **21**, a layered structure; $[Zn_2(\text{HBTC})_2((\text{Im})(H_2O))]$, **22**, ribbon like chain structure; $[Co_4(\text{BTC})_3(\text{BIm})_6][\text{solvent}]$, **23**, 3D-network with embedded paddlewheel SBUs; $[Cu_3(\text{BTC})_2(\text{BIm})_6][\text{solvent}]$, **24**, a layered structure with hexagonal sheet; and $[(CH_3CH_2)_2NH_2][Zn(\text{BTC})(\text{BIm})](H_2O)$ **25**, a 3D network. Compound **20** has a layered structure with hexanuclear Co cluster and show antiferromagnetic interaction between Co(II) ions. Compound **21** shows a wave like layered structure whereas compound **24** shows bronze hexagonal sheet. Compounds **23** and **25** were also found to have embedded helical assemblies. In all the crystal structure the added strength was provided by H-bonding and/or pi-stacking interactions. The compounds were well characterized by the single crystal X-ray diffraction, powder X-ray diffraction and thermogravimetric analysis. Compound **25** crystallizes in non-centrosymmetric space group and shows dielectric behaviour.

5.1 Introduction:

In the last two decades researcher are taking more interest in crystalline porous materials which is a most promising and emerging area for development in the architectural design and engineering for their novel topologies and their potential applications like catalysis, gas separation and storage, magnetism, and nonlinear optical phenomenon etc.^{1,2,3,4} The crystalline porous materials are divided into various types depending on the materials bonding and size of materials, which are the open-framework, metal-organic framework (MOF), proton conducting metal-organic framework (PC-MOF), coordination polymer, polyoxometalate cluster and covalent organic framework (COF). The synthesis of MOFs

depends on the various conditions like multi-nodal advanced engineered ligands, metal node, solvent, temperature, the stoichiometric ratio of metal to the ligand and pH.

The hybrid materials assimilating the properties of both organic and inorganic components have become a thrust area in material science^{5,6}. The most influential factors for achieving a certain coordination polymer are the nature and coordination ability of metal ions, flexibility and coordination mode inherited in the ligand system, the stoichiometry of the components and the reaction environments. Multi-carboxylate ligands have been widely explored for the synthesis of numerous metal-organic frameworks owing to its variable coordination mode towards metal ions e.g. monodentate, bridging and chelating etc.

In particular, C_{3v} symmetric 1, 3, 5-benzenetricarboxylic acid (H_3BTC) has served to construct a multitude of aesthetically pleasing MOF systems with interesting applications where the report of HKUST-1 serves as an emblematic example. Similarly, N-donor ligands in particular Im molecule have also been explored extensively to synthesize another class of coordination polymer known as zeolitic imidazolate frameworks (ZIF) which adopt crystalline architectures and in analogy with zeolites metal ions typically Zn^{2+} ions play mimics the role of silicon and the imidazolate anions acquire the role of oxygen atoms⁷. Additionally, Im entities have also been decorated with frameworks like benzene, biphenyl etc. to synthesize flexible or rigid ligands, for example, 1,3,5-tris(imidazol-1-ylmethyl)benzene, a tridentate ligand where Im moiety is decorated on benzene scaffold was used to construct diverse structures such as cages, honeycombs, interpenetrating networks and helical structures as a result of flexibility offered by the ligand⁸.

Recently, aromatic polycarboxylate ligands are combined with multidentate N-donor ligands like DABCO, 4,4'-bipyridine, longer and flexible bipyridyl and *bis*-(Im) to achieve

more complicated structures⁹⁻¹¹. For example, Rosi and co-workers have reported Bio-MOF using adenine molecule, a nucleic acid constituent, as N-donor ligand in conjunction with aromatic polycarboxylate ligand with interesting applications like drug release, gas adsorption, and luminescence properties¹²⁻¹⁵. These ligand combinations have afforded intriguing topologies of coordination polymer which assimilate the coordination behaviour of both polycarboxylate ligand and N-donor ligands providing materials with interesting application¹⁶⁻¹⁸.

In this chapter, we have explored the coordination behavior of Im and BIm along with benzenetricarboxylic acid (BTC) to synthesize six novel coordination materials with varying topology based on Co^{+2} , Cu^{+2} and Zn^{+2} metal ions using hydrothermal/solvothermal reaction conditions.

5.2 Experimental section

5.2.1 Materials and methods:

Zinc (II) acetate dihydrate ($\text{Zn}(\text{OAc})_2 \cdot 2\text{H}_2\text{O}$, 99.5%), Co (II) acetate tetrahydrate ($\text{Co}(\text{OAc})_2 \cdot 4\text{H}_2\text{O}$, 99.5%), Copper (II) acetate ($\text{Cu}(\text{OAc})_2$, 99.5%) Benzene-1,3,5-tricarboxylic acid (H_3BTC , 98%), N,N-dimethylformamide (DMF, 99%) and N,N-diethylformamide (DEF, 99%) were purchased from Sigma-Aldrich. The Imidazole (Im, 99%), Benzimidazole (BIm, 99%) were purchased from Spectrochem.

All the compounds **20-25** were characterized by X-ray diffraction (XRD), Fourier transform infrared spectroscopy (FTIR) and thermogravimetric analysis (TGA). The single crystal X-ray diffraction data were collected using a Bruker D8 advance. Powder X-ray diffractometer using $\text{CuK}\alpha$ radiation ($\lambda = 1.5418 \text{ \AA}$), radiation in the range of $5^\circ < 2\theta < 55^\circ$. The step size used was 0.02° and exposure time 1 s for each step and the voltage and current

used were 40 kV and 40 mA. Infrared spectra were recorded on a 'Perkin Elmer FTIR spectrometer' equipped with an attenuated total reflectance accessory. The samples were mixed with KBr and pressed. The pressed samples were scanned in the spectral region of 400-4000 cm^{-1} with a resolution of 4 cm^{-1} . Thermogravimetric analyses (TGA) were carried out using a Discovery TGA by TA Instruments-Waters Lab at a heating rate of 10 $^{\circ}\text{C}/\text{min}$ under nitrogen atmosphere.

5.2.2 Syntheses of compounds 20-25:

The compounds **20** and **21** were synthesized by the solvothermal condition in which 52 mg of BTC and 17 mg of Im were added in 1 mL of DMF and stirred for 60 min followed by the addition of cobalt acetate tetrahydrate and copper acetate respectively. The final reaction mixture with 1:1:1 molar ratio was sealed in 7 mL stainless steel autoclave and heated at 120 $^{\circ}\text{C}$. After 48 h the setup was cooled to room temperature, which afforded pink color crystals in 58% yield for compound **20** and blue crystals in 68% yield for compound **21**. Compound **22** was synthesized by the hydrothermal method where 52 mg of BTC and 17 mg of Im were added in 2 mL water, followed by the addition of 55 mg of zinc acetate dihydrate were added and the reaction mixture was stirred for 1 h. The reaction mixture having 1:1:1 molar ratio is sealed in 8 mL polypropylene bottle and heated at 110 $^{\circ}\text{C}$ for 48 h which afforded colorless crystals in 70% yield. Compounds **23-25** were obtained in a similar manner where 105 mg of BTC and 60 mg of BIm were dissolved in dimethylformamide (DMF, for compound **23**) or diethylformamide (DEF, for compounds **24** and **25**) and stirred for 30 min followed by the addition of metal acetate as given in Table 5.1. The final reaction mixture with molar ratio 1:1:1 was sealed into the 23 mL (7 mL, for compounds **23** and **24**) autoclave and heated at 120 $^{\circ}\text{C}$ for 72 h (48 h, for compounds **23** and **24**). The crystals of compounds **23-25** were obtained after cooling to room temperature in moderate yields.

Table 5.1. Synthetic conditions and molar ratios for the preparation of compounds 20-25.#

	Starting composition (in mM)[#]	T[°C]	t[h]	Formula	Yield (%)
20	Co(OAc) ₂ .4H ₂ O:BTC :Im:155 DMF	120	48	[Co ₆ (formate) ₆ (BTC) ₆ (Im) ₆]	58
21	Cu(OAc) ₂ :BTC :Im:155DMF	120	48	[(CH ₃) ₂ NH ₂][Cu(BTC)(Im)]	68
22	Zn(OAc) ₂ .2H ₂ O:BTC :Im:180 H ₂ O	110	72	[Zn ₂ (HBTC) ₂ ((Im)(H ₂ O))]	70
23	Co(OAc) ₂ .4H ₂ O:BTC :BIm:155 DMF	120	48	[Co ₄ (BTC) ₃ (BIm) ₆][solvent]	75
24	Cu(OAc) ₂ :BTC :BIm:155 DEF	120	48	[Cu ₃ (BTC) ₂ (BIm) ₆][solvent]	65
25	Zn(OAc) ₂ .2H ₂ O:BTC :BIm:155 DEF	120	72	[(CH ₃ CH ₂) ₂ NH ₂][Zn(BTC)(BIm)(H ₂ O)]	62

[#]BTC = benzene-1,3,5-tricarboxylic acid; Im = imidazole; BIm = Benzimidazole; DMF = dimethyl formamide and DEF = diethylformamide.

5.2.3 Characterization:

5.2.3.1 Single-Crystal Structure Determination:

Suitable single crystals of compounds **20-25** were carefully selected under a polarizing microscope and mounted at the tip of the thin glass fiber for X-ray diffraction data collection. Structures were solved by the direct method using SHELXTL and refined on F^2 by a full-matrix least-squares technique using the SHELXL-2014¹⁹ programs package. An empirical absorption correction based on symmetry-equivalent reflections was applied using SADABS.²⁰ The graphics programs DIAMOND²¹ and ORTEP²² were used to draw the structures. Non-hydrogen atoms were refined anisotropically. In the refinement, hydrogen atoms were treated as riding atoms using the SHELXL default parameters.

Details of crystal structure refinement parameters for compounds **20-25** are given in Table 5.2. Whereas the H-bonding interactions and other short interactions are provided in Table 5.4. (Appendix).

5.2.3.2 Elemental Analysis

FTIR (KBr, cm^{-1}) for compound **20**: 3431 br, 2924 m, 1638 s, 1532 m, 1478 s, 1413 s, 1221 s, 1144 b, 992 s, 968 s, 932 s, 884 s, 643 m, 490 m; for compound **21**: 3332 br, 2945 m, 1645 s, 1523 m, 1160 b, 960 s, 928 s, 616 m, 512 m; for compound **22**: 3323 br, 3018 m, 1616 s, 1472 m, 1112 b, 932 s, 875 s, 618 m, 512 m; for compound **23**: 3354 br, 3030 m, 1595 s, 14770 m, 1096 b, 969 s, 904 s, 618 m, 489 m; for compound **24**: 3258 br, 3020 m, 1628 s, 1458 m, 1096 b, 961 s, 910s, 636 m, 496 m; for compound **25**: 3406 br, 2985 m, 1595 s, 1467 m, 1237 s, 1030 s, 965 m, 934m, 621 m, 473 m;

5.3. Results and Discussion:

The three BTC-Im based compounds were synthesized under hydro/ solvothermal method in mild conditions by changing the metal ions and varying the solvents. Compound **20** and **21** showed a layered structure, whereas compound **22** featured a one-dimensional ribbon-like structure.

5.3.1. Structural analysis of $[\text{Co}_6(\text{formate})_6(\text{BTC})_6(\text{Im})_6]$, **20**:

The compound **20** has a layered structure. The compound **20** was synthesized by the solvothermal method, Cobalt acetate tetrahydrate, BTC and Im (1:1:1) were mixed in DMF and heated in 7 mL autoclave at 120 °C. After 2 days, pink color block shape crystals were filtered out and washed with DMF. Single crystal X-ray diffraction study reveals that compound **20** crystallizes centrosymmetrically in the $R\bar{3}$ space group with a trigonal crystal system featuring a layered structure which is formulated as

[Co₆(HCO₂)₆(BTC)₆(Im)₆], **20**. The fundamental unit contains 14 non-hydrogen atoms, which has one cobalt ion, one formate unit, one Im unit and one-third BTC units.

The part of the structure shown in Fig. 5.1, the central cobalt atom has an octahedral geometry where the coordination environment is composed of five oxygen atoms coming from two BTC anions, three formate anions and the sixth coordination is achieved by one of the nitrogen atom of Im unit. The Co-O bond lengths are in the range of 1.945-2.035 Å and Co-N bond length is 2.094 Å which are similar to the literature reports^{23,24}. Each BTC anions are coordinates to six Co(II) ions and each formate anions are connected to three Co(III) ions. The bond valence sum calculations show +2 oxidation state of cobalt ion.

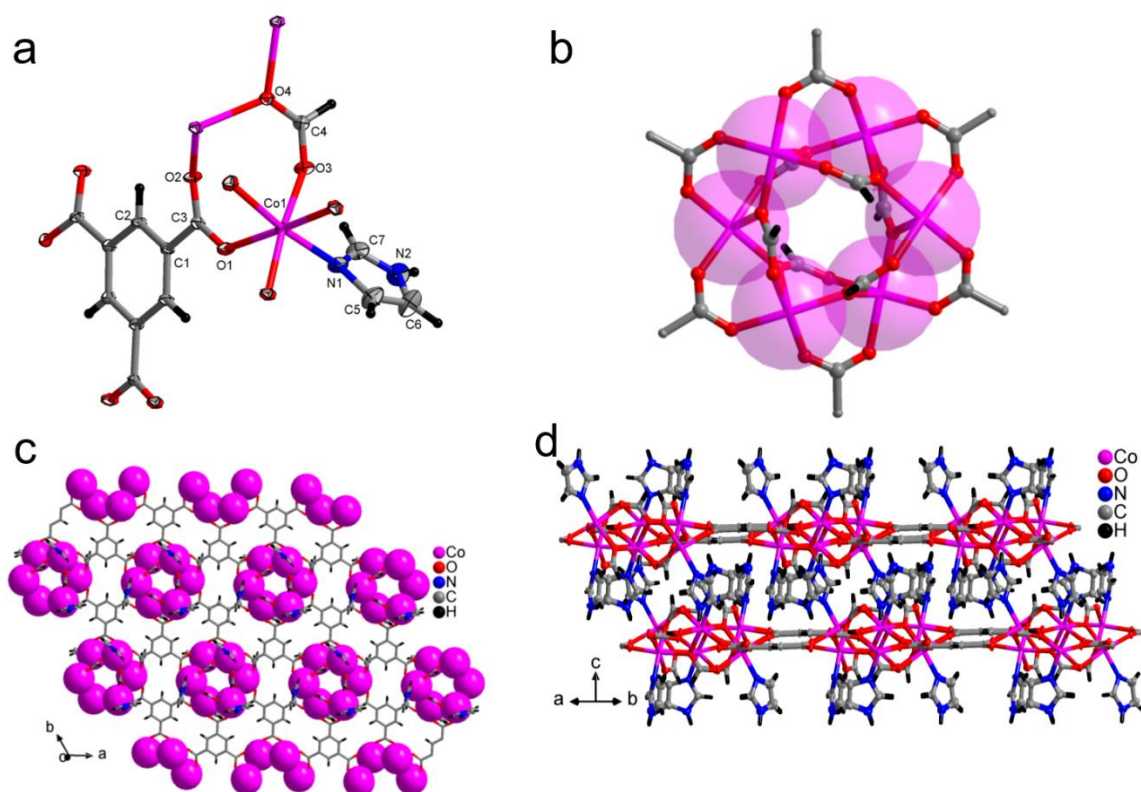


Fig. 5.1. (a) Asymmetric unit of [Co₆(formate)₆(BTC)₆(Im)₆], **20** with 35% ellipsoidal probability where unique atoms are labeled, (b) A hexagonal cluster of Co(II) ions, (c) A layer structure of compound **20** viewing along the *c*-axis and Co(II) ions were shown by space filling and (d) Lattice packing diagram of compound **20**.

The crystal lattice of compound **20** contains six Co(II) ions, six formate units, six BTC units and six Im moieties, which were arranged in anti-anti and syn-syn manner and forms a hexagonal Cobalt cluster. The BTC units are situated in the basal equatorial plane, whereas the other site i.e. axial site was bonded with formate and Im moieties. The two Co(II) ions are interconnected with the carboxylate and formate anions. The six formate anions connect six Co(II) ions and constructing hexaprismane structures as shown in Fig. 5.1b. The Co(II) ions are situated in a perfectly hexagonal manner and showing chair conformation. The distance between opposite Co(II) ions is 6.6995 Å and nearby two Co(II) ions separated by a distance 3.6290 Å. Two hexagonal Co cluster is further extended through six BTC unit and forms a layered structure in the *ab*-plane as shown in Fig. 5.1c. The distance between the two Co(II) ions in the hexagonal cluster is 7.8315 Å. These hexagonal Co clusters are situated in perfectly equilateral position²⁵.

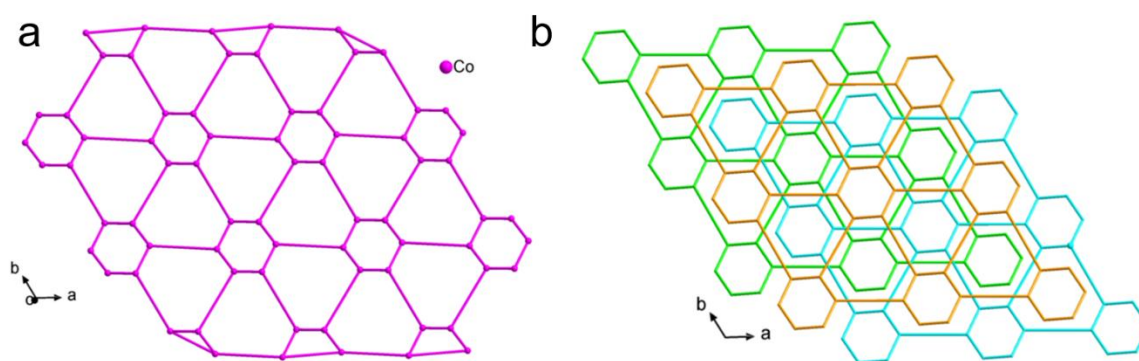


Fig. 5.2. (a) Crystal lattice of $[\text{Co}_6(\text{formate})_6(\text{BTC})_6(\text{Im})_6]$, **20**, with Co(II) ions are in hexagonal arrangement and (b) ABC-stacking of layers in $[\text{Co}_6(\text{formate})_6(\text{BTC})_6(\text{Im})_6]$, **20**, in the *ab*-plane.

In the crystal lattice, the layers are stacked in the ABC type (Fig. 5.2b) and these layers are separated by distance 7.1301 Å. The partially protonated Im and formate are connected to the Co(II) ions and protruding outside layer and situated in the interlayer space (Fig. 5.1d). Further compound **20** gets extra stability from H-bonding. The H-bonding involves in

between Im -NH (bifurcately) and carboxylate oxygen atoms in the *c*-axis. The two layers are interconnected by the H-bonding to construct an H-bonded three-dimensional framework. The H-bonding distances are 2.14 and 2.47 Å.

5.3.1.1. Magnetic properties of [Co₆(formate)₆(BTC)₆(Im)₆], **20**:

The Magnetic properties of compound **20** were performed on the crystalline sample, from the single crystal analysis of compound **20** shows hexagonal Co cluster, so it will show magnetic susceptibility, we measure magnetic susceptibility on Cryogenic PPMS system by VSM method, the Magnetic susceptibility χ_M versus T, χ^{-1} versus T and $\chi_M T$ versus T of compound **20** was recorded in presence of 100 Oe external magnetic field with varying temperature in the range of 2-350 K as shown in Fig. 5.3a and b.

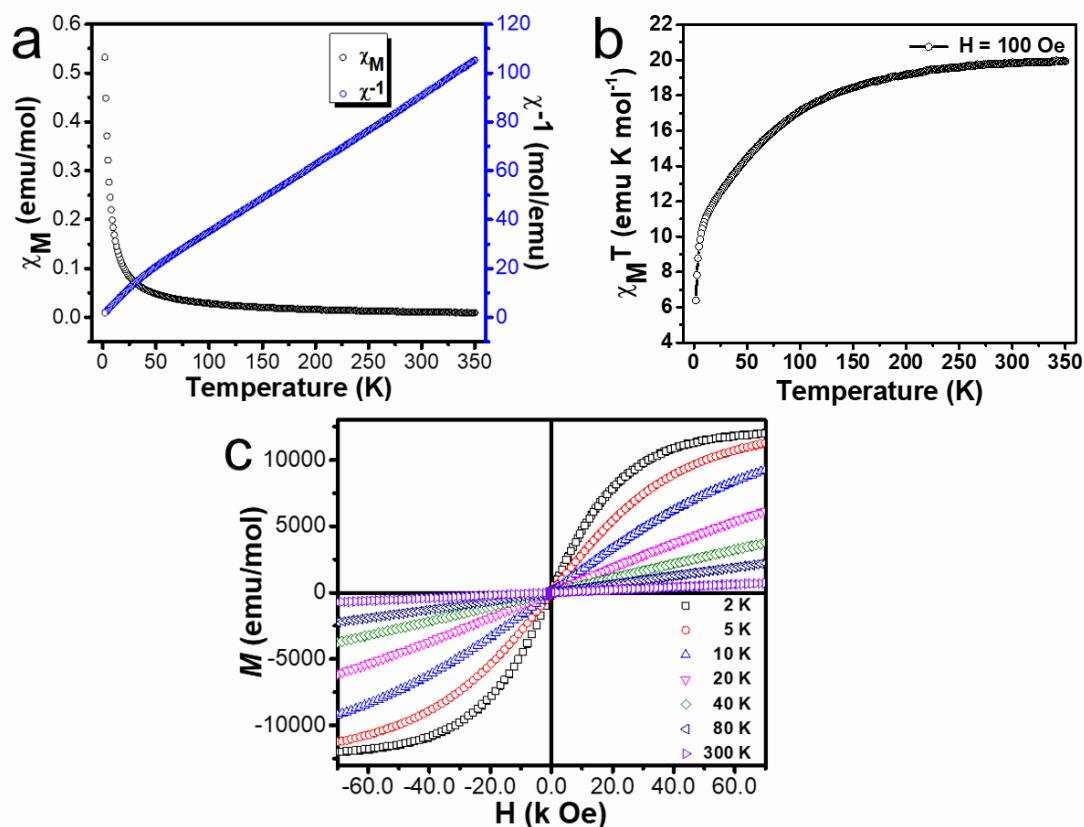


Fig. 5.3. (a) Temperature dependence graph of the magnetic susceptibility and χ^{-1} of compound **20** at external magnetic field 100 Oe, (b) Temperature dependent $\chi_M T$ curve of

compound **20** and (c) field dependent magnetization of compound **20** at 2, 5, 10, 20, 40, 80 and 300 K.

As shown in Fig. 5.1b, compound **20** composed of hexaprismane (hexanuclear cluster) Co(II) ions. The observed magnetic properties appear to be antiferromagnetic exchange coupling at low temperatures. The $\chi_{\text{M}}T$ value for hexaprismane Co_6 cluster at 300 K is $19.83 \text{ emu mol}^{-1} \text{ K}$, the value is larger than the value six magnetically isolated spin-only $S = 3/2$ Co(II) systems ($11.87 \text{ emu mol}^{-1} \text{ K}$). It reveals that the significant orbital contribution to high-spin, the Co(II) ions in an octahedral coordination environment. As temperature decreases, the $\chi_{\text{M}}T$ value decreases smoothly to reach a minimum value of $6.4 \text{ emu mol}^{-1} \text{ K}$ at 2 K. Above 50 K, the temperature dependence of χ^{-1} obeys the Curie-Weiss law with $C = 38.0 \text{ emu mol}^{-1} \text{ K}$ and Weiss constant -58 K , which suggests dominant antiferromagnetic interactions between the hexaprismane Co_6 cluster and the presence of spin-orbit couplings. The field dependent data indicate that the no hysteresis loop and as temperature decreases the magnetization is increasing and depicts the antiferromagnetic coupling between the Co(II) ions (Fig. 5.3c).

5.3.2 Structural analysis of $[(\text{CH}_3)_2\text{NH}_2][\text{Cu}(\text{BTC})(\text{Im})]$, **21**:

The $[(\text{CH}_3)_2\text{NH}_2][\text{Cu}(\text{BTC})(\text{Im})]$, **21** was synthesized under the solvothermal method under similar condition as used for compound **20**, provide a wave like layered structure with co-crystal of $[(\text{BTC})_4(\text{DMA})]$. From single crystal X-Ray diffraction data we can conclude that plate shape blue color crystal feature a layered structure, which is formulated as $[(\text{CH}_3)_2\text{NH}_2][\text{Cu}(\text{BTC})_3(\text{Im})]$. The compound **21** crystallizes centrosymmetrically in the monoclinic crystal system with $P2_1/n$ space group. The asymmetric unit contains 21 non-hydrogen atoms and it composed of one Cu(II) ion, one Im unit, one BTC unit and one protonated dimethylamine was trapped in the crystal lattice. The anionic $[\text{Cu}(\text{BTC})(\text{Im})]$

framework was balanced by one protonated dimethylamine cations which are formed *in-situ* by the decomposition of dimethylformamide solvent at the time of reaction. The part of the crystal structure of compound **21** is shown in Fig. 5.4.

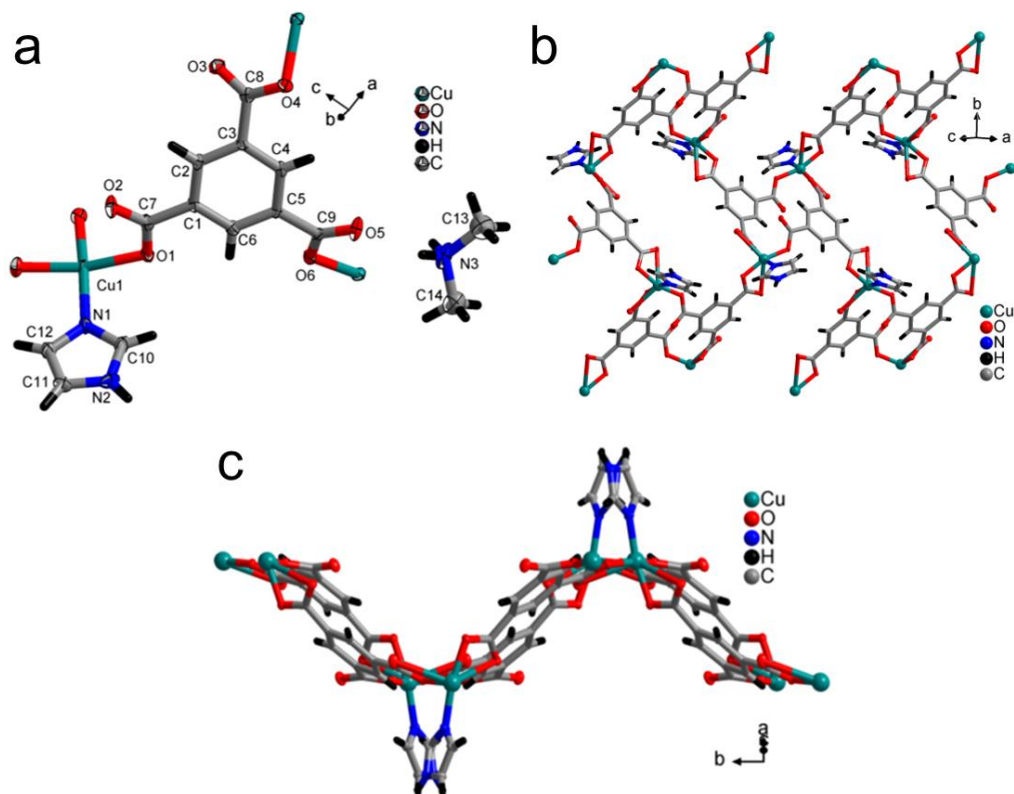


Fig. 5.4. (a) Asymmetric unit of $[(CH_3)_2NH_2][Cu(BTC)(Im)]$, **21**, where unique atoms are labeled, (b) crystal lattice view of a layered structure of $[(CH_3)_2NH_2][Cu(BTC)(Im)]$ with 8 and 4-membered rings and (c) A wave-like arrangement of $[(CH_3)_2NH_2][Cu(BTC)(Im)]$ layer in the bc - plane.

The central metal Cu atom has distorted square planar geometry and coordinated with three oxygen atoms from three different carboxylates group of BTC anions and one N atom from Im unit with the CuO_3N distorted square-planar structural unit. The average Cu-O bond distance is 1.98 Å and Cu-N has 2.05 Å bond length with acceptable range⁴. The bond valence sum calculations show +2 oxidation state of Cu metal center. Each deprotonated BTC anions are coordinated with three Cu(II) ions using its all carboxylate groups with

common oxygen atoms. The Im share its one N atom with Cu metal center, the other N atoms being protonated.

The crystallographic lattice of compound **21** shows that the distorted square-planar Cu polyhedra and tripodal BTC unit extend in the *bc*- plane and give a polymeric layered structure (Fig. 5.4c). There are two types of rings existed in the lattice of compound **21**, which are mainly 4-membered ring and 8-membered rings (Fig 5.4b). In one of the rings composed of two Cu(II) ions and two BTC units together form a 4-membered ring, whereas the other 8-membered rings are constructed from four Cu(II) ions and four BTC units. The 4-member ring and 8-member ring together extend and form a wave-like layered structure and running in the *bc*-plane.

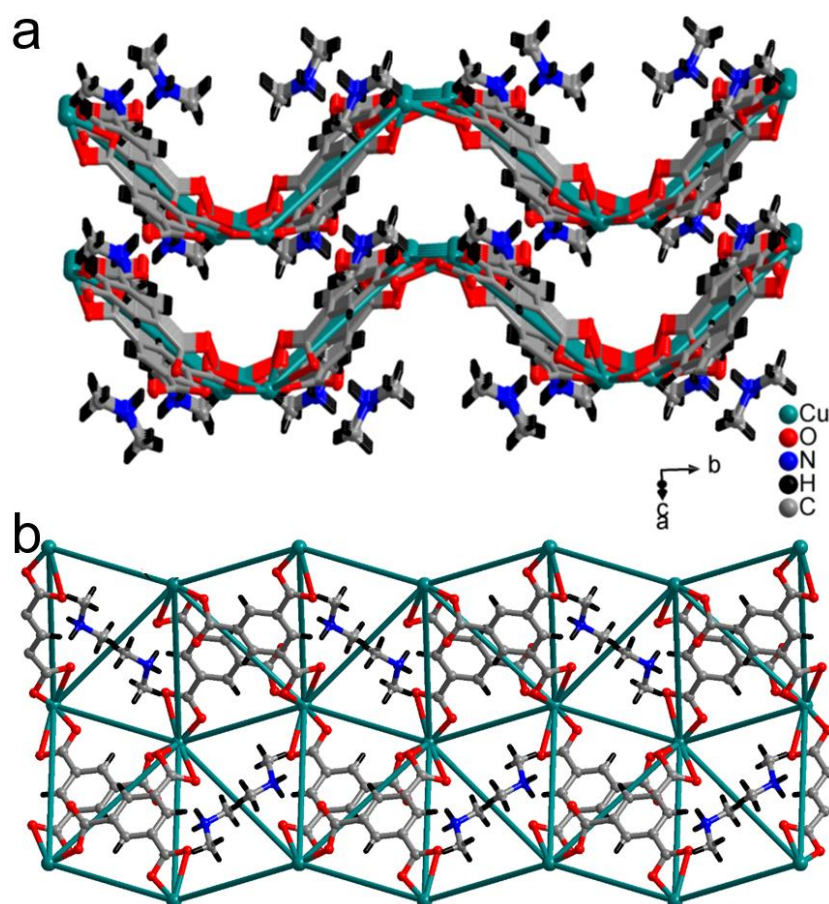


Fig. 5.5. (a) Lattice packing of two layers $[(\text{CH}_3)_2\text{NH}_2][\text{Cu}(\text{BTC})(\text{Im})]$, **21** and (b) The Cu-BTC layer in $[(\text{CH}_3)_2\text{NH}_2][\text{Cu}(\text{BTC})(\text{Im})]$, **21**, where Im unit omitted.

The two Cu(II) ions are separated by the distance 8.0773 Å and 8.9895 Å. In Fig. 5.5a and 5.5b, the Cu-Cu network shown. The other site of Cu(II) ions bonded with partially protonated Im which is protruding outside the layers and lying in between two [Cu-(BTC)] layers. Furthermore, the dimethylamine cations were situated in the interlayer space. The NH of Im, NH₂ of dimethylamine and carboxylate oxygen atoms are involved in the H-bonding. The H-bonding play a crucial role in the stability of compound **21** and form the H-bonded three-dimensional structure, the H-bond lengths are ranges from 2.05-2.56 Å.

5.3.3 Structural analysis of [Zn₂(HBTC)₂((Im)(H₂O))], **22**:

The compound **22** was synthesized by the hydrothermal method, where Zinc acetate dihydrate, BTC unit and Im unit (1:1:1) were mixed in water, and sealed in 15 mL polypropylene bottle and heated at 110 °C. After 2 days colorless crystals filtered out and washed with water.

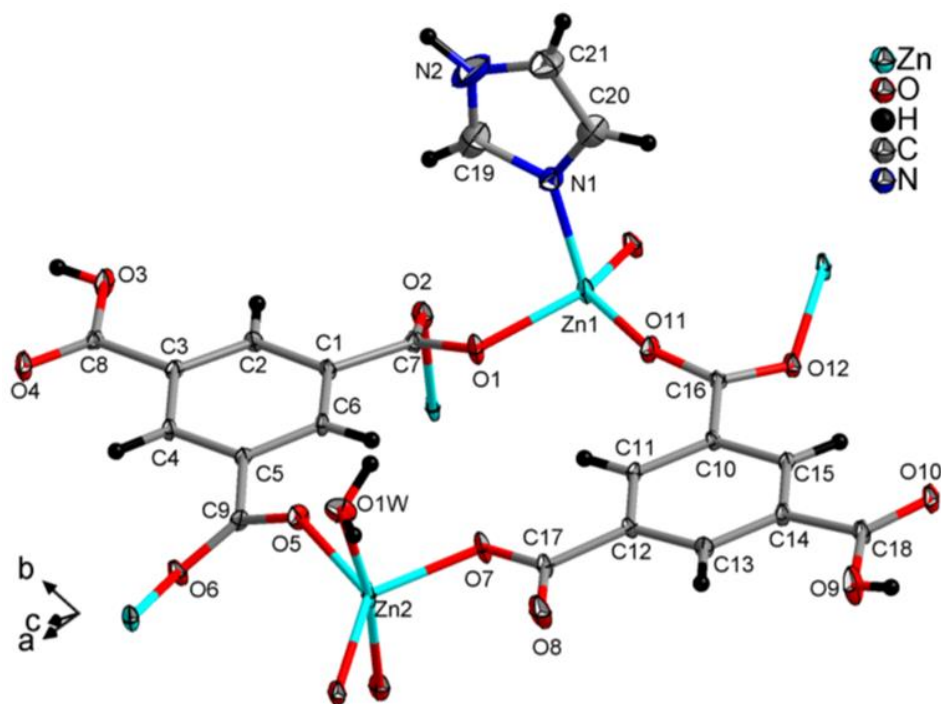


Fig. 5.6. The asymmetric unit of [Zn₂(HBTC)₂((Im)(H₂O))], **22**, with 20% ellipsoidal probability, where unique atoms are labeled.

The single crystal X-ray diffraction data was suggested that the colorless crystal of compound **22** crystallizes in centrosymmetrically $P-1$ space group in the triclinic crystal system featuring a one-dimensional ribbon-like structure and formulated as $[\text{Zn}_2(\text{HBTC})_2(\text{Im})(\text{H}_2\text{O})]$, **22**. The unit cell contains 38 non-hydrogen atoms which are formed by two Zn(II) ions, singly protonated two BTC units, one Im unit and one aqua ligand. The molecular crystal structure unit of compound **22** is shown in Fig. 5.6, there are two kinds of crystallographically unique Zn(II) ions namely Zn1 and Zn2 presents in the crystal lattice, which has different coordination environments with ZnO_3N tetrahedra and ZnO_5 polyhedral unit in the crystal structure.

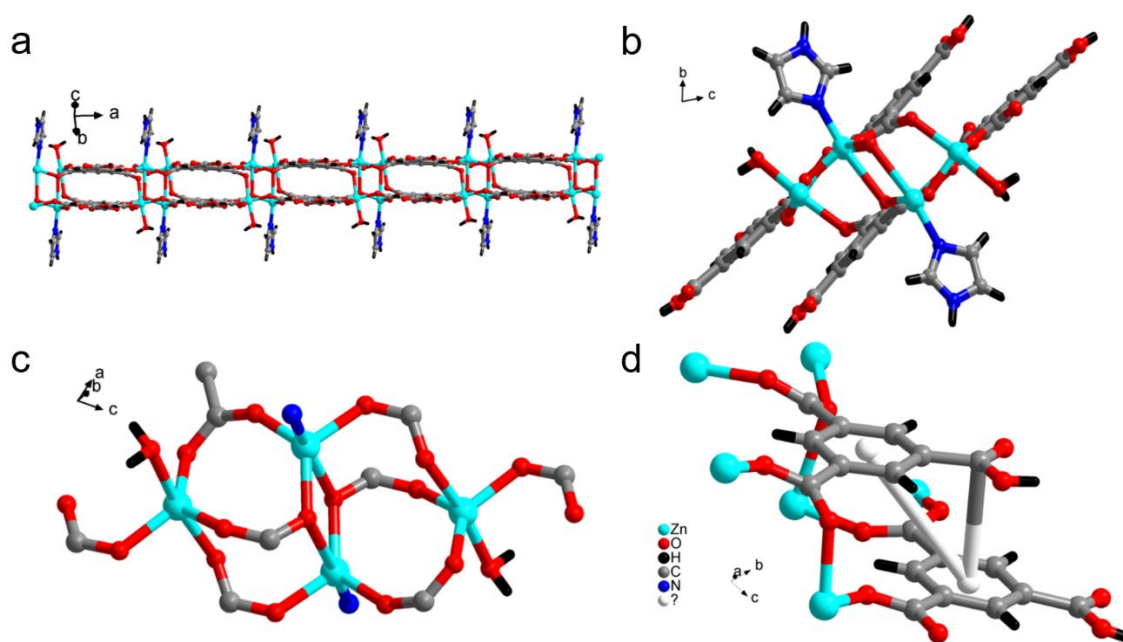


Fig. 5.7. (a) One dimensional ribbon running along a -axis in $[\text{Zn}_2(\text{HBTC})_2(\text{Im})(\text{H}_2\text{O})]$, **22**, (b) Crystal lattice of compound **22** viewing along a -axis, (c) Coordination mode of Zn(II) ions in compound **22**, and (d) A pi-pi interactions between two BTC units to provide extra stability.

The Zn1 metal centre is connected with three oxygen atoms of three different carboxylate group from BTC unit, and the fourth site of Zn1 is coordinated to the nitrogen atom of Im

with Zn-N bond length is 2.011 Å, and the Zn-O bond lengths are in the range of 1.947-1.969 Å²⁶. The other penta-coordinated central atom Zn2 has trigonal bipyramidal type geometry with five neighbor oxygen atoms, whereas the oxygen atoms namely O5, O7, and O12 of carboxylate oxygen atoms of BTC group are situated at the equatorial plane and aqua ligand O1w and carboxylate oxygen atom O2 of BTC anions are lying at the axial position of Zn(II) ions. The Zn2 atom surrounded with five oxygen atoms, where four oxygen atoms from four BTC unit and a fifth oxygen atom is bonded with an aqua ligand. However, equatorial Zn-O bond distance ranges in between 1.941-1.979 Å and axial bond distances are 2.115 Å and 2.210 Å which are in the acceptable range²⁶. The bond valence sum calculations suggested that Zn1 and Zn2 are in +2 oxidation state. There are two (HBTC)²⁻ units present in the structure, each BTC unit is singly protonated and connected with two surrounding Zn(II) ions with the different coordinated mode. One of the (HBTC)²⁻ unit bonded with five Zn(II) ions and other (HBTC)²⁻ anions share its oxygen with three Zn(II) ions.

In the crystal lattice of compound **22**, the Zn(II) ions are connected by (HBTC)²⁻ and Im unit, the alternate arrangement of tetrahedron ZnO₃N, pentacoordinate ZnO₅ and coordinate with (HBTC)²⁻ units, which is running along the *a*-axis and results into a 1D ribbon type structure. The Zn1O₃N connected to the other Zn1O₃N through O6 and Zn1-O6 have bond distance 2.717 Å, whereas the two units of ZnO₅ are interconnected with O2 of BTC unit with the bond distance 2.210 Å and form one-dimensional channel along *a*-axis (Fig. 5.7a). The inorganic node made up of two units of Zn(II) ions, each Zn inorganic node namely Zn(1)O₃N, and Zn(2)O₅ and organic linker BTC units are interconnected together and form a 4-membered rings. The distance between two opposite Zn(Zn1-Zn2) atoms is 7.3052 Å and nearest Zn1 and Zn2 is 3.7444 Å. The two closest Zn1 atoms are separated by the distance 3.7804 Å and two nearest Zn2 atoms are separated by 7.4913 Å distance.

Further, the molecule stabilized by the pi-pi interaction between the carboxylic unit and BTC unit, and separated by 3.3988 Å and two BTC unit is 4.5391 Å (Fig. 5.7d). The Im ions are connected to Zn1 ions and protruding outside to the [Zn(HBTC)] ribbon plane. The aqua ligand is coordinated with the Zn2 ions similar fashion with Im and perpendicular to [Zn(HBTC)] ribbon plane as shown in Fig. 5.7.

The compound **22** gets extra stability from the H-bonding. The H-bonding enhances the dimensionality and form an H-bonded three-dimensional network. The H-bonding involved in between the oxygen atoms of aqua ligand, oxygen atoms of carboxylate group from BTC unit and the nitrogen atom of Im. The bond distances of H-bonding are ranges in between 1.96-2.54 Å (Fig. 5.8).

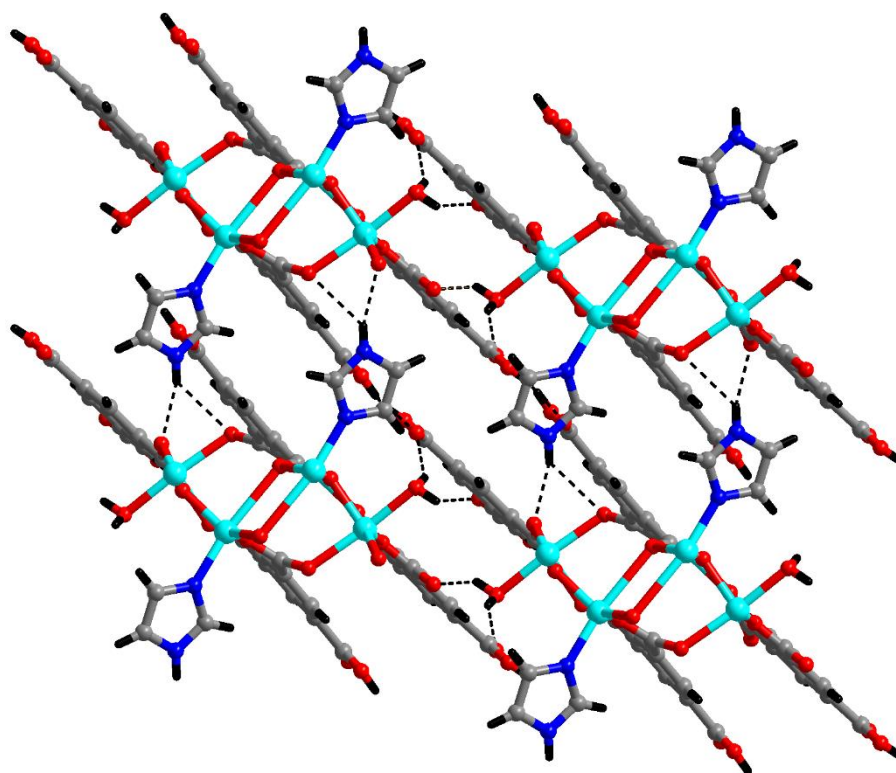


Fig. 5.8. H-bonding pattern in compound **22** along *a*-axis between the imine NH, carboxylate oxygen and aqua ligands.

Metal-BTC-BIm compounds:

We are using Im as a connecting bridge but we got a one-dimensional chain for compound **22**, and a layered structure in compounds **20** and **21** with different structural diversities. To explore and to increase the dimensionality, we replaced Im by BIm, which gives a layered and the 3D structure.

5.3.4 Structural analysis of [Co₄(BTC)₃(BIm)₆][solvent], **23:**

The paddlewheel type three dimensional [Co₄(BTC)₃(BIm)₆][solvent], **23** was synthesized similar to compound **21** under solvothermal conditions by heating the reaction mixture in DMF solution at 120 °C in an autoclave having cobalt acetate, BTC unit and BIm unit in 0.25: 0.25: 0.25 molar ratio. The X-ray crystallographic analysis reveals that rod-shaped pink color crystals of compound **23** crystallizes in the monoclinic crystal system with a C2/c space group with unit cell dimensions of a = 37.298(6) Å, b = 13.1819(19) Å, c = 19.249(5) Å, β = 113.855(14)° and V = 8656(3) Å³. The asymmetric unit composed of 53 non-hydrogen atoms having two Co⁺² ions, one and a half unit of BTC anions and three BIm units as shown in Fig. 5.9a. The anionic part of the crystal contains organic counter cations and a solvent molecule with high thermal parameters which are suppressed by squeezing the molecules by applying SQUEEZE program of PLATON software package to remove them. However, gross structural connectivity of the framework was established.

The crystallographically independent two Co(II) ions have unique positions. The Co(II) ions coordinated to 4 oxygen atoms of four carboxylate units and formed the paddlewheel like structure. Compound **23** constructed in paddlewheel Co₂ (II, II) type tetra-carboxylate and C_{3v} symmetric triangular BTC linkers and form an infinite three-dimensional framework. The two crystallographically equivalent Co(II) ions have a square pyramidal geometry where the four equatorial positions are occupied by carboxylate oxygen atoms. The average Co–O_{carboxylate} bond length is 2.010 Å. Each paddlewheel unit in compound **23**

is locked by four carboxyl groups from four equivalent BTC linkers, and each BTC linker connects three paddlewheels as SBU units, resulting in the 3D (3,4)-connected net in prismatic fashion. The fifth site of Co(II) atoms is connected with the terminal BIm unit at axial position. The bond length of Co-N atoms nearly 2.034 Å with acceptable range^{27,28}. From the bond valence sum calculations, we concluded that the Co present in the +2 oxidation states. The square planar Co(II) ions and BTC units forming helix running down along the *b*-axis and have the pitch length 13.19 Å. The BIm is protruding outside of the helix band. The crystallographically independent two Co(II) ions have unique positions with different geometries i.e. square pyramidal and tetrahedral.

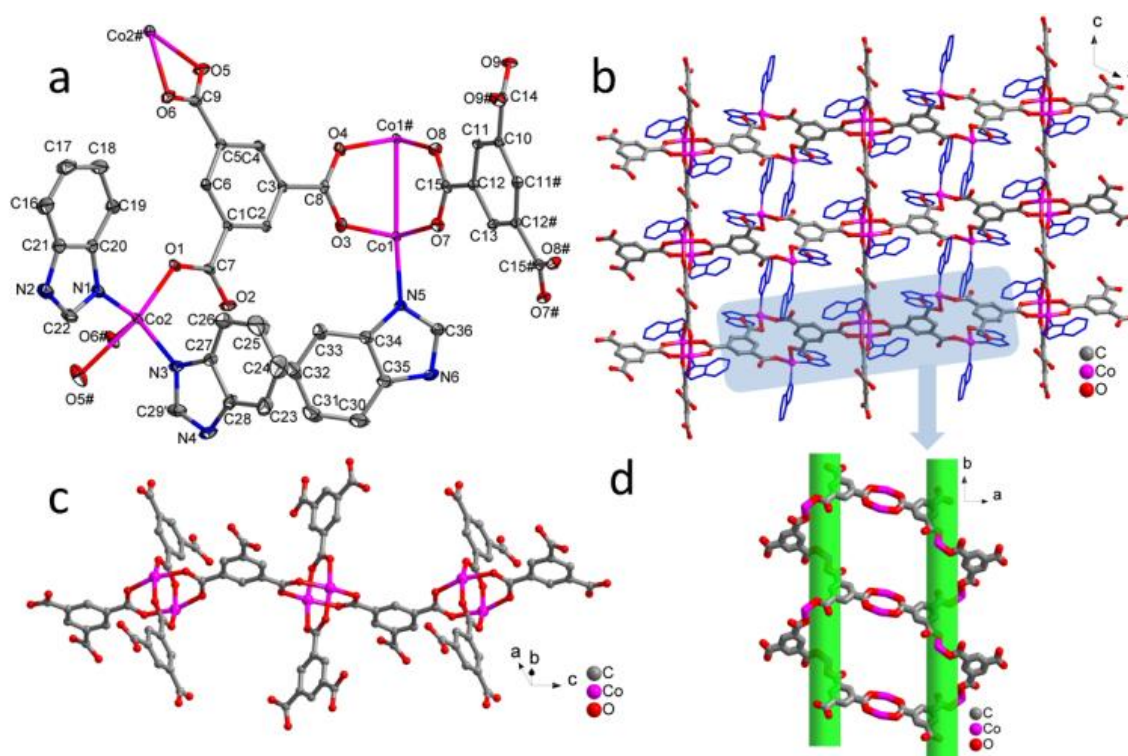


Fig. 5.9. (a) The asymmetric unit of $[\text{Co}_4(\text{BTC})_3(\text{BIm})_6][\text{solvent}]$, **23**, as ORTEP diagram with 15% probability level where unique atoms are labeled, (b) Part of the 3D-crystal lattice of compound **23**, (c) Interconnection of paddlewheel units along the *c*-axis and (d) Embedded helical assemblies running along the *b*-axis as a result of tetrahedrally coordinated Co^{+2} ions, interconnection of such assemblies through paddlewheel type of structure along the *a*-axis.

Part of the 3D-crystal lattice of compound **23** is shown in Fig. 5.9b as viewed along the *b*-axis. It can be dissected to visualize the presence of 1D chain structure, running along the *c*-axis, formed as a result of interconnected paddlewheel arrangements. Further, the crystal lattice also consists of alternate right and left-handed helical structures running along *b*-axis with a pitch length of 13.19 Å where the BIm units are protruding outwards with respect to the helix which is not shown. These helical structures are connected along the *a*-axis through paddlewheel secondary units as shown in Fig. 5.9d giving a layered structure in the *ab*-plane, thus resulting in an infinite 3D-lattice.

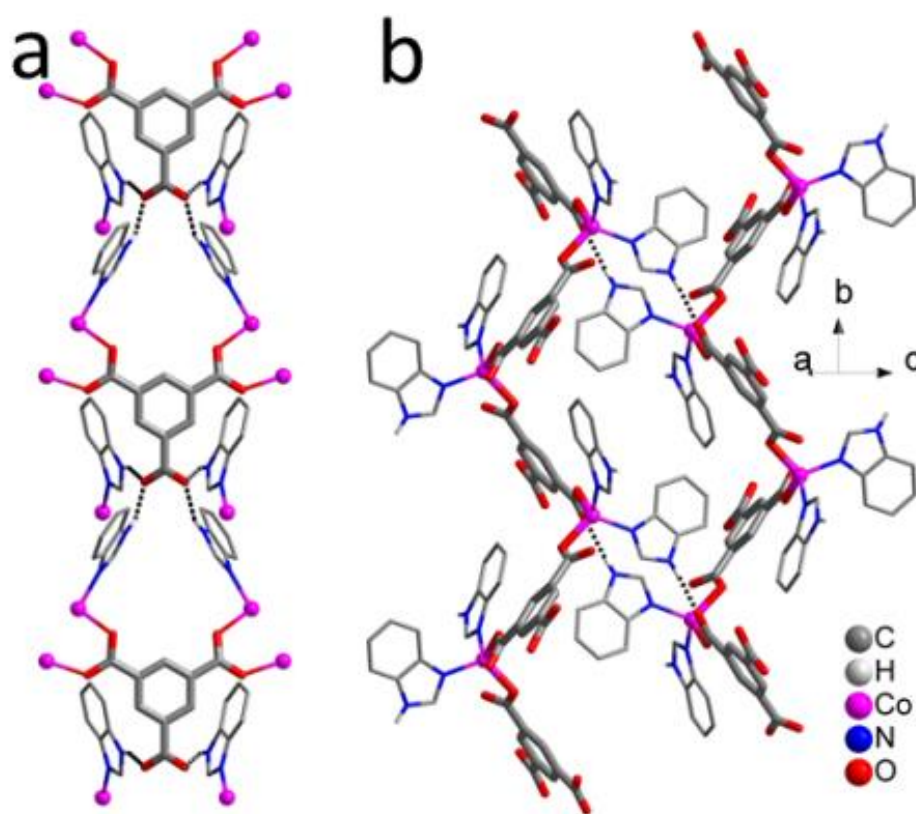


Fig. 5.10. (a and b) H bonding interaction between BIm NH group and carboxylate oxygen atoms.

From the PLATON program, the structure has contained 1D channel and possess voids 3013.4 Å³ (34.8%) porosity and 52.3 electrons which accounts two DMF and one dimethylamine cation, considering probing radius 1.20 Å. Interestingly, the coordination

modes of two crystallographically unique BTC ligands differ significantly where one type of BTC units offer its all three carboxylate groups (coordinating with two Co(1) and two Co(2) ions) whereas another type offers only two carboxylate groups (coordinating with four Co(1) ions) towards cobalt coordination. In this case, the third carboxylate moiety which also lies at the special position remains non-coordinated with both the C-O distances equal to 1.2467(1) Å. The added strength of the crystal lattice of compound **23** comes from H-bonding interaction between BIm -NH group towards carboxylate oxygen atoms. Both the oxygen atoms of non-coordinated carboxylate group acts as an acceptor for two crystallographically unique BIm group as shown in Fig. 5.10a. The other unique BIm is involved in H-bonding interaction interconnecting the helical assemblies.

5.3.5 Structural analysis of [Cu₃(BTC)₂(BIm)₆][solvent], **24**:

The solvothermal reaction of copper acetate dihydrate with 1,3,5-benzenetricarboxylic acid (H₃BTC) in presence of BIm results in a layered structure. Single crystal X-ray analysis of compound **24** shows that the plate shape blue colour crystals belong to the rhombohedral crystal system with *R*-3 space group. The asymmetric unit of compound **24** contains one copper ion with a half occupancy, one-third of BTC unit and one BIm molecule (Fig. 5.11a). There are certain intensities in the crystal structure which were not assigned and are squeezed using PLATON package. The metal centre Cu(II) ions show distorted square-planar geometry having two carboxylate groups and two imine N-atoms of BIm unit where ligands are arranged in a trans-manner forming a CuN₂O₂ polyhedron. The bond length for Cu-O is 2.076 Å and for Cu-N is 1.925 Å⁴. Bond valence sum calculations indicate +2 oxidation state for the central copper metal ion.

The six-distorted square planar Cu(II) ions and six C_{3v} symmetric BTC units are arranged alternately to form a 12-membered hexagonal ring resulting in a layered structure (Fig.

5.11). The distance between two successive Cu(II) ions in the hexagonal sheet is 9.4306 Å whereas the distance between opposite Cu centre is around 18.86 Å. The hexagonal copper rings are surrounded by the 6 small equilateral triangles of the Cu(II) ions, similarly, the small equilateral triangle which is occupied by the BTC unit is surrounded by three hexagonal copper rings. The BIm is out of the plane with respect to [Cu-BTC] plane and occupies in the interlayer space. The angle between the [Cu-BTC] and [Cu-BIm] planes is 83.29°. The hexagonal sheets are arranged in ABC-type of stacking. Interestingly, compound **24** shows isostructural with the previously published [Ni-BTC-Pyridine water] ($C_{131}H_{145}N_{15}Ni_5O_{37}$) one-dimensional coordinate polymer structure, which has water and pyridine coordinated to Ni(II) ions²⁹.

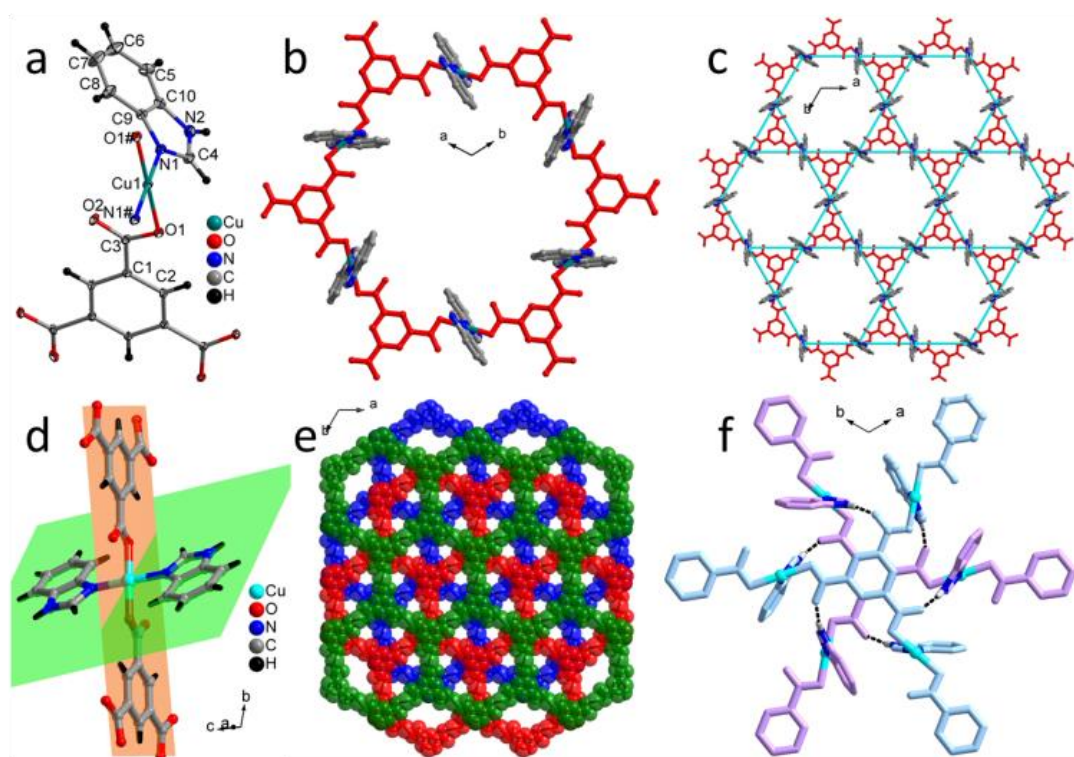


Fig. 5.11. (a) Asymmetric unit of $[Cu_3(BTC)_2(BIm)_6][\text{solvent}]$, **24** at 15% probability level where unique atoms are labelled, (b) A hexagonal 12-membered rings in compound **24**, (c) A bronze hexagonal sheet like structure in the lattice of compound **24**, (d) Intersection of BTC and BIm plane in compound **24**, (e) ABC-type stacking of layers in the crystal lattice and (f) H-bonding between -NH of BIm and carboxylate of BTC unit.

The compound **24** shows 31.7% voids which have 1714.8 Å³ void area with 346 electrons and accounting nearly 6 molecules of triethylamine which is calculated from the PLATON program. Further, the compound **24** gets extra stability and extends its dimensionality through H-bonding to result into an H-bonded 3D network. The H-bonding interaction between the carboxylate oxygen atoms of BTC and the -NH of BIm unit is observed with $d_{\text{N-H}\cdots\text{O}} = 2.19 \text{ \AA}$ which interconnects the layers along the *c*-axis as shown in Fig. 5.11e.

5.3.6 Structural analysis of [(CH₃CH₂)₂NH₂][Zn(BTC)(BIm)].(H₂O), **25**:

The solvothermal reaction of Zinc acetate dihydrate with 1,3,5-benzenetricarboxylic acid in presence of BIm results in a three-dimensional network of compound **25**. Single crystal X-ray analysis of compound **25** shows plate shape colorless crystals crystallizes in non-centrosymmetrically in an orthorhombic crystal system with *P2₁/n* space group. The asymmetric unit of compound **25** is shown in Fig. 5.12, which contains one zinc ion, one completely deprotonated BTC anion, one BIm unit, one diethyl ammonium cations and one lattice water molecule. Here the diethyl formamide decomposes and produces *in-situ* diethyl ammonium cations during reaction time, which involve in charge neutralization of anionic framework and one water molecule trapped in the crystal lattice and the distance between the diethyl ammonium cations and the water molecule is 2.875 Å. The central metal Zn(II) ions have tetrahedral geometry and linked with the surrounding three oxygen atoms of the three BTC unit through carboxylate group and one with the nitrogen atom of BIm moiety. The average bond length of Zn-O of the carboxylate of BTC unit is 2.076 Å whereas Zn-N is 1.925 Å which is in the normal range as accounted in the literature²⁶. From bond valence sum calculations, we concluded that Zn ion is present in +2 oxidation state.

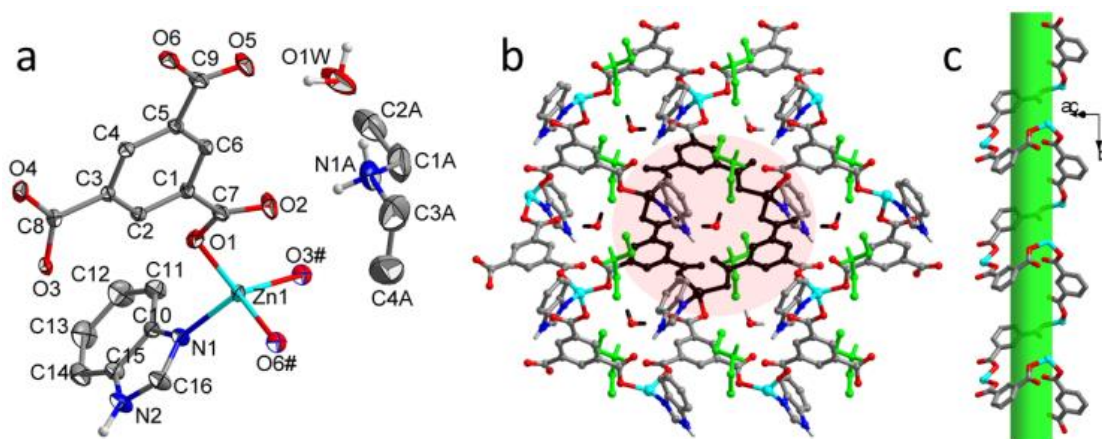


Fig. 5.12. (a) Asymmetric unit of $[(\text{CH}_3\text{CH}_2)_2\text{NH}_2][\text{Zn}(\text{BTC})(\text{BIm})]\cdot(\text{H}_2\text{O})$, **25**, as ORTEP diagram at 25% probability level, (b) Part of the crystal lattice of compound **25** (as viewed along the *b*-axis) where diethyl ammonium cations are shown in green color and (c) Embedded helical assembly in compound **25** as highlighted in 'b'.

The infinite 3D framework consists of ZnO_3N and tripodal BTC units arranged alternately. Each ring covered by the BIm which is connected to the framework, water and diethyl ammonium cation which improve the stability of the framework through strong $\text{N-H}\cdots\text{O}$ H-bonding interactions. The H-bonding distance ranges in between 2.07-2.28 Å. The crystal lattice of compound **25** is shown in Fig. 5.12b which contains helical assemblies (Fig. 5.12c) running along *b*-axis. These helices are joined along *a*- and *c*-axes to result in a 3D lattice. The helix assembly has a pitch length of 11.21 Å and coordinated BIm molecules are occupying the groove space. Further, the lattice water molecules and diethyl ammonium cations are involved in H-bonding interaction towards carboxylate oxygen atoms to provide added strength to the crystal lattice as shown in Fig. 5.13.

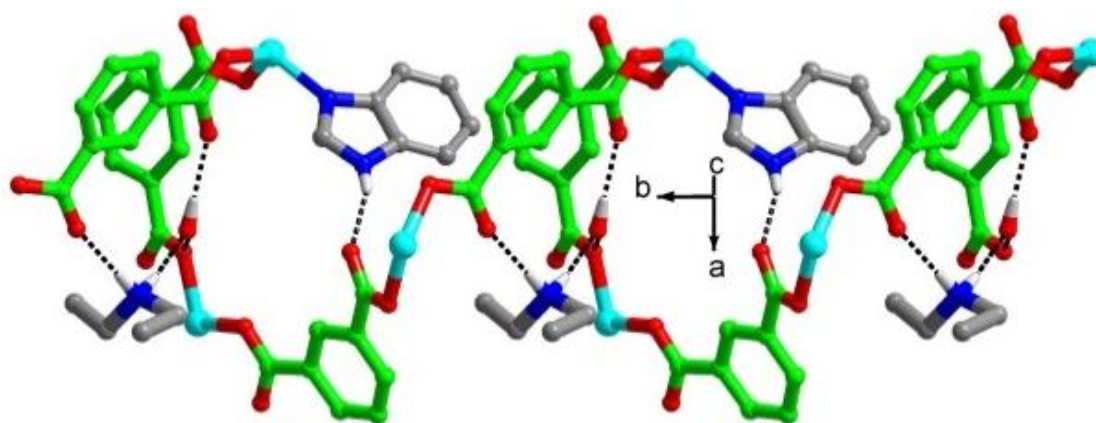


Fig. 5.13. A six-membered ring of Zn(II) ions and BTC unit in the 3D packing of $[(\text{CH}_3\text{CH}_2)_2\text{NH}_2][\text{Zn}(\text{BTC})(\text{BIm})].(\text{H}_2\text{O})$, **25**.

5.3.6.1. Dielectric measurement of $[(\text{CH}_3\text{CH}_2)_2\text{NH}_2][\text{Zn}(\text{BTC})(\text{BIm})].(\text{H}_2\text{O})$, **25**:

Compound **25** being polar, its dielectric behavior has been studied in the temperature range 25-75 °C at 1 kHz- 1 MHz frequencies. To observe an effect of temperature on dielectric constant, its variation on a function of temperature is plotted at the different frequencies as shown in Fig. 5.14a. It shows that the value of dielectric constant increases with increasing temperature. The dipole molecules cannot orient themselves at low temperature, as temperature increases, the orientation of dipoles is facilitated causing an increase in dielectric constant (K). The frequency dependence of dielectric constant at a different temperature is shown in Fig. 5.14b. It is clear from this Fig. 5.14 that the value of dielectric constant decreases with increasing frequencies. These observations indicate that dipole relaxation takes place at low frequencies. When frequency increases, the materials net polarisation decreases on each polarisation mechanism diminishes to contribute and hence the dielectric constant drops.

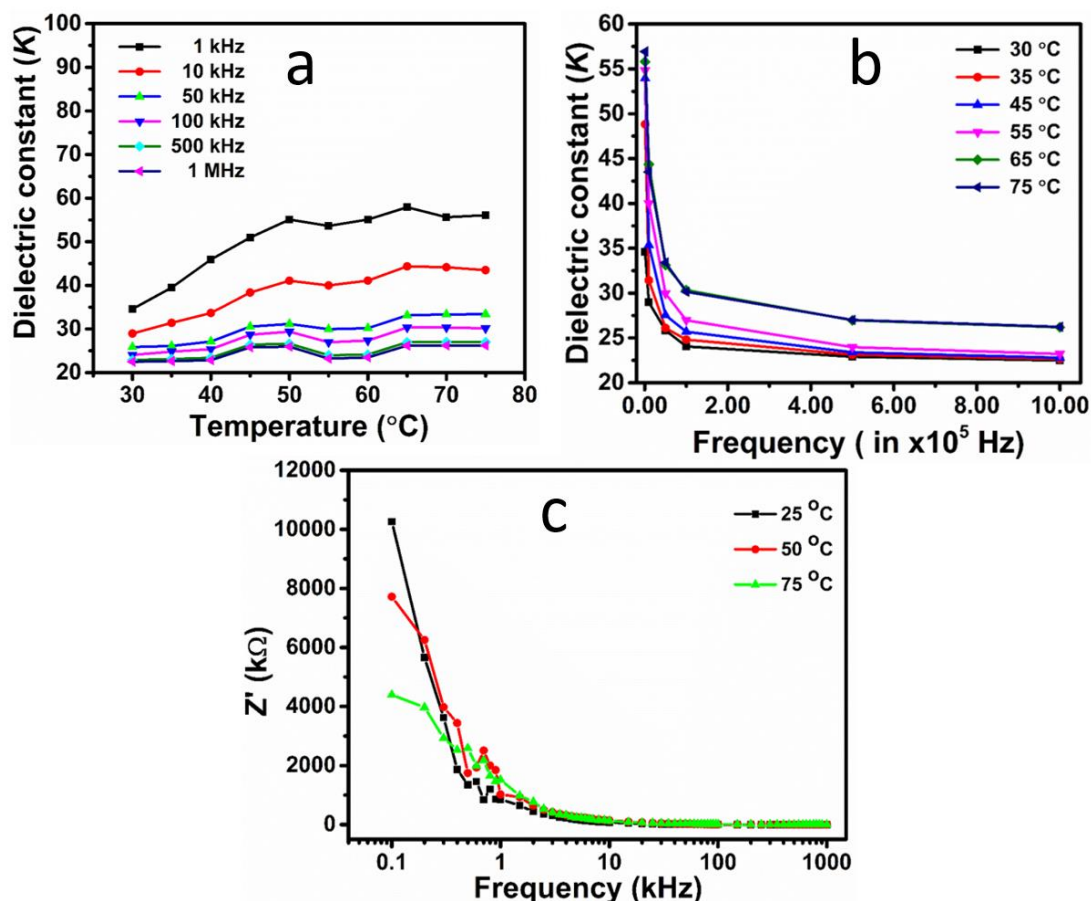


Fig. 5.14. Dielectric profile diagrams of compound **25** (a) Temperature dependent dielectric constant at various frequency, (b) Dielectric constant vs frequency at different temperature and (c) Frequency dependent real part of impedance graph.

5.4. Thermal analysis

5.4.1. Thermogravimetric Analysis (TGA):

To investigate the thermal stability of the framework for compounds **20-25**, thermogravimetric analyses (TGA) was performed. For thermal analysis study, crystalline powder sample was used and performed in the temperature range of 30–700 °C (Fig. 5.15) under a continuous flow of N_2 gas. TGA graph of compound **20** shows that compound **20** is stable up to 280 °C. Compound **20** start disintegrates from 280-340°C shows imidazole and carbon monoxide moiety which account 18.35 % (calculated 19.91 %), which is equivalent to 3 molecules. In the next step, the disintegration starts from 410-700°C which

accounts for the removal of nearly 4 molecules of BTC moiety (observed 53.38%, calculated 53.94%). The remaining residual product is identified as Cobalt oxide (CoO).

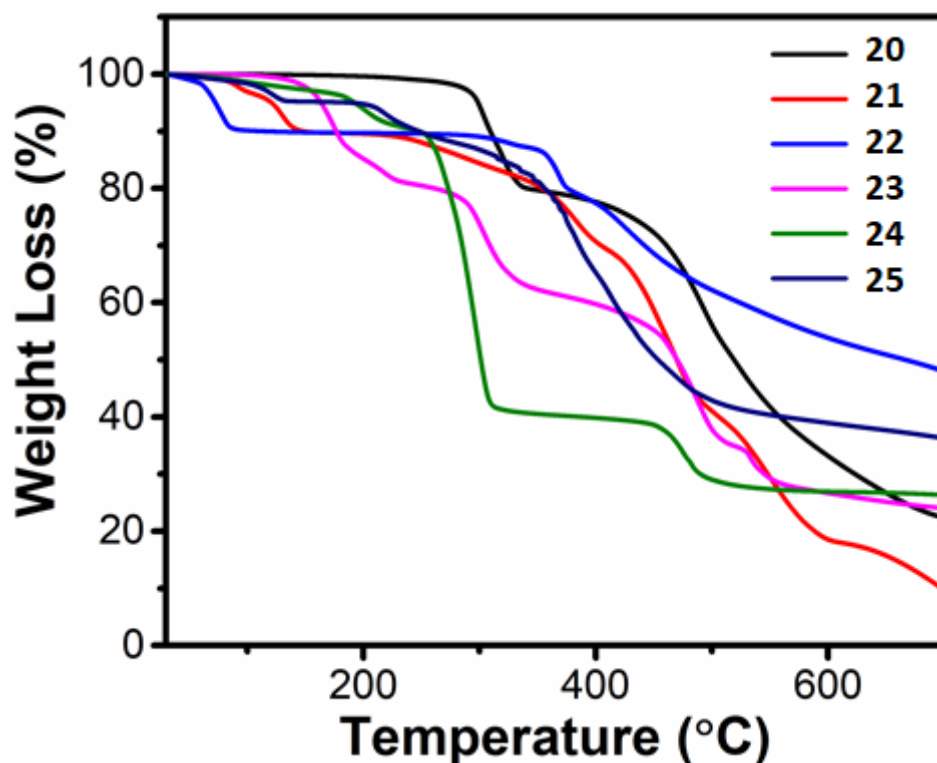


Fig. 5.15. TGA profile diagram of compounds **20-25**.

The TGA curve of compound **21** shows a gradual weight loss of 10.04% (60–150 °C), which corresponds to the removal of dimethylamine molecules and the weight loss is equal to ~10.95% (calculated 11.80%) dimethylamine molecules. The framework is stable up to 230 °C, and after that, it continuously decomposes up to 615 °C which accounts for 70.64% (calculated 71.06%) and corresponds to Im and BTC molecule. The calcined product identifies as CuO. TGA profile diagram of compound **22** indicates steady weight loss of 9.82% (calculated 10.24%) up to 90 °C which corresponds to water molecules. The dehydrated framework is stable up to 294 °C. Afterwards, it steadily decomposes into ZnO as a calcined product. The TGA graph of compound **23** shows a negligible weight loss up to 136 °C, and then it starts a continuous weight loss which corresponds to 17.9% up to 220 °C which indicates removal of guest molecules. The network is stable up to 260 °C, further,

it starts decomposing in the temperature range of 260-338 °C with loss of nearly three BIm molecules which accounts 17.40% (calculated 22.60%). In the next step, 24.40% weight loss occurs in the temperature range 425-650 °C which suggests removal of BTC units. The Final calcined product is CoO identified from the post calcined PXRD data.

TGA of compound **24** depicts 3.42 % weight loss up to 170 °C for adsorbed moisture followed by the removal of guest molecules up to 220 °C which accounts for 6.37%. Further, a sharp drop in weight occurs in the temperature range 240-315°C which accounts for 49.15%, which is equivalent to ~two BIm molecules (calculated 53.88%). The complex is stable up to 442 °C and it again decomposes and results into CuO as a calcined product at 550°C by removal of one third BTC units from compound **24** accounting 11.84% (calculated 14.53%). TGA profile reveals that compound **25** shows a gradual weight loss of 4.11% in between 60–90 °C, which corresponds to the loss of one guest water molecule (calculated 3.72%) from compound **25**. Furthermore, the dehydrated three-dimensional network is stable up to 200 °C with negligible weight loss. This is followed by a rapid decomposition to ZnO as the final product probably due to the decomposition of the frameworks.

5.5 Conclusion:

In this chapter, we have successfully synthesized and characterized six Metal-BTC-Im and Metal-BTC-Benzimidazole based coordination polymers with contrasting topologies namely, $[\text{Co}_6(\text{formate})_6(\text{BTC})_6(\text{Im})_6]$, **20**, a layered structure; $[(\text{CH}_3)_2\text{NH}_2][\text{Cu}(\text{BTC})(\text{Im})]$, **21**, a layered structure; $[\text{Zn}_2(\text{HBTC})_2((\text{Im})(\text{H}_2\text{O}))]$, **22**, a ribbon like chain structure; $[\text{Co}_4(\text{BTC})_3(\text{BIm})_6][\text{solvent}]$, **23**, a 3D-network with embedded paddlewheel SBUs; $[\text{Cu}_3(\text{BTC})_2(\text{BIm})_6][\text{solvent}]$, **24**, a layered structure with bronze hexagonal sheet; and $[(\text{CH}_3\text{CH}_2)_2\text{NH}_2][\text{Zn}(\text{BTC})(\text{BIm})].(\text{H}_2\text{O})$, **25**, a

3D network. The compound **20** has a layered structure with hexanuclear Co cluster which shows antiferromagnetic interaction between Co(II) ions. The compound **21** shows a wave like layered structure, whereas compound **24** have a bronze hexagonal sheet like structure. Compound **23** and **25** were also found to have embedded helical assemblies. In all the crystal structure the added strength was provided by H-bonding and/or pi-stacking interactions. The compounds were well characterized by the single crystal X-ray diffraction, powder X-ray diffraction and thermogravimetric analysis. Compound **25** crystallizes in polar (non-centrosymmetric) space group and shows the dielectric behaviour.

References:

- (1) Sabo, M.; Henschel, A.; Fröde, H.; Klemm, E.; Kaskel, S. *J. Mater. Chem.* **2007**, *17*, 3827.
- (2) Saha, D.; Wei, Z.; Deng, S. *Int. J. Hydrogen Energy* **2008**, *33*, 7479.
- (3) Black, C. A.; Costa, J. S.; Fu, W. T.; Massera, C.; Roubeau, O.; Teat, S. J.; Aromí, G.; Gamez, P.; Reedijk, J. *Inorg. Chem.* **2009**, *48*, 1062.
- (4) An, C.; Feng, X.; Zhao, N.; Liu, P.; Wang, T.; Lian, Z. *J. Clust. Sci.* **2015**, *26*, 889.
- (5) Cheetham, A. K.; Rao, C.; Feller, R. K. *Chem. Commun.* **2006**, 4780.
- (6) Alvaro, M.; Carbonell, E.; Ferrer, B.; Llabrés i Xamena, F. X.; Garcia, H. *Chem. Eur. J.* **2007**, *13*, 5106.
- (7) Lewis, D. W.; Ruiz-Salvador, A. R.; Gómez, A.; Rodriguez-Albelo, L. M.; Coudert, F.-X.; Slater, B.; Cheetham, A. K.; Mellot-Draznieks, C. *CrystEngComm* **2009**, *11*, 2272.
- (8) Luo, L.; Chen, K.; Liu, Q.; Lu, Y.; Okamura, T.-a.; Lv, G.-C.; Zhao, Y.; Sun, W.-Y. *Cryst. Growth Des.* **2013**, *13*, 2312.
- (9) Kondo, M.; Takashima, Y.; Seo, J.; Kitagawa, S.; Furukawa, S. *CrystEngComm* **2010**, *12*, 2350.
- (10) Zhang, J.; Wojtas, L.; Larsen, R. W.; Eddaoudi, M.; Zaworotko, M. J. *J. Am. Chem. Soc.* **2009**, *131*, 17040.
- (11) Shi, Z.; Li, G.; Wang, L.; Gao, L.; Chen, X.; Hua, J.; Feng, S. *Cryst. Growth Des.* **2004**, *4*, 25.
- (12) Li, T.; Kozłowski, M. T.; Doud, E. A.; Blakely, M. N.; Rosi, N. L. *J. Am. Chem. Soc.* **2013**, *135*, 11688.
- (13) An, J.; Geib, S. J.; Rosi, N. L. *J. Am. Chem. Soc.* **2009**, *131*, 8376.

- (14) An, J.; Fiorella, R. P.; Geib, S. J.; Rosi, N. L. *J. Am. Chem. Soc.* **2009**, *131*, 8401.
- (15) An, J.; Shade, C. M.; Chengelis-Czegan, D. A.; Petoud, S.; Rosi, N. L. *J. Am. Chem. Soc.* **2011**, *133*, 1220.
- (16) Xu, J.; Pan, Z.; Wang, T.; Li, Y.; Guo, Z.; Batten, S. R.; Zheng, H. *CrystEngComm* **2010**, *12*, 612.
- (17) Xu, J.; Yao, X.-Q.; Huang, L.-F.; Li, Y.-Z.; Zheng, H.-G. *CrystEngComm* **2011**, *13*, 857.
- (18) Qi, Y.; Luo, F.; Che, Y.; Zheng, J. *Cryst. Growth Des.* **2007**, *8*, 606.
- (19) Sheldrick, G. *SADABS, SHELXS-2008, SHELXL-2014*; University of Göttingen: Göttingen, Germany, 2014.
- (20) Sheldrick, G. M. *SADABS Siemens Area Correction Absorption Program*; University of Göttingen, Göttingen, Germany, 1994.
- (21) Pennington, W. T. *J. Appl. Crystallogr.* **1999**, *32*, 1028.
- (22) Farrugia, L. J. *J. Appl. Crystallogr.* **1997**, *30*, 565.
- (23) Miao, S.-B.; Ji, B.-M.; Wang, Y.-F.; Li, Z.-H.; Deng, D.-S.; Xu, C.-Y.; Zhou, L. *Inorg. Chem. Commun.* **2015**, *62*, 47.
- (24) Ko, I.-J.; Oh, H.-C.; Cha, Y.-J.; Han, C. H.; Choi, E.-Y. *Advances in Materials Science and Engineering* **2017**, 2017.
- (25) Zhao, J.-P.; Song, W.-C.; Zhao, R.; Yang, Q.; Hu, B.-W.; Bu, X.-H. *Cryst. Growth Des.* **2013**, *13*, 2858.
- (26) Li, M.; Liu, L.; Zhang, L.; Lv, X.; Ding, J.; Hou, H.; Fan, Y. *CrystEngComm* **2014**, *16*, 6408.
- (27) Zhao, J.; Dong, W.-W.; Wu, Y.-P.; Wang, Y.-N.; Wang, C.; Li, D.-S.; Zhang, Q.-C. *J. Mater. Chem. A* **2015**, *3*, 6962.

- (28) Meng, X.-m.; Fan, C.-b.; Bi, C.-f.; Zong, Z.-a.; Zhang, X.; Fan, Y.-h. *CrystEngComm* **2016**, *18*, 2901.
- (29) Prior, T.; Rosseinsky, M. *CrystEngComm* **2000**, *2*, 128.

Appendix

Table 5.2. Crystallographic structure refinement parameter tables for compounds 20-

25.

	20	21	22
Empirical formula	[Co ₆ (formate) ₆ (B TC) ₆ (Im) ₆]	[(CH ₃) ₂ NH ₂][Cu(B TC)(Im)]	[Zn ₂ (HBTC) ₂ ((Im)(H ₂ O)]
<i>Mr</i>	241	384.83	633.08
crystal system	Trigonal	Monoclinic	Triclinic
space group	<i>R</i> -3	<i>P</i> 21/ <i>n</i>	<i>P</i> -1
<i>a</i> /Å	14.1569(4)	8.054(2)	9.6764(2)
<i>b</i> /Å	14.1569(4)	15.781(5)	9.7358(2)
<i>c</i> /Å	21.3906(7)	12.584(3)	12.5954(3)
α /°	90	90	75.062(2)
β /°	90	96.724(16)	75.6550(10)
γ /°	120	90	76.146(2)
Volume/ Å ³	3712.7(2)	1588.4(8)	1091.02(4)
<i>Z</i>	18	4	2
<i>D_x</i> /Mg m ⁻³	1.941	1.609	1.927
μ / mm ⁻¹	2.067	1.411	2.279
θ range for data collection/°	1.915 to 25.464	2.079 to 25.497	1.707 to 25.499
Reflections collected	18079	16977	13136
unique reflections	1534	2945	4053
R(int)	0.0922	0.0996	0.0524
Data / restraints / parameters	1534 / 0 / 131	2945 / 0 / 217	4053 / 0 / 349
<i>R</i> 1 and <i>R</i> 2 [<i>I</i> >2 σ (<i>I</i>)]	0.0434, 0.1107	0.0405, 0.0892	0.0366, 0.0804
<i>R</i> 1 and <i>R</i> 2 (all data)	0.0615, 0.1246	0.0688, 0.1033	0.0540, 0.0875
Goodness-of-fit on <i>F</i> ²	1.046	1.028	1.048
Largest diff. Peak and hole/e.Å ⁻³	0.890 and -0.467	0.482 and -0.620	0.749 and -0.384
CCDC no	141585	141586	141587

	23	24	25
Empirical formula	[Co ₄ (BTC) ₃ (BIm) ₆]	[Cu ₃ (BTC) ₂ (BIm) ₆]	[(CH ₃ CH ₂) ₂ NH ₂][Zn(BTC)(BIm)].(H ₂ O)
<i>Mr</i>	1565.89	437.89	482.78
crystal system	Monoclinic	Trigonal	Orthorhombic
space group	<i>C2/c</i>	<i>R-3</i>	<i>Pna21</i>
<i>a</i> /Å	37.298(6)	18.8612(3)	15.634(13)
<i>b</i> /Å	13.1819(19)	18.8612(3)	11.214(8)
<i>c</i> /Å	19.249(5)	17.5446(4)	12.755(8)
α /°	90	90	90
β /°	113.855(14)	90	90
γ /°	90	120	90
Volume/ Å ³	8656(3)	5405.2(2)	2236.2(3)
<i>Z</i>	4	9	4
<i>D_x</i> /Mg m ⁻³	1.202	1.211	1.434
μ / mm ⁻¹	0.817	0.937	1.143
θ range for data collection/ °	2.132 to 25.483	2.636 to 25.496	2.235 to 25.498
Reflections collected	46914	34444	28440
unique reflections	7921	2227	4161
R(int)	0.859	0.0452	0.0294
Data / restraints / parameters	7921 / 0 / 466	2227 / 0 / 133	4161 / 1 / 200
<i>R</i> 1 and <i>R</i> 2 [<i>I</i> >2 σ (<i>I</i>)]	0.0458, 0.1184	0.0243, 0.0679	0.0248, 0.0673
<i>R</i> 1 and <i>R</i> 2 (all data)	0.0598, 0.1233	0.0274, 0.0691	0.0273, 0.0690
Goodness-of-fit on <i>F</i> ²	0.990	1.085	1.060
Largest diff. Peak and hole/e.Å ⁻³	0.46 and -0.53	0.23 and -0.15	0.32 and -0.35
CCDC no	141588	144589	144590

Table 5.3. Selected bond length tables of compounds 20-25.

[Co₆(formate)₆(BTC)₆(Im)₆], 20					
Co1-O1	2.078(3)	Co1-O2	2.100(3)	Co1-O3	2.120(3)
Co1-O4	2.149(3)	Co1-O4	2.120(3)	Co1-N1	2.106(4)
[(CH₃)₂NH₂][Cu(BTC)(Im)], 21					
Cu1-O1	1.944(2)	Cu1-O4	1.963(2)	Cu1-O6	1.940(2)
Cu1-N1	1.972(3)				
[Zn₂(HBTC)₂((Im)(H₂O))], 22					
Zn1-O1	1.947(2)	Zn1-O6	1.969(2)	Zn1-O11	1.953(2)
Zn1-N1	2.011(4)	Zn2 - O2	2.210(3)	Zn2-O5	1.979(2)
Zn2-O7	1.941(2)	Zn2-O12	1.949(2)	Zn2-O1W	2.115(3)
Zn2-O2	2.210(3)				
[Co₄(BTC)₃(BIm)₆][solvent], 23					
Co1-Co1	2.8713(8)	Co1-O3	2.024(2)	Co1-O4	2.058(2)
Co1-O7	2.048(2)	Co1-O8	2.039(2)	Co1-N5	2.025(3)
Co2-O1	1.971(2)	Co2-O5	2.405(3)	Co2-O6	2.019(2)
Co2-N1	2.037(3)	Co2-N3	2.014(3)		
[Cu₃(BTC)₂(BIm)₆][solvent], 24					
Cu1-O1	1.9702(9)	Cu1-O1	1.9702(9)	Cu1-N1	1.9851(14)
Cu1-N1	1.9851(14)				
[(CH₃CH₂)₂NH₂][Zn(BTC)(BIm)].(H₂O), 25					
Zn1-O1	1.951(2)	Zn1-O3	1.980(2)	Zn1-O6	1.986(2)
Zn1-N1	2.027(3)				

Table 5.4. Hydrogen bonding table for compounds 20-25.#

D—H...A	D—H	H...A	D—A	∠D—H...A
[Co₆(formate)₆(BTC)₆(Im)₆], 20				
N2—H2A...O2	0.86(4)	2.14(4)	2.841(6)	139(3)
N2—H2A...O1	0.86(4)	2.47(4)	3.197(6)	143(3)
[(CH₃)₂NH₂][Cu(BTC)(Im)], 21				
N2—H2...O6	0.86	2.14	2.9884(4)	170
N3—H3A...O5	0.89	2.35	2.722(5)	105
N3—H3A...O2	0.89	2.03	2.836(5)	151
N3—H3B...O5	0.89	2.27	2.722(5)	111
N3—H3B...O3	0.89	2.07	2.884(4)	151
[Zn₂(HBTC)₂((Im)(H₂O)], 22				
O1W—H1W1...O10	0.86	2.12	2.884(4)	147
O1W—H2W1...O8	0.86	1.94	2.694(4)	145
N2—H2A...O12	0.86	2.19	3.028(7)	164
O3—H3...O10	0.82	1.86	2.670(4)	168
O9—H9...O4	0.71(5)	1.94	2.630(5)	167
[Co₄(BTC)₃(BIm)₆][solvent], 23				
N2—H2A...O9	0.86	1.93	2.762(5)	161
N4—H4A...O2	0.86	1.83	2.687(5)	175
N6—H6A...O9	0.86	2.04	2.851(5)	158
[Cu₃(BTC)₂(BIm)₆][solvent], 24				
N2—H2...O2	0.86	1.88	2.729(5)	170
[(CH₃CH₂)₂NH₂][Zn(BTC)(BIm)].(H₂O), 25				
N1A—H1...O2	0.89	1.84	2.726(7)	170
N1A—H2...O1W	0.89	1.90	2.785(9)	171
O1W—H1W...O3	0.87	2.10	2.904(6)	155
O1W—H2W...O5	0.87	1.90	2.754(6)	168
N2—H2A...O4	0.86	1.89	2.700(4)	157

#Where 'D' is a donor and 'A' is acceptor, the bond lengths are in (Å) and angles are in (°).

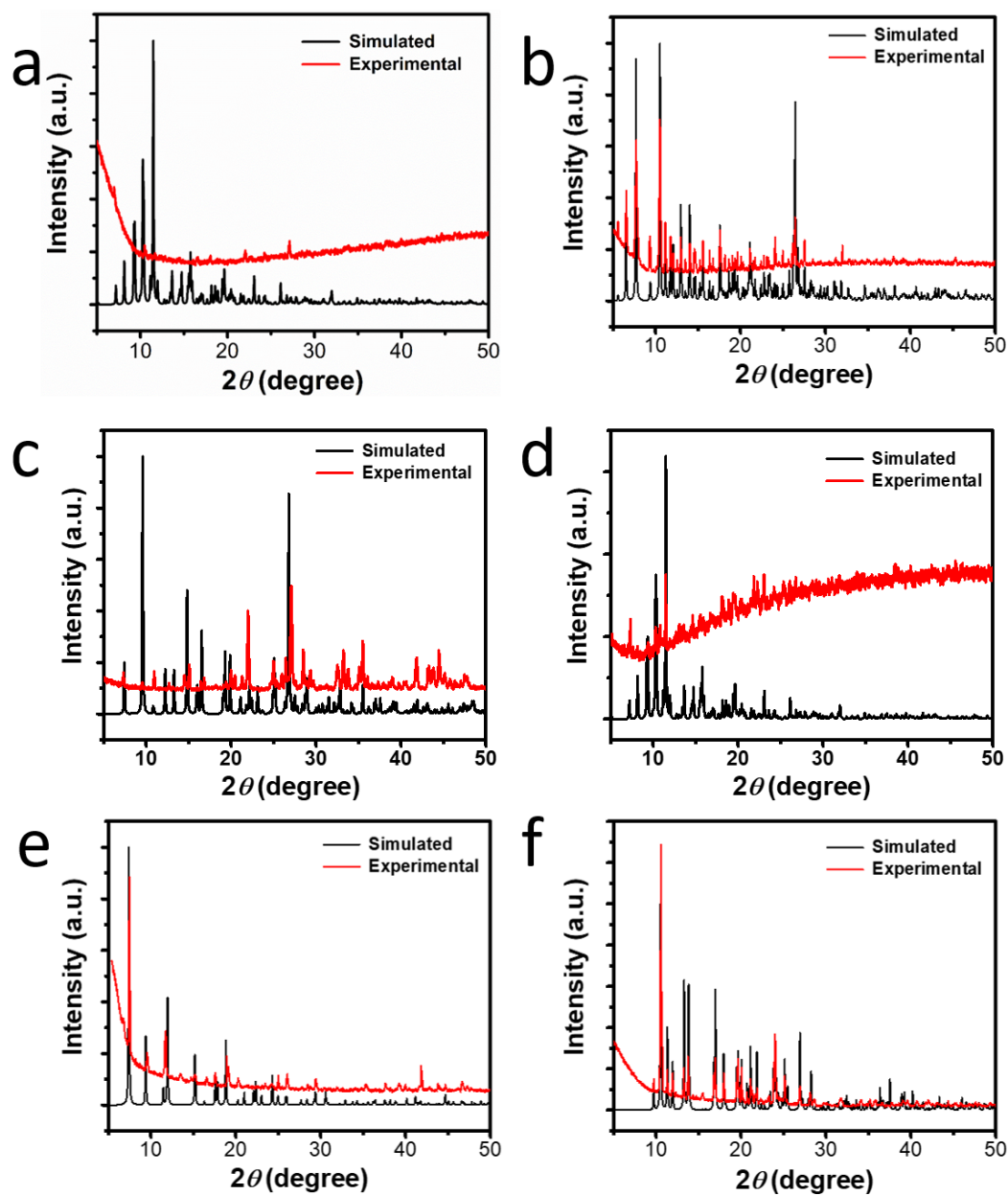


Fig. 5.16. PXRD pattern for (a) $[\text{Co}_6(\text{formate})_6(\text{BTC})_6(\text{Im})_6]$, **20**, (b) $[(\text{CH}_3)_2\text{NH}_2][\text{Cu}(\text{BTC})(\text{Im})]$, **21**, (c) $[\text{Zn}_2(\text{HBTC})_2((\text{Im})(\text{H}_2\text{O}))]$, **22**, (d) $[\text{Co}_4(\text{BTC})_3(\text{BIm})_6][\text{solvent}]$, **23**, (e) $[\text{Cu}_3(\text{BTC})_2(\text{BIm})_6][\text{solvent}]$, **24** and (f) $[(\text{CH}_3\text{CH}_2)_2\text{NH}_2][\text{Zn}(\text{BTC})(\text{BIm})].(\text{H}_2\text{O})$, **25**.

Summary of Chapter 5

